UNIVERSITY OF SOUTHAMPTON

FACULTY OF ENGINEERING AND THE ENVIRONMENT

Novel Smart Magnetorheological Elastomer Vibration Controller: Experiment, Modelling and Development

By

Wei Wang

Thesis for the degree of Doctor of Philosophy

November 2017

UNIVERSITY OF SOUTHAMPTON

ABSTRACT

FACULTY OF ENGINEERING AND THE ENVIRONMENT

Thesis for the degree of Doctor of Philosophy

Novel Smart Magnetorheological Elastomer Vibration Controller: Experiment, Modelling and Development

Wei Wang

Magnetorheological elastomer (MRE) is a new kind of smart material. MRE materials are composed of micro-sized ferromagnetic particles and non-magnetic elastomer. The stiffness and damping properties of MRE can be controlled continuously, rapidly and reversibly by an external magnetic field which makes MRE as an ideal material for vibration control. Currently, the applications of the materials are at an exploratory stage. Challenges include a better understanding of the dynamic behaviour of MRE materials, to accurately and continuously model the dynamic properties of MRE and to use MRE properly in the engineering application.

In this thesis, the dynamic shear and compression mechanical properties of MRE are investigated. Three different MRE samples with 10%, 30% and 50% iron particle concentrations are used for dynamic properties testing. MRE samples are tested at different strain amplitudes, frequencies, magnetic fields and pre-strain amplitudes. The experiment results show that the dependence of the pre-strain is an important parameter that needs to be considered. The new findings are large pre-strain amplitude deteriorates the controllability of MRE; coupling effects between pre-strain amplitude and magnetic field, frequency and strain amplitude, strain amplitude and magnetic field on the dynamic mechanical properties are obvious. These coupling effects are considered for modelling the dynamic properties of MRE. Based on the experimental results, a nonlinear mathematical model is proposed to describe the dynamic properties of MRE. The mathematical model considers the dependences of pre-strain, frequency, strain amplitude, magnetic field and their coupling effects. The proposed mathematical model can accurately and continuously model the dynamic shear and compression properties of MRE. A hybrid shear and squeeze MRE based isolator is designed. The MRE isolator is optimised to have a compact size, lower power consumption and high load-bearing capacity. The isolation performance of the hybrid MRE isolator is experimentally and numerically studied. By comparing with the experimental results and simulation results, it is found that the resonance frequencies of the isolation system shifted from 30.1 Hz to 36.8 Hz at a magnetic field of 500 mT. With a simple on-off control, the maximum force transmissibility of the hybrid MRE isolation system is reduced from 6.6 to 3.2 (51.5%).

Table of Contents

List of Tables

List of Figures

Academic Thesis: Declaration Of Authorship

I, Wei Wang

declare that this thesis and the work presented in it are my own and has been generated by me as the result of my own original research.

Novel Smart Magnetorheological Elastomer Vibration Controller: Experiment, Modelling and Development

I confirm that:

1. This work was done wholly or mainly while in candidature for a research degree at this University;
2. Where any part of this thesis has previously been submitted for a degree or any other qualification at this University or any other institution, this has been clearly stated;
3. Where I have consulted the published work of others, this is always clearly attributed;
4. Where I have quoted from the work of others, the source is always given. With the exception of such quotations, this thesis is entirely my own work;
5. I have acknowledged all main sources of help;
6. Where the thesis is based on work done by myself jointly with others, I have made clear exactly what was done by others and what I have contributed myself;
7. Parts of this work have been published as listed in publications.

Signed: .....

Date: .....

Acknowledgements

The author would like to thank Associate Prof. Yeping Xiong. Without her advice, encouragement and support, this thesis would not have been possible. The author would also like thank to Prof. Shoufeng Yang for generously offering his lab and providing useful advice for this research. Thanks also go to Prof. Ajit Shenoi and Dr. Mingyi Tan for their critical comments and advice at the transfer viva.

The author would like to thank Dr. Guanghong Zhu, Ms Kyriaki Sapouna, Dr Andy Robinson and the Engineering Development and Manufacture Centre team for the suggestion, training and manufacture for the experimental work.

The author would also like to thank Mr Li Zhu, Dr Zhe Sun, Dr Chuan Wang, Dr Yuan Li, Mr Yanxiang Wan and Mr Yu Cao for their encouragements and friendships.

The author would like to thank his parents for their selfless love. Thanks for them being financially and mentally supportive during the research life.

Last but not least, the author would like to thank the Faculty of Engineering and the Environment, University of Southampton for the sponsorship.

Nomenclatures

σ	Stress
γ	Strain
γ_p	Pre-strain amplitude
$\boldsymbol{\gamma}$	Matrix for strain amplitude
$\boldsymbol{\gamma_f}$	Matrix for strain amplitude and frequency coupling effect
$\boldsymbol{\gamma_B}$	Matrix for strain amplitude and magnetic field strength
η	Viscosity/ MPa*s
μ_0	Magnetic permeability in vacuum / H/m
μ	Relative magnetic permeability
Φ	Magnetic flux / Wb

A	Cross section area / m^2
$\boldsymbol{A'}$	Parameter matrix for storage modulus
$\boldsymbol{A''}$	Parameter matrix for loss modulus
B	Magnetic field strength/ T
$\boldsymbol{B}$	Matrix for magnetic field strength
$\boldsymbol{C}$	Damping of the isolator / kN*s/mm
d	Wire diameter / mm
f	Frequency/ Hz
$\boldsymbol{f}$	Matrix for frequency
$\boldsymbol{f_B}$	Matrix for frequency and magnetic field strength

F	Excitation force / N
G'	Storage modulus / MPa
G''	Loss modulus / MPa
$\overline{G_e}$	Mean experiment value of storage modulus or loss modulus / MPa
G_s	Simulated value of storage modulus or loss modulus / MPa
G_p'	Compensation value of storage modulus due to pre-strain / MPa
G_p''	Compensation value of loss modulus due to pre-strain / MPa
H	Thickness of the sample / mm
i	Current / A
K	Stiffness of the isolator / kN/mm
L_t	Total length of wire / m
L_w	Winding length / mm
M	Mass of isolated object / kg
N	Turns of winding
N	Turns of winding
N	Turns of winding
P	Power
R	Magnetic reluctance / A*n/Wb
R_r	Electric resistance / ohm
T_f	Force transmissibility
V	Voltage
X	Steady state response / mm
W_{coil}	Weight of coil / g
W_{core}	Weight of magnetic core / g

mmf	Magnetomotive force / A*n
MRE	Magnetorheological elastomer
MRF	Magnetorheological fluid
TVA	Tuned vibration absorber

Chapter 1: Introduction

1.1 Background

Vibration is a mechanical phenomenon which can be described as an object oscillates around an equilibrium point. In the engineering field, vibration is undesirable in most of cases. This is because vibration can create noise and waste energy in the system. Table 1.1 summarises typical vibration sources and effects in different engineering fields.

Table 1.1 Vibration sources and effects in different engineering fields

	Sources	Effects
Vehicle	• Vibration due to engine unbalance • Whirling of shaft • Road Roughness	• Affect the comfortability of the human on the vehicle, serious vibration will cause injure of the human.
Ship	• Main and auxiliary machines vibration • Unbalanced shaft • Hydrodynamic load on ship hull • Cavitation of propeller • Slamming load	• Impair health and working efficiency of the crews. • Damage the ship hull structure and endanger the safety of the marine vessel
Aeroplane	• Engine vibration • Aerodynamic force on hull structures	• Affect the comfortability of the human on board • Damage the aeroplane structures

The sources of vibration can be categorised into two groups, internal sources and external sources. The internal sources include vibration of the engine, whirling shaft, etc. The external sources are the interaction of the vehicle with road, the fluid (liquid and air) and structure hull interaction. The vibration in different engineering fields will affect the health and comfort of the humans on board and cause potentially damage to the entire system. Thus, how to eliminate or minimize the vibration and provide a safe working environment are crucial for engineering applications. In this study, the control of the vibration from an internal source (engine vibration) is considered.

Vibration control techniques are widely used in the engineering field to suppress the engine vibration. Basically, there are three kinds of vibration control techniques which are passive vibration control,

active vibration control and semi-active vibration control. Passive vibration control benefits from its simplicity. However, effective control frequency bandwidth in the passive vibration control is narrow. Active vibration control uses an actuator to transfer electric power to an active force to minimize vibration. Thus, active vibration control is effective for a broad range of vibration frequencies and can provide control of the system with time-varying vibration sources. However, the power consumption of an active vibration control is high (Andre, 2011). Semi-active vibration control combining the advantages of passive and active vibration control has attracted much attention during the past decades. By adjusting natural frequencies with low energy consumption, semi-active vibration control system can deal with time-varying vibration control problem and achieve a wide range of effective frequencies. Therefore, semi-active vibration control has greater potential compared with the others in engineering application.

In order to achieve controllable stiffness and damping properties in a semi-active control system, smart materials are widely used. Smart materials are a group of materials in which the mechanical properties can be controlled by external stimuli, such as stress, temperature, electric or magnetic field (Rubby et al., 2012). Magnetorheological (MR) material is a class of a new generation of smart materials whose elastic and rheological properties can be changed continuously, rapidly and reversibly corresponding to an applied external magnetic field (Gong et al., 2012). The MR phenomenon was first discovered by Rabinow in 1948 (Rabinow, 1948). Then, MR materials have been developed into a large family including MR foam, MR fluid, MR gel and MR elastomer (Zhang et al., 2012).

Compared with MR fluid, MRE overcomes a lot of shortcomings, such as low yield stress, sealing problem and particle sedimentation. This has drawn great concern during recent years (Zhu et al., 2015). MRE is normally composed of two primary components, which are micro-sized ferromagnetic powder and non-magnetic elastomer (Zajac et al., 2010). MRE's stiffness and damping properties can be changed corresponding to an applied external magnetic field and exhibit a quick response to external stimuli at an order of a millisecond. Since, MRE has advantages in controllable stiffness and damping properties compared with conventional materials. Then, MRE is regarded as a promising material for vibration control.

1.2 Aim and Objectives

Currently, the applications of MRE are still at an exploratory stage. The aim of this thesis is to enhance the applications of MRE in a semi-active control system to reduce the vibration. The principal objectives of this thesis are accordingly

- To investigate the dynamic mechanical properties of MRE

The dynamic shear and compression mechanical properties of MRE will be investigated. An Instron E1000 Plus is used to perform the dynamic test of MRE samples. Then, the experiment data is processed by dynamic mechanical analysis to obtain the storage and loss modulus of MRE. MRE samples will be tested at different strain amplitudes, frequencies, magnetic fields and pre-strain amplitudes.

- To propose a mathematical model to describe the dynamic properties of MRE

A nonlinear mathematical model is proposed to describe the dynamic mechanical properties of MRE by including the dependences of strain amplitude, frequency, magnetic field, pre-strain and their coupling effects. The model is based on a viscoelastic Kelvin Voigt model.

- To design a hybrid MRE based isolator

A hybrid shear and squeeze MRE based vibration isolator is designed. The designed isolator is aimed to have a compact size, low power consumption, high load-bearing capacity and wide effective frequency control bandwidth.

- To experimentally and mathematically analyse the isolation efficiency of the hybrid isolator

The isolation efficiency of the designed isolator will be experimentally and mathematically investigated. A non-linear equation of motion of the isolation system is formulated based on the proposed mathematical model. The displacement response and force transmissibility of the isolation system are calculated and compared with the experimental results.

1.3 Novelty

1. Dynamic mechanical properties of MRE

The dynamic mechanical properties of MRE are dependent on external stimuli. The dependences include strain amplitude, excitation frequency, magnetic field and pre-strain condition. Currently, most of the researchers focus on the magnetic field, frequency and strain amplitude effect on the dynamic properties of MRE. The investigation of pre-strain effect on the dynamic properties of MRE is limited. In engineering application, MRE based vibration control device will withstand the gravity force of an instrument. This initial loading will cause an inevitable pre-strain of MRE. The changes of mechanical properties of MRE due to pre-strain could induce an inefficiency of a control system. In this thesis, characterization of the dynamic shear and compression properties of MRE is experimentally investigated by considering the dependences of pre-strain, frequency, strain amplitude and magnetic field. The benefits of consideration of these four dependences to characterize the dynamic mechanical properties of MRE include, better understanding of MRE materials and use MRE effectively in engineering applications.

2. Mathematical model of MRE

Based on the experimental results, a new mathematical model is proposed to continuously describe the dynamic properties of MRE. The dependences of the strain amplitude, frequency, magnetic field, pre-strain amplitude and their coupling effect are considered in the mathematical model. This has not been done by other researchers.

3. Application and assessment of the MRE in isolation system

A hybrid MRE based isolator is designed and assembled. By using a combination of the shear and squeeze mode of MRE, the isolator is designed to have a high load-bearing capacity and a wide effective control bandwidth. The conventional design of a MRE based isolator is usually heavy and bulk. In this thesis, a better solution is found to design a MRE based isolator with a compact size and low power consumption.

For the evaluation of MRE isolation system, most of the researchers only consider MRE isolation system to be a linear vibration isolation system. By using the proposed mathematical model, the non-linear dynamic performance of the isolator could be assessed.

1.4 Thesis Structure

Chapter 2 gives a review of the current research of MRE materials. The review contains an introduction to smart materials, MR fluid and MRE. The review of the MRE contains mechanical properties of MRE, mathematical models of MRE and applications of MRE. The summary of the current literatures and research gaps are given at the end of this chapter.

Chapter 3 states the methodology to experimentally characterise the dynamic properties of MRE material. The manufacture of MRE samples will be introduced at first. Then, the dynamic test procedures of MRE and data processing method are explained.

Chapter 4 and Chapter 5 investigate the dynamic shear and compression properties of MRE material. The dependences of pre-strain, frequency, strain amplitude and magnetic field are considered. Coupling effects between these dependences are also compared and discussed.

Chapter 6 comes up with a new mathematical model to describe the dynamic properties of MRE. The mathematical model is based on the classical viscoelastic Kelvin-Voigt model. The dependences of pre-stain, frequency, strain amplitude, magnetic field and their coupling effect are considered by this mathematical model. The simulation results show good agreement with the experimental results.

Chapter 7 proposes a hybrid squeeze and shear based MRE isolator. This chapter includes design and optimisation of a closed-loop magnetic circuit, simulation of the magnetic circuit in COMSOL MULTIPHYSICS, manufacture and assemble the designed hybrid MRE isolator.

Chapter 8 evaluates the isolation efficiency of the design isolator. The results show that the resonance frequency of the isolation system can be shifted from 30.1 Hz to 36.8 Hz at a 500 mT magnetic field. The maximum force transmissibility of the hybrid isolation system is reduced at 51.5% (from 6.6 to 3.2). The numerical results are compared with the experimental results and show good agreement.

Chapter 2: Literature Reviews

2.1 Smart Materials

The definition of smart materials is a group of materials in which can respond to external environmental stimuli by changing their properties. The external stimuli include temperature, electric or magnetic field, etc. Since almost all the materials will respond to such stimuli, in order to clearly distinguish a smart material from a conventional material, Bouge (2014) indicated that the response of a smart material should have a potential to enhance the capabilities and functionalities of a material. Depending on the response of smart materials to external stimuli, the smart materials can be classified as shape memory alloys, piezoelectric materials and magnetic rheological materials, etc. Table 2.1 shows the classification of smart materials in terms of stimulus and response.

Table 2.1 Classification of smart materials

Type of smart material	Stimulus	Response
Shape memory alloys	Temperature	Deformation
Piezoelectric	Electric potential difference	Deformation
Magnetorheological material	Magnetic field	Stiffness and damping difference
Thermoelectric	Temperature	Electric potential difference
Photochromic	Radiation	Colour change

In this study, the smart materials are selected to deal with a vibration control problem. The mechanical properties of a smart material respond to the external stimuli are considered. It is seen that mechanical properties of shape memory alloys, piezoelectric material and magnetorheological material will be changed by external stimuli.

Shape memory alloys are a group of metallic alloys which can transform to their pre-form geometry by an external stimulus (temperature). Aguiar et al., (2012) made a smart spring by using shape memory alloys. He experimentally investigated shape memory alloys in vibration reduction. It was found that by controlling the temperature, the stiffness of the smart spring changed. Then, the resonant frequency of the system was altered. The advantages of shape memory alloys were lightweight and could undergo a large strain deformation. However, the response of shape memory alloys by a temperature stimulus was slow. This limited the application of shape memory alloys in the engineering field. (Jani et al. 2014)

Piezoelectric materials generate voltage on the surface of the materials as a stress is applied. This phenomenon is reversible. An applied voltage could induce a geometry deformation of piezoelectric materials. Wu et al., (2014) used piezoelectric materials as an actuator to increase the damping of a cantilever beam. The experiment results showed that the first three modes of vibration of the cantilever beam was well controlled. The piezoelectric material had a quick response time and was very sensitive to small strains. The main drawbacks were the brittle nature of ceramic which made them vulnerable to accidental breakage. Also, a high voltage was required to achieve a relative large deformation of this material. Moreover, the small range of mechanical motion (30 parts per million) would not be suitable to a large motion vibration system.

Magnetorheological materials are a new generation of the smart materials. Since the stiffness and damping properties of these materials can be changed corresponding to an applied magnetic field and exhibit a quick response to a stimulus at an order of milliseconds. Thus, MR materials have advantages in controllable stiffness and damping properties comparing with the other smart materials. These offer MR materials wider applications to vibration control in various engineering fields. In the following sections, magnetorheological materials are intensively reviewed.

2.2 Magnetorheological fluid

Magnetorheological fluid (MRF) is a kind of smart fluid materials. The rheological properties of MRF can be controlled under an applied magnetic field. MRF consists of micro sized magnetisable particles and an inert, non-magnetic carrier fluid with additives (Baranwal and Deshmukh, 2012). Basically, there are three components in MRF which are carrier fluid, micro-sized magnetic particles and stabilizing additives, respectively.

The carrier fluid is a kind of non-magnetic fluid in which the magnetic particles are suspended. An ideal carrier fluid should have certain features, such as natural lubrication, damping and most importantly, a low viscosity property which will not vary significantly with temperature. Thus, the magnetic field effect on the variation of the viscosity of the carrier fluid is dominant compared to the temperature effect on the viscosity variation (Carlson and Jolly, 2000).

The size of the magnetic particle in MRF typically ranges from 10^{-7} m to 10^{-5} m (Huang et al., 2002). Nowadays, the magnetic particles used in MRF include carbonyl iron, powder iron and iron cobalt alloys. A larger magnetic particle enables the fluid to become more stable and to have higher magnetisable ability. This allows the magnetic particles form a stronger chain-like structure under a magnetic field, i.e. increases the MR effect of MRF. Typically, the particle volume fraction of MRF can go up to 50%.

The additives added into MRF are stabilizers and surfactants (Turczyn and Kciuk, 2008). The particles in MRF have a tendency to aggregate and settle down due to gravity. Because the sedimentation of particles, the volume of the active magnetic particles suspended in MRF decreases and thus the MR effect also decrease. The stabilizers are used to preserve the magnetic particles suspended in the fluid and increase the life time of MRF (Kciuk and Turczyn, 2006). The surfactants are adsorbed on the surface of the magnetic particles to increase the polarization of particles under a magnetic field. Thus, the MR effect of MRF is enhanced. The application of the MR fluid could also be broaden.

The magnetorheological properties of MRF are determined by all these three components together. In order to enhance the MR effect of MRF, an optimum procedure to combine these three components is always required.

In the absence of a magnetic field, magnetic particles are dispersed randomly inside MRF. At this time, MRF behaves like a Newtonian-like fluid. However, as a magnetic field is applied, the magnetic particles form chain-like structures and MRF changes from a liquid state to a solid state. Meanwhile, the behaviour of MRE can be regarded as a Bingham fluid. Essentially, the operational mode of MRF applied in all devices can be classified into four groups. There are valve mode, shear mode, squeeze mode and a combination of these modes. The schematic of MRF operations of these modes are

illustrated in Figure 2.1 below. H means the magnetic field and the thick arrow shows the direction of the magnetic field. The symbols g, w and L mean the height, width and length of MRF in valve mode. The dark grey colour is container boundary of MR fluid. The shallow grey colour is MR fluid.

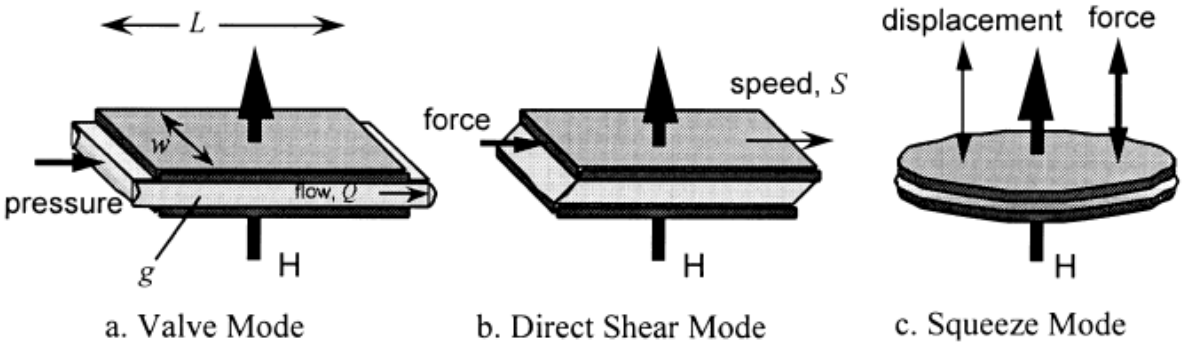

Figure 2.1 Three operation modes of MR fluid. (Carlson and Jolly, 2000)

MR fluids have been researched since 1940. However, the potential applications of MR fluid have only been recognised widely in recent years. Since the rheological and viscosity properties of MR fluid can be changed by an external magnetic field, MR fluid can be used in semi-active vibration control system or impact energy dissipation device. The current successful applications of MR fluid include, brake/clutch, engine mount, semi-active vibration isolator and vibration absorber (Baranwal and Deshmukh, 2012, Huang et al., 2002, Turczyn and Kciuk, 2008, Kciuk and Turczyn, 2006).

However, there are still some problems for MRF which limit its applications. For the real industrial applications, the devices sometimes are required for a high yield stress. In order to achieve a high yield stress, a large volume concentration of magnetic particles is required to disperse within MRF. However, a high concentration of the iron particles will arouse particles sedimentation and reduce the particles content in MRF. Therefore, the MR effect of MRF is decrease. This phenomenon has been regarded as a serious disadvantage of MRF. (You et al., 2008) Furthermore, environmental contamination and sealing problems also prevented its further application.

2.3 Magnetorheological elastomer

In recent years, MR elastomer (MRE) has drawn more and more attention by researchers due to its promising dynamic characteristics. The dynamic properties of MRE are suitable to apply in various vibration systems and offer more innovative solutions for many engineering challenges.

2.3.1 Mechanical properties of MRE

MRE is a kind of smart material analogous to MRF. However, the carrier fluid in MRF is replaced by a cross-linked material such as natural rubber or silicone rubber which makes the MRE materials become a solid. Thus, the magnetic particles in a MRE are suspended in a solid non-magnetic matrix.

The classifications of MRE can be dependent on several parameters, such as particles type, distribution of particles and matrix structure and properties (Boczkowska and Awietjan, 2012). The details of these classifications are listed in table 2.2.

Table 2.2 Classifications of MRE (Boczkowska and Awietjan, 2012)

Parameters	Classifications
1.Particles magnetic properties	(a) soft magnetic particles (b) hard magnetic particles (c) magnetostrictive particles (d) magnetic shape-memory particles
2. Matrix structure	(a) solid matrix (b) porous matrix
3. Matrix electrical properties	(a) isolating matrix (b) conductive matrix
4. Distribution of particles	(a) isotropic (b) anisotropic

The classification of MRE due to the distribution of particles is widely used. Depending on the distribution of magnetic particles in a matrix, there are two kinds of MRE materials: isotropic MRE and anisotropic MRE.

An anisotropic MRE is also called a pre-structured magnetic elastomer. During the curing process, a magnetic field is applied to a mixture of a matrix and magnetic particles. At this stage, the matrix is in a liquid state and the magnetic particles are able to move through the matrix due to a magnetic force. After the curing procedure, the matrix solidifies and the magnetic particles are locked in the elastomer. The magnetic particles are aligned parallel to the magnetic field to form chain-like or column structures (Figure 2.2 (a)). Then, an anisotropic MRE is fabricated (Farshad, and Benine, 2004, Boczkowska et al. 2007, Li et al., 2013). Otherwise, if no magnetic field is applied to a MRE during the curing procedure, the magnetic particles will distribute uniformly in the matrix. Then, an isotropic MRE material is fabricated (Figure 2.2 (b)) (Varga et al. 2005, Hua et al. 2005, Wang et al. 2006, Tian et al. 2011)

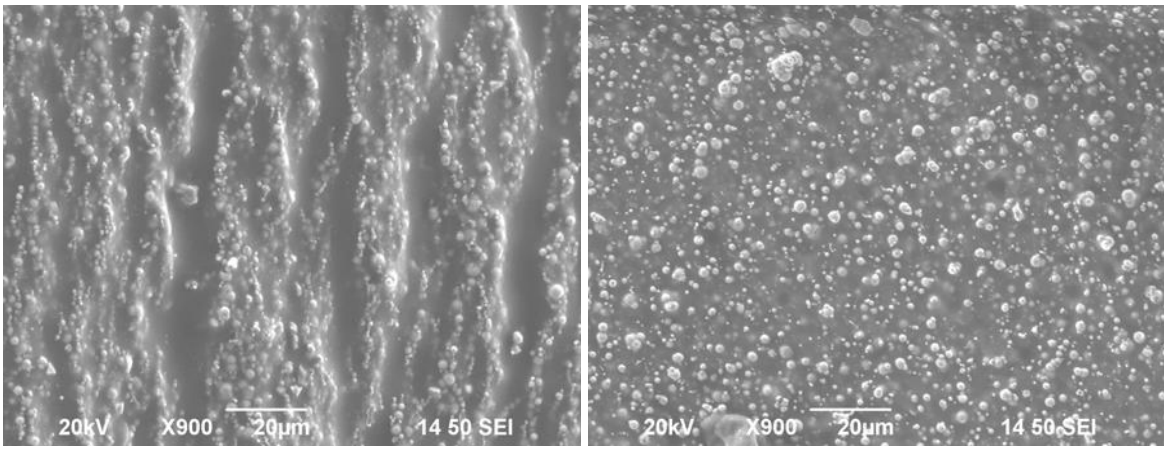

(a) (b)

Figure 2.2 SEM of the microstructure of MRE material (a) anisotropic MRE, (b) isotropic MRE (Tian et al., 2011)

The fabrication of an isotropic MRE material does not require an external magnetic field during the curing process. Therefore, the manufacture procedure of isotropic MRE material is simpler comparing with that of anisotropic MRE. It makes a great potential to manufacture large quantities of isotropic MRE material in industry application.

2.3.1.1 Payne Effect

MRE is the composite of a non-magnetic polymer matrix and magnetic particles. Therefore, MRE can be classified as a kind of filled rubber materials. Since being composite polymer material, the MRE exhibits the Payne effect (Payne, 1962) and the Mullins effect (Mullins, 1969). These two effects are known to be particular feature of the stress-strain behaviour of the filled rubber.

The Payne effect is observed under cyclic loading and manifests as a dependence of the storage and loss modulus on the strain amplitude. The storage modulus demonstrates a steady decrease as the strain amplitude increases from 0.1% to 20%. The Payne effect is dependent on the concentration of the filler and will vanish for unfilled rubber. It has been shown that MRE demonstrates a small Payne

effect under a dynamic loading without the magnetic field. As a MRE material is subjected to a magnetic field, the Payne effect becomes more obvious (Sorokin et al., 2014). The filled particles configuration and concentration of a MRE also have an impact on the Payne effect. Kallio, et al. (2007) found that the Payne effect on anisotropic MRE was more distinctive comparing with isotropic MRE. An increasing concentration of the iron particle induces a higher Payne effect of MRE (Ginder et al., 2002).

2.3.1.2 Mullins effect

The Mullins effect is also known as stress-softening effect for filled rubber. It has been reported that the rubber initial stress-stain curve of the deformation is unique and cannot be retraced. Under cyclic loadings, the stiffness of the rubber decreases and trends to a steady value (Mullins, 1969). Ogden and Roxburgh (1999) had proposed a constitutive model to describe the Mullins effect for an isotropic filled rubber. This model had been used for commercial FE codes. Coquelle and Bossis (2006) developed a two sphere de-bonding model to describe the Mullins effect for isotropic MRE.

2.3.1.3 MR effect

Magnetorheological (MR) effect is a unique mechanical property of MR materials which makes MR materials different from the other smart materials.

The MR effect can be described as the increase in the elasticity of MR materials under the influence of a magnetic field (Stepanov et al., 2009). For MRE materials, the elasticity is usually defined as shear modulus or compression modulus. Since, MRE is a kind of viscoelastic material, the shear modulus or compression modulus is composed of storage modulus and loss modulus. Storage modulus is associated with the ability to store energy due to the materials deformation which is related to the stiffness of the materials. Meanwhile, the loss modulus describes the ability of the materials to dissipate energy as heat which contributes to the damping of the material.

The mechanism of the MR effect is that the magnetic iron particles dispersed in the elastic matrix changing their positions to form chain-like structure under an external magnetic field. The schematic of the MR effect is showed in Figure 2.3.

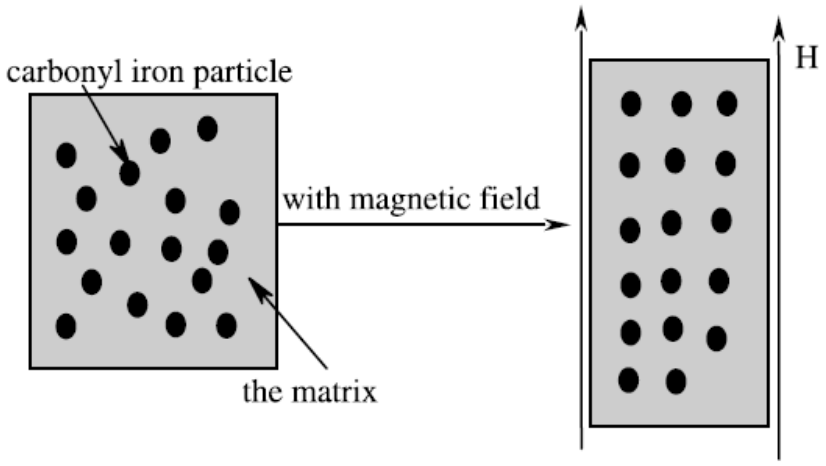

Figure 2.3 Schematic of MR effect of MRE under a magnetic field (Wang et al., 2006)

The magnetic field will induce dipole moments among the magnetic particles within the matrix. In order to obtain the minimum energy state of these particles, the magnetic particles will align parallel to the magnetic field. The movement of these particles will also induce a deformation of the matrix, resulting in an increase of the stiffness of the elastomer. Furthermore, the attractions between iron particles under a magnetic field also make contributions to an increase stiffness of MRE (Bose and Roder, 2009).

The magnetorheological effect can be categorised into absolute MR effect and relative MR effect (Lokander and Stenberg, 2003). The absolute MR effect (ΔG) is the maximum modulus (G_{max}) of MRE achieved under an external magnetic field minus the modulus of MRE without a magnetic field. The modulus of MRE without a magnetic field also called zero field modulus (G_0). The equation to calculate the absolute MR is given in Eq. 2.1.

$$\Delta G = G_{max} - G_0 \qquad \text{Eq. 2.1}$$

The relative MR effect (ΔG_r) is defined as the absolute MR effect divided by the zero field modulus. The equation is given in Eq. 2.2.

$$\Delta G_r = \frac{\Delta G}{G_0} * 100\% \qquad \text{Eq. 2.2}$$

In order to broaden the application of MRE in industrial, a MRE material with higher MR effect is required. The MR effect of MRE materials is related to magnetic particles and elastic matrix selections. Based on the current research, the MR effect can be increased in the following methods.

The MR effect increases with the strength of a magnetic field, so the magnetic particle selected to fabricate the MRE should have a high saturation magnetization (Bose and Roder, 2009). A high concentration of iron particles also increases the MR effect. That is because a high iron particle concentration increases the attractions among the particles under a magnetic field. It has been proved that the 27% magnetic particle volume concentration achieves a better MR effect (Davis, 1999).

Furthermore, according to Eq. 2.2, a decrease of the zero field modulus of MRE leads to an increase MR effect. The zero field modulus of MRE decreases as a soft material selected to be a matrix material. However, the decrease stiffness limits the application of MRE materials where a high stiffness is required. The using of additives also increases the MR effect of MRE materials. Jiang et al., (2008) indicated that the MR effect of MRE was improved by using a surfactant.

2.3.2 Composition effect on MRE properties

MRE typically consists of two components which are non-magnetic polymer matrix and magnetic filler. Currently, lots of materials have been used to fabricate MRE materials. The following section summarises the materials used to manufacture MRE and their effect on MRE properties.

2.3.2.1 Effect of matrix materials

The matrix materials have a great influence on the dynamic properties of MRE. A proper matrix material selection could increase the dynamic performance of MRE (stiffness, MR effect, etc.). The matrix material to synthesize MRE should have two properties. There are rheological property and low magnetic permeability. The rheological property enables the particles to form chain-like structures as a magnetic field is applied. The particle-chain-structure increases the MR effect of MRE. Low magnetic permeability of a matrix makes magnetic polarisation of the particles be more effective, thus increase the MR effect.

Nowadays, there are various materials have been used as a matrix of MRE. Based on the curing procedure, the matrix materials can be categorised into three groups. There are unsaturated elastomer (natural rubber (Chen et al., 2007, Jeong et al., 2013, Ubaidillah et al., 2016), synthetic rubber (Fan, Y.C., 2010, Zhu et al., 2013)), saturated elastomer (silicone rubber (Gong et al., 2007, Eem, S.H. et al., 2012, Li and Sun, 2013)) and thermoset-thermoplastic elastomer (Fan et al., 2013). The curing procedure of an unsaturated elastomer requires a vulcanization process. Meanwhile, a saturated elastomer can cure at room temperature. For a thermoset-thermoplastic elastomer, it can be cured with or without vulcanization process (depend on the polymer chain). The fabrication process of MRE with saturation elastomer (silicone rubber) is the simplest. Thus, it attracts more interest among the researchers. However, the mechanical properties of the unsaturated elastomer (stiffness and damping) are higher than the saturated elastomer and thermoset-thermoplastic elastomer (Ubaidillah et al., 2015).

Stiffness of a raw matrix material has a significant effect on the mechanical properties of MRE. The first effect is on the MR effect. For a hard matrix MRE, the MR effect is relative lower comparing with a soft matrix MRE (Lokander and Stenberg, 2003). According to the current literatures, the maximum MR effect achieved for a hard matrix is 133% which contain 80% (weight fraction) iron particles and 20% nature rubber under 1 Tesla magnetic field (Chen et al., 2007). The maximum MR

effect achieved for a soft matrix is 878% containing 10% (weight fraction) silicone rubber, 10% silicone oil and 80% of iron particles under 1 Tesla magnetic field (Gong et al., 2007). The second effect is the zero-field modulus. A harder matrix MRE results in a higher zero-field modulus. By contrast, a softer matrix MRE has a relative lower zero-field modulus.

2.3.2.2 Effect of filled particles

Particles selected for MRE materials should have some particular features, such as high magnetic permeability, low remnant magnetisation and high saturation magnetization (Munoz and Jolly, 2001). A high magnetic permeability and saturation magnetization induce a higher interaction among the particles of MRE under a magnetic field. Therefore, the MR effect of MRE material is increased (Lokander and Stenberg, 2003). A low remnant magnetisation enables the particles to get de-magnetisation instantaneous as a magnetic field is removed. This phenomenon is described as reversible MR effect (Genc, S and Phule, P.P., 2002). Based on current reviews, the carbonyl iron particle is selected as magnetic particles in most of MRE materials.

Particle size also has an effect on the mechanical properties of MRE materials. The particle size selected to manufacture MRE materials ranges from 10 μm to 200 μm. It is found that for a MRE material fabricated with smaller size iron particles, the zero field modulus is higher comparing with that of larger size iron particles. Meanwhile, the damping of a MRE material with smaller size particles is also higher. This is due to the interfacial frictions between the particles and matrix is higher for a MRE material with smaller particles. For a MRE material manufactured with larger size particles, a higher increase modulus is observed under an applied magnetic field (Ubaidillah et al. 2014).

Magnetic particle concentration is another factor that affects the mechanical properties of MRE. Bose and Roder (2009) had investigated the storage modulus and loss modulus of isotropic and anisotropic MRE with different iron concentrations. They found that by increasing the concentration of the iron particles lead to a steady increase of the storage modulus and loss modulus (see Figure 2.4). Davis (1999) used finite element method to simulate the MR effect with different iron particle concentrations. He found that the MR effect is higher for MRE samples with a 27% iron particle concentration.

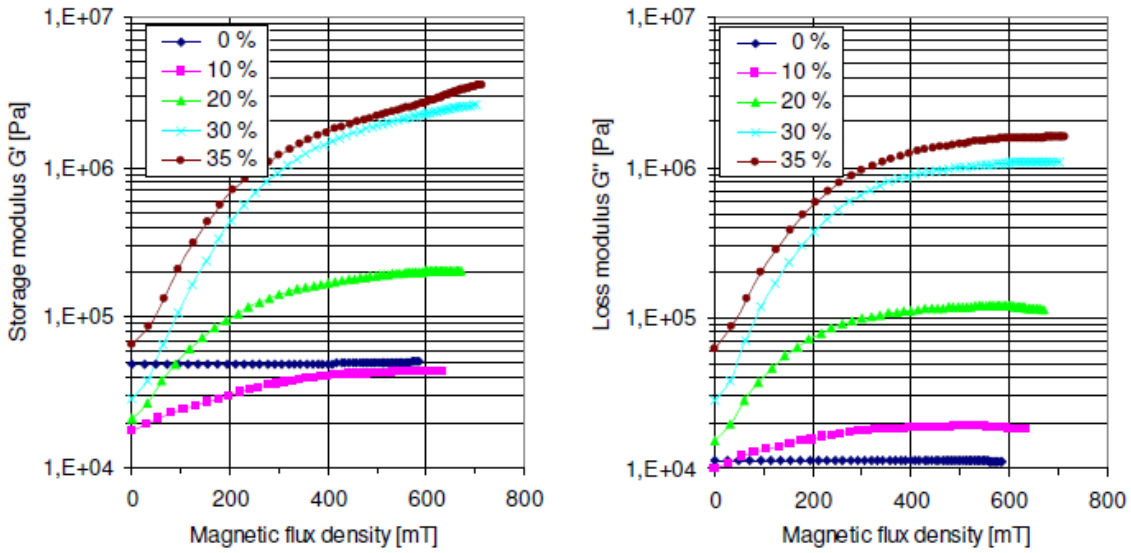

Figure 2.4 Storage modulus and loss modulus of isotropic MRE with different concentration of iron particles under magnetic field (Bose and Roder (2009))

2.3.3 Quasi-static and dynamic properties of MRE

The quasi-static and dynamic mechanical properties of MRE material are different.

2.3.3.1 Quasi-static mechanical properties of MRE

Figure 2.5 illustrates the stress-strain curve of MRE at a quasi-static loading with different magnetic fields various from 0 mT to 750 mT. The shear modulus of MRE can be obtained from the slope of the stress-strain curves. It can be seen from Figure 2.5, the shear modulus of MRE increases with the magnetic field strength. For shear strain less than 10%, the stress-stain curves show that the shear stress has a linear relationship with the shear strain. This phenomenon demonstrates that MRE has a linear viscoelastic property at a quasi-static loading less than 10% shear strain. However, as the shear strain continues to increase, the shear stress of MRE will reach to a maximum value and decrease to a steady value. At this region, the shear stress of MRE has a nonlinear relationship with the shear strain. Then, it is said that MRE has a nonlinear viscoelastic property for the shear strains above 10%.

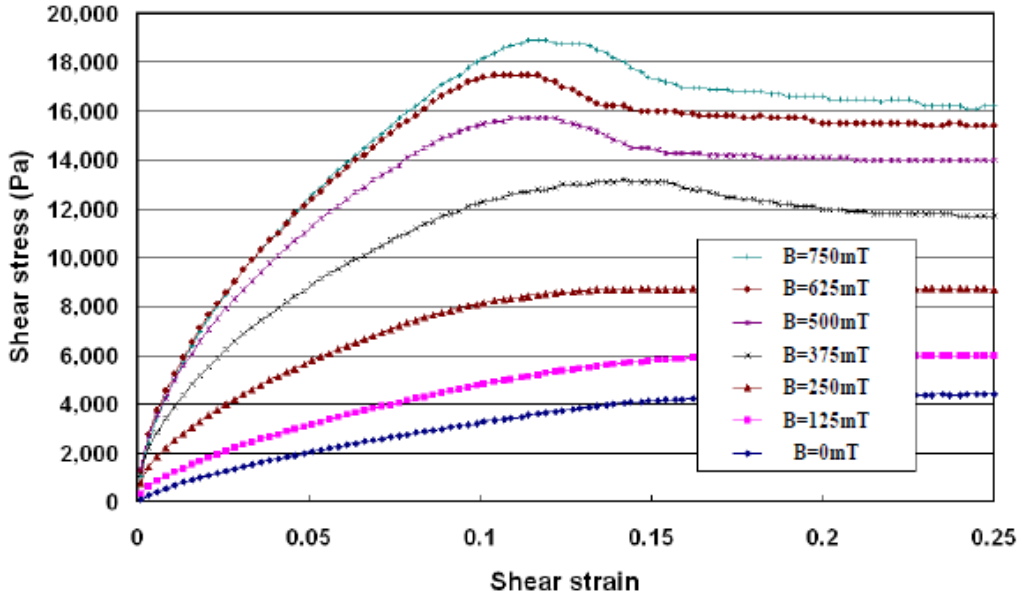

Figure 2.5 Quasi-static shear stress-strain curves with different magnetic fields (Li et al., 2013)

2.3.3.2 Dynamic mechanical properties of MRE

The dynamic mechanical properties of the MRE are different compared with those at a quasi-static state. The MRE is a kind of viscoelastic material which the stress does not respond instantaneously as a strain is applied. The stress-strain curve of the MRE material that subjected to a dynamic sinusoidal loading exhibits a hysteresis loop. This is shown in Figure 2.6.

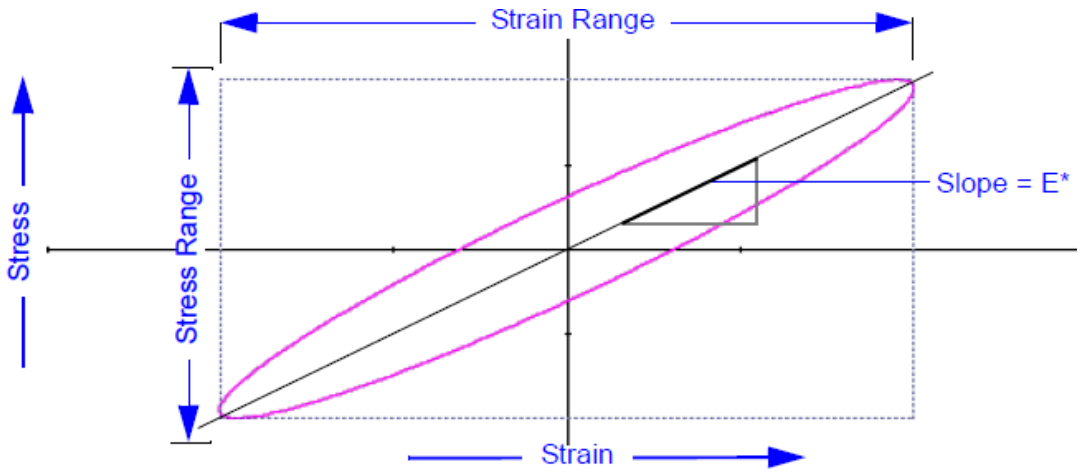

Figure 2.6 Hysteresis loop of viscoelastic material under a dynamic loading (Instron, 2008)

The dynamic mechanical analysis (DMA) is used to study the dynamic properties of the viscoelastic material. The complex dynamic modulus $E^*$of the MRE material is defined by the storage modulus and loss modulus.

$$E^* = E' + iE'' \qquad \text{Eq. 2.3}$$

Where, $i^2 = -1, E'$ is the storage modulus of MRE and E'' is the loss modulus of MRE. The storage modulus and loss modulus can be expressed as

$$E' = |E^*| * cos\delta \quad \text{Eq. 2.4}$$

$$E'' = |E^*| * sin\delta \quad \text{Eq. 2.5}$$

$|E^*|$ is the absolute value of the complex dynamic modulus. $|E^*|$ is equal to the slope of stress range to strain range (Eq. 2.6).

$$|E^*| = \frac{Stress\ Range}{Strain\ Range} \quad \text{Eq. 2.6}$$

δ is the loss angle. The loss angle is calculated as the arcsine of the ratio of the area of the hysteresis loop and the area of the ellipse bounded by the stress range and stain range. The equation to calculate the loss angle is defined in Eq. 2.7. (Instron, 2008)

$$\delta = arcsine\left(\frac{enclosed\ area\ of\ the\ hysteresis\ loop}{\pi * Strain\ Range * Stress\ Range/4}\right) \quad \text{Eq.2.7}$$

Li et al. (2010) had studied the dynamic properties of MRE material under different magnetic field.

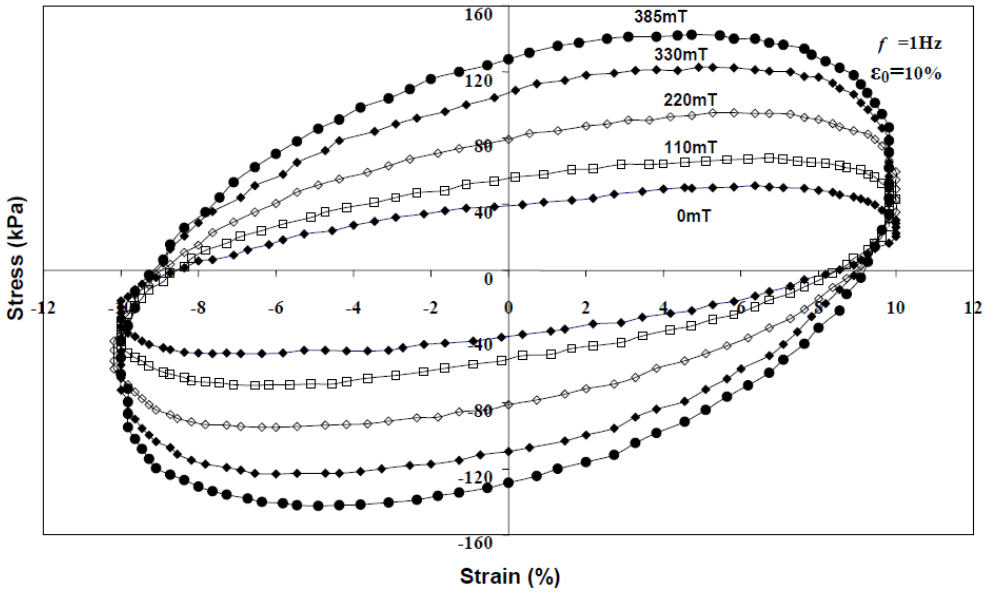

Figure 2.7 Stress-strain curves of MRE material under dynamic loading with different magnetic field (Li et al., 2010)

Figure 2.7 demonstrates the stress-strain curves of MRE under dynamic loadings. The excited frequency is 1Hz and the strain amplitude is 10%. The magnetic field strength various from 0 mT to 385 mT. It is seen from Figure 2.7, the slope of the stress to strain and the area of the stress-strain

ellipse vary with the magnetic field. This phenomenon indicates that MRE exhibits a controllable stiffness and damping properties by an external magnetic field.

Sorokin et al. (2014) investigated the strain amplitude effect on the dynamic properties of MRE with and without magnetic field. The strain amplitude effect was also known as Payne effect (Payne, 1962). They found that the Payne effect on the storage modulus and loss modulus of MRE material was more obvious by the presence of a magnetic field (shown in Figure 2.8).

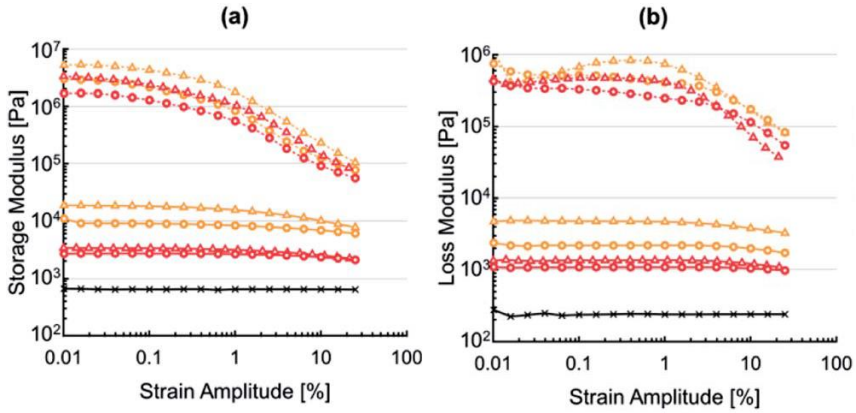

Figure 2.8 Storage modulus and loss modulus of MRE samples without (solid lines) and with (dashed lines) the magnetic field (Sorokin et al., 2014)

The vibration frequency also has an effect on the dynamic properties of MRE. The experiment results show that both of the storage modulus and loss factor vary with different excitation frequencies. As the excitation frequency increases, the storage modulus of MRE increases. Meantime, a decrease of the loss factor is observed (Gong et al., 2012).

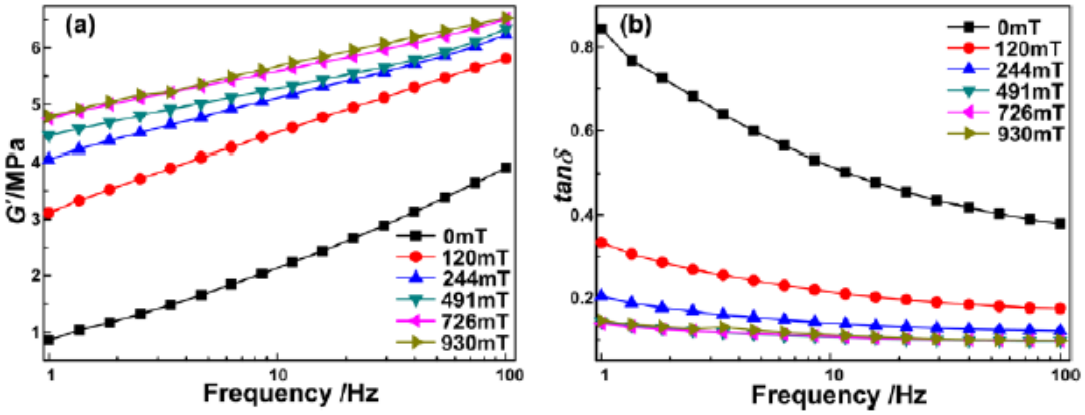

Figure 2.9 Storage modulus and loss factor variations with increase frequency (Gong et al., 2012)

Lejon and Kari (2009) investigated the pre-strain effect to the dynamic shear mechanical properties of an isotropic MRE. They found that the pre-strain was an important parameter need to be considered in describing the mechanical properties of MRE material.

2.4 Mathematical models of MRE

The mathematical models of MRE material can be categorised into two groups. The first one is to model the magnetic induced modulus of MRE and the other one is to model the mechanical properties of MRE under a dynamic loading.

2.4.1 Magnetic induced modulus of MRE

A quasi-static and one-dimensional dipole model was proposed by Jolly et al. (1996) to model the magnetic induced modulus of the MRE. Since the model was quasi-static, therefore the dynamic effect of the magnetic field was neglected.

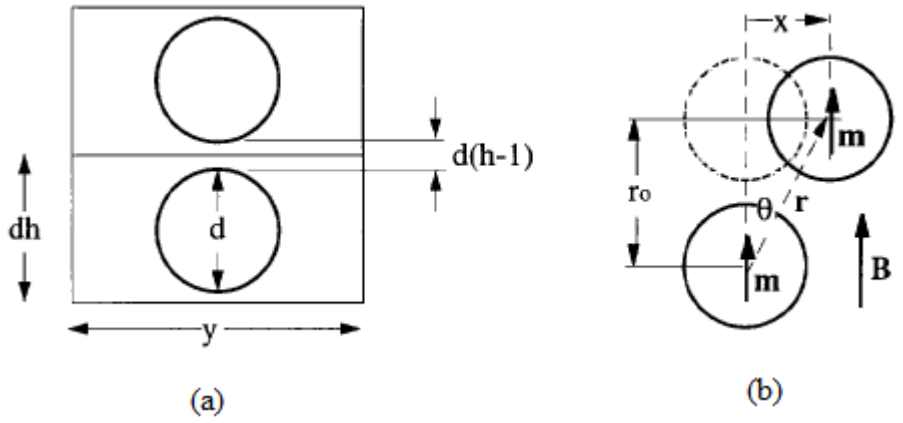

Figure 2.10 (a) Two particle within a particle chain with adjacent chain at a distance of y, (b) Magnetic dipole moment between two adjacent particles (Jolly et al., 1996)

The interaction energy of the two dipoles of equal magnetic strength $|m|$ was given in Eq. 2.8

$$E = \frac{(\epsilon^2 - 2)|m|^2}{4\pi\mu_1\mu_0 r_0^3(\epsilon^2 + 1)^{2.5}} \quad \text{Eq. 2.8}$$

Where, $\epsilon = x/r_0$ was the shear strain, $\mu_1$was the relative permeability of the rubber. They assumed that the dimensions of the particles were the same and there were no multi-pole interactions within MRE. Thus, the magnetic interaction energy density was calculated by multiplying the magnetic dipole moment to the total particle number and dividing the volume of MRE.

$$U = \frac{3\phi(\epsilon^2 - 2)|m|^2}{2\pi^2\mu_1\mu_0 d^3 r_0^3(\epsilon^2 + 1)^{2.5}} \quad \text{Eq. 2.9}$$

The shear stress was obtained from the derivative of the energy density with respect to the shear strain. By dividing the shear strain to the shear stress, the field-induced shear modulus was calculated by Eq. 2.10.

$$G = \frac{\phi J_p^2}{2\mu_1 \mu_0 h^3} \qquad \text{Eq. 2.10}$$

Where, J_p was the particle polarization and was related to the magnetic dipole strength.

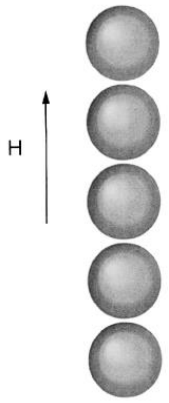

Figure 2.11 The iron particle chain in MRE along an applied magnetic field H (Davis, 1999)

Davis (1999) used finite element method to model the field-induced modulus of MRE with different magnetic particle concentrations. A finite length of the iron particle chain (see Figure 2.11) was built to calculate the dipole moment within MRE material. The dipole moments of the entire particles chain were considered.

Shen, et al. (2004) proposed a quasi-static finite chain model to study the field-induced modulus of MRE. The dipole interactions induced by all iron particles along the chain were measured. Besides, the nonlinear stress-strain relationship of the host materials was also considered. This increased the accuracy of the model by comparing with the previous models (Jolly et al., 1996, Davis, 1999). The interactions between the adjacent magnetic particle chains were neglected.

Zhu et al. (2006) developed a model to analyse the field-induced modulus of MRE by including the interactions of the adjacent chains. The structure of the particles was modelled as a body-centred tetragonal structure (shown in Figure 2.12).

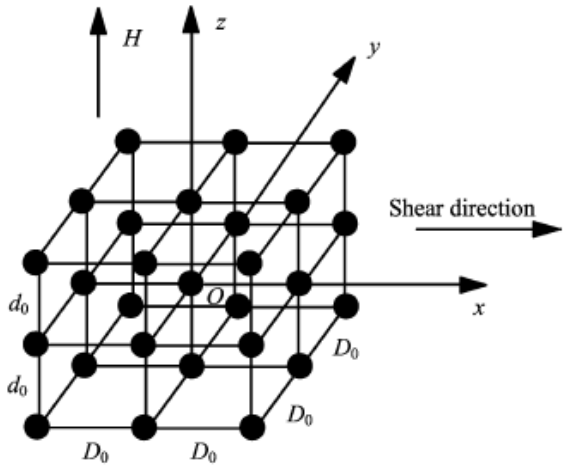

Figure 2.12 Body-centred tetragonal structures of MRE (Zhu et al., 2006)

Where, D_0 was the distance of the adjacent chains and d_0 was the distance between the iron particles in a chain. The Cartesian coordinate was used to locate the coordinate of the iron particles. The original coordinate of the iron particle was (x, y, z). After a horizontal shear deformation, the new coordinate of the iron particle became $(x + \gamma z, y, z)$, where γ was the shear strain. The interaction energy of a specific particle was given in Eq. 2.11.

$$E = \frac{|m|^2}{4\pi\mu_1\mu_0}\left[\frac{(x+\gamma z)^2 + y^2 - 2z^2}{(x+\gamma z)^2 + y^2 + z^2}\right] \quad \text{Eq. 2.11}$$

Then, the Cartesian coordinate of the iron particle was replaced by the distance of the adjacent particles chains D_0 and the adjacent particles d_0.

$$\begin{cases} x = kD_0 \\ y = lD_0 \\ z = nd_0 \end{cases} \quad \text{Eq. 2.12}$$

k, *l* and *n* were all integers. The total magnetic interaction energy density was derived by integrations for all the *k*, *l* and *n*. Then, the shear stress was calculated from the derivative of the energy density with respect to shear strain. The field induced modulus was obtained by dividing the shear stress to the shear strain. By comparing the results with previous methods, Zhu et al. (2006) indicated that as the ratio of the distance of the adjacent particle chains to the distance of the adjacent particles was large, the results were compatible with the single chain model. However, as the ratio was small, the differences of the results were significant. This multi-chains model provided a more accurate result as it considered the interactions between the particle chains.

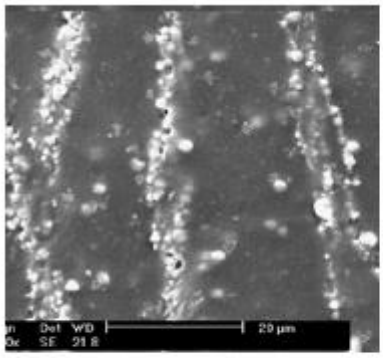

(a)

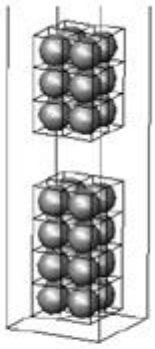

(b)

Figure 2.13 (a) SEM image of MRE, (b) sketch of finite column model of MRE (Chen et al., 2007)

Most of the previous models have assumed that MREs have a perfect infinite chain structure. Chen et al. (2007) developed a finite-column model which had a discontinuous column structure within a MRE. The distribution of the column of the iron particle was observed by scanning electron microscope (SEM) image and calculated with the iron particle volume concentration. The results indicated that the field-induced shear stress of MRE was related to the magnetic permeability (Eq. 2.13).

$$\tau = -\frac{1}{2}\mu_0 \frac{\partial \chi}{\partial \theta} H_0^2 \qquad \text{Eq. 2.13}$$

Where, H_0 was the magnetic field strength, χ was MRE's effective magnetic susceptibility which parallel to the applied magnetic field. By applying Wiener bounds (Neelakanta, 1995) and Maxwell Garnett mixing rule (Maxwell-Garnett, 1904) to the finite column model of MRE, the effective magnetic susceptibility of MRE were separated into two components. There were parallel and perpendicular to the column. Then, the field-induced modulus was equalled to the shear stress divided to the shear stress shown in Eq. 2.14.

$$G = \frac{\tau}{\theta} = (\mu_{\parallel} - \mu_{\perp}) \frac{H_0^2 sin\theta cos\theta}{\theta} \qquad \text{Eq. 2.14}$$

2.4.2 Dynamic properties modelling of MRE

The dynamic properties of MRE materials exhibit viscoelastic characterisation within certain ranges of frequency and strain. Therefore, the viscoelastic models are widely used to model the dynamic properties of MRE.

Norouzi et al. (2016) used a classical Kelvin-Voigt model to model the dynamic behaviour of an isotropic MRE material. The Kelvin-Voigt model was comprised of a stiffness component and a damping component with parallel connection.

Guo et al. (2014) used the Maxwell viscoelastic model (shown in Figure 2.14) to model the dynamic properties of MRE. The elastic part of the material was modelled by the spring element k_2 and the viscosity part of the material was modelled by the damping element c. The spring element k_1 represented the magnetic induced modulus of MRE. Olabide et al. (2017) also used Maxwell viscoelastic model to model the dynamic properties of MRE. In their model, k_1 was the static modulus of MREl. The chain of k_1 and c was used to represent viscoelastic properties of MRE.

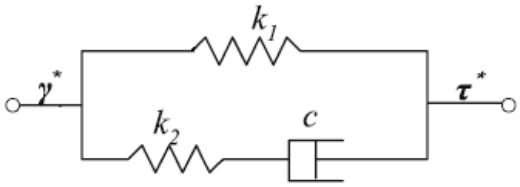

Figure 2.14 Three parameters Maxwell viscoelastic model of MRE

Three-parameter Maxwell viscoelastic model is shown in Figure 2.14. Where, γ^* is the input complex strain of MRE, τ^* is the output complex stress of MRE. The relationship of γ^* and τ^* is given in Eq. 2.15.

$$\tau^* = E^*\gamma^* = (E' + iE'')\gamma^* \quad \text{Eq. 2.15}$$

The storage modulus and loss modulus of the three-parameter model is defined in Eq. 2.16 and Eq. 2.17.

$$E' = k_1 + \frac{k_2(c\omega)^2}{k_2 + (c\omega)^2} \quad \text{Eq. 2.16}$$

$$E'' = \frac{k_2^2(c\omega)}{k_2^2 + (c\omega)^2} \quad \text{Eq. 2.17}$$

Li, et al. (2010) proposed a four-parameter viscoelastic model to model the mechanical properties of MRE (see Figure 2.15). In this model, a standard viscoelastic solid model (contains k_1, k_2 and c)

was used to model the viscoelastic properties of MRE. k_b represented the magnetic induce modulus of MRE.

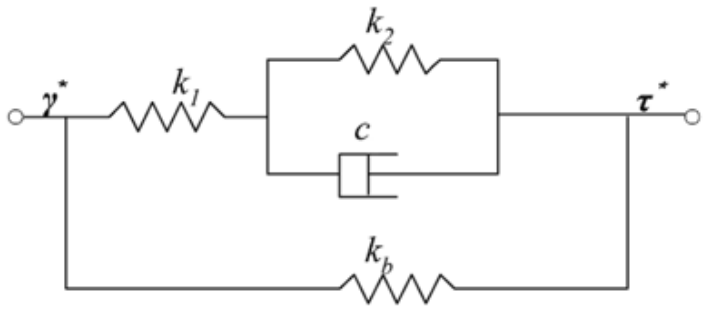

Figure 2.15 Four parameters viscoelastic model for MRE (Li, et al. (2010))

The storage modulus and the loss modulus of the four-parameter viscoelastic model were given in Eq. 2.18 and Eq. 2.19 below.

$$E' = \frac{(k_1k_b + k_2k_b + k_1k_2)[(k_1 + k_2)^2 + (c\omega)^2] + (c\omega)^2k_1^2}{(k_1 + k_2)[(k_1 + k_2)^2 + (c\omega)^2]} \quad \text{Eq. 2.18}$$

$$E'' = \frac{k_1^2c\omega}{(k_1 + k_2)^2 + (c\omega)^2} \quad \text{Eq. 2.19}$$

As the strain amplitude increase, a high non-linear stress strain curve of the MRE under dynamic excitation is observed. At this time, the general viscoelastic model is not capable to predict the stress-strain curve of MRE. Yang et al. (2013) and Zhu and Rui (2014) used a Bouc-Wen component parallel connected with the Kelvin-Voigt model to simulate hysteretic behaviour of MRE. The results showed that by using the Bouc-Wen component, the high non-linear stress-strain relationship of MRE was accurately predicted (shown in Figure 2.16).

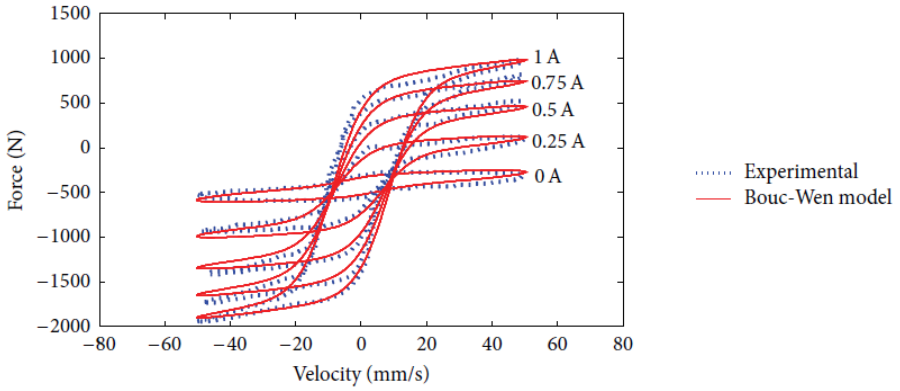

Figure 2.16 Hysteretic stress-strain curve of MRE modelled by a Bouc-Wen component (Zhu and Rui, 2014)

2.5 MRE applications

The mechanical properties of MR materials, i.e. stiffness and damping can be controlled continuously, rapidly and reversibly by the external magnetic field. Due to these promising mechanical properties, MR materials have advantages in vibration control in various engineering fields by comparing with conventional materials. The current potential applications of MRE materials include variable stiffness suspension systems (Du et al., 2011), vibration absorbers (Ginder et al., 2001, Deng et al., 2006, Deng and Gong, 2007, Sun et al., 2015, Sun et al., 2017) and vibration isolators (Kavlicoglu et al., 2011, Opie and Yim, 2011, Li et al., 2013, Wahab et al., 2016), etc.

2.5.1 MRE based vibration absorbers

Vibration absorbers are mainly used to eliminate or minimize the vibration of a system. Typically, there are three kinds of the absorbers. There are passive tuned vibration absorber (TVA), semi-active TVA and active TVA. For the passive TVA, the stiffness and damping properties is unchangeable. Therefore, the effective frequency bandwidth of the passive TVA is narrow. The passive TVA loses its effectiveness or even amplifies the vibration of a system as an excitation frequency out of the designed effective frequency bandwidth. The magnetic field dependent stiffness properties make MRE as a suitable candidate for the development of semi-active TVA which has a wider range of effective frequencies for vibration absorption.

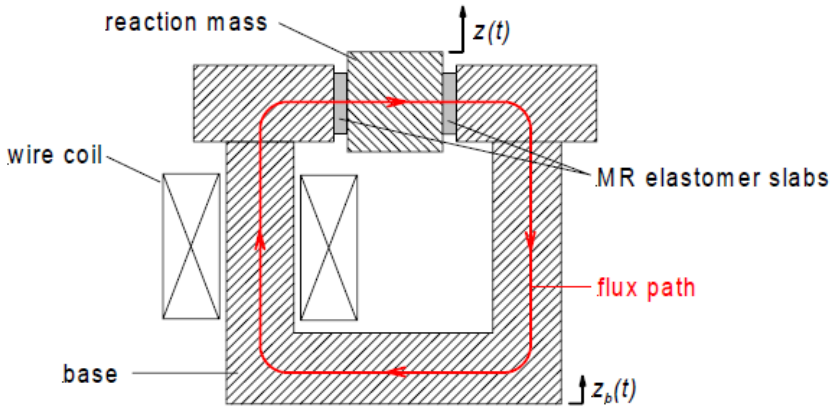

Figure 2.17 Schematic of the construction of MRE TVA (Ginder et al., 2001)

The first MRE TVA (shown in Figure 2.17) was prototyped by Ginder (2001). The TVA was constructed by using a closed magnetic circuit, a wired coil and two MRE samples. The reaction mass was mounted between two MRE samples and excited by a vertical motion. The experiment results showed that the resonance frequency of this system could shift from 500 Hz to 600 Hz.

Deng et al. (2006) improved the design of MRE TVA by adding another wired coil to strengthen the magnetic field strength of this system (shown in Figure 2.18). The resonance frequency of MRE TVA was controlled by electrical currents from 55 Hz at 0 A to 81.25 Hz at 1.5 A.

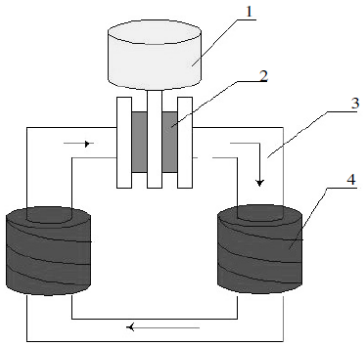

Figure 2.18 Sketch of adaptive tuned vibration absorber: 1. Oscillator, 2. MRE, 3. Magnetic conductor, 4. Coils (Deng et al., 2006)

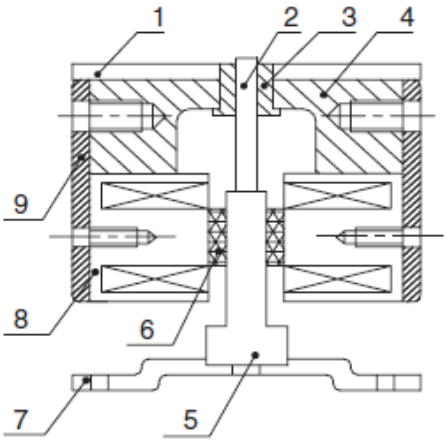

Figure 2.19 A compact MRE adaptive TVA 1. Cover, 2. guide rod, 3. linear bearing, 4. Magnetic conductor, 5. shear plate, 6. MRE, 7. Base, 8. Electromagnet, 9. mounting shell (Deng and Gong, 2007)

Deng and Gong (2007) designed a compact shear mode adaptive TVA using MRE (shown in Figure 2.19). The electromagnets and magnetic conductor formed a closed magnetic path. In a meanwhile, the electromagnets also served as a dynamic mass. It was found that this device had a more compact configuration than the previous ones.

In order to deal with large amplitude vibration problem, Sun et al. (2015) developed a multi-layered MRE based absorber. It was found that the vibration amplitude of the designed multi-layered MRE absorbed could reach as large as 13.6mm. Recently, the non-linear behaviour of the MRE based absorbed was analysed by Sun et al. (2017).

2.5.2 MRE based vibration isolators

Vibration isolator is used to isolate an object from the source of vibrations. Since, the stiffness and damping properties of MRE can be controlled by an external magnetic field. Therefore, MRE materials have better isolation performance comparing with the conventional materials.

Kavlicoglu et al. (2011) proposed a MRE mount for shock and vibration isolation. The mount used a 0.5-inch thick MRE layers and two electromagnets. The configuration of the designed mount was shown in Figure 2.20. It was found that the proposed MRE mount could reduce a 5g shock impulse to 3.42g.

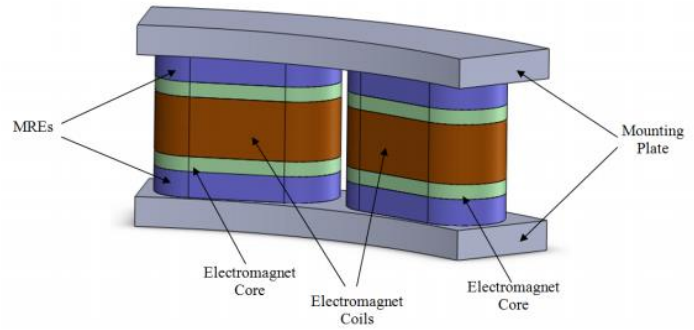

Figure 2.20 Schematic of MRE mount proposed by Kavlicoglu et al. (2011)

Opie and Yim (2011) developed and tested a semi-active shear-mode vibration isolator with a semi-active controller. By comparing the semi-active control isolator and the passive control isolator, it was found that the semi-active control system can reduce the resonance and payload velocity by 16-30%.

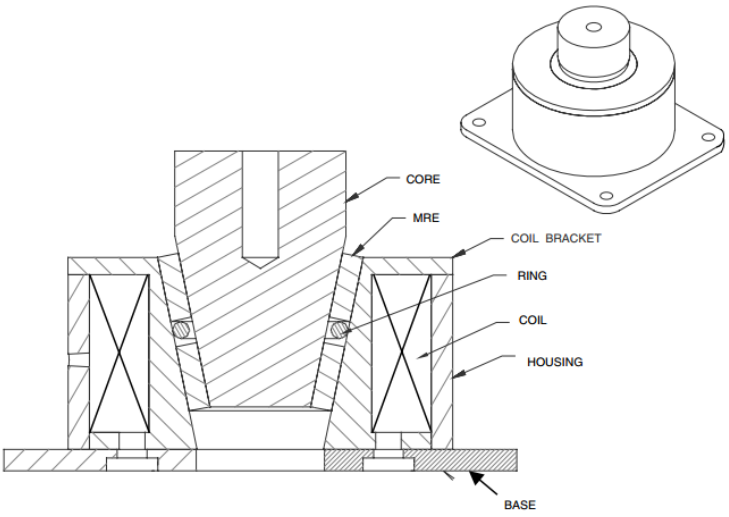

Figure 2.21 Schematic diagram of the MRE seat isolator (Du et al., 2011)

Du et al. (2011) proposed a stiffness control of the seat suspension system by using MRE isolator. By comparing with the acceleration response, it was found that a continuous control of the stiffness achieved a better isolation performance comparing with a simple on-off control.

Most of researches analysed the characteristic of MRE based isolator to a small scale structure. The investigation of the MRE based isolator on a large-scale structure is limited. Li et al. (2013) and Wahab et al. (2016) adopted a new structure of MRE isolator which comprised of layers MRE samples and thin steel plates. The designed isolator had a high vertical stiffness and was capable for seismic isolation.

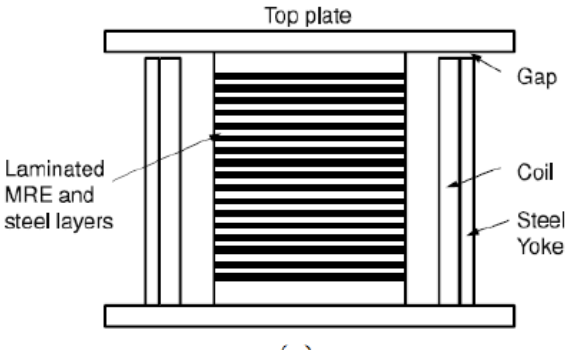

Figure 2.22 Laminated MRE isolator (Li et al., 2013)

2.5.3 MRE based actuator

Soft actuators can produce force or displacement by external stimuli (such as heat or a magnetic field) is applied. As a soft matrix material is selected to fabricate MRE and a strong magnetic field applied, MRE materials demonstrate a noticeable actuation effect (Bose, 2007). By applying a magnetic field to a soft MRE material, the shape of MRE is deformed. MRE returns to its original shape when the magnetic field is removed. Due to a quick response of MRE to a magnetic field, the soft MRE materials have promising advantages over other soft actuators (Mitsumata et al., 2006 and Mitsumata, 2008).

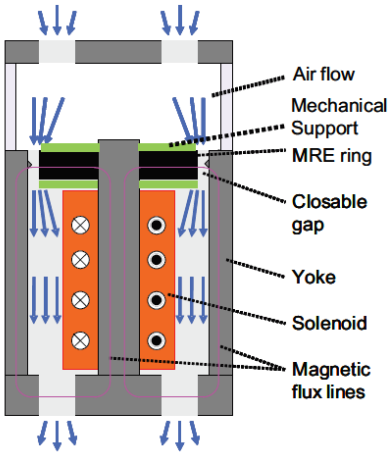

Figure 2.23 Scheme of the soft MRE air valve (Bose et al., 2011)

Bose et al. (2011) designed an air valve actuator by using a soft MRE material. The scheme of the soft MRE air valve was shown in figure 2.23. By applying a magnetic field to the soft MRE ring, the MRE ring expanded and blocked the gap between the MRE ring and the yoke. Then, the air flow

through the gap was blocked. By controlling the magnetic strength, the air flow rate could be changed between $0 - 0.4\, m^3/h$.

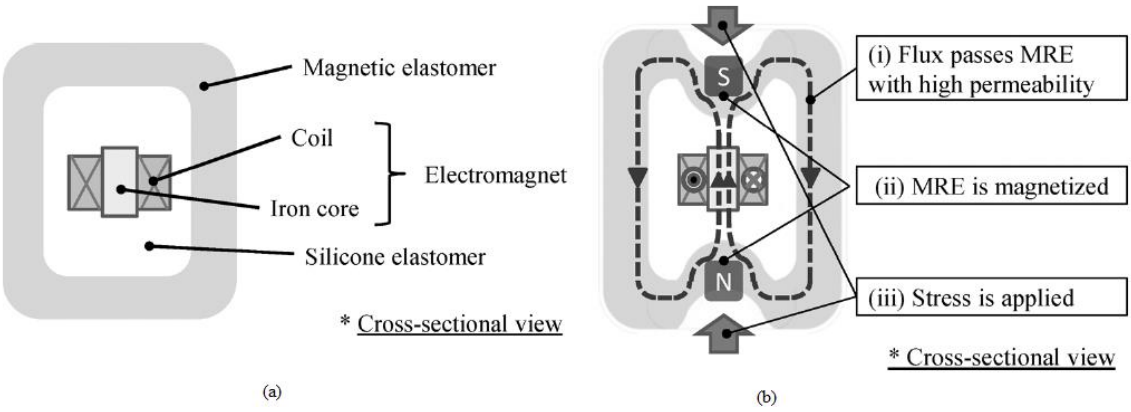

Figure 2.24 (a) structure of the MRE actuator ,(b) operation principle of the actuator (Kashima et al., 2012)

Kashima et al. (2012) developed a displacement actuator by using MRE. By applying a magnetic field to the actuator, MRE facing the iron core became magnetized. Then, this section of MRE was contracted towards to the iron core. The contraction of MRE induced a displacement change of the actuator. Kashima et al. (2012) found that a 2.5 mm vertical displacement was achieved by applying a magnetic field to the actuator.

2.5.4 Other applications

Apart from vibration absorber, isolator and actuator, MRE materials also have other promising applications, such as sandwich beam structure, sensor and medical equipment.

The concept of MRE sandwich beam was firstly proposed by Zhou and Wang (2006). The experimental verifications of the effectiveness of MRE sandwich beam were conducted by Nayak et al. (2011) and Aguib et al. (2016). It was found that the structure vibration of a sandwich beam could be significantly reduced by the presence of a magnetic field.

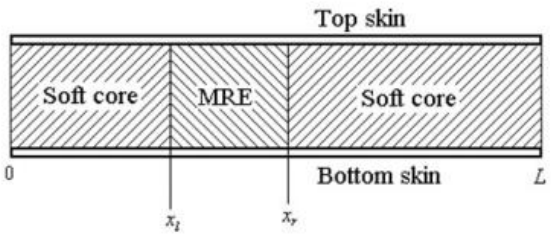

Figure 2.25 Sandwich beam proposed by Zhou and Wang (2006)

Li et al. (2009) developed a force sensor with MRE. The developed MRE force sensor was able to detect a static force. A simple MRE position sensor was proposed by Ausanio et al. (2014). By measuring the magneto-piezo-resistance of MRE, the variations of the positions were recorded.

Thorsteninsson et al. (2013) used MRE material as a shock energy absorber on a prosthetic leg. By changing the stiffness of MRE based shock energy absorber, the vibration of the prosthetic leg was reduced to an activity level of user.

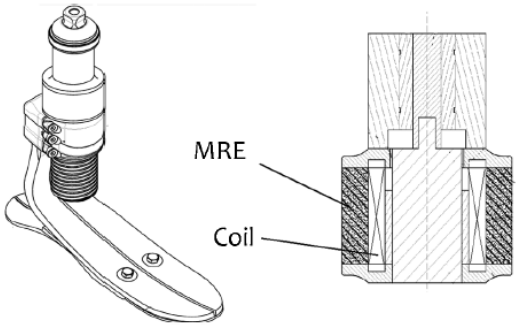

Figure 2.26 MRE-based prosthetic leg (Thorsteninsson et al., 2013)

2.6 Summary

- Dynamic properties of MRE materials

Lots of researchers experimentally investigate the dynamic mechanical properties of MRE materials composed of different polymer matrix and magnetic filler. It was shown that the MR effect of an anisotropic MRE was higher comparing with that of an isotropic MRE (Gong et al., 2005, Boczkowska et al., 2007). Sorokin et al. (2014) indicated that the mechanical properties (i.e. stiffness and damping) of an anisotropic MRE material were higher. Therefore, the applications of anisotropic MRE materials in the engineering vibration attenuation problem will achieve a better performance. The dynamic mechanical properties of MRE depend on many factors, such as strain amplitude, frequency, magnetic field and pre-strain amplitude. The Table 2.3 and 2.4 below summarise the testing conditions of the dynamic mechanical properties of anisotropic MRE materials.

Table 2.3 Testing conditions of the dynamic shear mechanical properties of anisotropic MRE materials

Author	Pre-strain	Frequency	Strain amplitude	Magnetic field	Particle volume
Popp et al. (2009)		1-100 Hz	0.1, 1, 5, 10, 15%	0-0.15 T	17%
Bose and Roder (2009)		10 Hz	1%	0-0.7 T	0% - 35%
Li et al. (2010)		1,5,10 Hz	10%	0-0.44 T	17.1%
Opie and Yim (2011)		1-100 Hz	1-20%	0, 0.6 T	30%
Tian et al. (2011)		6-100 Hz	1%	0-0.44 T	13%-20%
		5 Hz	0.01%-100%		
Xu et al. (2011)		5 Hz	0.2%	0-0.86 T	7.7%, 15.8%, 23%, 33%
Zhu et al. (2012)		1, 2, 5, 10 Hz	12.5, 25, 50%	0-0.3 T	30%
Li and Sun (2013)		0.1-100 Hz	1%	0 T, 0.1 T, 0.2 T	10%, 20%, 30%
		10 Hz	0.5-5%		
Fan et al. (2013)		1-30 Hz	0.3%	0-1 T	17%
Sorokin et al. (2014)		0.01-10 Hz	1%	0 T	22%, 35%
		1-9 Hz	0.01-25%	0-0.7 T	
Guo et al. (2014)		1, 10, 100 Hz	0.01-10%	0-0.1 T	13, 18, 25, 34, 46%
		1-40 Hz	0.1%		
Wen et al. (2017)		5 Hz	0.1%	0-1.5 T	7.7%, 15.8%, 33%

Table 2.4 Testing conditions of the dynamic compression mechanical properties of anisotropic MRE materials

Author	Pre-strain	Frequency	Strain amplitude	Magnetic field	Particle volume
Boczkowska et al. (2007)	NA	0.1-60 Hz	0.1%	0 T, 0.2 T	1.5%,11.5%, 33%
Padalka et al. (2010)	NA	1 Hz	1,2,3%	0, 0.1, 0.2 T	10%
Mitsumata and Ohori (2011)	NA	1 Hz	0.001-1%	0 T	0-29%
			0.01%	0, 0.5 T	
Li and Sun (2013)	NA	0.1-100 Hz	1%	0 T, 0.1 T, 0.2 T	10%, 20%, 30%
		10 Hz	0.5-5%		
Shuib and Pickering (2016)	NA	0.01-130 Hz	0.5%	0T	6.4%-7.7%
		100 Hz	0.1-4.5%		

It is seen from Table 2.3 and 2.4 that, there is no experiment testing of MRE cover all four dependences of strain amplitude, frequency, magnetic field and pre-strain amplitude. The experimental investigation of the dependence of the pre-strain effect on the dynamic properties of anisotropic MRE materials is limited. The applications of MRE materials in the engineering field will withstand initial force (gravity force of the instrument) which will cause a pre-strain of MRE. This initial pre-strain could change the mechanical properties of MRE materials and affect the efficiency of the entire system. Thus, consideration of the dependence of the pre-strain is important.

MRE materials can be categorised as a kind of filled rubber material. The dynamic properties of MRE materials with different compositions have similar characteristics (such as Payne effect, MR effect). The benefits of characterization of the MRE material by consideration of these four dependences include, better understanding of this kind filled rubber material, use the MRE material properly in engineering applications, a more accurate model to describe the dynamic properties of MRE. Therefore, in this study, characterization of MRE considering pre-strain, frequency, strain amplitude and magnetic field is experimentally investigated.

It is also observed that, most of the researches use the iron particle concentration up to 30%. Because Davis (1999) showed that the MR effect of MRE samples was higher at an iron particle concentration at 27%. In engineering application, the MR effect is an important factor need to be considered. On the other hand, the mechanical properties of MRE are also important for engineering applications. By increasing the iron particle concentration of MRE, the mechanical properties (stiffness and damping) of MRE increase. There are few researches investigate the dynamic properties of MRE

material with a high iron particle concentration (up to 50%). In this thesis, the dynamic properties of MRE samples with high iron particle concentration (50%) are also investigated.

- Mathematical models of MRE

The mathematic models of MRE can be categorised into two groups. The first one is to model the magnetic induced modulus of MRE and the other is to model the dynamic mechanical properties of MRE. The reviews of the mathematical models of MRE are given in section 2.4. In order to better control MRE to deal with engineering vibration problem, the model of MRE should not only contain the magnetic effect, the effect of the strain amplitude, frequency and the pre-strain effect should also be included. Table 2.5 summarises the models used to model the dynamic properties of MRE.

Table 2.5 Summary of the viscoelastic model used for MRE

Author	Pre-strain	Frequency	Strain amplitude	Magnetic field	Coupling	Continuity
Li et al. (2010)	No	1-10 Hz	10%	0-0.385 T	No	1-10 Hz at specified strain amplitude and magnetic field
Eem et al. (2012)	No	0.5-3 Hz	8,23,40%	0.05-0.5 T	No	No
Zhu et al. (2012)	No	1-10 Hz	No	No	No	1-10 Hz at specified strain amplitude and magnetic field
Guo et al. (2014)	No	1-40 Hz	0.1%	0-0.1T	Frequency-magnetic	Continue in frequency and magnetic field
Norouzi et al. (2015)	No	0.1-8 Hz	2, 4, 8, 16%	0-0.272 T	Frequency-strain	Continue in frequency and strain.
Olabide et al. (2017)	No	0.01-40 Hz	0.06%	0-0.7 T	No	0.01-40 Hz at specified strain amplitude and magnetic field

It is seen from table 2.5 that there is no such viscoelastic model considered all the dependences of pre-strain, frequency, strain amplitude and magnetic field. The investigations of the coupling effects between these dependences are also limited. For the current literatures, the coupling effects between selected dependences are discussed (frequency-magnetic, frequency-strain). In this thesis, the coupling effects between the dependences are experimentally analysed and considered in the mathematical model. The continuity of the viscoelastic model in the literatures is only valid in a

certain region. There is no such model can satisfy to continuously model the dynamic properties of MRE with the dependences of frequency, strain amplitude, magnetic field and pre-strain amplitude. In this study, a new mathematical model is proposed. The dependences of the pre-strain, frequency, strain amplitude and magnetic field and their coupling effects are considered. The proposed model is able to continuously describe the dynamic properties of MRE material with these four dependences.

- Applications of MRE in engineering field

The stiffness and damping properties of MRE materials can be controlled continuously, rapidly and reversibly by an external magnetic field. Therefore, MRE materials have advantages in vibration control in various engineering fields comparing with conventional materials.

An overview of the development of the MRE based vibration control devices is given in section 2.5. It is found that the MRE devices are become more compact and with higher load bearing capacity. In this thesis, a hybrid shear and compression MRE based isolator is designed. The designed isolator has a compact size and a high load bearing capacity. The non-linear dynamic properties of the MRE based isolation system are also experimentally and numerically analysed.

Chapter 3: Experimental Setup for Characterising the Dynamic Properties of MRE

3.1 Introduction

This chapter gives an introduction of the experiment setup to characterise the dynamic shear and compression mechanical properties of MRE. The manufacture of MRE samples is introduced in the beginning. Then, the dynamic test procedures for MRE materials and the data processing method are explained.

3.2 Manufacture process of MRE samples

MRE samples are manufactured in three steps:

1. Mixing silicone rubber with iron powder

MRE samples are manufactured with two-component silicone rubber (RTV-2, ELASTOSIL® M 4644 A/B) and Carbonyl-Iron powder (size 5-9μm, 44890 ALDRICH). For the mixing procedure, two-component silicone rubber A and B are mixed by weight ratio of 10:1. Then, iron powder is added into the silicone rubber. Three different MRE samples are fabricated with iron particle concentrations of 10%, 30% and 50%. The mixture is stirred for 30 minutes to ensure the iron powder thoroughly mixed with the silicone rubber.

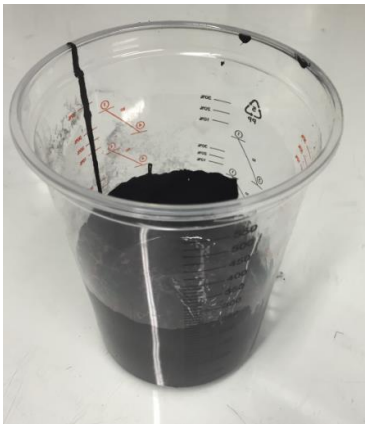

Figure 3.1 The mixture of the iron powder and silicone rubber

2. Removing air bubbles from the mixture

There are many air bubbles generated within the mixture during the stirring process. In order to remove the air bubbles, the mixture is placed into a vacuum chamber at room temperature and vacuumed for 30 minutes to eliminate the air bubbles trapped inside.

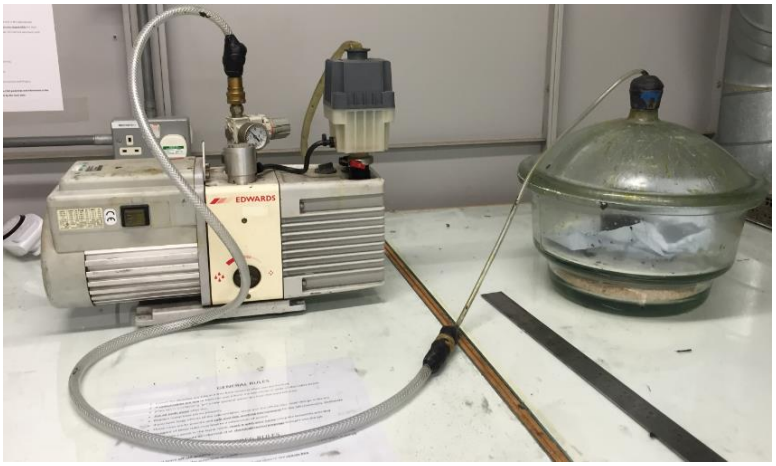

Figure 3.2 Vacuuming procedure of the mixture

3. Curing of MRE samples

The mixture is poured into the alumina mould for solidification. The size of the mould is $22\ mm \times 22\ mm \times 6.5\ mm$. The geometry configuration of MRE samples is designed referred to the BS ISO 4664-1:2001. During the curing procedure, two strong permanent magneto discs (N42 Neodymium magnet) are placed parallel beside the mould to produce a 260 mT magnetic field. The moulds are left for 24 hour to ensure MRE samples completely cured. Then, anisotropic MRE samples are fabricated.

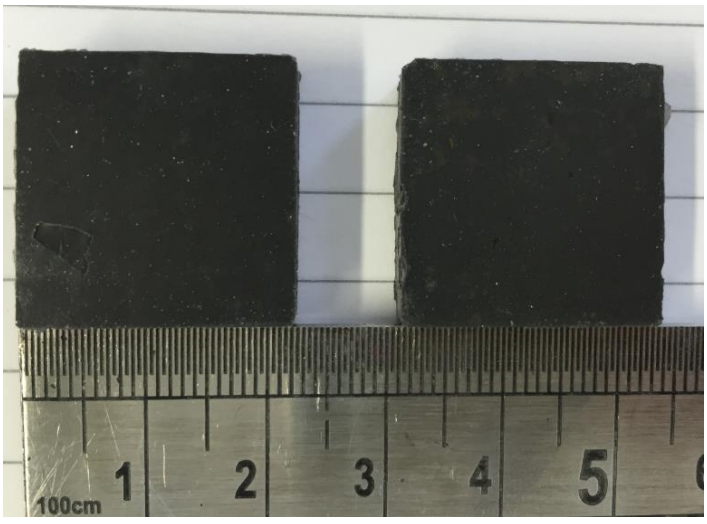

Figure 3.3 Manufactured anisotropic MRE samples

3.3 Dynamic testing method

The dynamic testing of the anisotropic MRE samples is performed by the ElectroPlus E1000. The configuration of the dynamic testing of MRE material is shown in figure 3.4. The figure on the left is the experimental setup for MRE shear test and the other is for MRE compression test. For MRE shear test, MRE samples are glued to the test fixture by an adhesive (Araldite ®, extra strong adhesive). A sinusoidal excitation is generated by the actuator and the responded force is recorded by the load cell. An external magnetic field is generated by circular disc permanent magnets (shining silver disc shown in figure 3.4). For shear test, the magnets are placed beside the test fixtures (left and right). For compression test, the magnets are placed above and below a MRE sample. By adding pairs of the permanent magnets, the magnetic field can be increased with several discrete values.

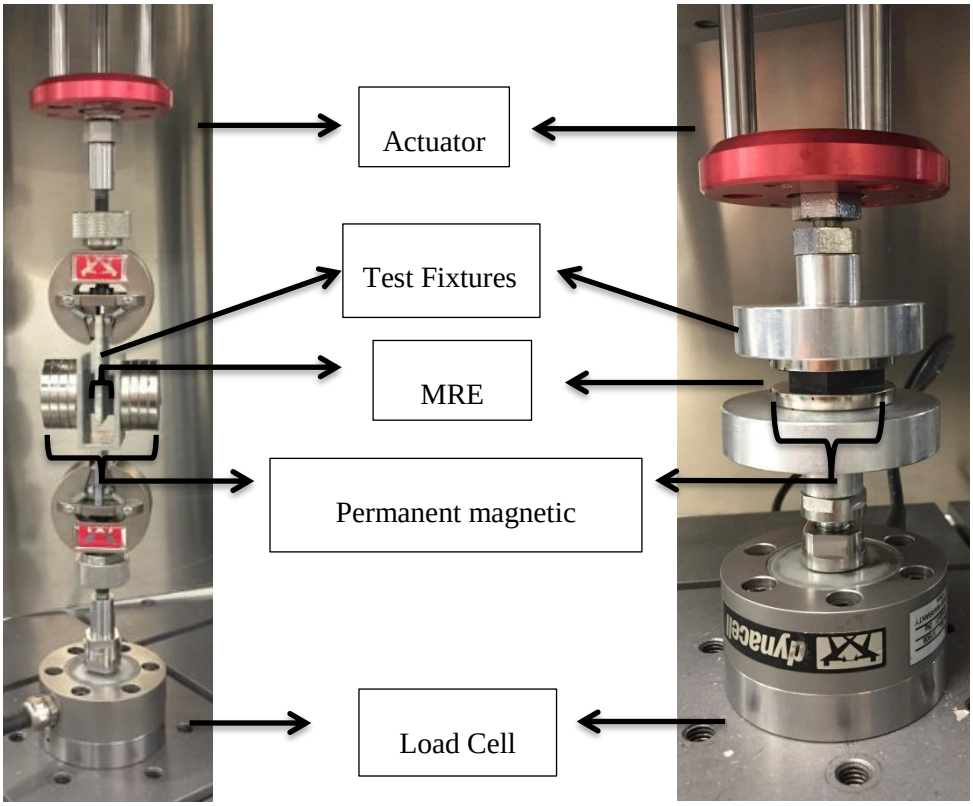

Figure 3.4 Configuration of the dynamic testing of MRE material performed by ElectroPuls

In this experiment, a strong N42 Neodymium magnet is chosen to generate the magnetic field. The dimension of the N42 Neodymium magnet is 40 mm in diameter and 5 mm in thickness. The magnetic field strength generated by N42 Neodymium magnets is measured with a Gauss meter (GM08, Hirst Magnetic Instruments). The magnetic field strengths with different pairs of magnets for both shear and compression MRE test are shown in figure 3.5. By controlling pairs of N42 magnetic discs, the magnetic field strength can be changed from 0 T to 0.48 T.

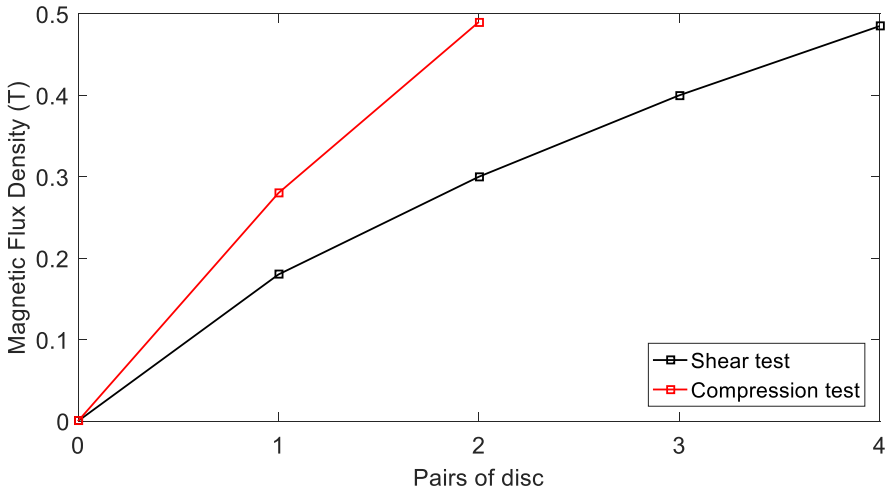

Figure 3.5 Magnetic flux density with different pairs of magnetic disc

Dynamic mechanical analysis (DMA) is used to characterise the dynamic properties of MRE. The procedures of the dynamic mechanical properties testing of MRE samples are as followed. The first step is to apply a preliminary pre-strain to MRE samples. The MRE material is a kind of viscoelastic material which show stress relaxation phenomenon. The stress relaxation is described as a gradual stress reduction with time as a constant strain is applied to the material. In order to eliminate the stress relaxation effect on the dynamic properties of MRE, a certain time is required to ensure the relaxation stress at the pre-strain condition is reduced to a steady-state value. In this experiment, the initial pre-strain is maintained for 40 second. Then, a sinusoidal motion as an input is applied by the actuator. The corresponding stress is recorded by the load cell. The dynamic tests of MRE samples are performed with different pre-strain amplitudes, frequencies, strain amplitudes and magnetic field strengths. A summary of all the testing parameters for shear and compression testing conditions is listed in Table 3.1. For each testing condition, three groups of MRE samples are used and each group is tested at three times under the same testing condition. The testing temperature is at room temperature (20℃). The dynamic tests of MRE follow the standard of BS ISO 4664-1:2011. (BSI, 2011)

Table 3.1 Summary of the testing conditions

	Shear test	Compression test
Iron particle percentage (%)	10, 30, 50	10, 30, 50
Pre-strain amplitude (%)	0, 0.5,1,1.5, 2	2,3,4,5,6
Frequency Sweep (Hz)	1, 5,10,20,30,40,50,60	1, 5,10,20,30,40,50,60
Strain Sweep (%)	0.25, 0.5, 0.75, 1, 1.25, 1.5, 1.75, 2	0.25,0.5,0.75,1,1.25,1.5
Magnetic strength (mT)	0, 180, 300, 400, 485	0, 300,490

3.4 Processing of experiment data

The raw MRE experiment data is shown in Table 3.2. The experiment results of displacements of the actuator and force response of the load cell are recorded. Total time means the time period of the experiment. Cycles means the current cycle of the input excitation. Position (ElectroPuls: Position) is the real position of the actuator. Displacement (ElectroPuls:Digital Position) is the position of the actuator after calibration. Load (ElectroPuls:Load) is the force recorded by the load cell.

Table 3.2 Raw data of dynamic properties test of MRE for one motion cycle

Total Time (s)	Cycles	Position(ElectroPuls: Position) (mm)	Load(ElectroPuls: Load) (N)	Displacement(ElectroPuls :Digital Position) (mm)
49.3624	71	-16.09520994	-139.4324899	-0.183339935
49.3726	71	-16.06910668	-67.96506792	-0.156343781
49.3828	71	-16.02477155	-9.491847828	-0.114125365
49.393	71	-15.97484134	21.74852788	-0.067852175
49.3946	71	-15.97184263	22.04519883	-0.065401139
49.3952	71	-15.97172283	21.78789303	-0.064893922
49.398	71	-15.96994184	18.35662127	-0.065248086
49.3998	71	-15.97200356	14.55801725	-0.067183076
49.4098	71	-15.99908136	-29.5038037	-0.096903516
49.42	71	-16.04707323	-103.3902988	-0.143684537
49.4302	71	-16.08065091	-161.1110866	-0.174750328
49.4402	71	-16.10051892	-193.1626946	-0.191295813
49.4444	71	-16.10413633	-196.9362795	-0.193999424
49.4474	71	-16.10534332	-195.011884	-0.195125672
49.451	71	-16.10616944	-190.8357739	-0.194040663

The stress-strain curve of MRE is plotted by the force response (ElectroPuls: Load) and the calibrated displacement (EletroPuls: Digital Position). The stress-strain curve of MRE exhibits a hysteresis loop under a sinusoidal excitation. This is because MRE is a kind of viscoelastic materials. The stress does not respond instantaneously as a strain is applied. The stress response has a phase lag due to the viscosity of the material (shown in Figure 3.6).

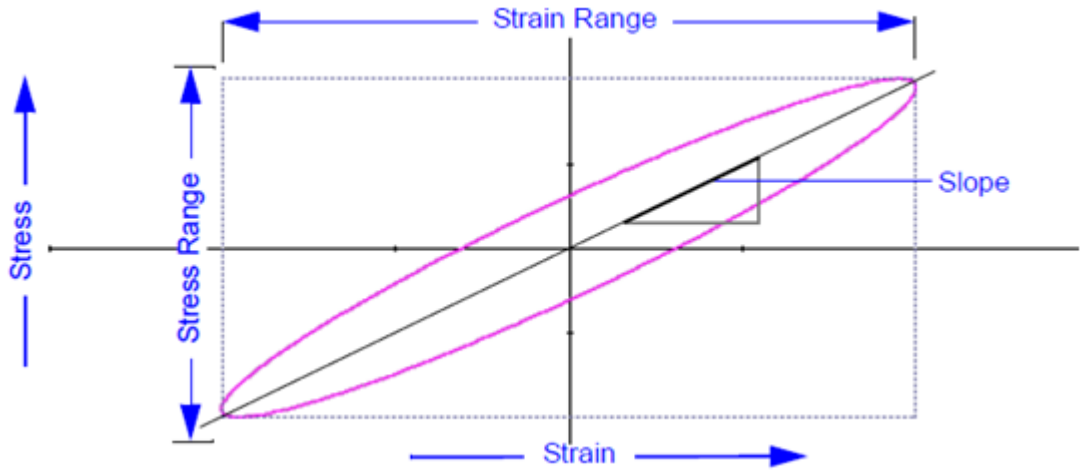

Figure 3.6 Stress-strain plot for MRE under a harmonic load

The complex modulus G^* is used to present the shear or compression modulus of MRE. The calculation of the absolute value of complex G^* is given in Eq. 3.1 which is the slope of stress to strain.

$$|G^*| = \frac{Stress\ Range}{Strain\ Range} \quad \text{Eq. 3.1}$$

The complex modulus G^* comprises a real elastic component and an imaginary viscous component which are called storage modulus G' and loss modulus G'', respectively.

$$G^* = G' + iG'' \quad \text{Eq. 3.2}$$

$$G' = |G^*| * cos\delta \quad \text{Eq. 3.3}$$

$$G'' = |G^*| * sin\delta \quad \text{Eq. 3.4}$$

δ is the loss angle which is calculated from energy method, the equation is given in Eq.3.5.

$$\delta = arcsine\left(\frac{enclosed\ area\ of\ the\ hysteresis\ loop}{\pi * Stress\ range * Strain\ Range/4}\right) \quad \text{Eq. 3.5}$$

Chapter 4: Experiment results of Dynamic Shear Properties of MRE

4.1 Introduction

In this chapter, experiment results of the dynamic shear mechanical properties of MRE samples are shown. Discussion on the dependences of pre-strain, frequency, strain amplitude and magnetic field strength are presented. The coupling effects between the dependences on the dynamic mechanical properties of MRE in shear mode are also discussed.

4.2 Stress relaxation of MRE under a constant shear strain

Stress relaxation describes the ability of the viscoelastic materials relieves stress under a constant strain. In order to ensure MRE samples respond to a dynamic excitation at a steady state pre-strain condition, the stress relaxation properties of MRE are initially tested. For the stress relaxation test of MRE, a constant strain is applied to MRE material in 2 seconds. Then, the strain is maintained for 40 second and the corresponding stress is recorded.

The relationship between the stress response at a constant strain of MRE samples and relaxation time are plotted in the Figure 4.1. An initial strain is applied to MRE sample with a sharp stress increase. Then, the strain is maintained for a constant value and the stress response of MRE corresponding to time is recorded by the load cell of the Instron plus.

As can be seen from the Figure 4.1 (a)-(c), there is a non-linear relationship between the stress response and the relaxation time. The stress reduces obviously at the initial 5 seconds. Then, a slow and continuous reduce of stress at a decrease rate is observed. As the relaxation time is more than 40 seconds, the response stress decays to a steady state and remains unchanged. Three parameters namely pre-strain amplitude, iron powder concentration and magnetic field strength are investigated to analyse the stress relaxation properties of MRE. Figure 4.1 (a) demonstrates the effect of the magnetic field on the stress relaxation of MRE. For MRE samples with same iron particle concentration and pre-strain amplitude, an increase of the magnetic field strength induces an increase of the maximum stress and the stress at the steady state of MRE. However, as comparing the data in Table 4.1, the stress reduction rate and the relaxation time of MRE to release stress at a steady state are almost the same. Figure 4.1 (b) presents the effect of iron particle concentrations on the stress relaxation of MRE. The maximum stress and the stress at the steady state increase significantly by increasing the concentration of iron particle. Table 4.2 shows that MRE samples with higher iron particle concentration release more stress at a constant strain. In the meantime, the period required for MRE samples with different iron particle concentrations to release stress to a steady state remains

the same. Figure 4.1 (c) illustrates the strain amplitude effect on the stress relaxation of MRE. By increasing the amplitude of a strain, an increment of magnitude of the maximum stress and the steady state stress are observed. The rate of the stress reduction curve and the time required to achieve the steady state pre-strain condition remain the same.

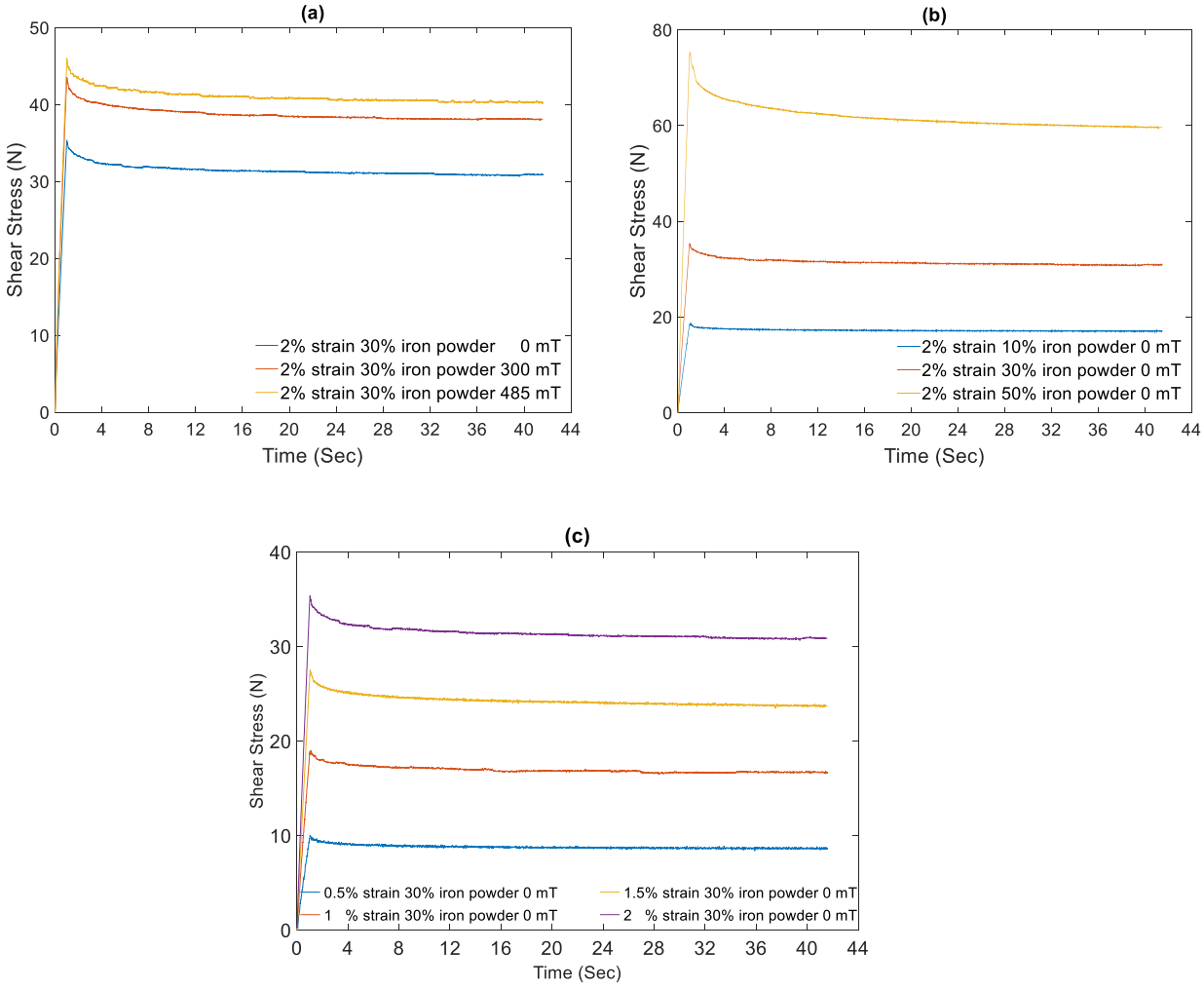

Figure 4.1 Stress relaxation of MRE (a) 2% pre-strain amplitude for samples with 30% iron powder volume percentage under 0, 300 and 485 mT magnetic field strength (b) 2% pre-strain amplitude for samples with 10%, 30% and 50% powder volume percentage under 0 mT magnetic field strength (c) 0.5%, 1%, 1.5% and 2% pre-strain amplitude with 30% iron powder under 0 mT magnetic field strength

Table 4.1 Stress response of 30% iron particle MRE at constant strain under different magnetic field

Magnetic field (mT)	Maximum Stress (N)	Stress at 20s (N)	Stress at 30s (N)	Stress at 40s (N)	Stress Reduction rate (%)
0	35.37	31.30	31.00	30.91	12.61
300	43.55	38.37	38.13	38.10	12.51
485	46.04	40.90	40.51	40.42	12.21

Table 4.2 Stress response of MRE at constant strain under 0 mT magnetic field with different iron particle concentration

Iron powder concentration (%)	Maximum Stress (N)	Stress at 20s (N)	Stress at 30s (N)	Stress at 40s (N)	Stress Reduction rate (%)
10	18.43	17.19	17.03	17.04	7.54
30	35.37	31.30	31.00	30.91	12.61
50	74.76	61.12	60.14	60.05	19.67

Table 4.3 Stress response of 30% MRE under 0 mT magnetic field with different strain amplitude

Pre-strain amplitude (%)	Maximum Stress (N)	Stress at 20s (N)	Stress at 30s (N)	Stress at 40s (N)	Stress Reduction rate (%)
0.5	10.02	8.68	8.63	8.59	14.27
1	18.89	16.80	16.69	16.67	11.75
1.5	27.42	24.13	23.88	23.77	13.31
2	35.37	31.30	31.00	30.91	12.61

The stress reduction rate is calculated by Eq. 4.1

$$Stress\ reduction\ rate = \frac{Maximum\ Stress - Steady\ state\ Stress}{Maximum\ Stress} \quad \text{Eq.4.1}$$

It can be concluded that an increase of the magnetic field or pre-strain amplitude induces an increment of the maximum stress. A higher iron particle concentration leads to a higher stress reduction as a constant strain is maintained. For all the cases, the steady-state stress response is achieved as the stress relaxation time is at 40 seconds. Then, in order to eliminate the stress relaxation effect on the dynamic properties of MRE, at least 40 seconds is required to enable the MRE to approach a stable pre-strain condition.

4.3 Pre-strain effect on the dynamic shear properties of MRE under different frequencies

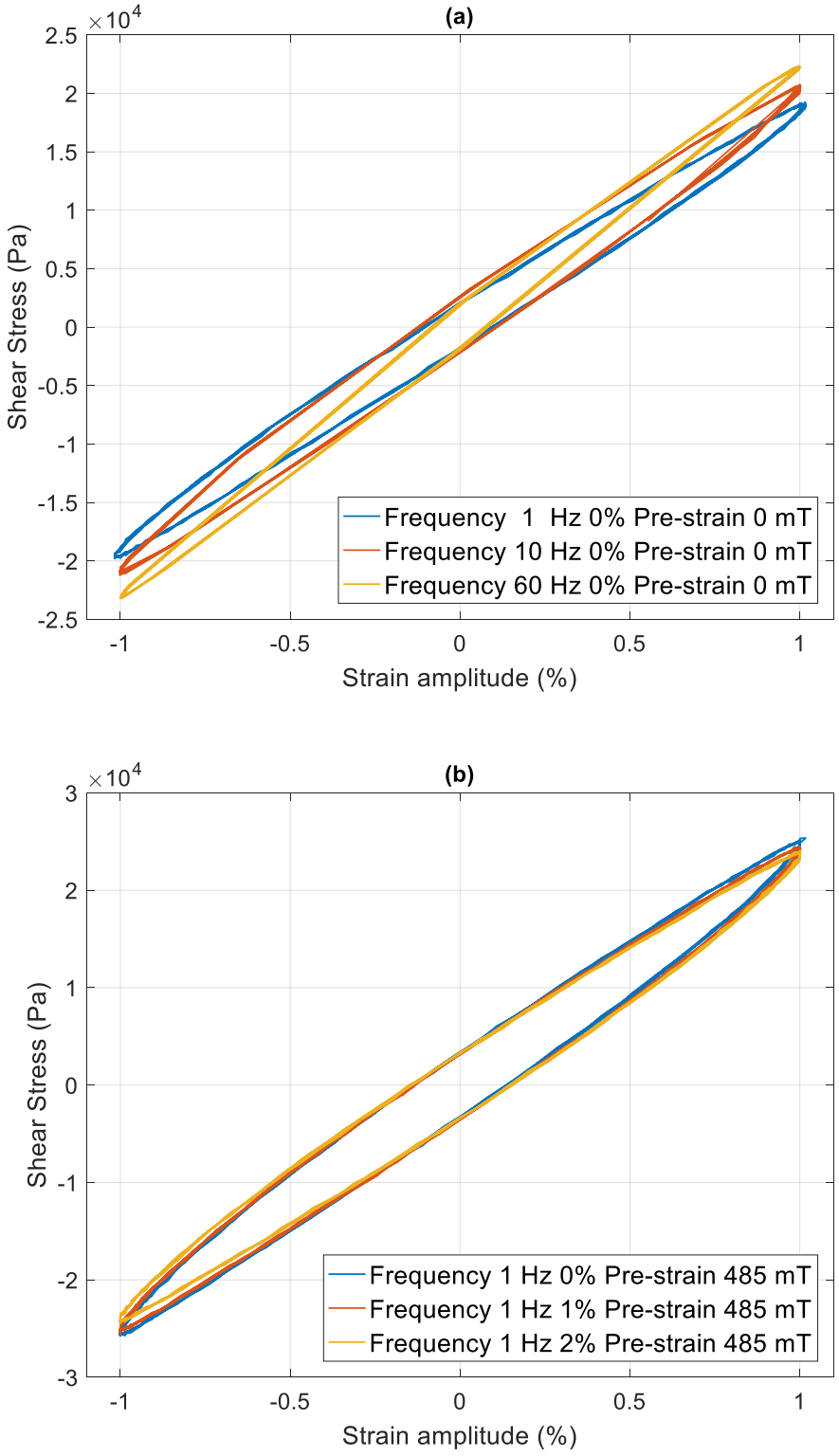

Figure 4.2 Stress-strain hysteresis curve plot of the 30% iron particle concentration MRE (a) 1,10,60 Hz frequency, 0% pre-strain condition, 0 mT magnetic flux density, (b) 1 Hz frequency, 0%,1% and 2% pre-strain condition, at 500 mT magnetic flux density.

Figure 4.2 (a) shows the stress-strain hysteresis curves of the 30% iron particle concentration MRE sample under different excitation frequency with 1% strain amplitude at 0 mT magnetic flux density and Figure 4.2 (b) illustrates the stress-strain curves with pre-strain effect at 1 Hz excitation frequency, 1% strain amplitude at 485mT magnetic flux density. The complex modulus of MRE is the slope of stress to strain. It is seen from Figure 4.2 (a), the complex modulus increases gradually with the excitation frequency. Figure 4.2 (b) indicates that the slope of the stress to strain decreases slightly when a pre-strain is applied which means that the complex modulus of MRE decreases as a pre-strain increases. As pre-strain increases from 1% to 2%, the decrease rate of the stress-strain slope subsides, referring to MRE is starting to stiffen.

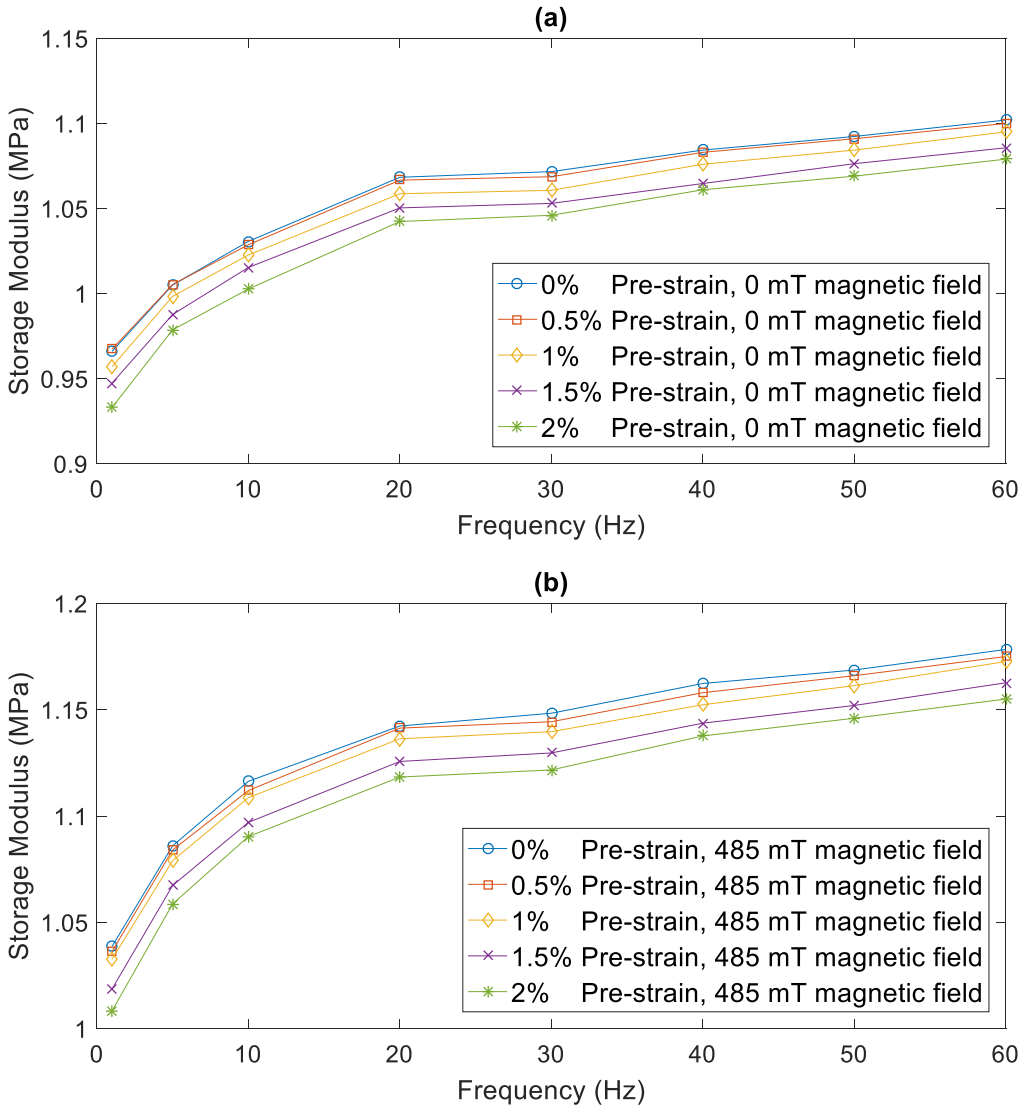

Figure 4.3 Storage modulus of MRE with 10% iron powder under different pre-strain amplitude with 1% strain amplitude (a) under 0 mT magnetic field (b) under 485 mT magnetic field

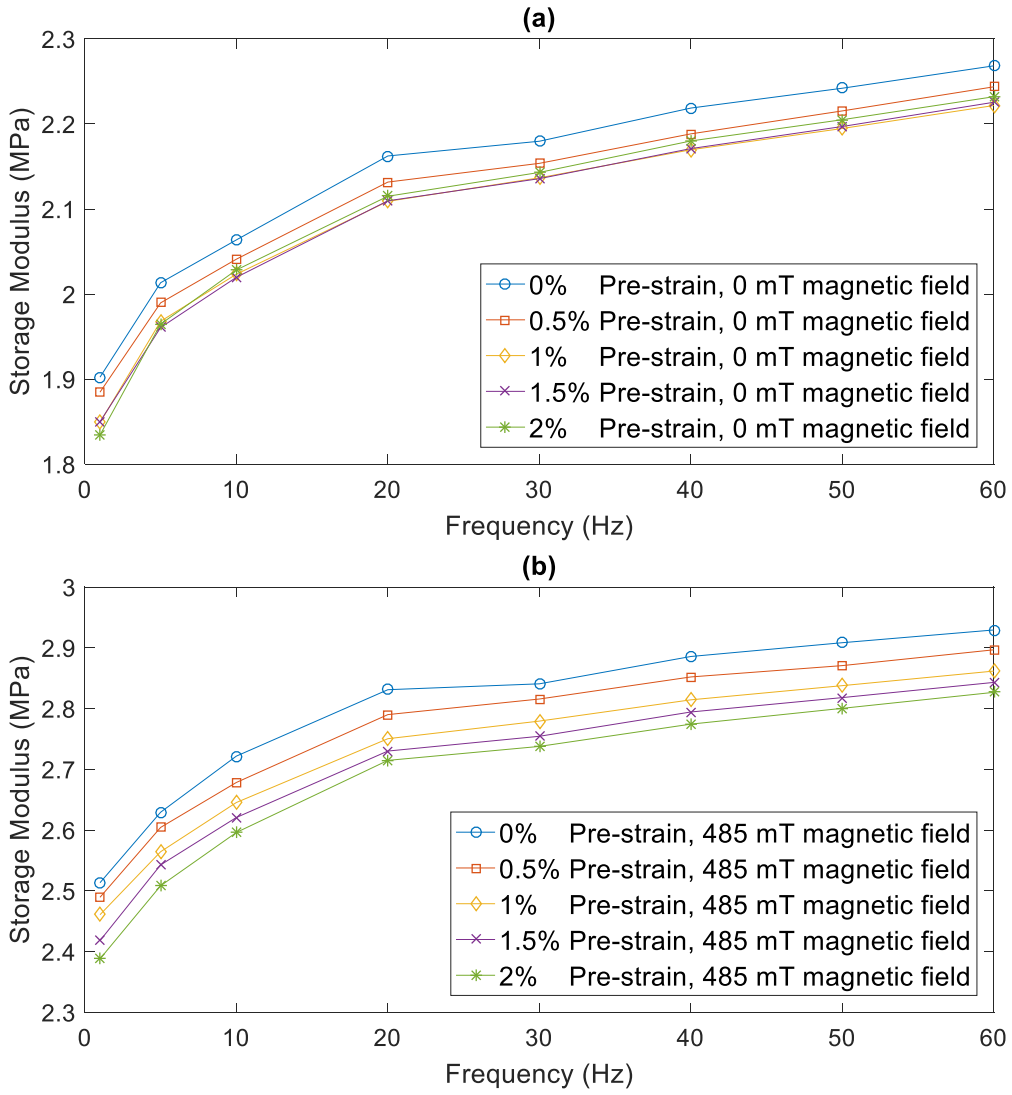

Figure 4.4 Storage modulus of MRE with 30% iron powder under different pre-strain amplitude with 1% strain amplitude (a) under 0 mT magnetic field (b) under 485 mT magnetic field

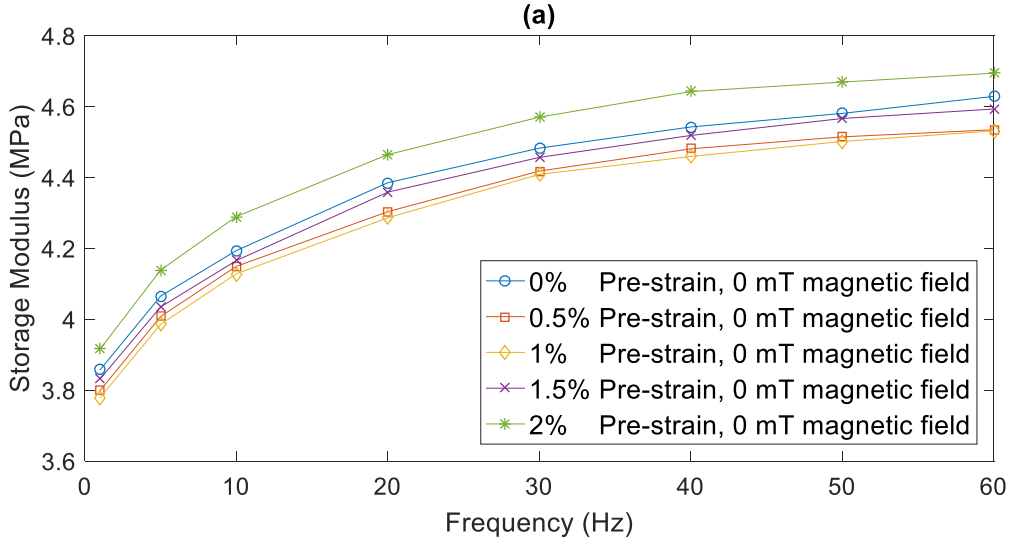

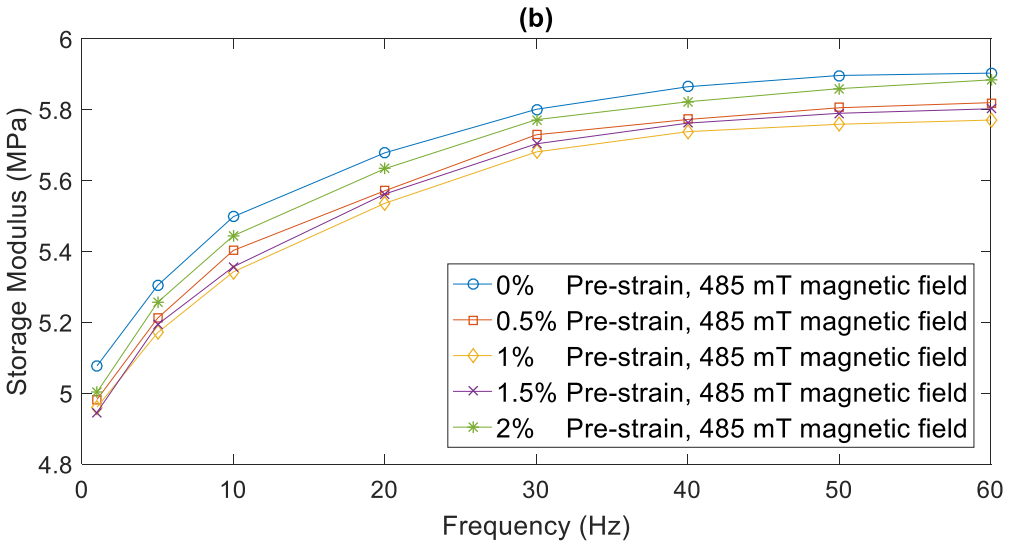

Figure 4.5 Storage modulus of MRE with 50% iron powder under different pre-strain amplitude with 1% strain amplitude (a) under 0 mT magnetic field (b) under 485 mT magnetic field

The storage modulus is calculated by Eq. 3.1 and Eq. 3.3. Figure 4.3-4.5 demonstrate the pre-strain effect on the dynamic shear storage modulus of MRE under different frequency varies from 1Hz to 60 Hz. The strain amplitude is set to 1% and two magnetic field strengths 0 mT and 485 mT are selected for the frequency sweep tests. For MRE samples with different iron particle concentrations, an increase frequency induces an increment of storage modulus of MRE which means MRE becomes stiffer at a higher excitation frequency. The storage modulus increases rapidly as frequency increases from 1Hz to 20Hz. Then, a slow and continuous increase of the storage modulus at a decrease rate is observed for frequency over 20Hz.

The pre-strain effect on the dynamic shear storage modulus of MRE is different among MRE samples with different iron particle concentrations. For MRE sample with 10% iron particle concentration, the pre-strain effect leads to a decrease of storage modulus shown in Figure 4.3 (a). As pre-strain amplitude increases from 0% to 2%, the dynamic storage modulus induces a further decrease. For MRE samples with a higher iron particle concentrations, i.e. 30% and 50% (Figure 4.4 (a) and Figure 4.5 (a)), pre-strain also induces a material soften phenomenon for pre-strain amplitude smaller than 1%. As pre-strain amplitude increases from 1% to 2%, storage modulus starts to increase. At this time, the storage modulus soften phenomenon due to pre-strain vanishes and MRE becomes stiffer. As iron particle concentration increases from 30% to 50%, storage modulus increment due to pre-strain amplitude over 1% becomes more obvious. Figure 4.5 (a) shows that storage modulus at 2% pre-strain amplitude is even higher than that without pre-strain amplitude. In the meantime, the trend of storage modulus remains unchangeable by the effect of pre-strain at different frequencies. The plots of storage modulus at various pre-strain conditions are parallel to each other. The couple effect between pre-strain and frequency is small and can be neglected. The dependence of frequency on storage modulus is independent of pre-strain.

Figures 4.3 (b) to 4.5 (b) illustrate the effect of the pre-strain on the dynamic storage modulus of MRE with different frequency at 485 mT magnetic field. The external magnetic field induces an increase of the storage modulus. The increase trend of the storage modulus does not vary with the applied magnetic field. Comparing with the results at 0 mT magnetic field, the storage modulus shows a further decrease due to the presence of the pre-strain under a magnetic field. By increasing the pre-strain amplitude, the decrement of magnitude of the storage modulus also increase under the influence of the magnetic field. The storage modulus reduction due to pre-strain under the magnetic field is more obvious for the samples with higher iron particle concentration (30% and 50%).

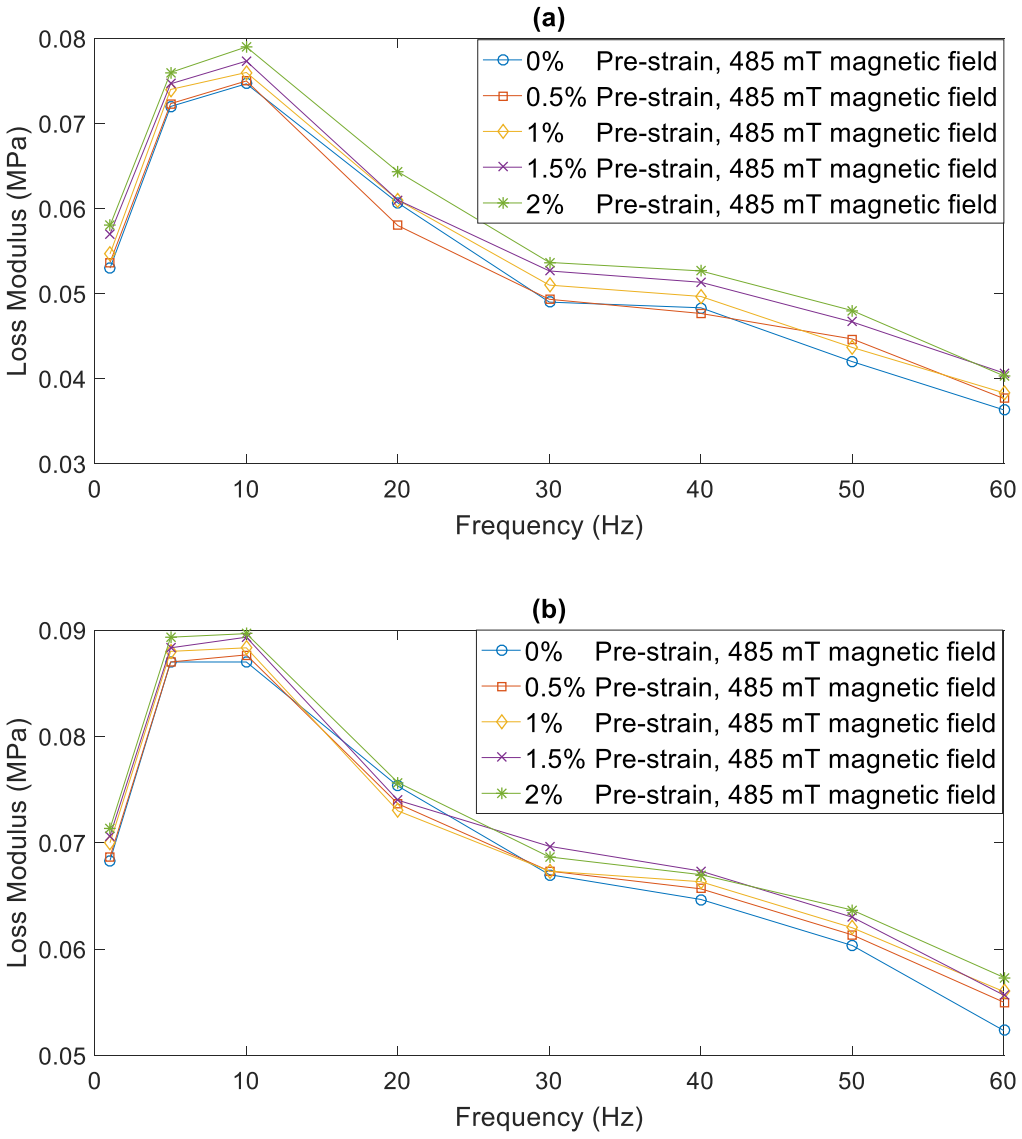

Figure 4.6 Loss modulus of MRE with 10% iron powder under different pre-strain amplitude with 1% strain amplitude (a) under 0 mT magnetic field (b) under 485 mT magnetic field

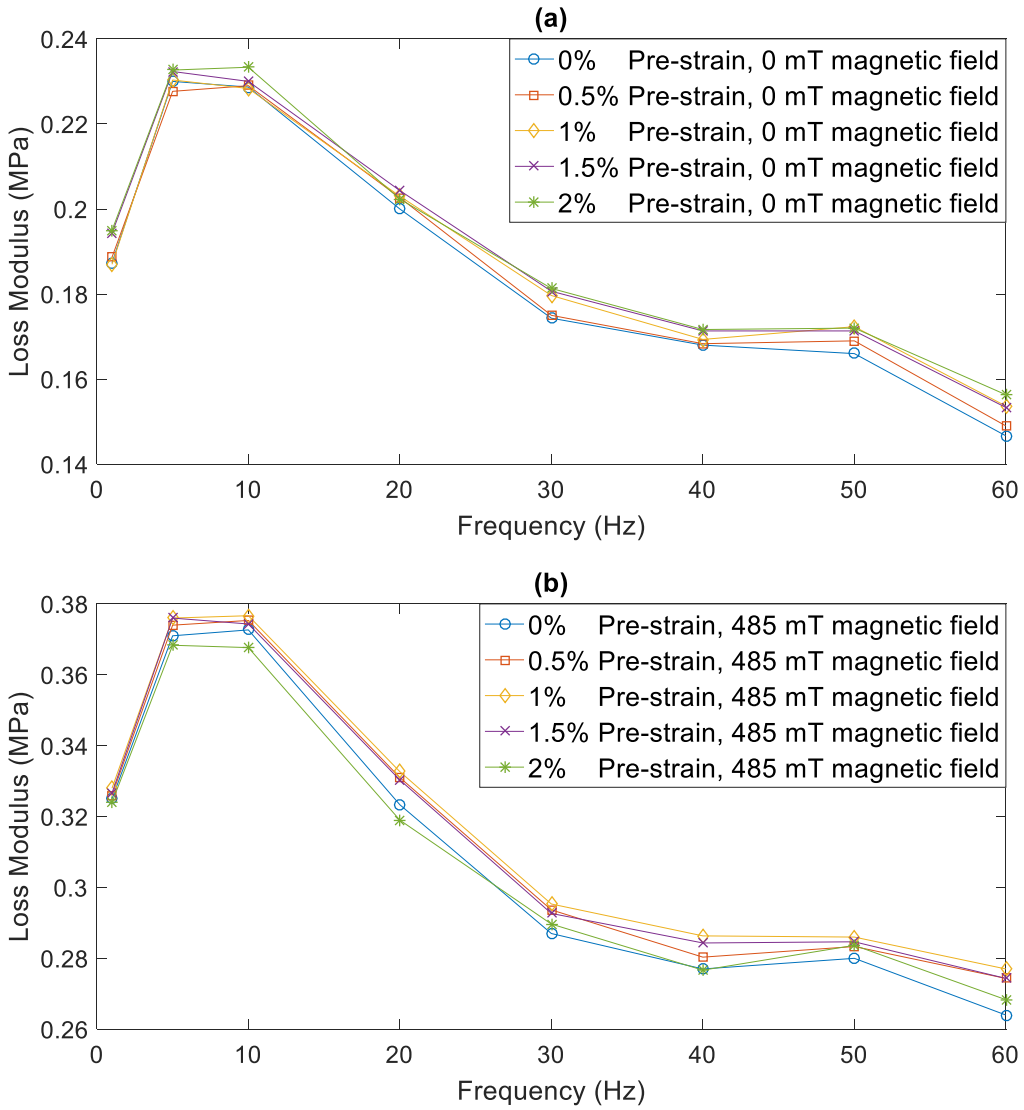

Figure 4.7 Loss modulus of MRE with 30% iron powder under different pre-strain amplitude with 1% strain amplitude (a) under 0 mT magnetic field (b) under 485 mT magnetic field

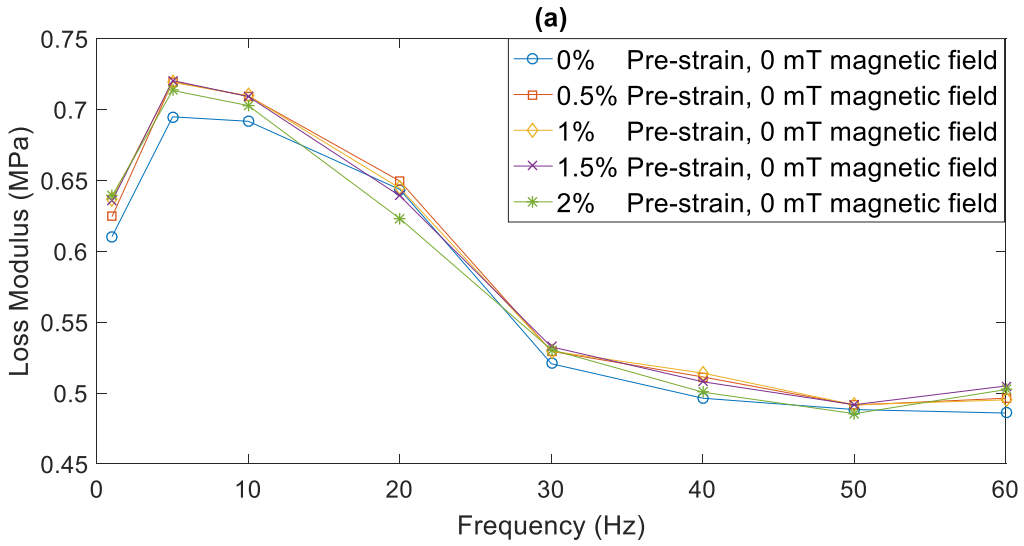

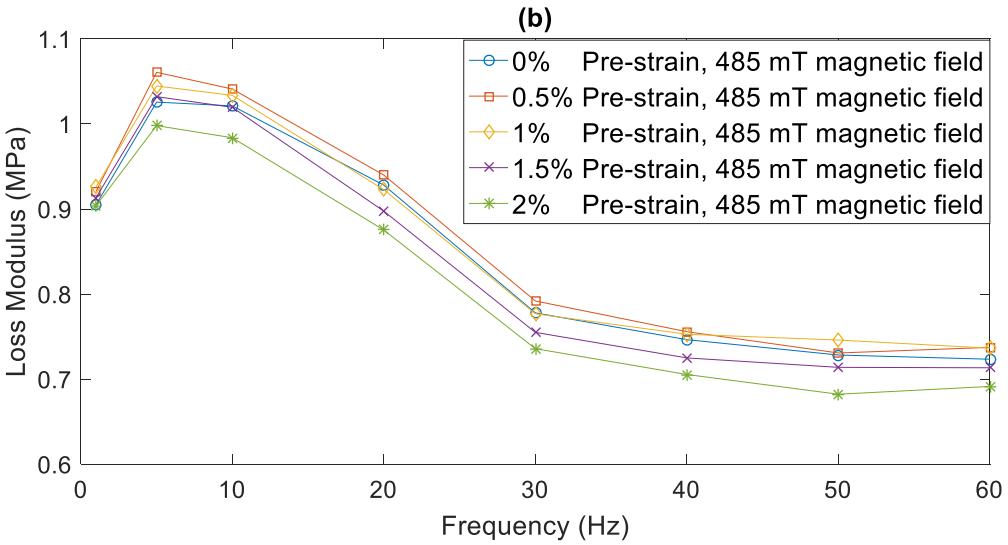

Figure 4.8 Loss modulus of MRE with 50% iron powder under different pre-strain amplitude with 1% strain amplitude (a) under 0 mT magnetic field (b) under 485 mT magnetic field

The loss modulus is calculated by Eq. 3.1 and Eq. 3.4. Figures 4.6-4.8 display the pre-strain effect on the dynamic shear loss modulus of MRE under different frequencies from 1Hz to 60 Hz with 1% strain amplitude at two magnetic field strengths 0 mT and 485 mT. The loss modulus increases with the frequency and reaches a maximum value between 5-10 Hz. After reaching the maximum value, the loss modulus starts to decrease as the frequency further increase. Loss modulus describes the energy dissipation of a material under dynamic loading. MRE is a rubber-like material with composition of silicone rubber and iron particle. The silicone rubber is polymer material contains long chain molecule. The movement of the molecule segment cause energy dissipated, such as heat. By increasing the frequency, the movement of a molecule segment increases which lead to an increase of the loss modulus. As the frequency continues increase, the movement of a molecule chain segment cannot keep up with the external excitation. At the time, the energy generated by the movement of the molecule segment starts to decrease which leads to a decrease of the loss modulus of MRE for the frequency over 10 Hz (Ward and Sweeney, 2004). The maximum loss modulus is observed between 5 Hz to 10 Hz for all MRE samples with 10%, 30% and 50% iron particle concentrations. Then, it is concluded that the maximum loss modulus frequency of the MRE is largely dependent on the matrix material selection.

The pre-strain effect induces a slightly increase of the loss modulus for MRE samples with 10% iron particle concentration. For the samples with 30% and 50% iron particle concentrations, as the pre-strain amplitude increase from 1% to 2%, the loss modulus starts to decrease. By applying a pre-strain to MRE, the trend of the loss modulus along with the frequency remains the same. Then, it is concluded that the dependence of the loss modulus on the frequency is independent of the pre-strain.

An external magnetic field leads to an increment of the loss modulus (Figure 4.6 (b) –Figure 4.8 (b)). Meanwhile, the trend of the loss modulus under different frequencies remains the same as a magnetic

field is applied. Comparing with the loss modulus of MRE at 0 mT magnetic field, a decrement of the loss modulus is observed at 2% pre-strain amplitude for the 10% iron particle concentration MRE samples (Figure 4.6 (b)). This phenomenon is more obvious for the samples with 30% and 50% iron particle (Figure 4.7 (b) and Figure 4.8 (b)). To conclude, there is no obvious coupling effect between the frequency and pre-strain on MRE shear loss modulus.

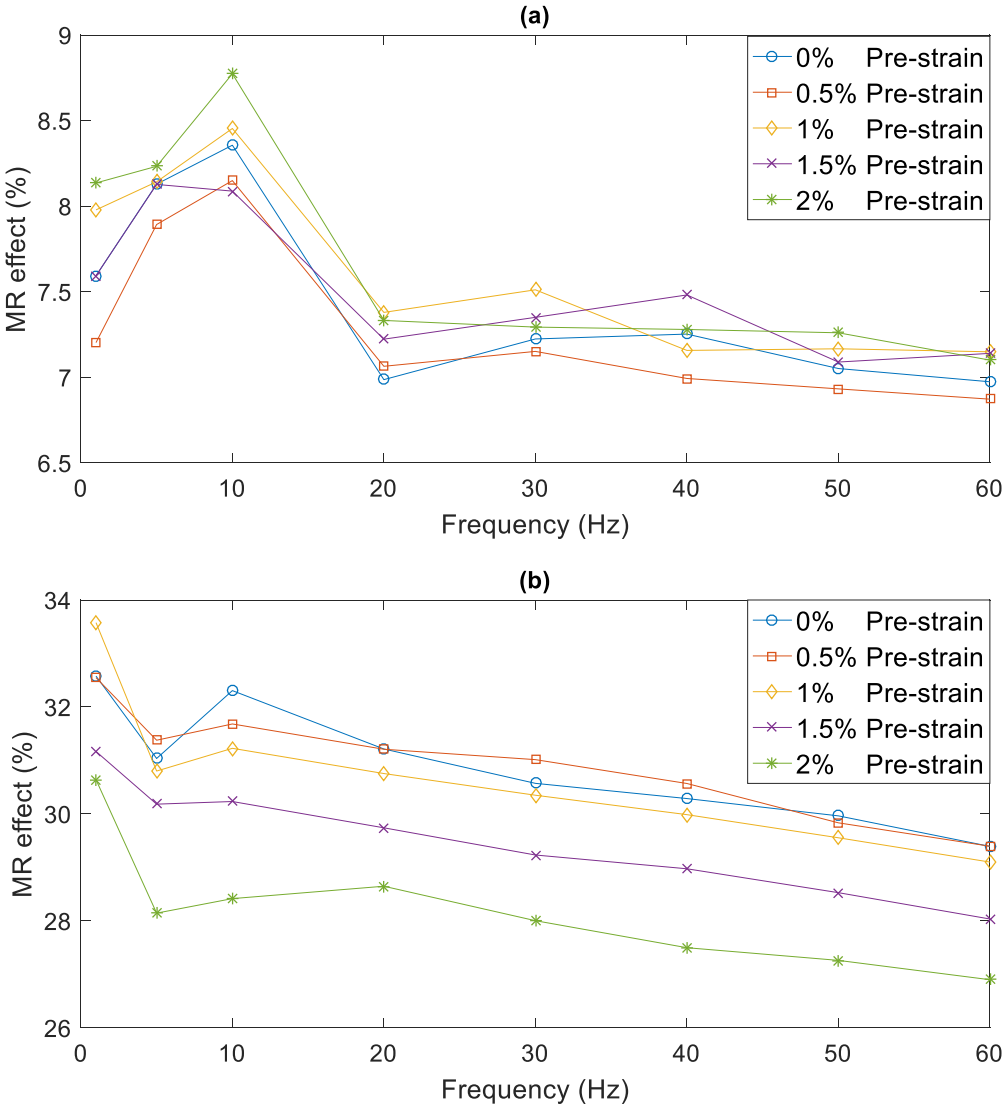

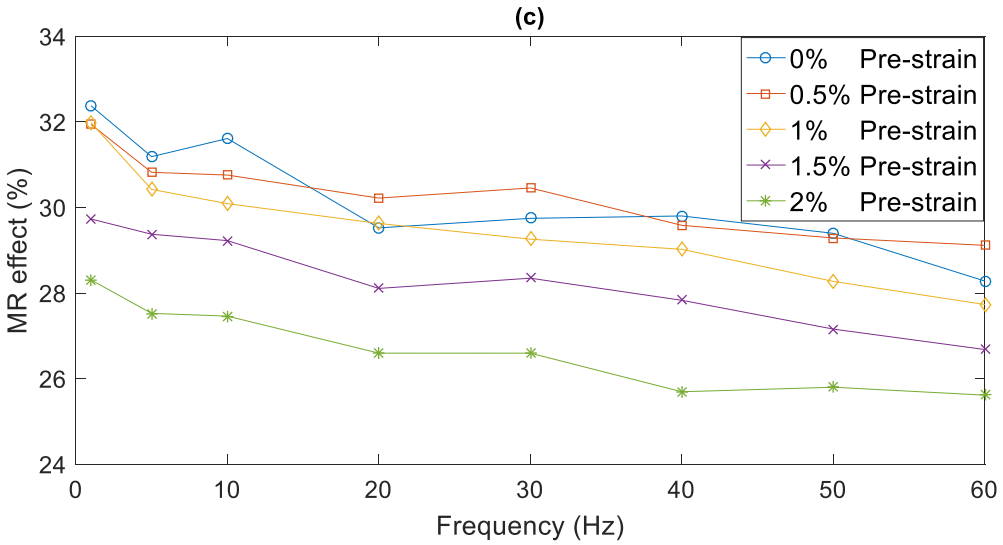

Figure 4.9 MR effect of MRE samples under different pre-strain with 1% strain amplitude at 485 mT magnetic field (a) 10% iron particle (b) 30% iron particle (c) 50% iron particle sample

The MR effect is calculated by Eq. 2.2. Figure 4.9 shows the MR effect of MRE samples with 10%, 30, and 50% iron particle concentrations under different pre-strain amplitude with frequencies from 1 Hz to 60 Hz. The strain amplitude is set to 1% and the magnetic field strength is 485 mT. The MR effect describes the controllability of MRE. A higher MR effect means a higher stiffness increase can be achieved by applying a magnetic field to MRE material. Figure 4.9 (a) shows that the MR effect of MRE samples with 10 % iron particle concentration is around 7% to 9% from 1 Hz to 60 Hz which is the lowest compared to the 30% and 50% iron particle concentration samples. By increasing the iron particle concentration, more iron particle chains are formed within MRE. The interactions among the iron particle chains become stronger under a magnetic field. Thus, a higher MR effect is achieved for a higher iron particle concentration MRE sample. The MR effect demonstrates a steady decrease as the frequency increase from 1 Hz to 60 Hz for the samples with 30% and 50% iron particle concentration (Figure 4.9 (b) and (c)). For the sample with 10 % iron particle concentration, the MR effect increases as the frequency varies from 1 Hz to 10 Hz. Then, the MR effect decreases as the frequency further increase.

Pre-strain induces an obvious decrease of the MR effect for MRE samples with 30% and 50% iron particle concentrations. As pre-strain amplitude increases from 0.5% to 2%, a further decrease of the MR effect is observed. For the 10% iron particle concentration MRE, there is fewest iron particle chains formed within MRE. Since iron particle chains are separated sparsely among the 10% MRE samples. The interactions between the iron particle chains are weak under a magnetic field. In consequence, the MR effect for the 10% iron particle concentration MRE sample is not obvious and there is no clearly relationship between pre-strain amplitude and MR effect obtained. By comparing Figure 4.9, it is concluded that MRE has a better controllability at a low frequency and a low pre-strain condition. A higher iron particle concentration increases the MR effect. The maximum MR effect is achieved for MRE samples with 30% iron particle concentration.

4.4 Pre-strain effect on the dynamic shear properties of MRE under different strains

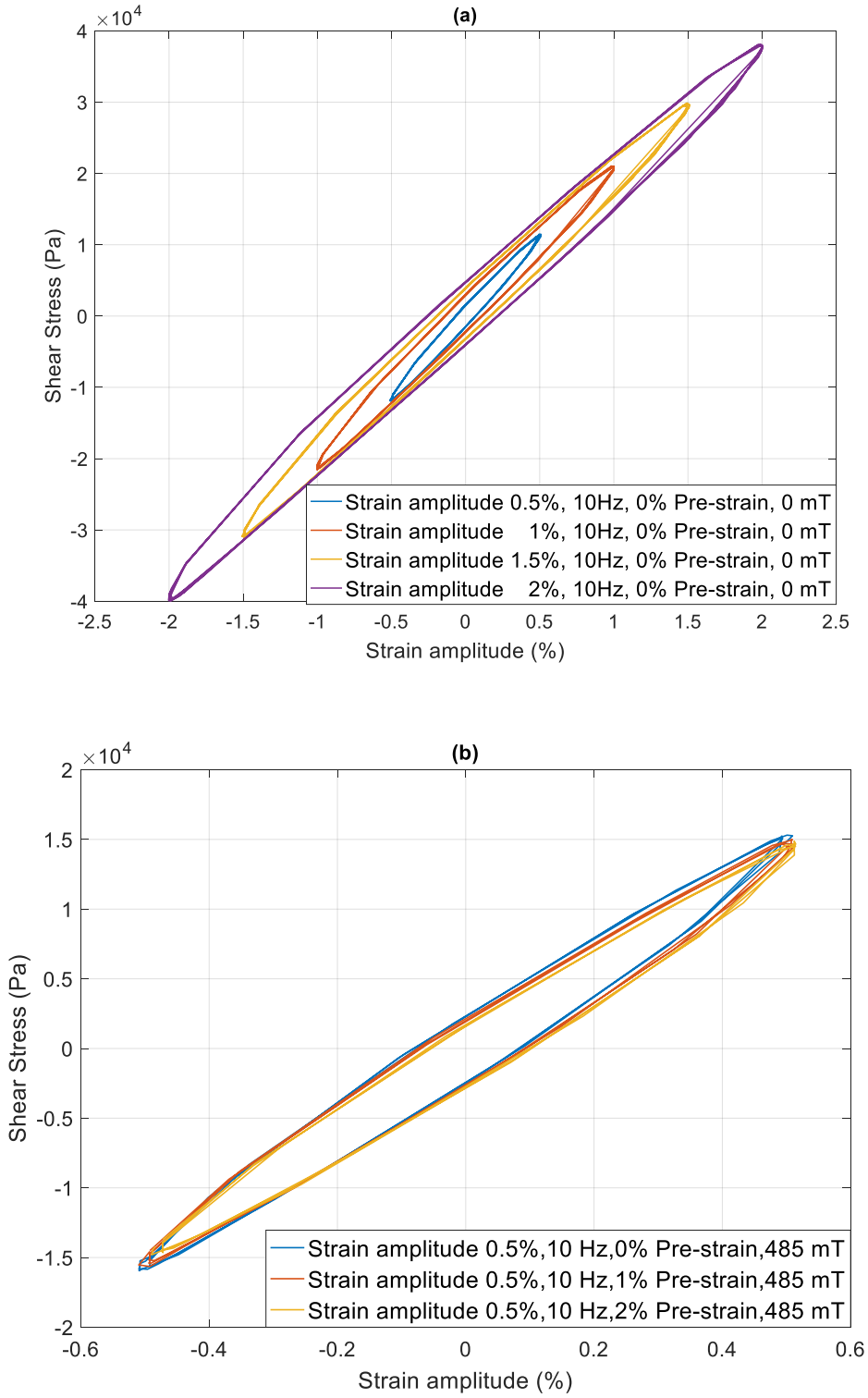

Figure 4.10 Stress-strain hysteresis curve plot of the 30% iron particle concentration MRE (a) 0.5%, 1%, 1.5%, 2% strain amplitude, 10 Hz frequency, 0% pre-strain condition, 0 mT magnetic flux density, (b) 0.5% strain amplitude, 10 Hz frequency, 0%,1% and 2% pre-strain condition, at 485 mT magnetic flux density.

Figure 4.10 (a) shows the stress-strain hysteresis curves of 30% iron particle concentration MRE under different strain amplitude from 0.5% to 2% at a 0.5% increment, at 10 Hz and 0 mT magnetic flux density with 0% pre-strain. Figure 4.10 (b) illustrates the stress-strain curves with pre-strain effect at 10 Hz, 0.5% strain amplitude with 485 mT magnetic flux density. As can be seen from Figure 4.10 (a), the slope of the stress to strain indicates a slight decrease with the increase strain amplitude. The complex modulus of MRE decreases with the increase stain amplitude. Figure 4.10 (b) illustrates the slope of the stress to strain decreases marginally as a pre-strain is applied. The complex modulus of MRE decrease as a pre-strain continuously increases. As pre-strain increases from 1% to 2%, the decrease rate of the stress-strain slope reduces, indicating that MRE starts to stiffer. A similar phenomenon can be observed from Figure 4.2 (b).

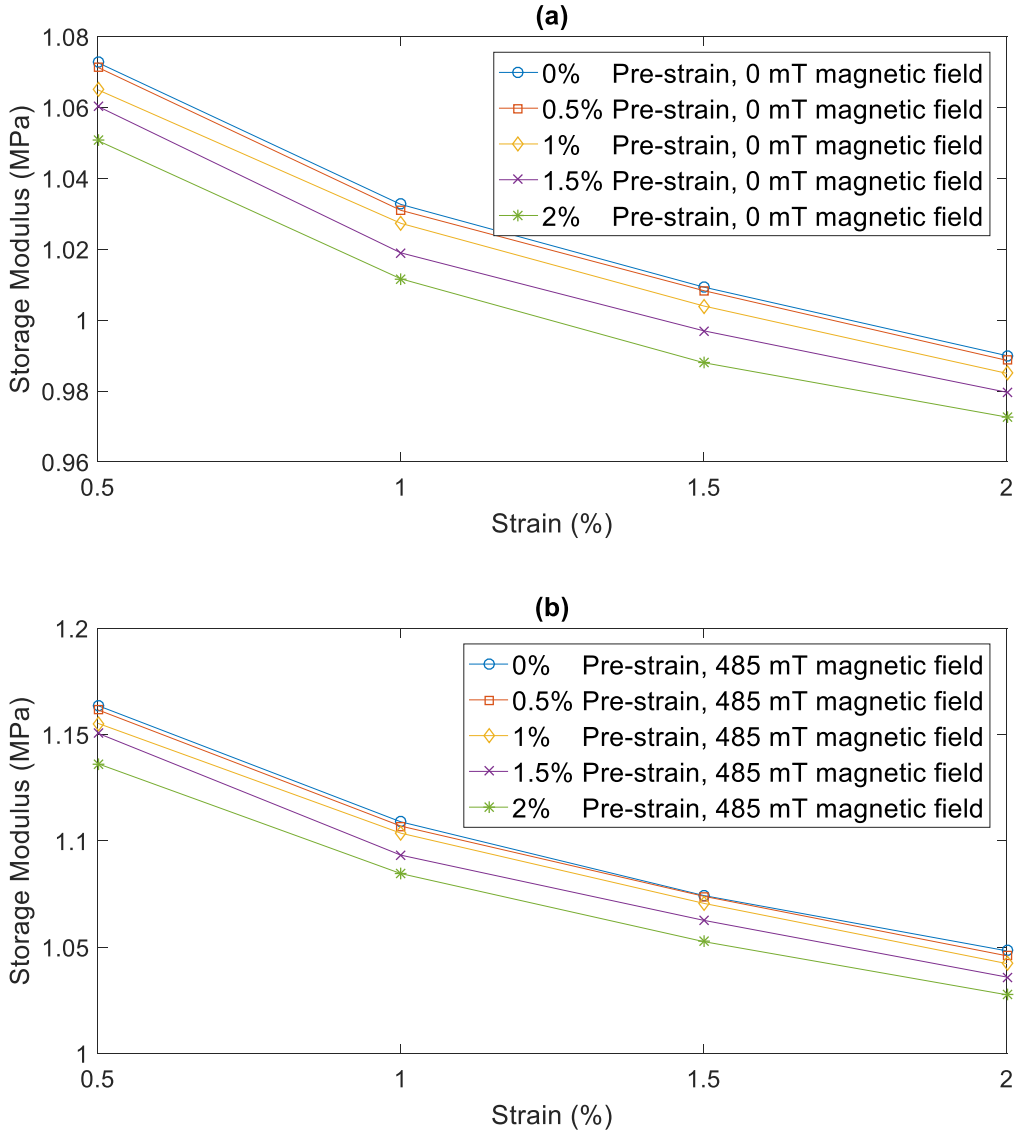

Figure 4.11 Storage modulus of MRE with 10% iron powder under different pre-strain amplitude with 10 Hz frequency (a) under 0 mT magnetic field (b) under 485 mT magnetic field

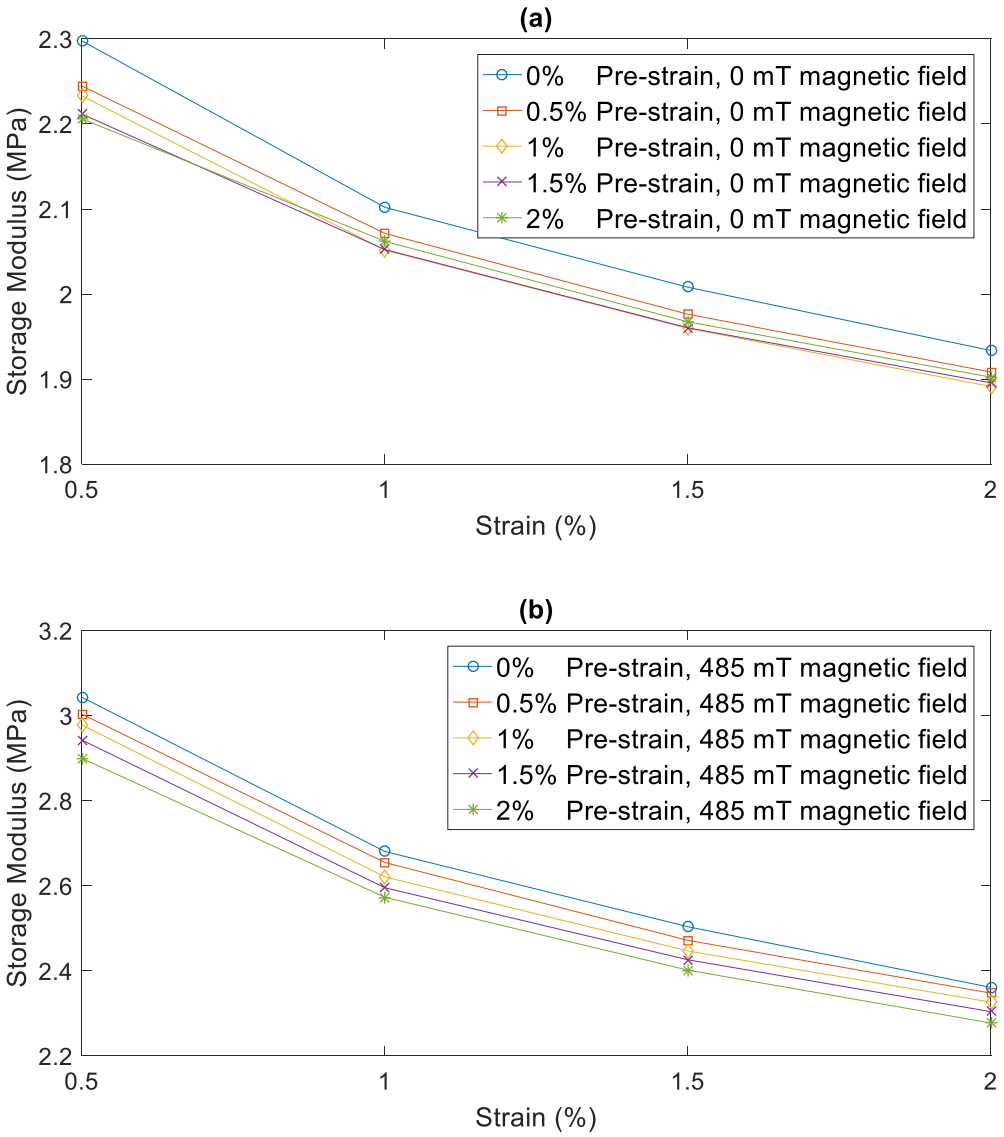

Figure 4.12 Storage modulus of MRE with 30% iron powder under different pre-strain amplitude with 10 Hz frequency (a) under 0 mT magnetic field (b) under 485 mT magnetic field

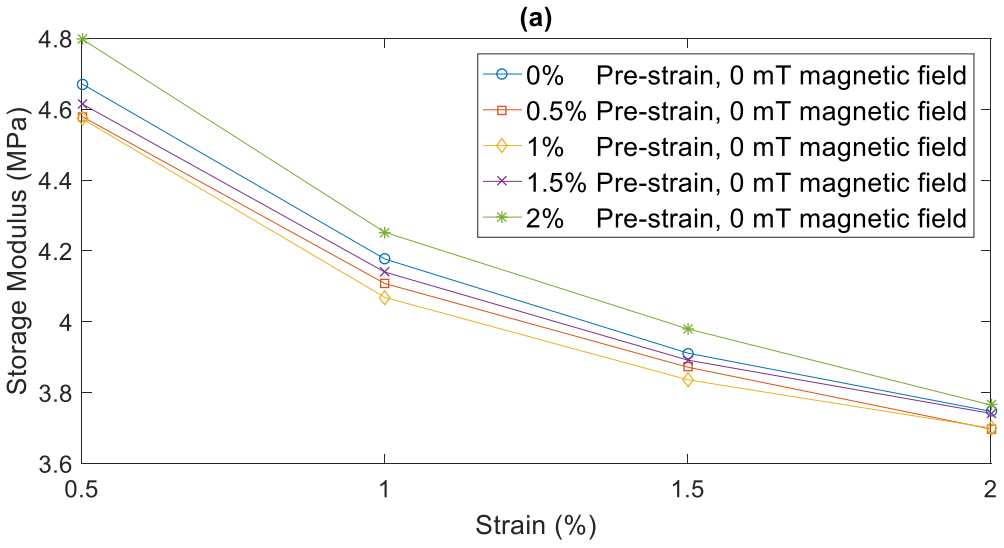

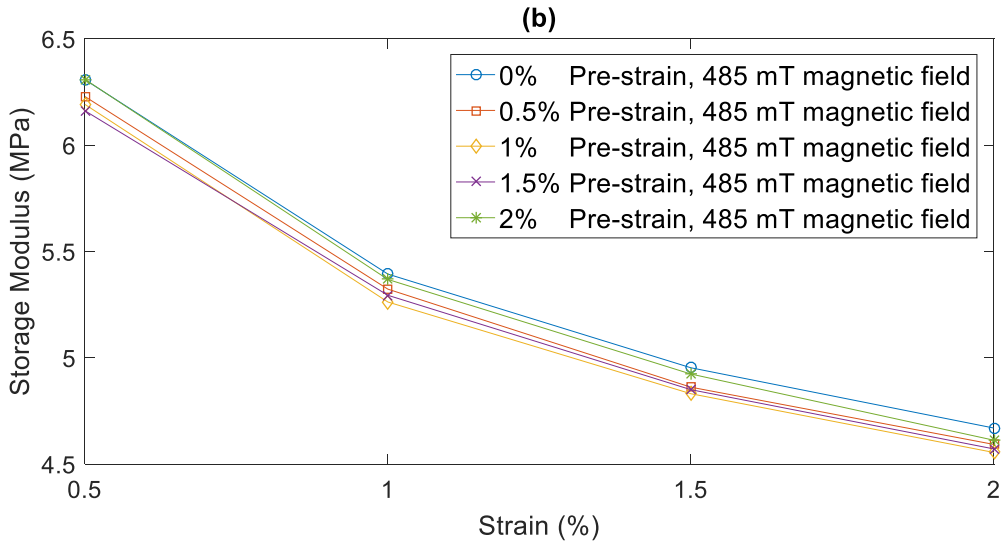

Figure 4.13 Storage modulus of MRE with 50% iron powder under different pre-strain amplitude with 10 Hz frequency (a) under 0 mT magnetic field (b) under 485 mT magnetic field

Figure 4.11-4.13 demonstrate the pre-strain effect on the dynamic storage modulus of MRE under different strain amplitudes from 0.5% to 2%. The excitation frequency is set as 10 Hz. Two magnetic field strengths 0 mT and 485 mT are selected for the strain amplitude sweep tests. Due to Payne effect, the storage modulus of MRE shows a magnitude reduction as a strain amplitude increases (Payne, 1962). The Payne effect becomes more obvious as iron particle concentration increases from 10% to 50%. The storage modulus reduction has a linear relationship with the strain amplitude. The external magnetic field does not change the dependence of the storage modulus on the dependence of strain, but induces an increment of the storage modulus.

The pre-strain effects on the dynamic storage modulus of MRE for the strain amplitude sweep show similar results for those of frequency sweep. For 10% iron particle concentration MRE samples, a pre-strain leads to a storage modulus reduction and an increase of the pre-stain amplitude lead to a further decrease of the storage modulus (Figure 4.11 (a)). For MRE samples with higher iron particle concentrations (Figure 4.12 (a) and 4.13 (a)), a storage modulus reduction is observed for the pre-strain condition from 0% to 1%. As the pre-stain amplitude continues to increase from 1% to 2%, the shear modulus starts to increase and MRE becomes stiffer. Since the trend of the storage modulus at different pre-strain amplitudes does not change with the strain amplitude. Then, it is said that the dependence of the pre-strain amplitude on the dynamic storage modulus is independent of the strain amplitude. The coupling effect between the pre-strain and strain amplitude is weak and can be neglected.

Figure 4.11 (b)-4.13 (b) show the effect of the pre-strain on the storage modulus of MRE under a 485 mT magnetic field. A magnetic field magnifies the pre-strain effect on the storage modulus. A further storage modulus reduction is observed comparing with the results without magnetic field. This phenomenon becomes more noticeable for high iron particle concentration samples

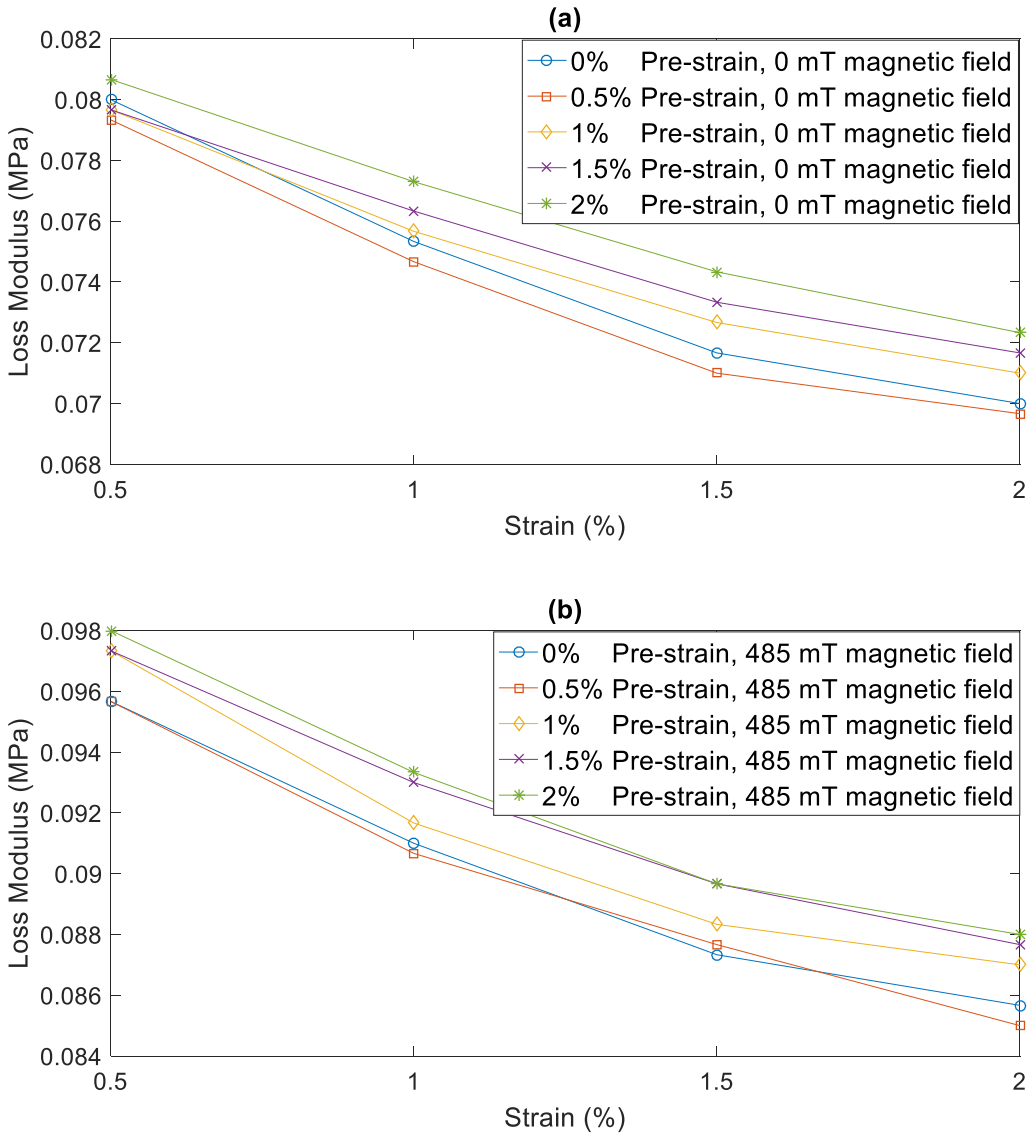

Figure 4.14 Loss modulus of MRE with 10% iron powder under different pre-strain amplitude with 10 Hz frequency (a) under 0 mT magnetic field (b) under 485 mT magnetic field

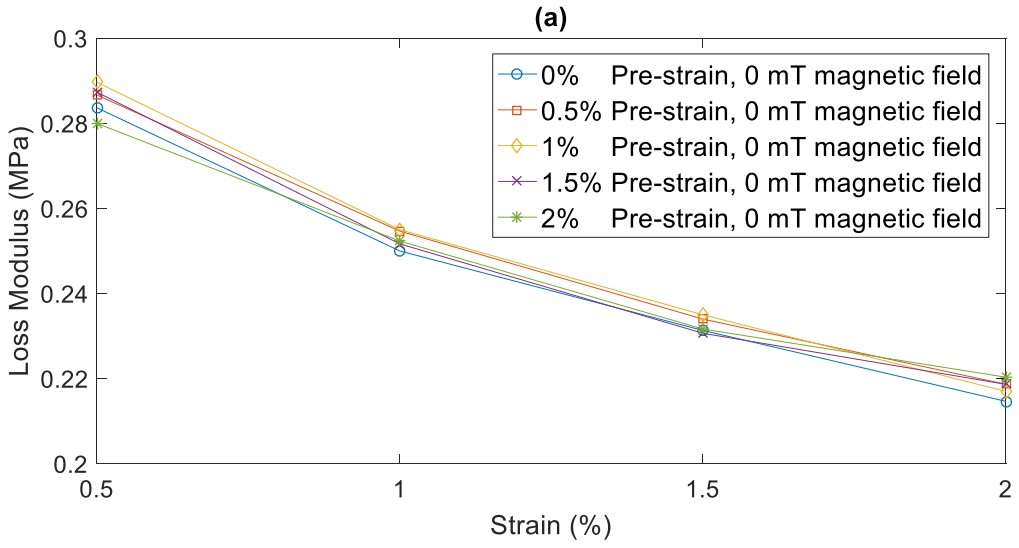

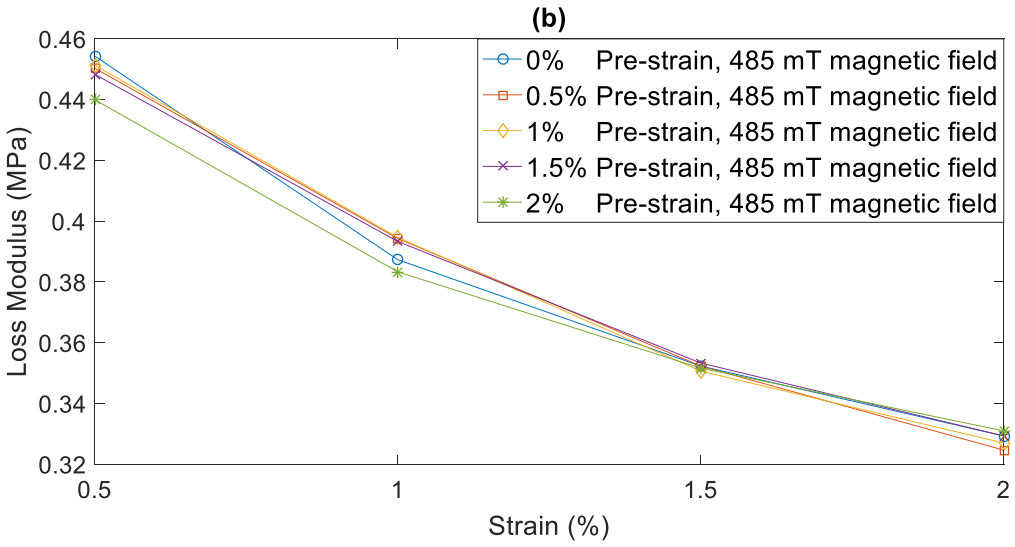

Figure 4.15 Loss modulus of MRE with 30% iron powder under different pre-strain amplitude with 10 Hz frequency (a) under 0 mT magnetic field (b) under 485 mT magnetic field

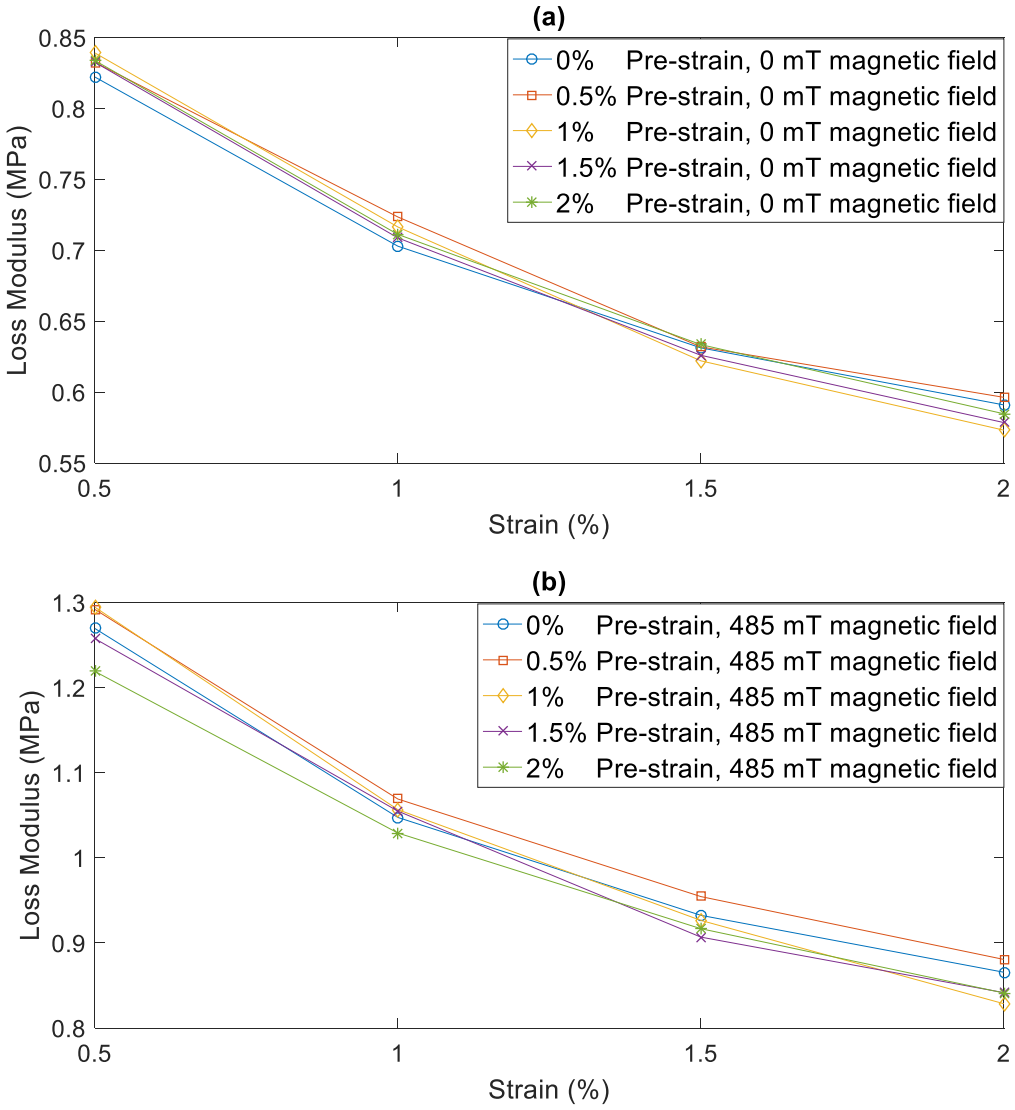

Figure 4.16 Loss modulus of MRE with 50% iron powder under different pre-strain amplitude with 10 Hz frequency (a) under 0 mT magnetic field (b) under 485 mT magnetic field

Figure 4.14-4.16 illustrate the pre-strain effect on the dynamic shear loss modulus of MRE under different strain amplitudes from 0.5% to 2% at 10 Hz with two magnetic field strengths 0 mT and 485 mT. Due to Payne effect, the loss modulus also decreases with an increase strain amplitude for all the MRE samples. A steady decrease of the loss modulus is observed as the strain amplitude increase from 0.5% to 2%. The loss modulus for the higher iron particle concentration MRE samples is higher compared with the lower ones.

Pre-strain effect leads to an increase of the loss modulus for 10% iron particle concentration MRE samples at 0 mT magnetic field (Figure 4.14 (a)). This means more energy is dissipated by MRE samples as a pre-strain is applied. For MRE samples with 30% and 50% iron particle concentration, the loss modulus shows a slight increase as a pre-strain is applied. As the pre-strain amplitude continues to increase from 1% to 2%, the loss modulus starts to decrease. By applying a magnetic field, a further decrease of the loss modulus due to the pre-strain increase from 1% to 2% is observed (Figure 4.15 (b)-4.16 (b)). The magnetic field effect on the loss modulus due to a pre-strain for 10% iron particle concentration MRE sample is not obvious comparing with the other samples. The trend of the loss modulus remains unchangeable due to a pre-strain with the strain amplitude from 0.5% to 2%. Then, it is concluded that the dependence of the loss modulus on the strain amplitude is independent of the pre-strain.

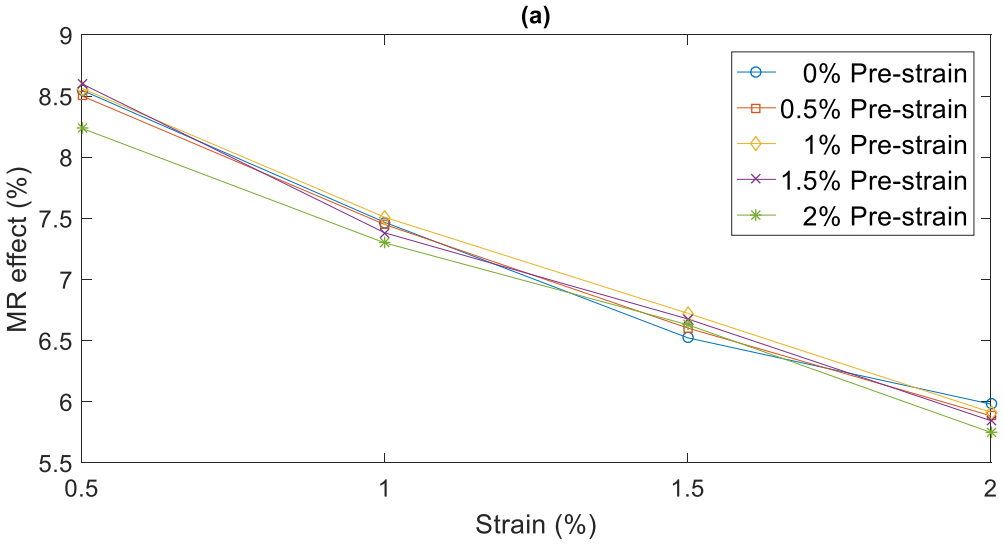

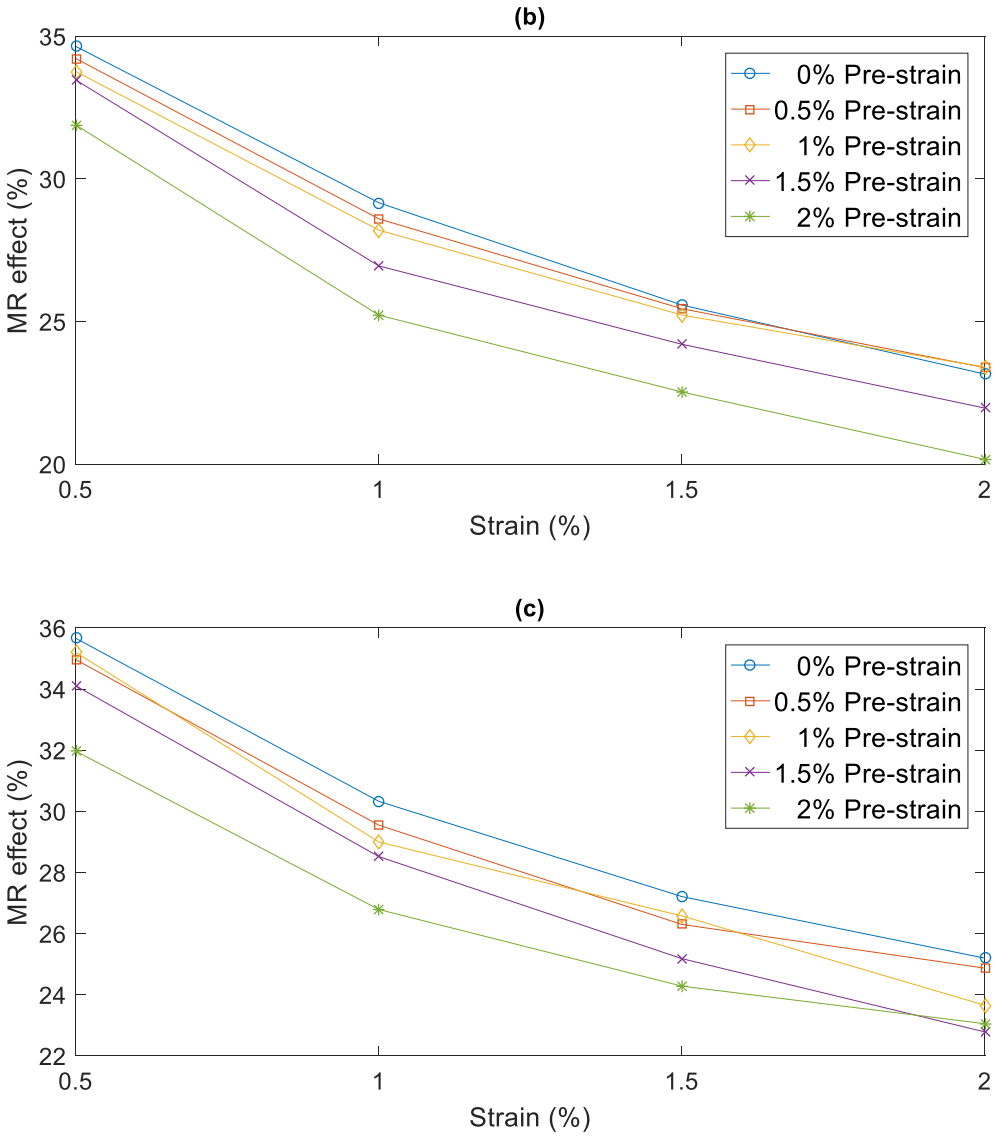

Figure 4.17 MR effect of MRE sample under different pre-strain amplitude with 10 Hz at 485 mT magnetic field (a) 10% iron particle sample (b) 30% iron particle sample (c) 50% iron particle sample

The dependence of the MR effect on pre-strain under different strain amplitude of MRE samples with 10%, 30, and 50% iron particle concentration can be observed in Figure 4.17. It can be seen that the MR effect of MRE samples decreases rapidly with the increased strain. The MR effect of the 10 % iron particle concentration sample (Figure 4.17 (a)) reduces from 8.5% to 6% as the strain amplitude increases from 0.5% to 2%. For MRE samples with 30% and 50% iron particle concentration, the MR effect decreases from 35% to 25% as the strain amplitude increases from 0.5% to 2% (Figure 4.17 (b) and (c)). The pre-strain effect on the MR effect of 10% iron particle sample is not significant. While, the pre-strain effect on the MR effect for 30% and 50% iron particle samples is more obvious. An initial pre-strain to the MRE samples induces a reduction of the MR effect. As pre-strain amplitude increases from 0.5% to 2%, the MR effect continuous decrease which means that the controllability of MRE sample deteriorates.

4.5 Pre-strain effect on the dynamic shear properties of MRE under different magnetic fields

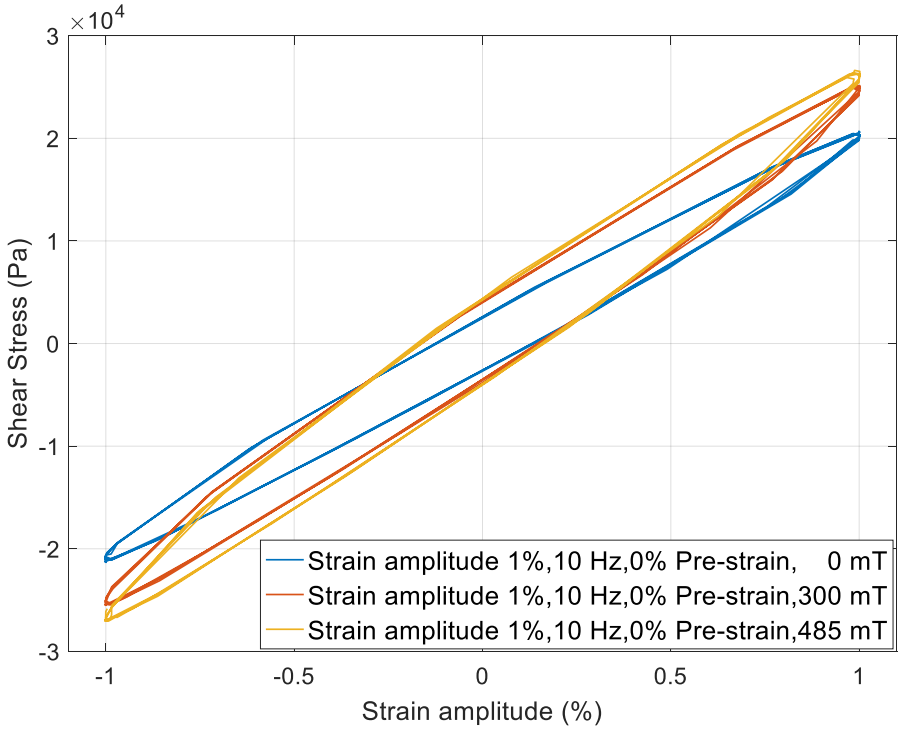

Figure 4.18 Stress-strain hysteresis curve plot of 30% iron particle concentration MRE with 0 mT, 300 mT and 500 mT at 10 Hz frequency with 1% strain amplitude

Figure 4.18 demonstrates the stress-strain hysteresis curves of the 30% iron particle concentration MRE under 0, 300 mT and 500 mT magnetic flux density, at 10 Hz, 1% strain amplitude with no pre-strain condition. It is seen from Figure 4.18, the slope of the stress to strain increase with the magnetic flux density. There is an obvious increase of the shear modulus of MRE as the magnetic field increase from 0 mT to 300 mT. Due to the magnetic saturation of iron particle, the increasing rate of the shear modulus subsides for the magnetic field strength increase from 300 mT to 485 mT.

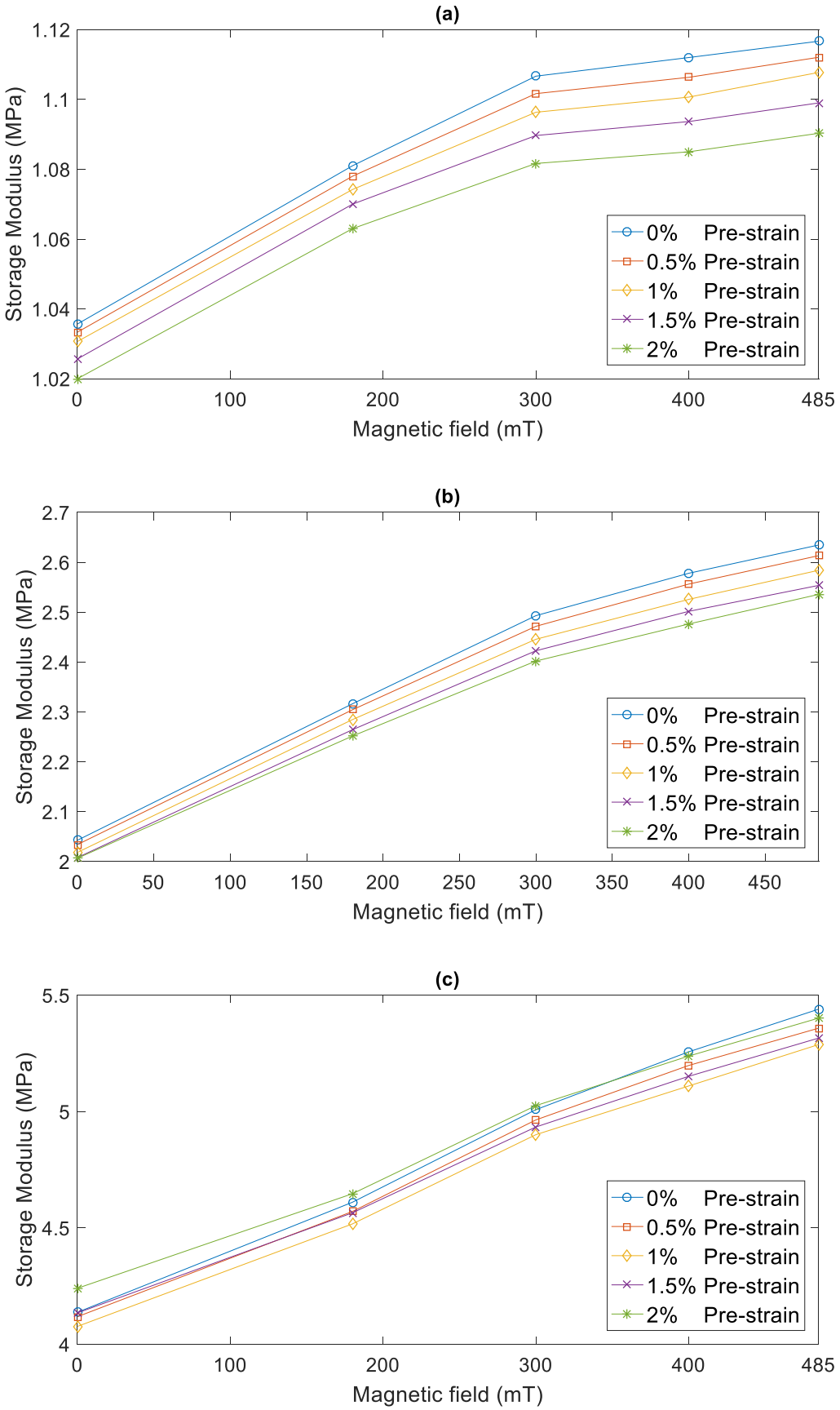

Figure 4.19 Storage modulus of MRE under different magnetic field with 1% strain amplitude at 10 Hz (a) 10% iron particle concentration (b) 30% iron particle concentration (c) 50% iron particle concentration

Figure 4.19 (a)-(c) are the plots of the pre-strain effect on the storage modulus of MRE with different iron particle concentrations under various magnetic fields. A stronger magnetic field strength induces a higher magnetic interaction between magnetic particle chains. Thus, the storage modulus increases significantly by increasing the magnetic field strength. For MRE samples with higher iron particle concentration, this phenomenon is more obvious (Figure 4.19 (b) and (c)). As the strength of the magnetic field increase to 300 mT, the magnetic saturation phenomenon is observed. The increase rate of the storage modulus decreases. The pre-strain effect induces a decrease of the shear modulus of MRE samples. By increasing the strength of the magnetic field, a further reduction of the storage modulus due to a pre-strain is observed. The microstructure of MRE has a significant impact on the mechanical properties of MRE (Chen et al., 2007). The storage modulus increase due to a magnetic field is mainly dependent on the magnetic interaction among iron particles within MRE. By applying a pre-strain to MRE, iron particle chains are elongated and the distance between iron particles is increased. Thus, the magnetic interactions between iron particles are decreased which lead to a reduction of the storage modulus.

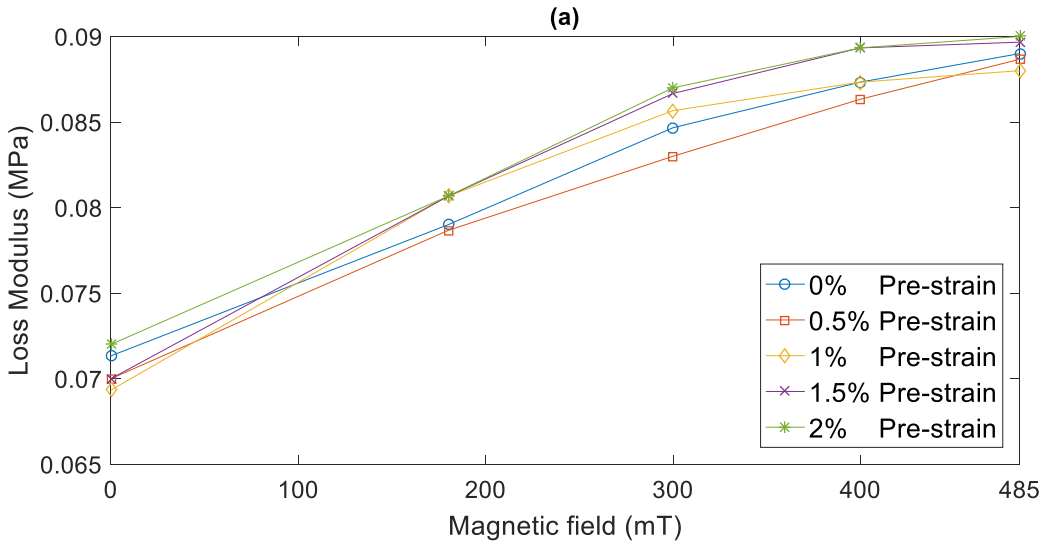

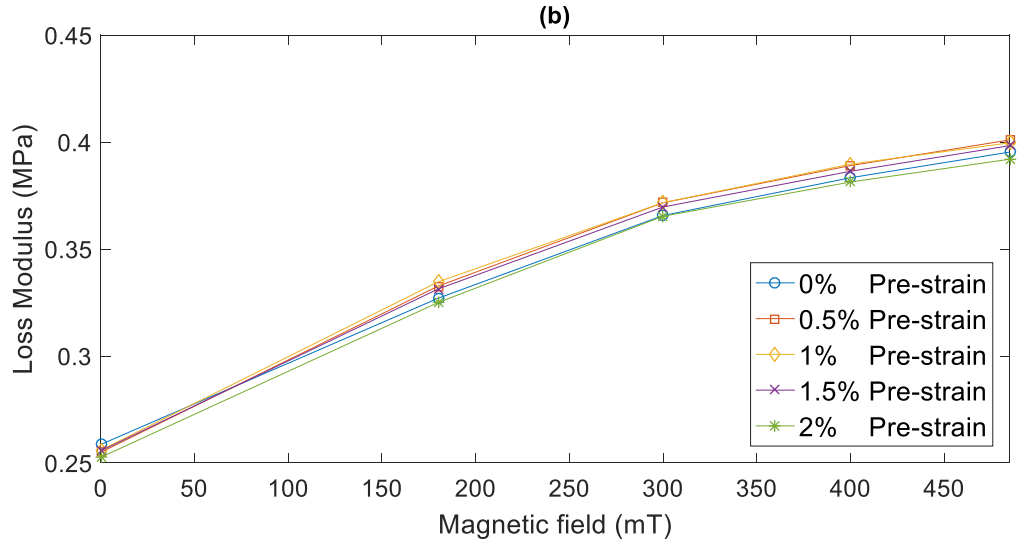

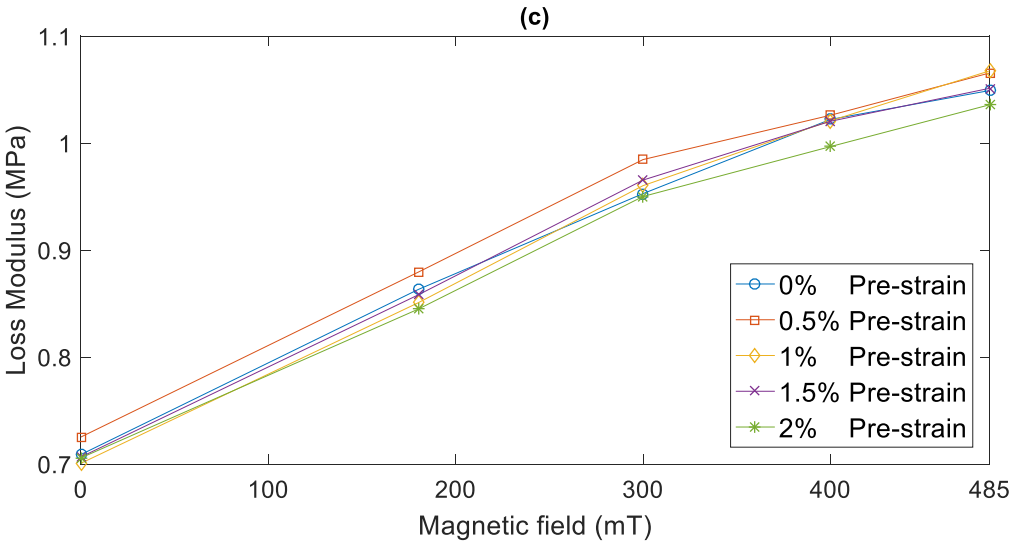

Figure 4.20 Loss modulus of MRE under different magnetic field with 1% strain amplitude at 10 Hz (a) 10% iron particle concentration (b) 30% iron particle concentration (c) 50% iron particle concentration

Figure 4.20 (a)-(c) illustrate the loss modulus of MRE samples with 10%, 30, and 50% iron particle concentrations under different pre-strain amplitudes with magnetic field strengths various from 0 mT to 485 mT. The loss modulus of MRE also increases with the magnetic field strength. The iron particles become more aggregate as an external magnetic field is applied. The friction between the iron particles is increased. This friction between the iron particles generates more energy dissipated which leads to an increase of the loss modulus. There is no clear relationship between pre-strain and magnetic field effect on the loss modulus of MRE obtained. The pre-strain causes a slight loss modulus increase for the 10% iron particle concentration MRE sample. For higher iron particle concentration samples, by increasing the pre-strain amplitude from 1% to 2%, the loss modulus starts to decrease.

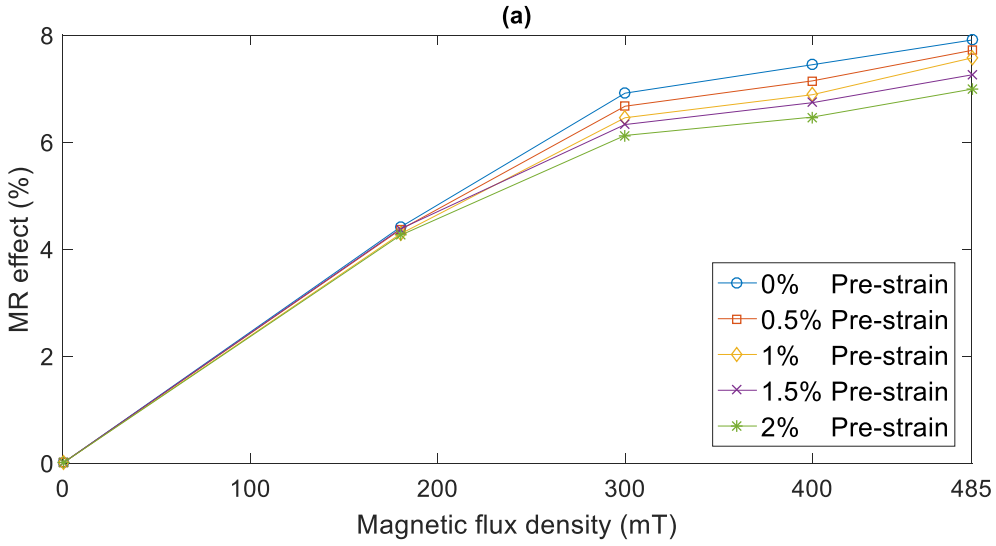

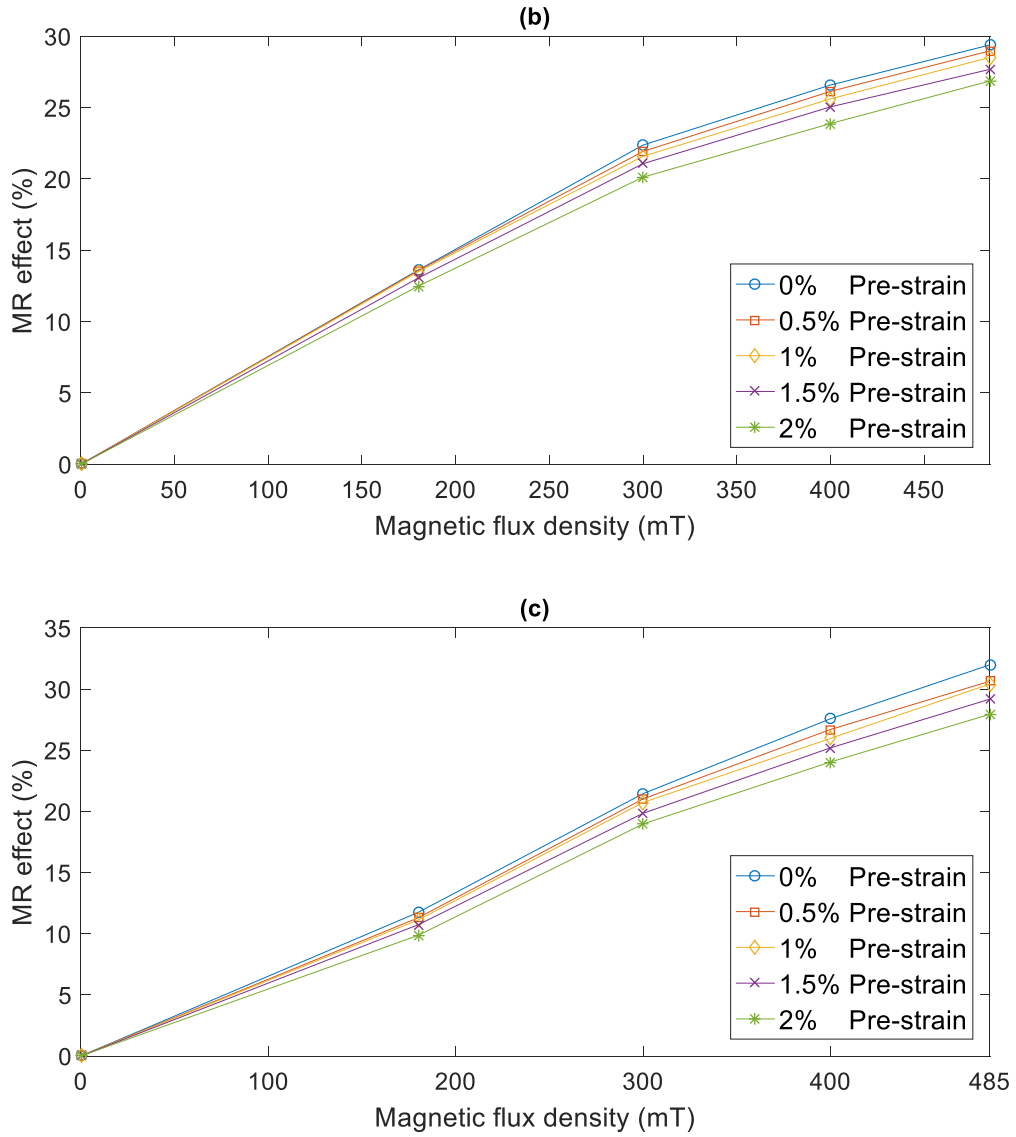

Figure 4.21 MR effect of MRE samples under different magnetic field with 1% strain amplitude at 10 Hz (a) 10% iron particle sample (b) 30% iron particle sample (c) 50% iron particle sample

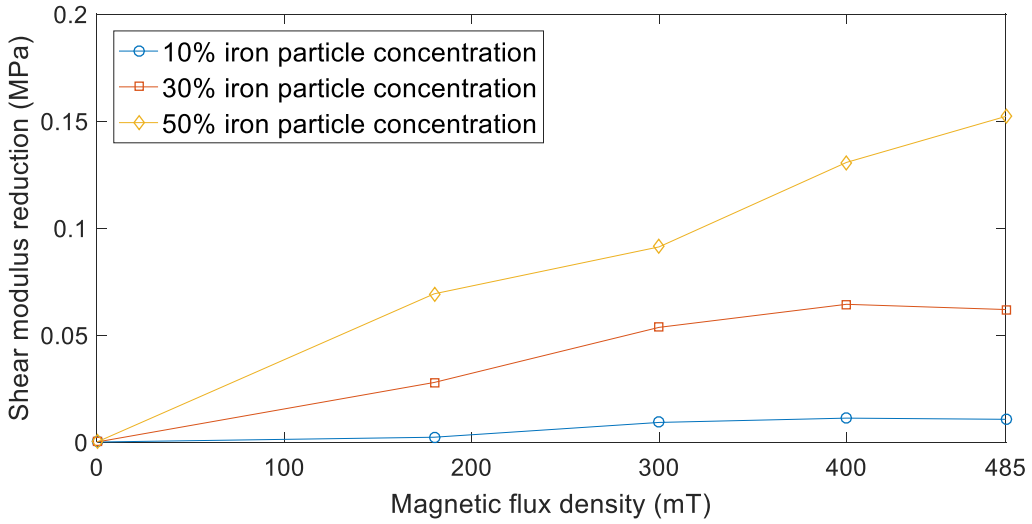

Figure 4.22 Shear modulus reduction due to a 2% pre-strain effect under different magnetic field at 1% strain amplitude, 10 Hz excitation frequency

The dependence of pre-strain on MR effect under different magnetic fields with 10%, 30, and 50% iron particle concentrations can be seen in Figure 4.21. The pre-strain effect causes a reduction of the MR effect. This is mainly dependent on the magnetic interactions between the iron particles are decreased due to the elongation of the magnetic particle chains. The reduction of the MR effect due to a pre-strain is magnified by increasing the magnetic strength field and the iron particle concentration. By increasing the pre-strain amplitude, a further reduction of the MR effect is observed.

Figure 4.22 compares the value of the shear modulus reduction at 2% pre-strain amplitude under different magnetic fields with 10%, 30% and 50% iron particle concentrations. MRE sample with 50% iron particle concentration shows a larger shear modulus reduction by a presence of a pre-strain. A higher iron particle concentration MRE sample forms stronger iron particle chains in. The elongation of the stronger iron particle chain causes to a higher magnetic interaction reduction. Thus, the shear modulus reduction due to a pre-strain is higher for MRE sample with a higher iron particle concentration.

4.6 Coupling effect between strain amplitude and frequency on the dynamic shear properties of MRE

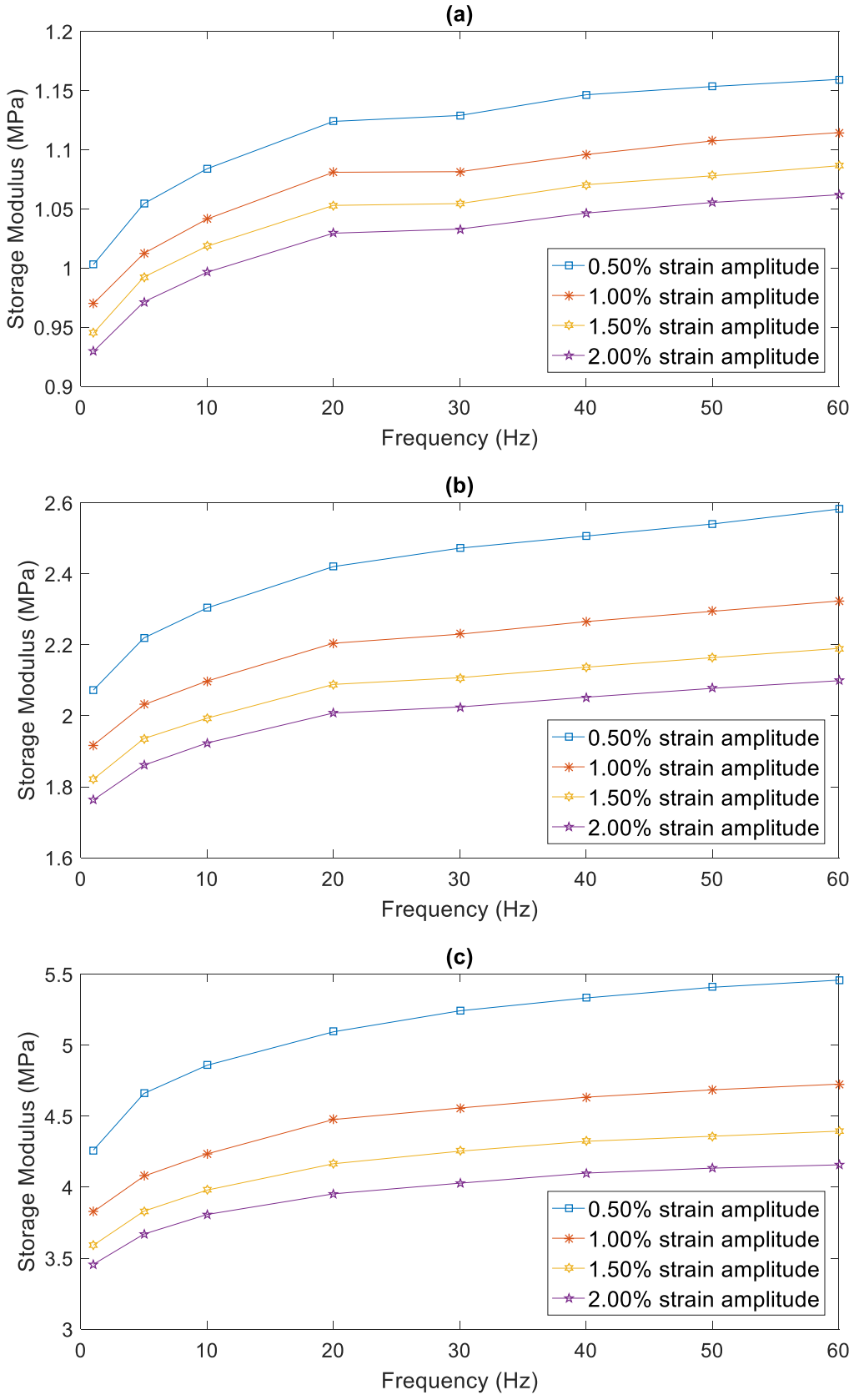

Figure 4.23 Strain amplitude and frequency coupling effect on the storage modulus of MRE at 0 mT magnetic field (a) 10% (b) 30% (c) 50% iron particle concentration MRE sample

Figure 4.23 above illustrates strain amplitude and frequency coupling effect on the storage modulus of MRE samples with different iron particle concentrations. Due to Payne effect, storage modulus demonstrates an obvious reduction as strain amplitude increase. This phenomenon is more noticeable for higher iron particle concentration MRE samples (Figure 4.23 (b) and (c)). In the meantime, storage modulus also increases smoothly as frequency increase. By comparing storage modulus with increase frequency, it is found that the increment of storage modulus by an increasing frequency is higher for lower strain amplitude for all MRE samples with different iron particle concentrations. Then, it is concluded that frequency and strain amplitude have a coupling effect on storage modulus of MRE samples. The increment of the storage modulus for smaller strain amplitude by the increasing frequency is higher comparing with larger strain amplitude.

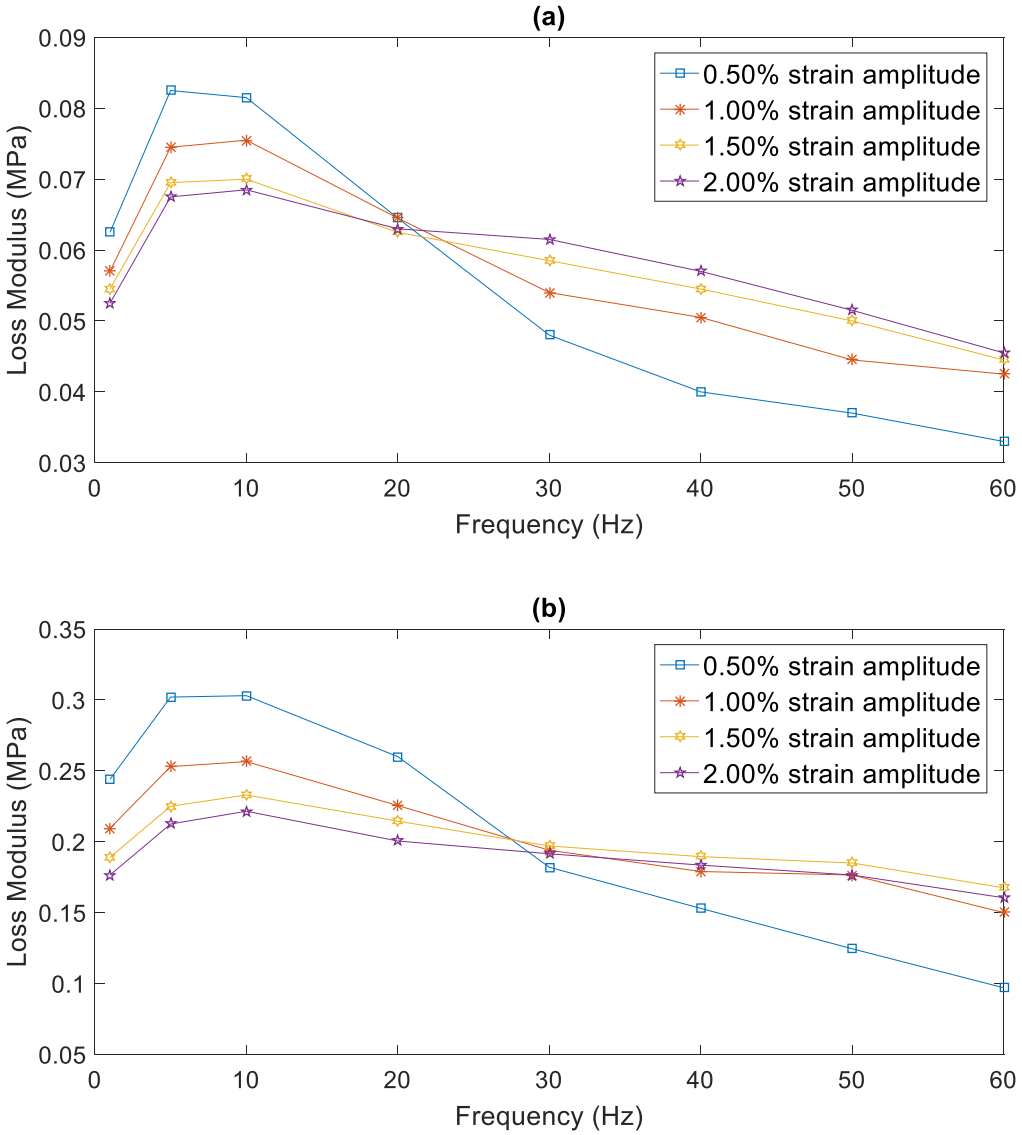

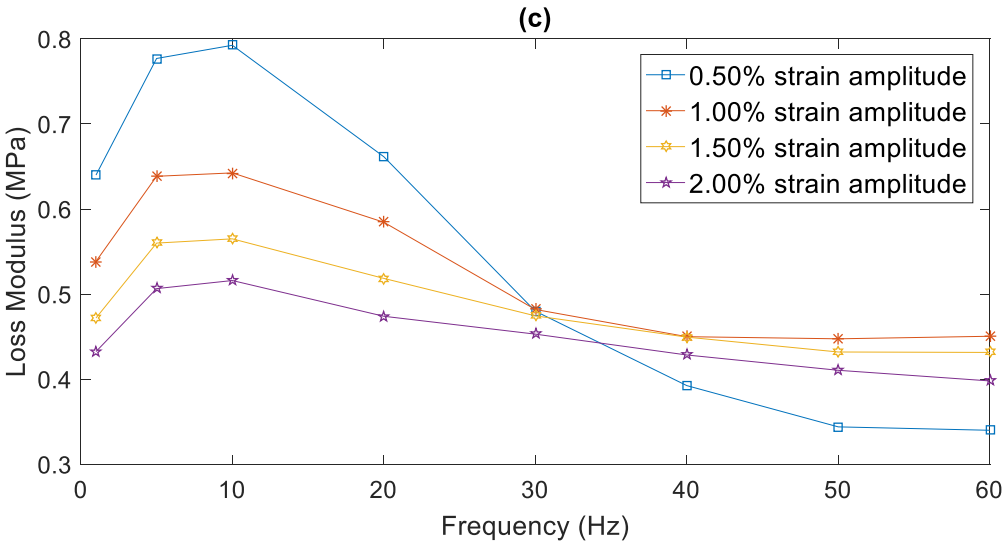

Figure 4.24 Strain amplitude and frequency coupling effect on loss modulus of MRE at 0 mT magnetic field (a) 10% (b) 30% (c) 50% iron particle concentration MRE sample

Figure 4.24 (a)-(c) are the plot of strain amplitude and frequency coupling effect on loss modulus of MRE samples with 10%, 30% and 50% iron particle concentration. The coupling effect between strain amplitude and frequency on loss modulus is more obvious than the effect on storage modulus. Loss modulus decreases with an increasing strain amplitude at a low-frequency region. By increasing the frequency, loss modulus increase to a peak value around 10 Hz and then starts to decrease as the frequency further increase. In the meantime, a decreasing reduction rate of the loss modulus with the increasing strain amplitude is obtained. The loss modulus reduction due to the increasing frequency is faster for smaller strain amplitude. This phenomenon indicates that Payne effect on loss modulus reduction is more obvious for smaller strain amplitude. A crossing point is observed for the loss modulus reduction by the increasing frequency with different strain amplitude. The crossing point is around 20 Hz for the 10% iron particle concentration MRE sample and 30 Hz for the 30% and 50% iron particle concentration MRE samples.

4.7 Coupling effect between strain amplitude and magnetic field on the dynamic shear properties of MRE

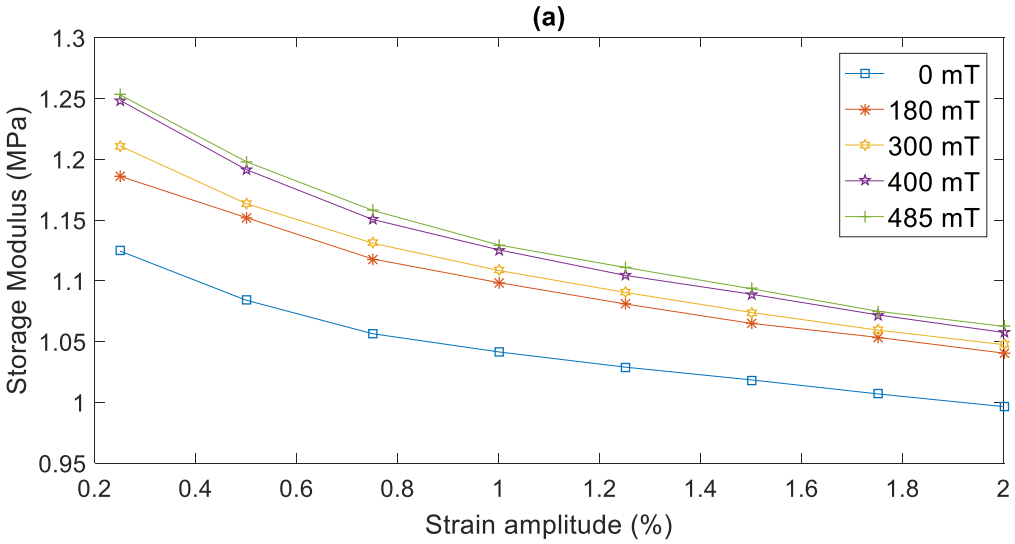

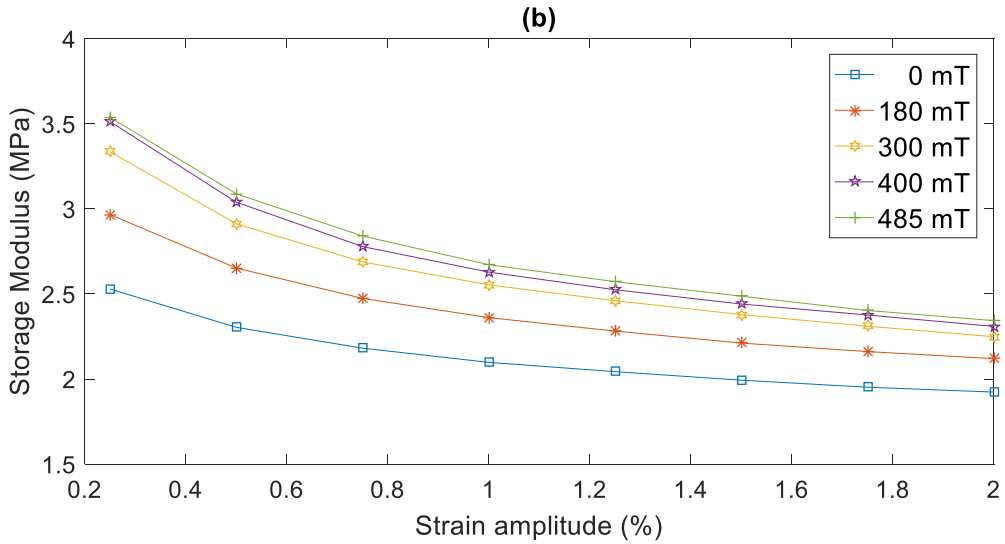

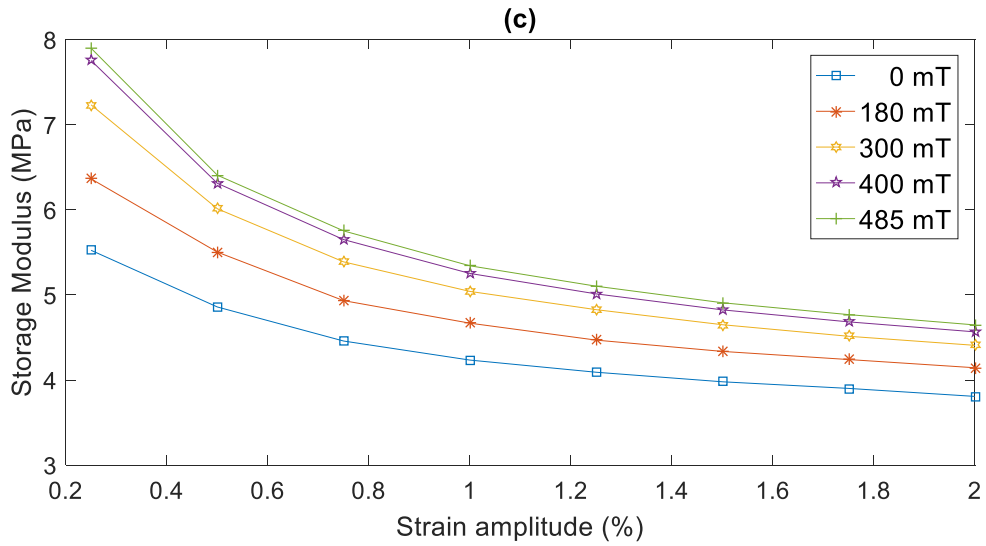

Figure 4.25 Strain amplitude and magnetic field coupling effect on storage modulus of MRE at 10 Hz (a) 10% (b) 30% (c) 50% iron particle concentration MRE sample

Figure 4.25 demonstrates strain amplitude and magnetic field coupling effect on storage modulus of MRE with 10%, 30% and 50% iron particle concentrations. Due to Payne effect, the storage modulus decreases with an increase strain amplitude. The same conclusion is drawn from Chapter 4.4. Storage modulus decreases steeply as strain amplitude increases from 0.25% to 1%. A further increase of strain amplitude leads to a slight decrease of storage modulus. Storage modulus increases with an increase external magnetic flux density. The increment of storage modulus due to a magnetic field is more obvious at small strain amplitude (less than 1%). As strain amplitude increases, the effect of magnetic field to storage modulus subsides for all MRE samples. It is concluded that the coupling between strain amplitude and magnetic field has an effect on storage modulus of MRE.

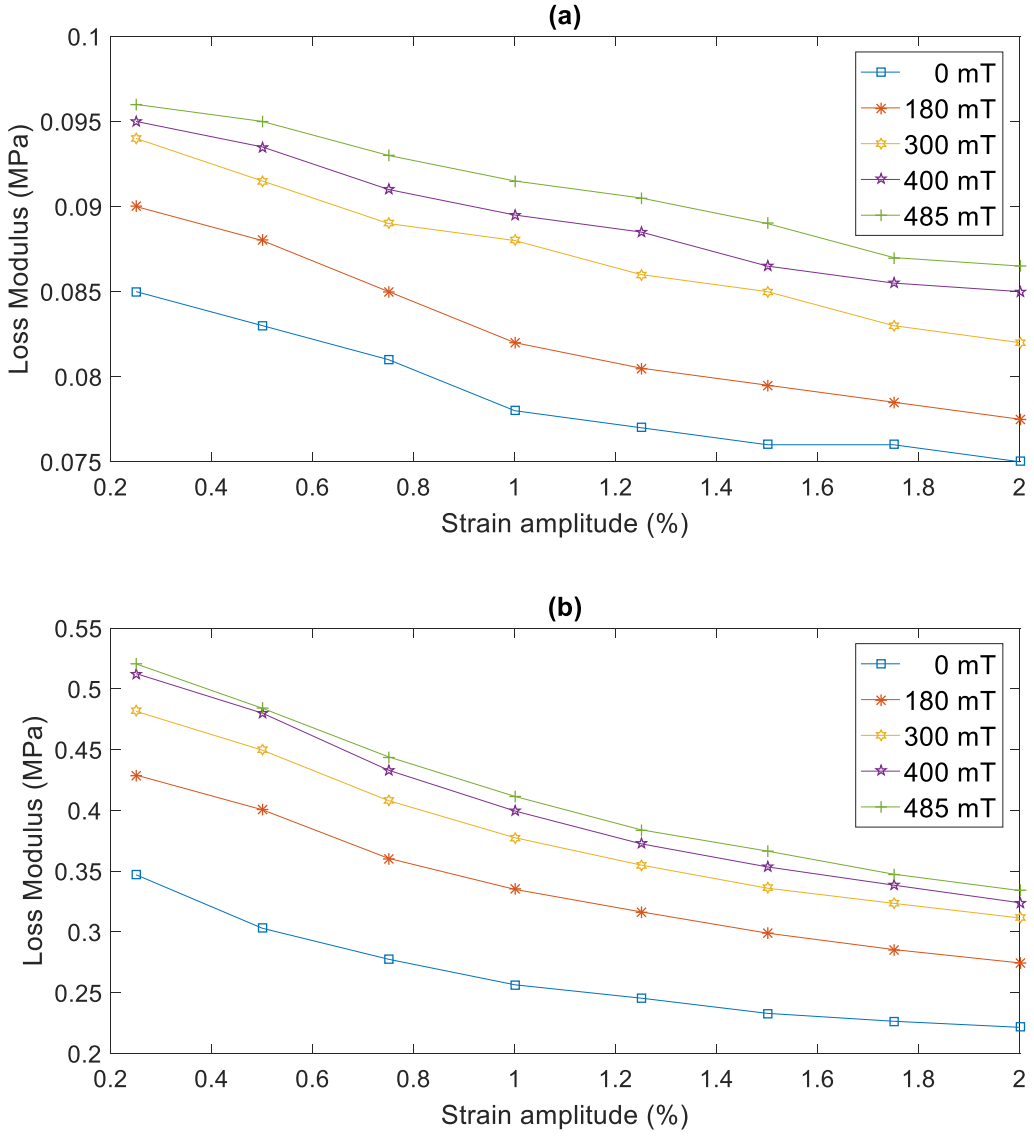

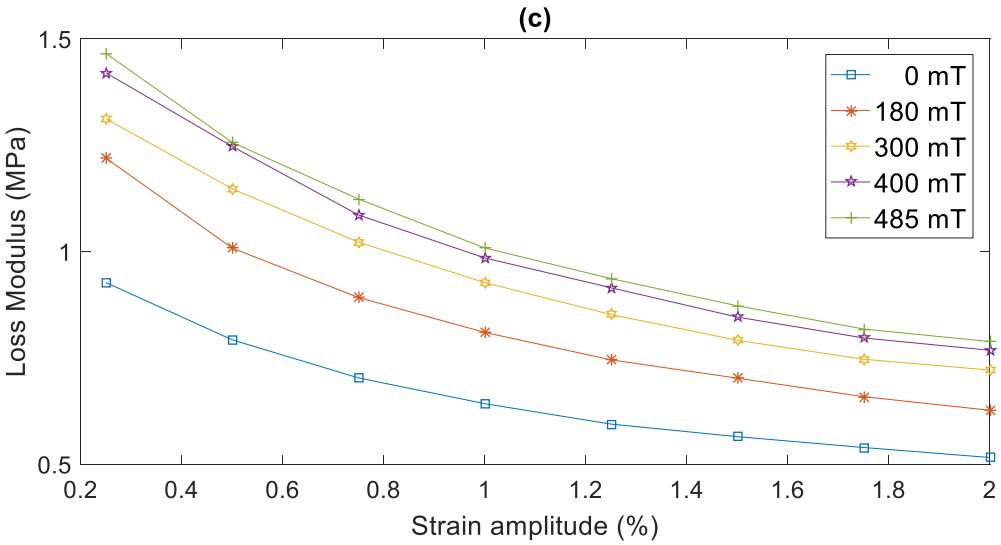

Figure 4.26 Strain amplitude and magnetic field coupling effect on loss modulus of MRE at 10 Hz (a) 10% (b) 30% (c) 50% iron particle concentration MRE sample

Strain amplitude and magnetic field coupling effect on loss modulus of MRE are shown in Figure 4.26. The increment of loss modulus due to an increase magnetic field is more noticeable at smaller strain amplitude. As strain amplitude increases, the effect of the magnetic field to loss modulus of MRE diminishes. This phenomenon is more obvious for the 30% and 50% iron particle concentration MRE samples.

4.8 Coupling effect between frequency and magnetic field on the dynamic shear properties of MRE

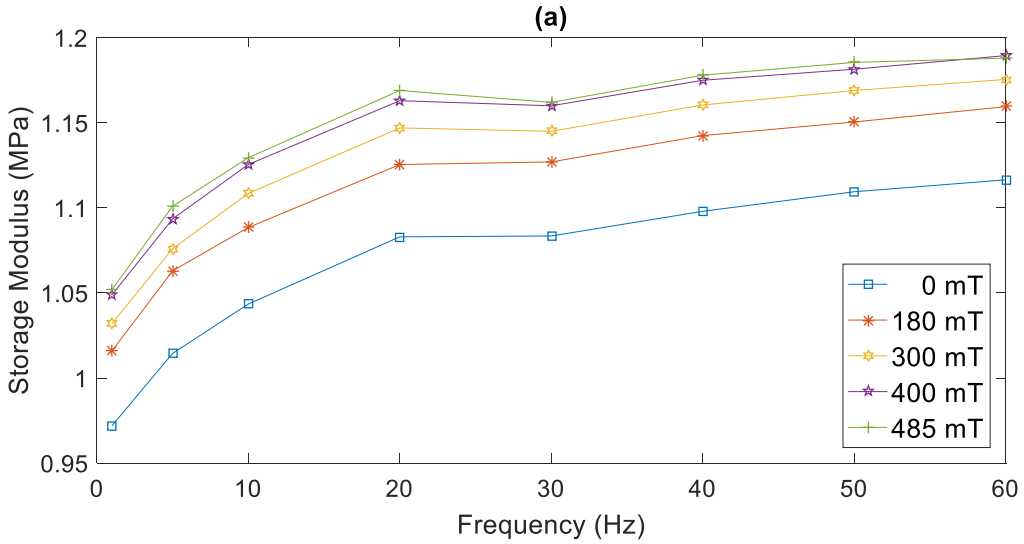

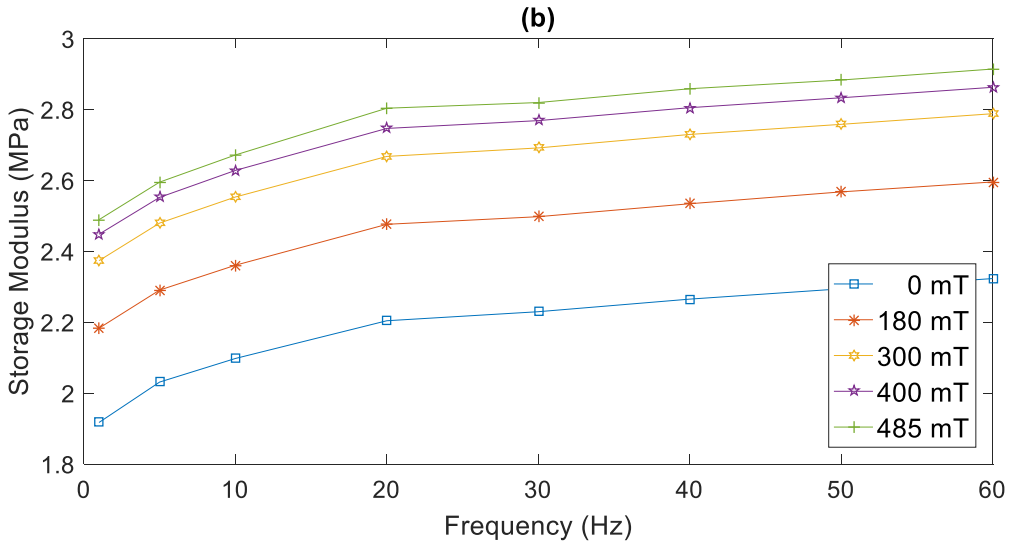

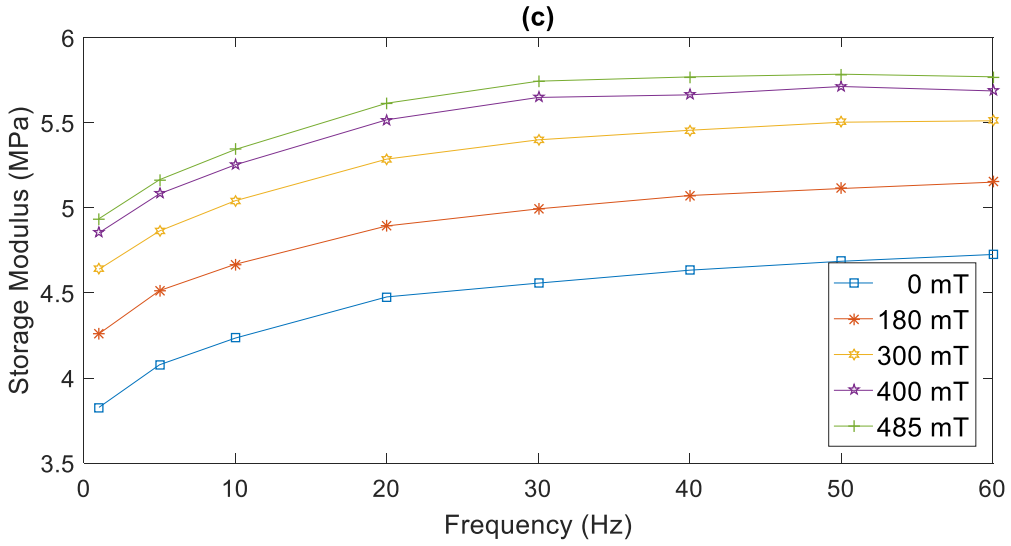

Figure 4.27 Frequency and magnetic field coupling effect on storage modulus of MRE at 1% strain amplitude (a) 10% (b) 30% (c) 50% iron particle concentration MRE sample

Figure 4.27 and Figure 4.28 demonstrate frequency and magnetic field coupling effect on storage modulus and loss modulus of MRE, respectively. By comparing with storage and loss modulus of the 10%, 30% and 50% iron particle samples, it is found that the trend of storage modulus and loss modulus at different frequencies is not affected by an increase magnetic field. The plots of storage modulus and loss modulus are parallel with each other at different magnetic fields. Then, it is concluded that the coupling effect between frequency and magnetic field on MRE dynamic mechanical properties, such as storage modulus and loss modulus is weak and can be neglected.

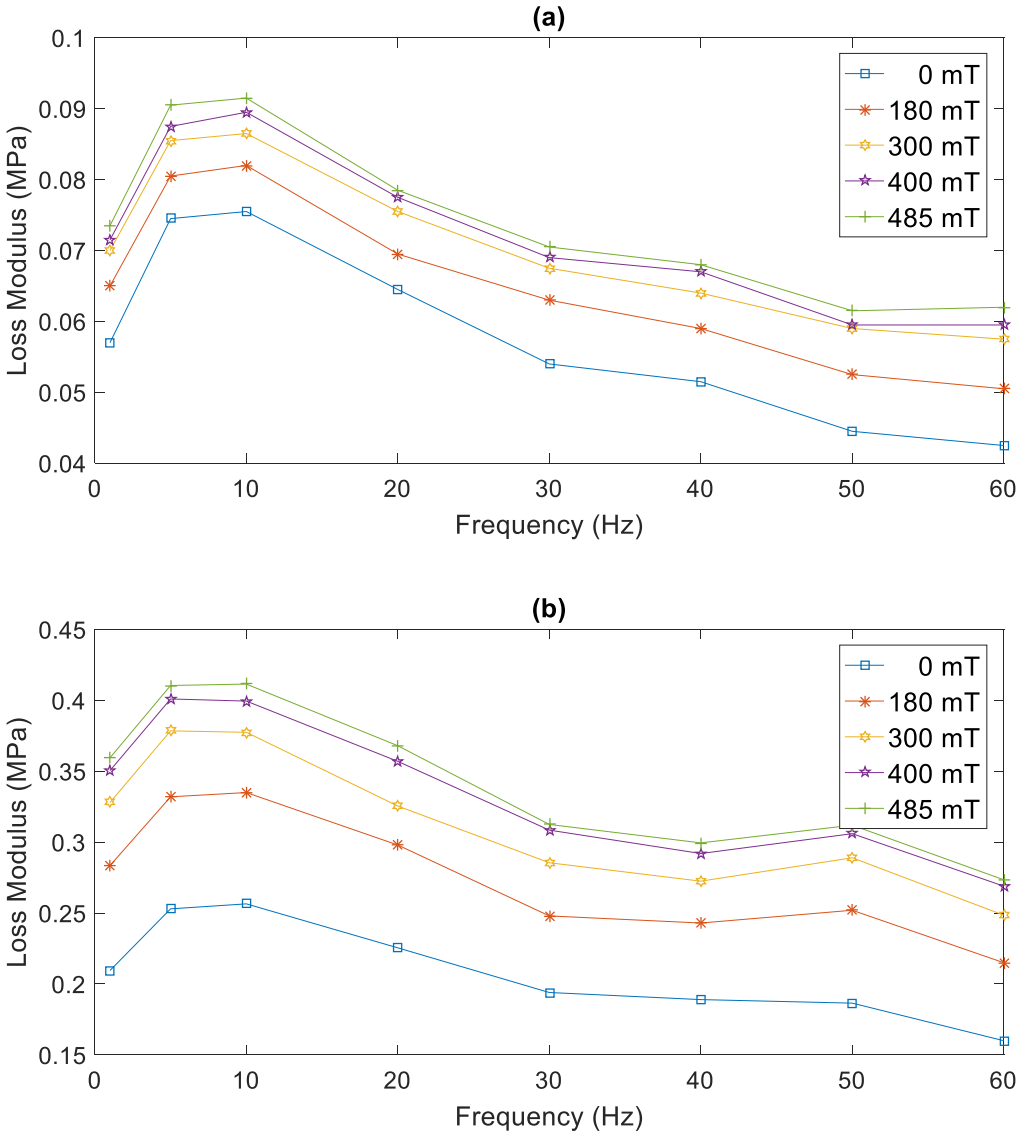

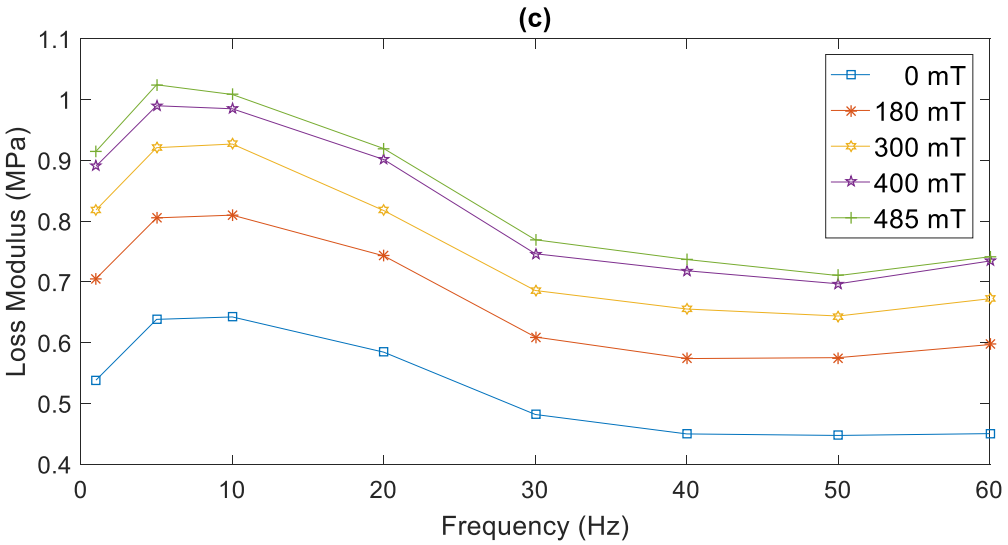

Figure 4.28 Frequency and magnetic field coupling effect on the loss modulus of MRE at 1% strain amplitude (a) 10% (b) 30% (c) 50% iron particle concentration MRE sample

4.9 Experimental error analysis of dynamic shear tests of MRE

For dynamic shear tests of MRE, three groups of MRE samples are used for each test condition. Error bar is used to represent the experiment error of the dynamic shear test of MRE. The equation to calculate the error bar is given in equation 4.2.

$$Error\ Bar = \bar{G} \pm stdDev \qquad \text{Eq. 4.2}$$

Where $\bar{G}$ is the average experiment results (shear storage modulus or shear loss modulus) for each test condition, stdDev is the standard deviation of three groups of MRE samples at this test condition.

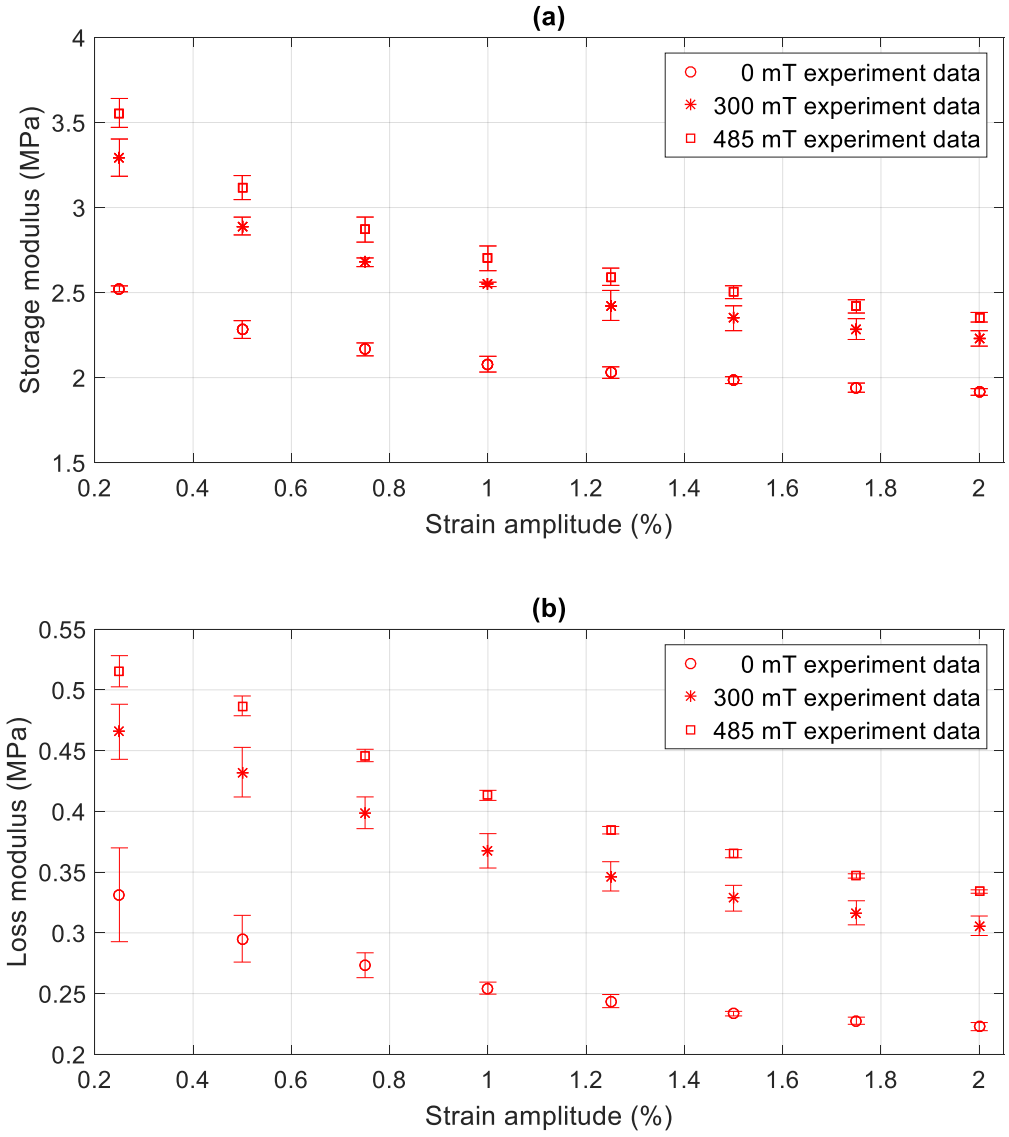

Figure 4.29 Error bar of (a) shear storage modulus and (b) shear loss modulus of 30% iron particle concentration MRE samples at 10 Hz with 0 mT, 300 mT and 485 mT.

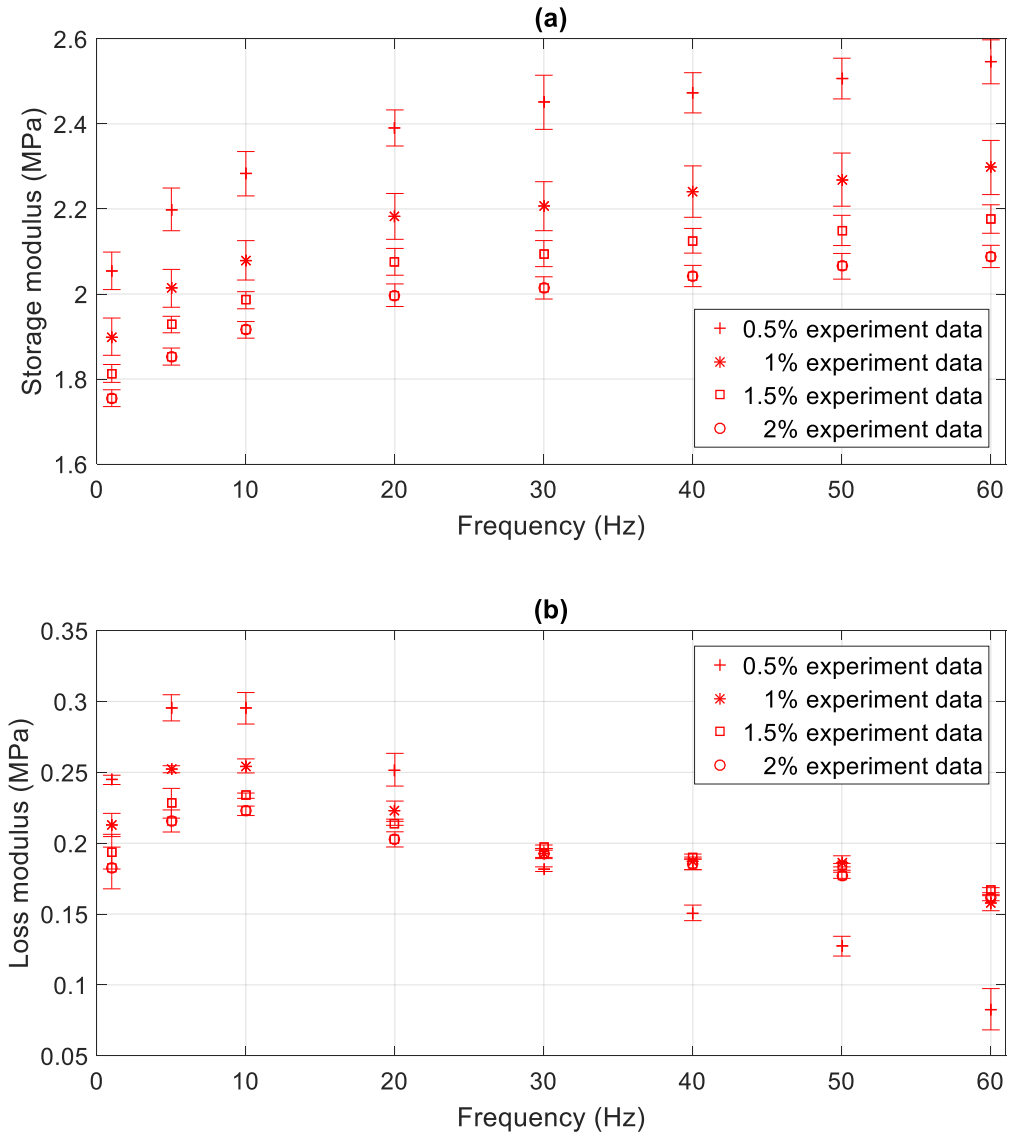

Figure 4.30 Error bar of (a) shear storage modulus and (b) shear loss modulus of 30% iron particle concentration MRE samples at 0.5%, 1%, 1.5% and 2% strain amplitude at 0 mT.

Experiment error of the dynamic shear tests of MRE are presented in figure 4.29 and figure 4.30. The experiment error occurs mainly due to two factors. There are vibration environmental disturbance and sample differences.

Vibration environmental disturbance is another factor that affects the experiment results of MRE shear test. The shear tests of MRE are done by Instron Plus in TSRL LAB in Southampton University. There are many test machines in the TSRL Lab. The operations of other experiment apparatus induce vibration which makes a contribution to the experiment error of MRE.

For MRE samples with same iron particle concentration, there is always difference between each MRE samples. In order to reduce the difference among MRE samples, MRE samples used for shear tests are fabricated at the same time.

It is found that the error of loss modulus is higher than that of storage modulus. The error of experiment results of smaller stain amplitude is also higher. For experiment results with small strain amplitude (0.5%), the stress response of MRE is small. At this time, an environmental disturbance makes a major contribution to the experiment error. As strain amplitude increase, the value of stress response also increases. Then, the effect of an environmental disturbance decrease.

4.10 Summary

This chapter investigates the dependence of the pre-strain to the dynamic shear mechanical properties of MRE under different frequency, strain and magnetic field conditions. The coupling effects of strain amplitude, motion frequency and magnetic flux density are also discussed. The dynamic shear properties considered are shear storage modulus and shear loss modulus. MRE samples are comprised silicone rubber ELASTOSIL 4644 A/B and 9 μm carbonyl iron powder (ALDRICH-44890) and cured at a 260 mT magnetic field. 10%, 30% and 50% iron particle concentrations MRE samples are fabricated. Shear stress relaxation of MRE samples is tested with different magnetic fields, iron particle concentrations and pre-strain amplitudes. It is found that a steady state responds to shear stress is achieved at 40 seconds. Then, a dynamic sinusoidal excitation is applied to MRE samples at a 40-second delay after a pre-strain is added on MRE samples. The dependences of the pre-strain, frequency, stain amplitude and magnetic field and their coupling effects on the dynamic shear properties of MRE are summarized as followed.

- The pre-strain effect on shear storage modulus is different for MRE samples with different iron particle concentrations. For 10% iron particle concentration, the pre-strain induces a decrease on storage modulus. A further decrease of shear storage modulus is observed as pre-strain amplitude continues to increase. For 30% and 50% iron particle concentration samples, shear storage modulus demonstrates a decrease as a pre-strain is applied. As pre-strain amplitude continues to increase, MRE becomes stiffer and shear storage modulus starts to increase. The dependence of pre-strain on shear storage modulus is independent of frequency and strain amplitude. While, a magnetic field induces a magnitude reduction on storage modulus for all MRE samples. This phenomenon is more obvious for MRE samples with higher iron particle concentration.
- The pre-strain effect on shear loss modulus is also different for MRE samples with different iron particle concentrations. Pre-strain leads to an increase of loss modulus for the 10% iron particle concentration MRE. As iron particle concentration increases, loss modulus starts to decrease for large pre-strain amplitude (1.5%-2%). An external magnetic field leads to a decrease of loss modulus. This becomes more obvious for larger pre-strain amplitude and higher iron particle concentration samples. The dependence of pre-strain on shear loss modulus is also independent of frequency and strain amplitude.
- The coupling effect between frequency and strain amplitude is obvious. The increase of storage modulus with increased frequency is higher at lower strain amplitude for all MRE samples. The decrease of loss modulus for lower strain amplitude is higher with increasing frequency.
- The coupling effect between strain amplitude and magnetic field is also noticeable. The increase strain amplitude attenuates the effect of magnetic field. The increase of shear storage modulus and loss modulus is higher for lower strain amplitude under the same magnetic field.

- The coupling effect between the frequency and magnetic field is weak and can be neglected.
- The MR effect is different with dynamic excitation conditions and iron particle concentrations of MRE. The MR effect decreases with the increase strain amplitude and frequency, while increases with an increase magnetic field. The pre-strain leads to a reduction of magnetic induce modulus of MRE. Then, the MR effect is also reduced under a pre-strain condition. The MR effect of the 10% iron particle concentration is the lowest among all MRE samples. The MR effect for the 30% and 50% iron particle concentration MRE samples is almost the same.

Chapter 5: Experiment results of Dynamic Compression Properties of MRE

5.1 Introduction

In this chapter, experiment results of the dynamic compression tests of MRE samples are shown. Firstly, the stress relaxation of MRE under a constant compression strain is discussed. Then, pre-strain effects on the dynamic compression mechanical properties of MRE coupling with frequency, strain amplitude and magnetic field are presented. Finally, coupling effects between strain amplitude, frequency and magnetic field are discussed.

5.2 Stress relaxation of MRE under a constant compression strain

The stress relaxation phenomenon of MRE samples under a constant compression strain is plotted in Figure 5.1. For all stress relaxation of compression strain tests, an initial compression strain is applied to MRE samples within 2 second. Then, the compression strain is held for a fixed value and the relaxation stress of MRE sample is recorded by the load cell of Instron plus.

Stress relaxation of MRE samples under constant compression strain has a non-linear relationship corresponding to relaxation time. A sharp decline of relaxation stress is observed at the initial 4 seconds. Then, a slow and continuous reducing of stress is obtained. As a constant strain is maintained for more than 40 seconds, the response stress decays to a steady state and remains unchanged. There are three parameters pre-strain amplitude, iron powder concentration and magnetic field strength investigated to analyse the stress relaxation properties of MRE under a constant compression strain.

Figure 5.1 (a) demonstrates the effect of magnetic field on compression stress relaxation of the 30% iron particle MRE sample. An increase of magnetic field strength leads to an increase of the maximum compression stress and stress response at the steady-state of MRE. From Table 5.1, it is found that stress reduction rate for MRE sample with no magnetic field is slight higher. Figure 5.1 (b) presents strain amplitude effect on the stress relaxation of MRE. By increasing the strain amplitude, a significant magnitude increment of the maximum stress and steady-state response stress is observed. Table 5.2 shows that an increase of compression strain amplitude induces a higher stress relaxation of MRE. In the meantime, the stress reduction rates of MRE samples with different compression strains are almost the same. Time required to achieve a steady state pre-strain condition is 40 seconds. Figure 5.1 (c) shows the effect of iron particle concentrations on the stress relaxation of MRE. Compression stress relaxation of MRE samples are compared with 10%, 30% and 50% iron particle concentrations. The maximum stress and stress at a steady state increase markedly by

increasing the concentration of iron particle. Table 5.3 indicates that by increasing iron particle concentration of MRE samples, a higher compression stress relaxation is obtained. Stress relaxation rate for a higher iron particle sample is also higher.

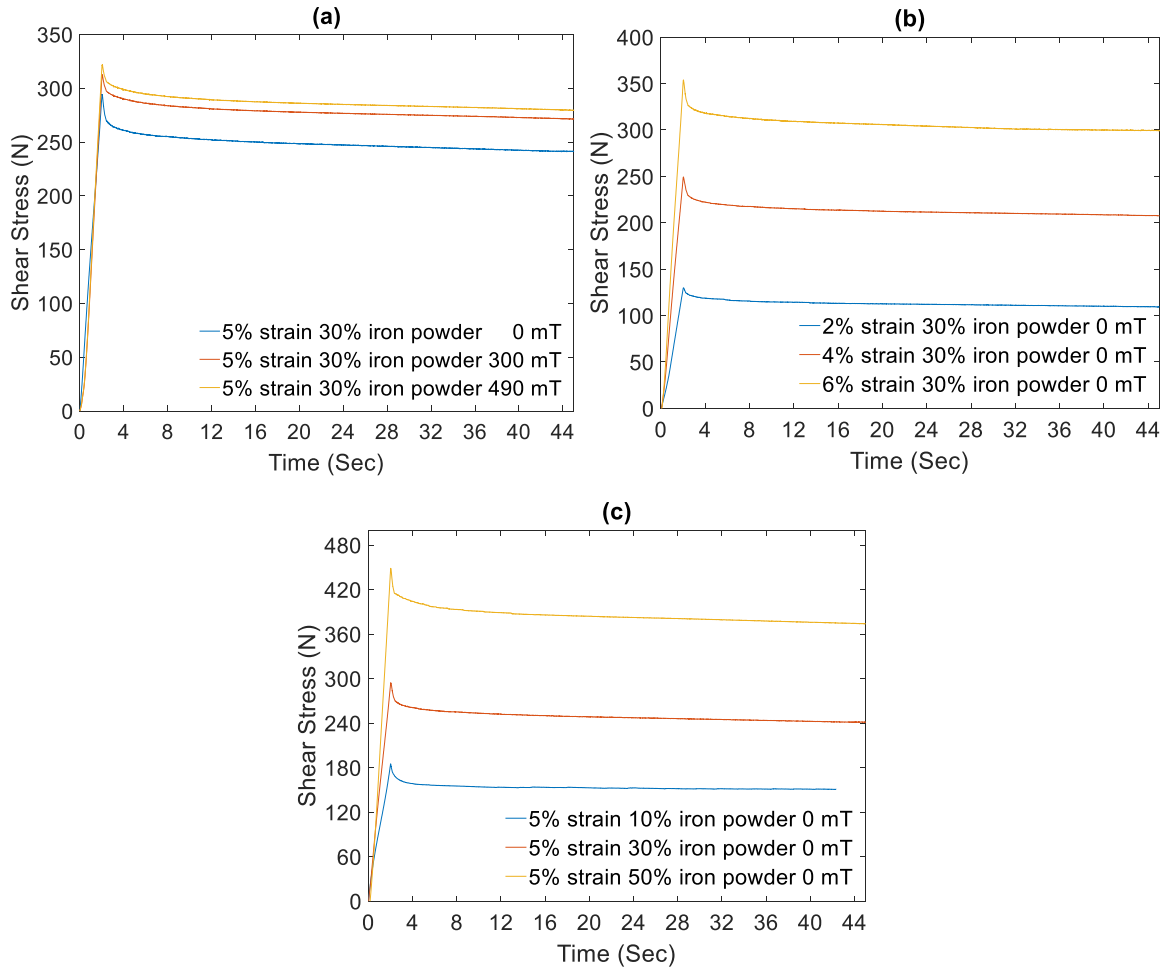

Figure 5.1 Stress relaxation of MRE (a) 5% pre-strain amplitude for samples with 30% iron powder volume percentage under 0, 300 and 490 mT magnetic field strength (b) 2%, 4% and 6% pre-strain amplitude with 30% iron powder under 0 mT magnetic field strength (c) 5% pre-strain amplitude for samples with 10%, 30% and 50% powder volume percentage under 0 mT magnetic field strength

Table 5.1 Stress response of 30% iron particle MRE at 5% compression strain under different magnetic fields

Magnetic field (mT)	Maximum Stress (N)	Stress at 20s (N)	Stress at 30s (N)	Stress at 40s (N)	Stress Reduction rate (%)
0	291.74	248.29	245.46	244.38	16.19
300	312.37	277.64	274.24	273.85	12.23
490	321.74	285.97	282.44	281.87	12.39

Table 5.2 Stress response of 30% MRE under 0 mT magnetic field with different compression strains

Compression Strain amplitude (%)	Maximum Stress (N)	Stress at 20s (N)	Stress at 30s (N)	Stress at 40s (N)	Stress Reduction rate (%)
2	129.82	112.57	111.17	110.89	14.58
4	249.15	212.23	209.53	208.80	16.19
6	353.55	305.72	301.03	299.87	15.18

Table 5.3 Stress response of MRE at constant strain under 0 mT magnetic field with different iron particle concentrations

Iron powder concentration (%)	Maximum Stress (N)	Stress at 20s (N)	Stress at 30s (N)	Stress at 40s (N)	Stress Reduction rate (%)
10	183.69	152.59	151.58	158.89	13.50
30	291.74	248.29	245.46	244.38	16.19
50	450.31	383.87	377.96	375.81	16.54

It can be concluded that an increase magnetic field or compression strain induces an increment of the maximum compression stress. A higher iron particle concentration leads to a higher stress reduction for a same compression strain. A steady-state stress response is observed as a compression strain is maintained for 40 seconds. In order to eliminate the stress relaxation effect on the dynamic properties of MRE, at least 40 second is required to enable MRE to approach a stable pre-strain condition.

5.3 Pre-strain effect on the dynamic compression properties of MRE under different frequencies

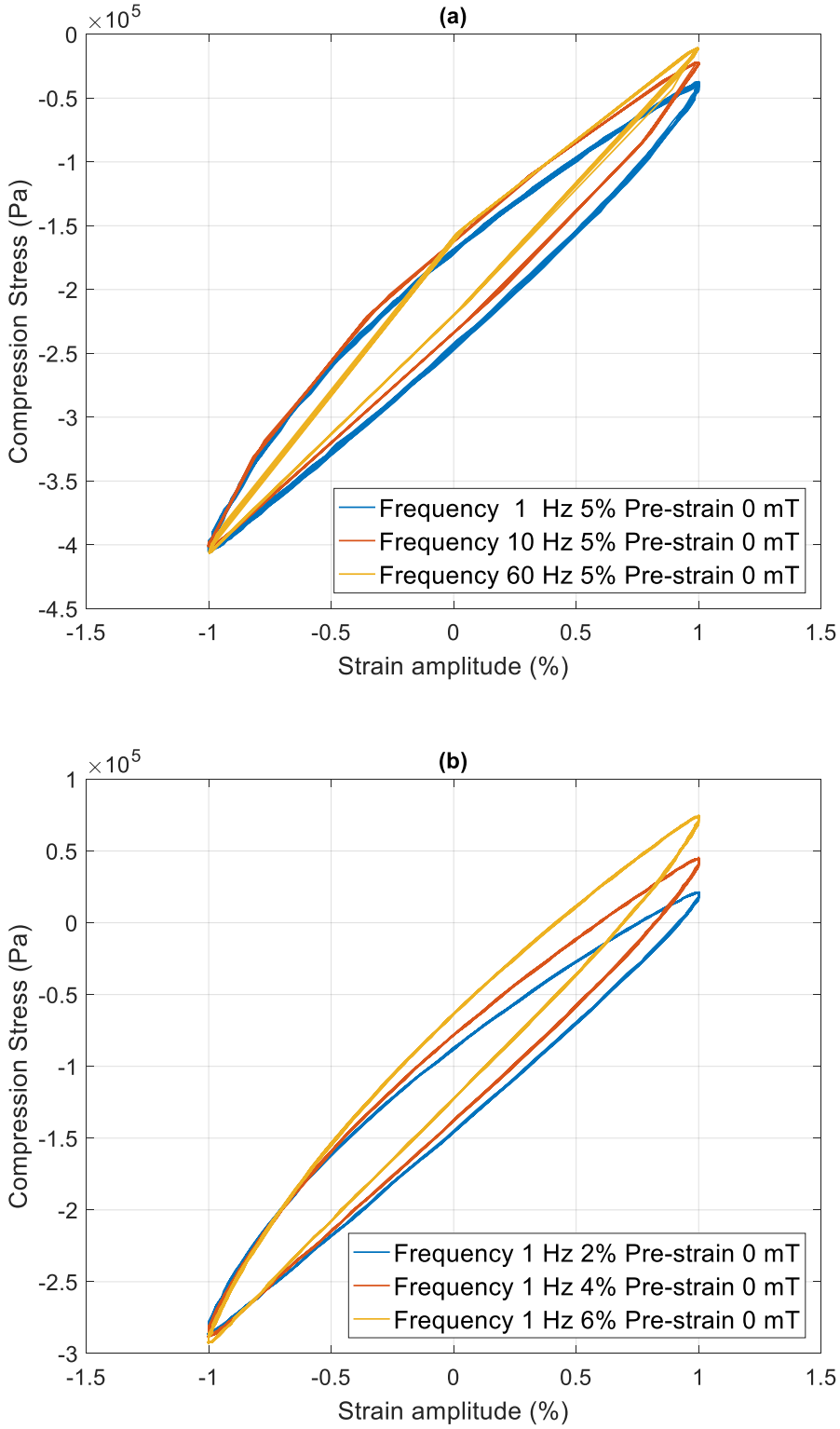

Figure 5.2 Stress-strain hysteresis curve plot of the 30% iron particle concentration MRE (a) 1,10,60 Hz frequency, 5% pre-strain condition, 0 mT magnetic flux density, (b) 1 Hz frequency, 2%,4% and 6% pre-strain condition, at 0 mT magnetic flux density.

Figure 5.2 (a) shows stress-strain hysteresis curves of 30% iron particle concentration MRE samples under dynamic compression load with different frequencies and 1% strain amplitude at 0 mT magnetic flux density. Figure 5.2 (b) illustrates compression stress-strain curves of MRE samples with different compression pre-strains at 1 Hz motion frequency, 1% strain amplitude at 0 mT magnetic flux density. The complex modulus of MRE is calculated as the slope of stress to strain. Figure 5.2 (a) illustrates that by increasing frequency, a higher stress response is achieved. It is concluded that compression complex modulus increases gradually with frequency which is in accord with the shear test results (Figure 4.2 (a)). Figure 5.2 (b) indicates that the slope of the stress to strain increases steadily as a compression pre-strain increases. This is means that complex modulus of MRE increases with an increase compression pre-strain.

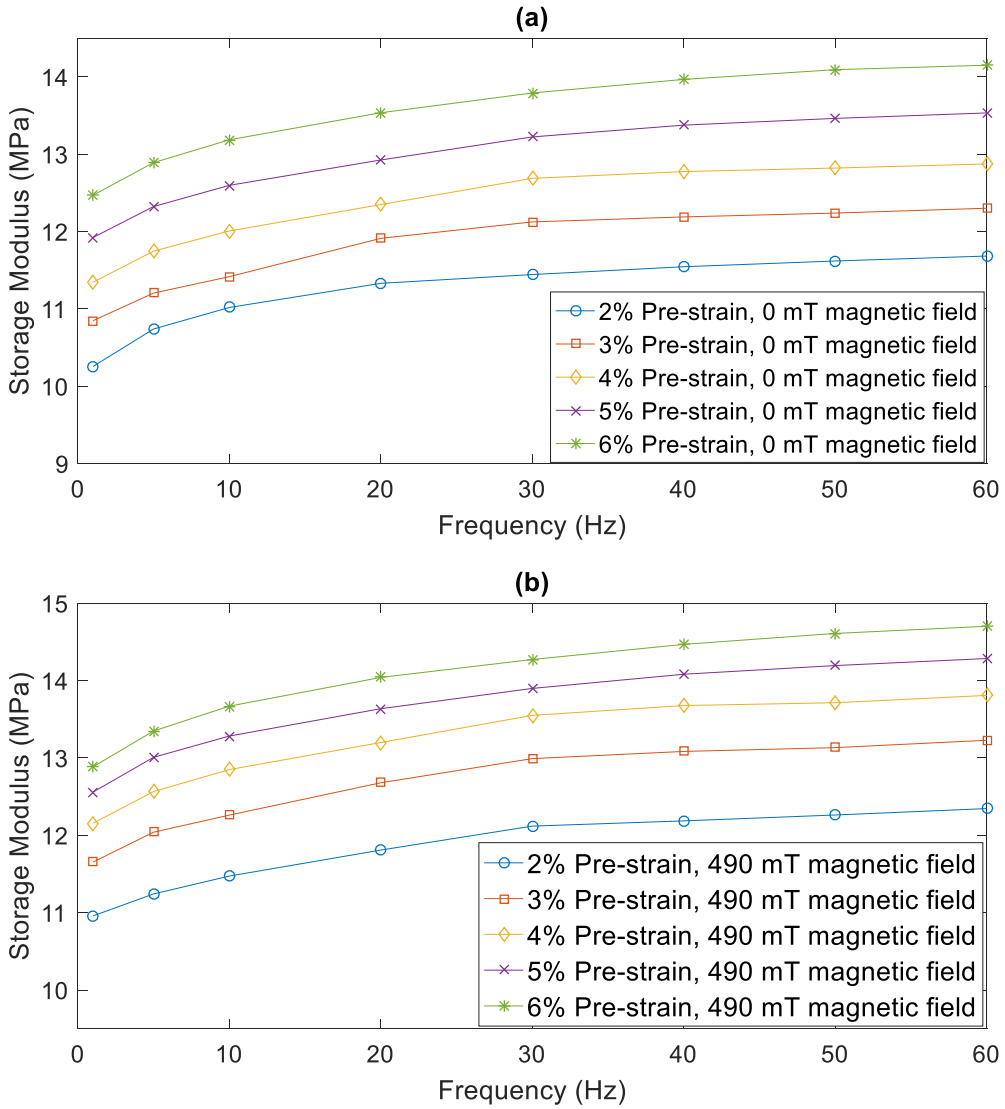

Figure 5.3 Compression storage modulus of MRE with 10% iron powder under different pre-strain amplitude with 1% strain amplitude (a) under 0 mT magnetic field (b) under 490 mT magnetic field

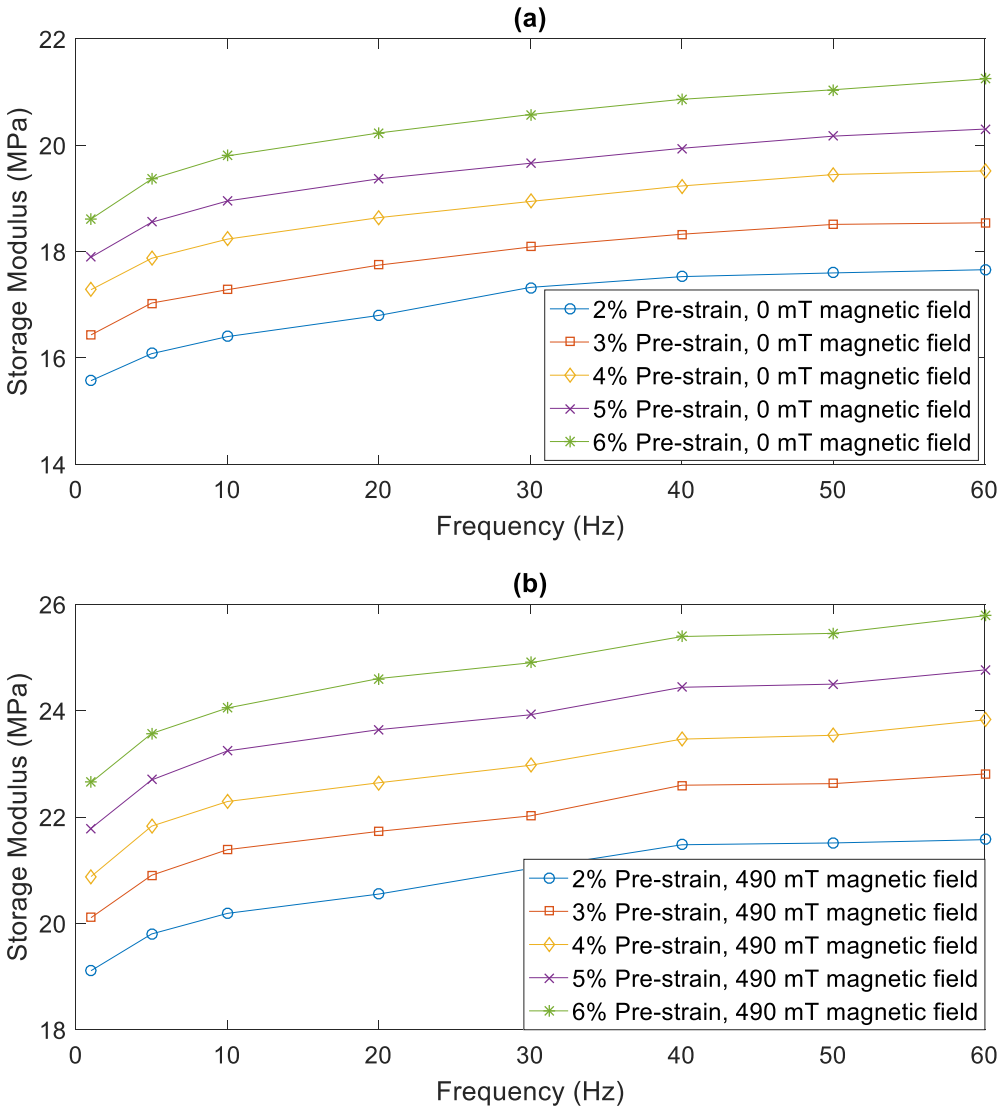

Figure 5.4 Compression storage modulus of MRE with 30% iron powder under different pre-strain amplitude with 1% strain amplitude (a) under 0 mT magnetic field (b) under 490 mT magnetic field

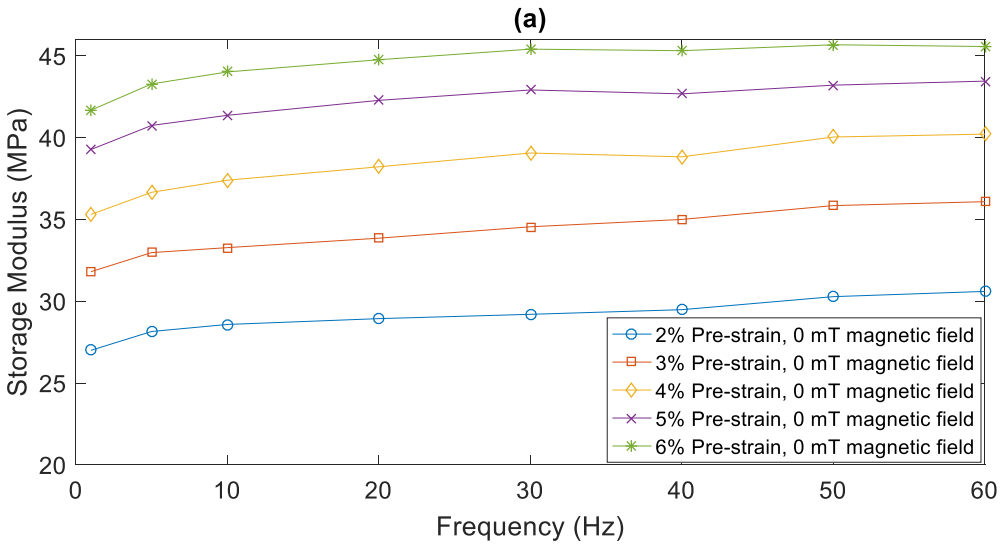

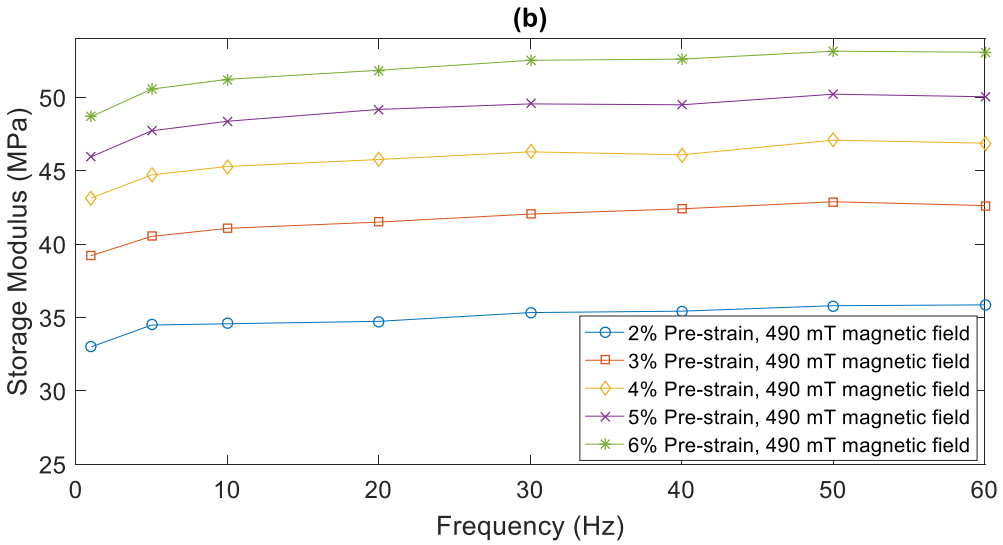

Figure 5.5 Compression storage modulus of MRE with 50% iron powder under different pre-strain amplitude with 1% strain amplitude (a) under 0 mT magnetic field (b) under 490 mT magnetic field

Figure 5.3-5.5 demonstrate compression pre-strain and frequency coupling effect on the dynamic compression storage modulus of MRE. The strain amplitude is set to 1% and two magnetic field strengths 0 mT and 490 mT are used for frequency sweep tests. Compression storage modulus increases with frequencies from 1 Hz to 60 Hz for all MRE samples with different iron particle concentrations. MRE samples become stiffer at a higher excitation frequency. This phenomenon is also observed for MRE with shear tests (Figure 4.3-4.5). A steady increment of compression storage modulus is observed as frequency increase from 1 Hz to 10 Hz. Then, a slow and continuous increase of storage modulus at a decrease rate is achieved for further frequency increase. By increasing iron particle concentration of MRE, compression storage modulus increases significantly.

It is clearly seen that a compression pre-strain induces a steady increase of storage modulus of MRE samples with different iron particle concentrations. For the 10% iron particle concentration MRE samples (Figure 5.3 (a)), the plots of storage modulus are parallel with each other. The gaps between the adjacent plots are almost the same. Then, it is concluded that for the 10% iron particle concentration MRE, as compression pre-stain amplitude increases from 2% to 6%, a linear increment of the compression storage modulus is observed with frequency from 1-60 Hz. The dependence of compression pre-strain on storage modulus of MRE is independent of frequency. The coupling effect between compression pre-strain and frequency is weak and can be neglected. The same conclusion can be drawn for MRE samples with 30% iron particle concentration (Figure 5.4 (a)). For MRE samples with 50% iron particle concentration, as compression pre-strain increases from 5% to 6%, the increment of storage modulus subsides. This means that, storage modulus no longer demonstrate a linear increase due to pre-strain.

Figure 5.3 (b) –figure 5.5 (b) illustrate the effect of compression pre-strain on the dynamic storage modulus of MRE with different frequencies at 490 mT magnetic field. An external magnetic field

induces an increment of storage modulus. Meanwhile, the trend of storage modulus remains unchangeable by the effect of magnetic field.

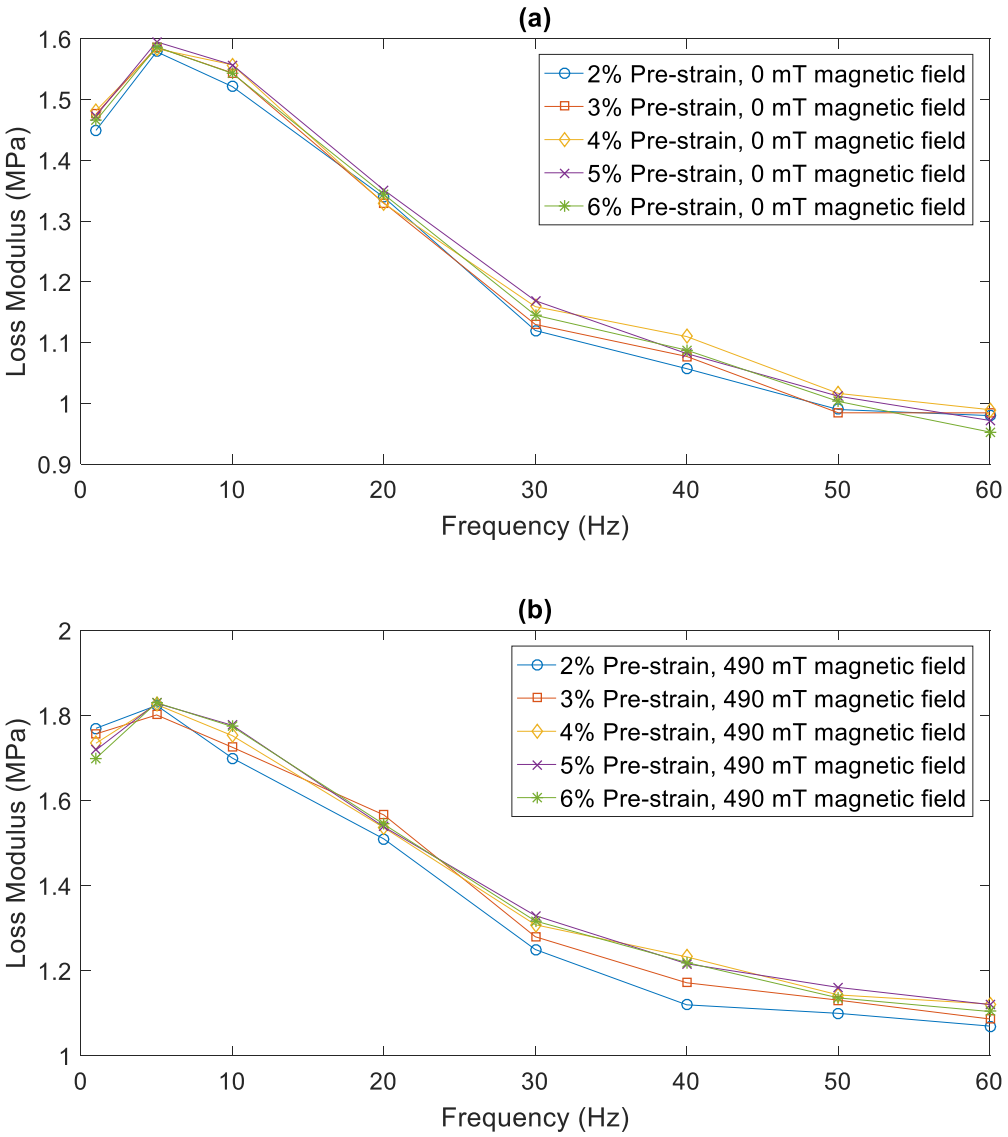

Figure 5.6 Compression loss modulus of MRE with 10% iron powder under different pre-strain amplitude with 1% strain amplitude (a) under 0 mT magnetic field (b) under 490 mT magnetic field

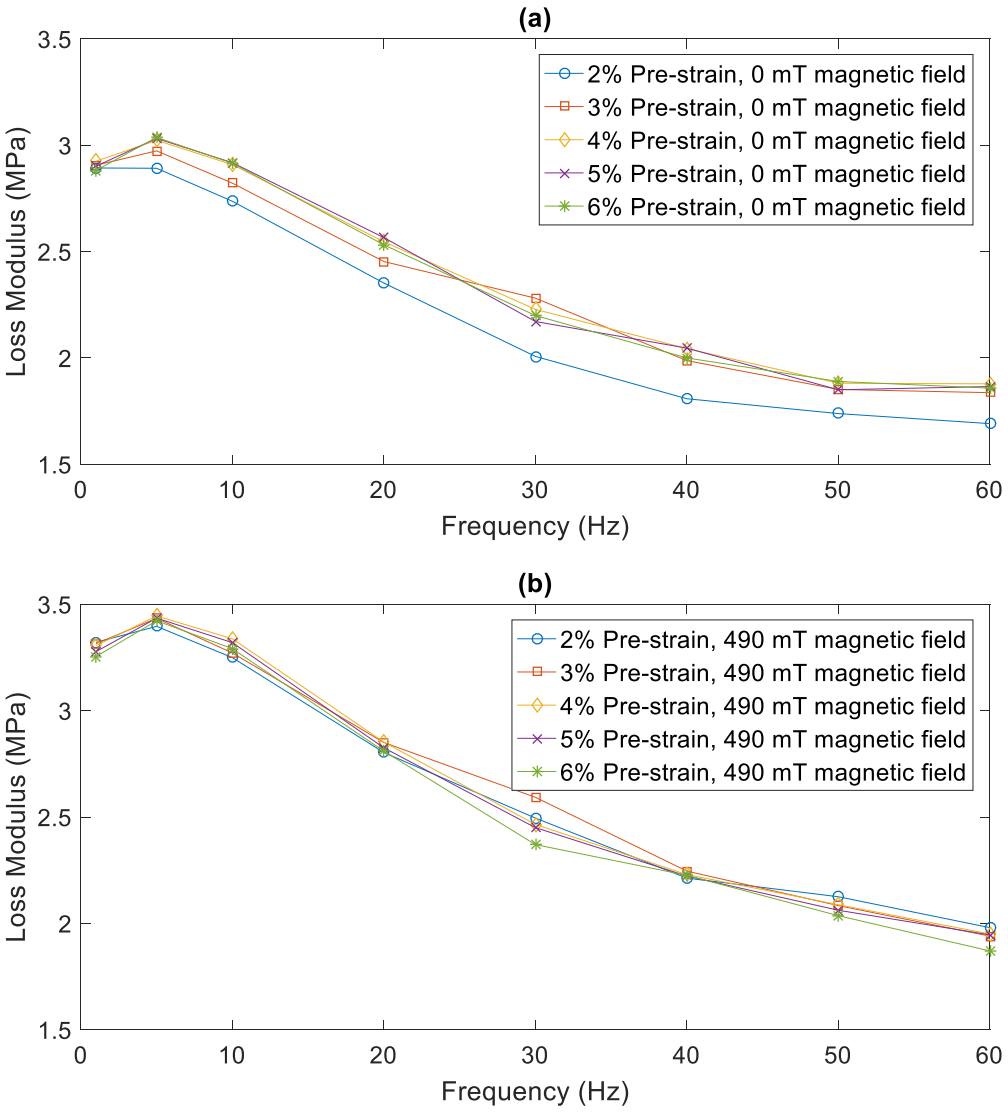

Figure 5.7 Compression loss modulus of MRE with 30% iron powder under different pre-strain amplitude with 1% strain amplitude (a) under 0 mT magnetic field (b) under 490 mT magnetic field

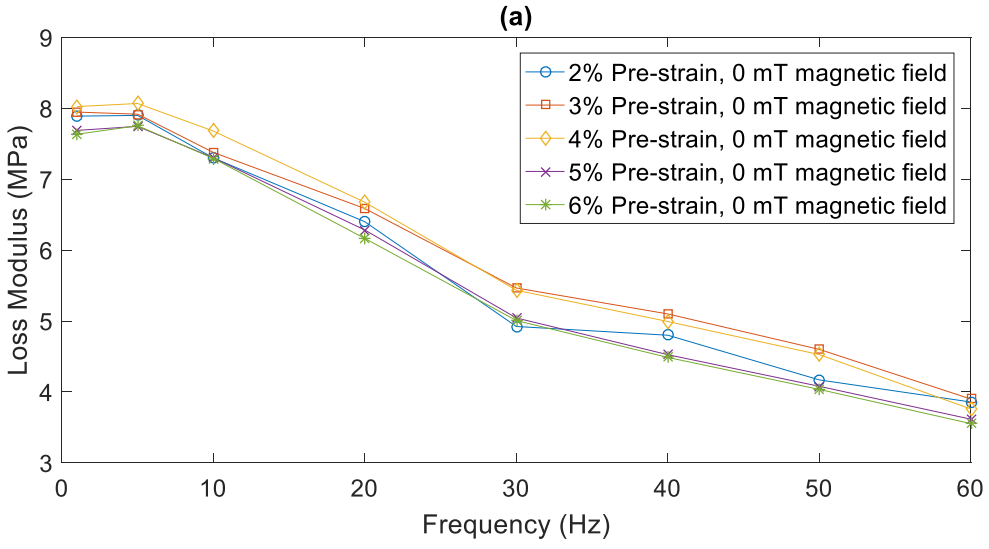

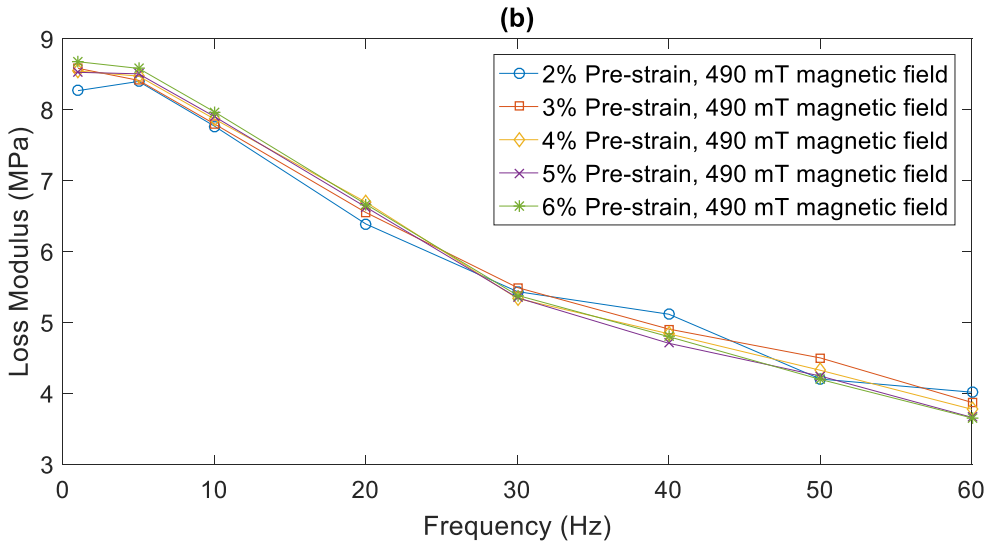

Figure 5.8 Compression loss modulus of MRE with 50% iron powder under different pre-strain amplitude with 1% strain amplitude (a) under 0 mT magnetic field (b) under 490 mT magnetic field

Figure 5.6-5.8 illustrate compression pre-strain and frequency coupling effect on the dynamic compression loss modulus of MRE samples with 1% strain amplitude at two magnetic field strengths 0 mT and 490 mT. For MRE samples with different iron particle concentrations, loss modulus increases with frequency and reaches a maximum value around 5 Hz. Then, loss modulus starts to decrease as frequency further increases. This phenomenon is also observed for MRE samples with shear test. The dependence of frequency on loss modulus of MRE is explained in Section 4.3. The frequency to achieve the maximum loss modulus is around 5 Hz for all MRE samples with compression test which is slightly lower comparing with MRE samples with shear test. Therefore, it is concluded that the frequency to achieve the maximum loss modulus is largely dependent on matrix material selection and the dynamic shear or compression deformation also has an impact on frequency to achieve the maximum loss modulus.

Compression pre-strain effect on loss modulus is not obvious comparing with that of storage modulus. The trend of loss modulus with different compression pre-strains with an increase frequency is the same. For MRE samples with 10% and 50% iron particle concentrations, loss modulus varies slightly as compression pre-strain amplitude increases from 2% to 6%. For MRE sample with 30% iron particle concentration, an increment of loss modulus demonstrates is observed at compression pre-strain increases from 2% to 3%. Then, there is no noticeable increase of loss modulus as compression pre-strain further increases.

An external magnetic field induces an increase of loss modulus (Figure 5.6 (b) –Figure 5.8 (b)). The dependent of frequency on loss modulus remains the same. There is no obvious variation of loss modulus observed by the effect of compression pre-strain under a magnetic field. To conclude, the coupling effect between frequency and compression pre-stain on the loss modulus is small and can be neglected.

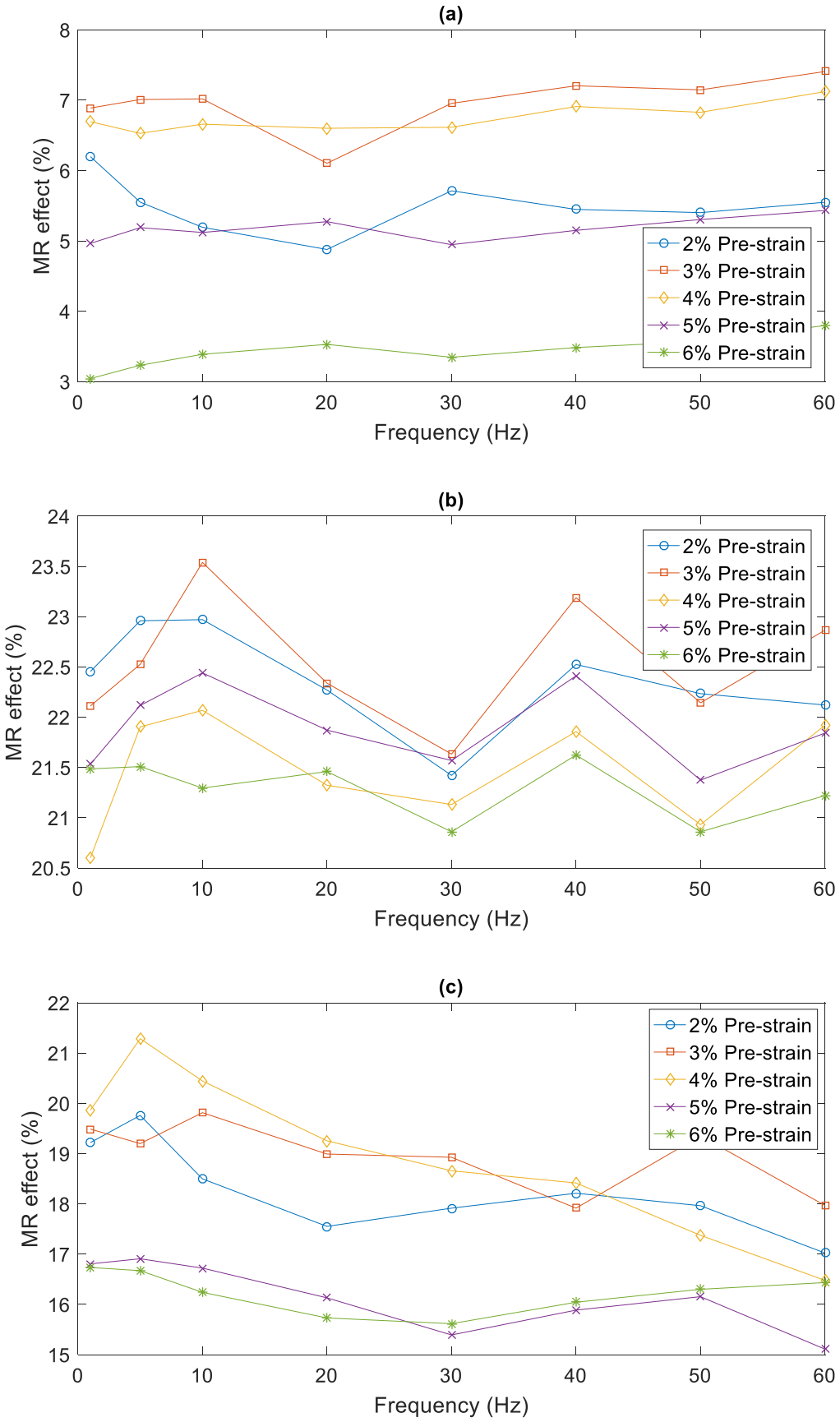

Figure 5.9 MR effect of MRE samples under different compression pre-strain amplitude with 1% strain amplitude at 490 mT magnetic field (a) 10% iron particle sample (b) 30% iron particle sample (c) 50% iron particle sample

Figure 5.9 illustrates the MR effect of MRE samples with 10%, 30, and 50% iron particle concentrations at 490 mT magnetic field strength under different compression pre-strain amplitudes with frequency from 1 Hz to 60 Hz. The MR effect of the 10% iron particle concentration MRE (Figure 5.9 (a)) is the lowest compared with the other two. There are fewest iron particle chains formed in the 10% iron particle concentration MRE sample. The interaction between these iron particle chains is weakest. By increasing concentration of iron particle, more iron particle chains are formed in MRE and interactions among the iron particle chains become stronger. Then, the MR effect is increased for a higher iron particle concentration MRE sample. The same conclusion is drawn for MRE with shear test. By comparing the MR effect with different iron particle concentrations MRE samples, it is found that the MR effect of the 30% iron particle concentration MRE is the highest. The MR effect is calculated as ratio of increased young's modulus due to magnetic field divided by young's modulus at no magnetic field. Even though the increment of young's modulus due to a magnetic field is higher for the 50% iron particle concentration MRE sample. However, the increment of young's modulus at zero magnetic field is more significant for the 50% iron particle concentration MRE sample. Thus, MR effect of the 50% iron particle concentration MRE sample is lower than the 30% iron particle concentration MRE sample.

The value of the MR effect demonstrates a slight fluctuation with same compression pre-strain at frequency increases from 1 Hz to 60 Hz for MRE samples with 10% and 30% iron particle concentration. For MRE samples with 50% iron particle concentration, the MR effect decreases slightly for compression pre-stain 2% to 4%. As compression pre-strain continues to increase, the phenomenon of the MR effect decreases due to increasing frequency vanished. Compression pre-strain effect on the MR effect is different comparing with the results of MRE with shear test. The MR effect increases slightly as a compression pre-stain increases from 2% to 3% for MRE samples with different iron particle concentrations. By applying compression pre-strain, iron particles in MRE samples become closer. Thus, interactions between iron particles become stronger which induce an increase of the MR effect. As compression pre-strain continues increase, the increment of young's modulus at zero magnetic field is more significant comparing with the increment of young's modulus due to a magnetic field. Then, the MR effect demonstrates a steady decrease as compression pre-strain continues to increase.

5.4 Pre-strain effect on the dynamic compression properties of MRE under different strains

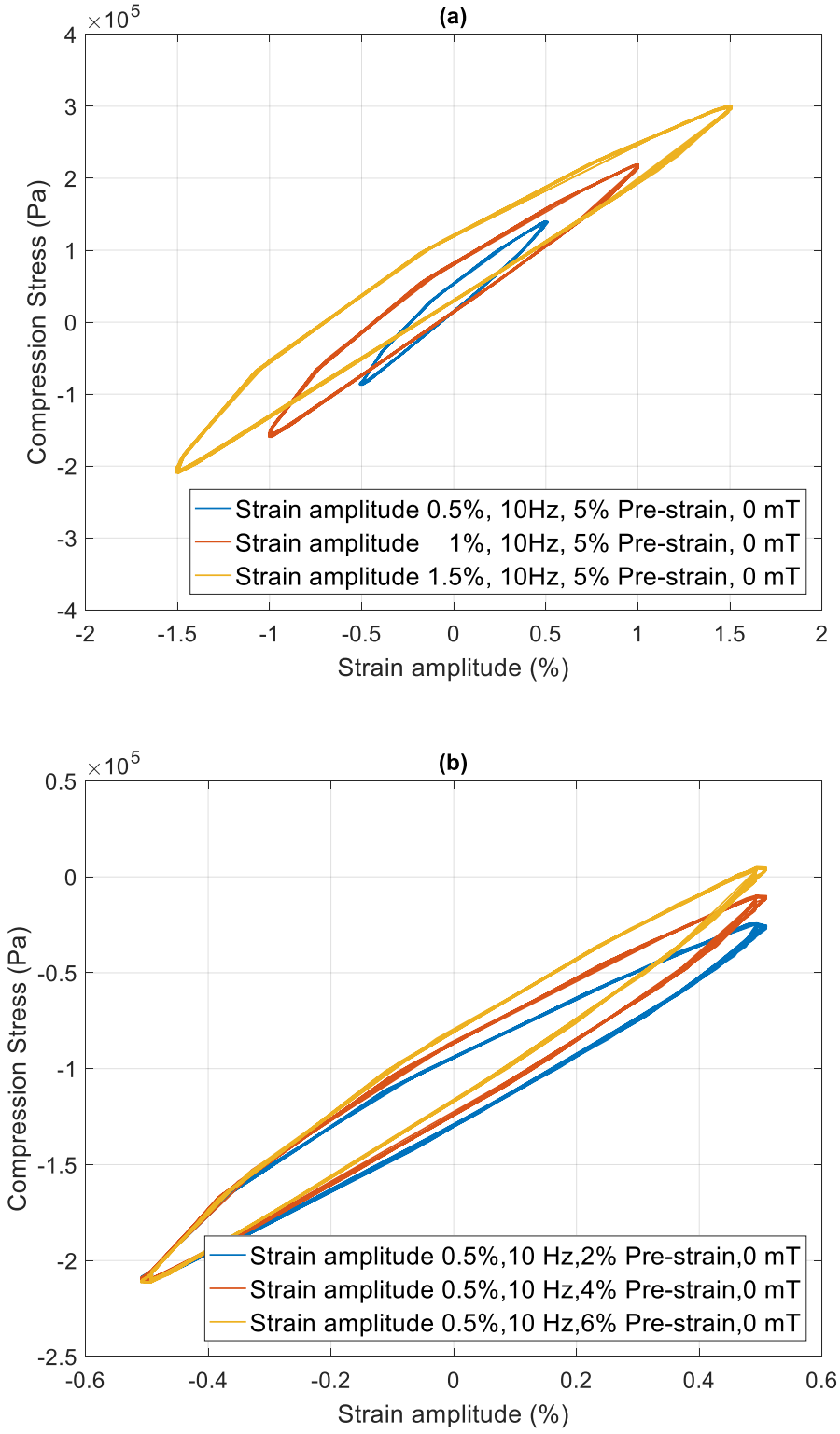

Figure 5.10 Stress-strain hysteresis curve plot of the 30% iron particle concentration MRE (a) 0.5%, 1%, 1.5%, strain amplitude, 10 Hz frequency, 5% pre-strain condition, 0 mT magnetic flux density, (b) 0.5% strain amplitude, 10 Hz frequency, 2%,4% and 6% pre-strain condition, at 0 mT magnetic flux density.

The stress-strain hysteresis curves of 30% iron particle concentration MRE sample under different strain amplitudes at 10 Hz and 0 mT magnetic field with 5% compression pre-strain is shown in Figure 5.10 (a). Figure 5.10 (b) illustrates the stress-strain curves with 2%, 4% and 6% compression pre-strains at 10 Hz and 0.5% strain amplitude. As can be seen from Figure 5.10 (a), the slope of the stress to strain of MRE decreases as strain amplitude increases. This indicates the complex modulus of MRE decrease with an increase strain amplitude. The same conclusion is drawn for MRE samples with shear test. Figure 5.10 (b) shows there is a steady increase of the slope of stress to strain as compression pre-strain increases from 2% to 6%. Then, it is concluded that MRE becomes stiffer as a higher compression pre-stain is applied.

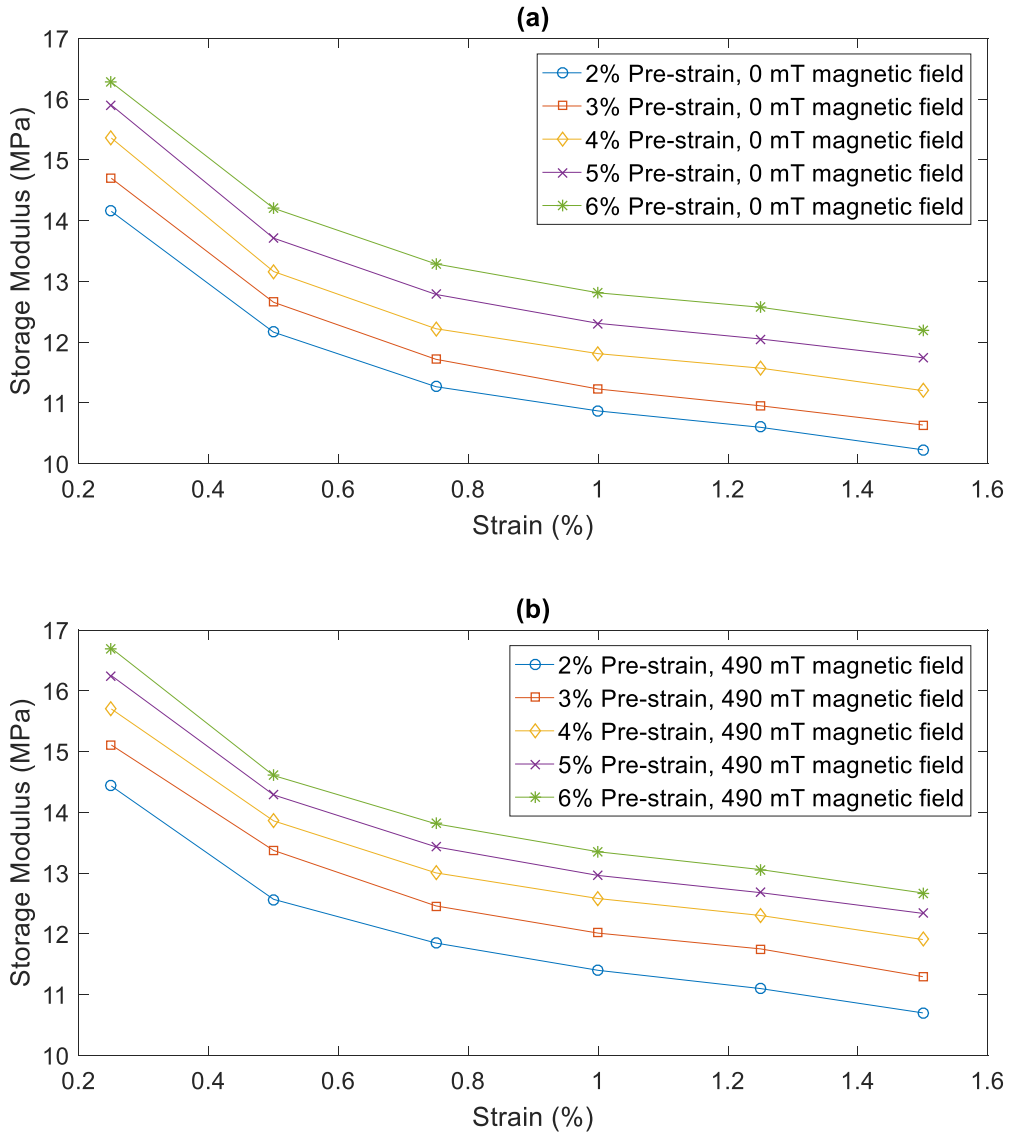

Figure 5.11 Compression storage modulus of MRE with 10% iron powder under different pre-strain amplitude with 10 Hz frequency (a) under 0 mT magnetic field (b) under 490 mT magnetic field

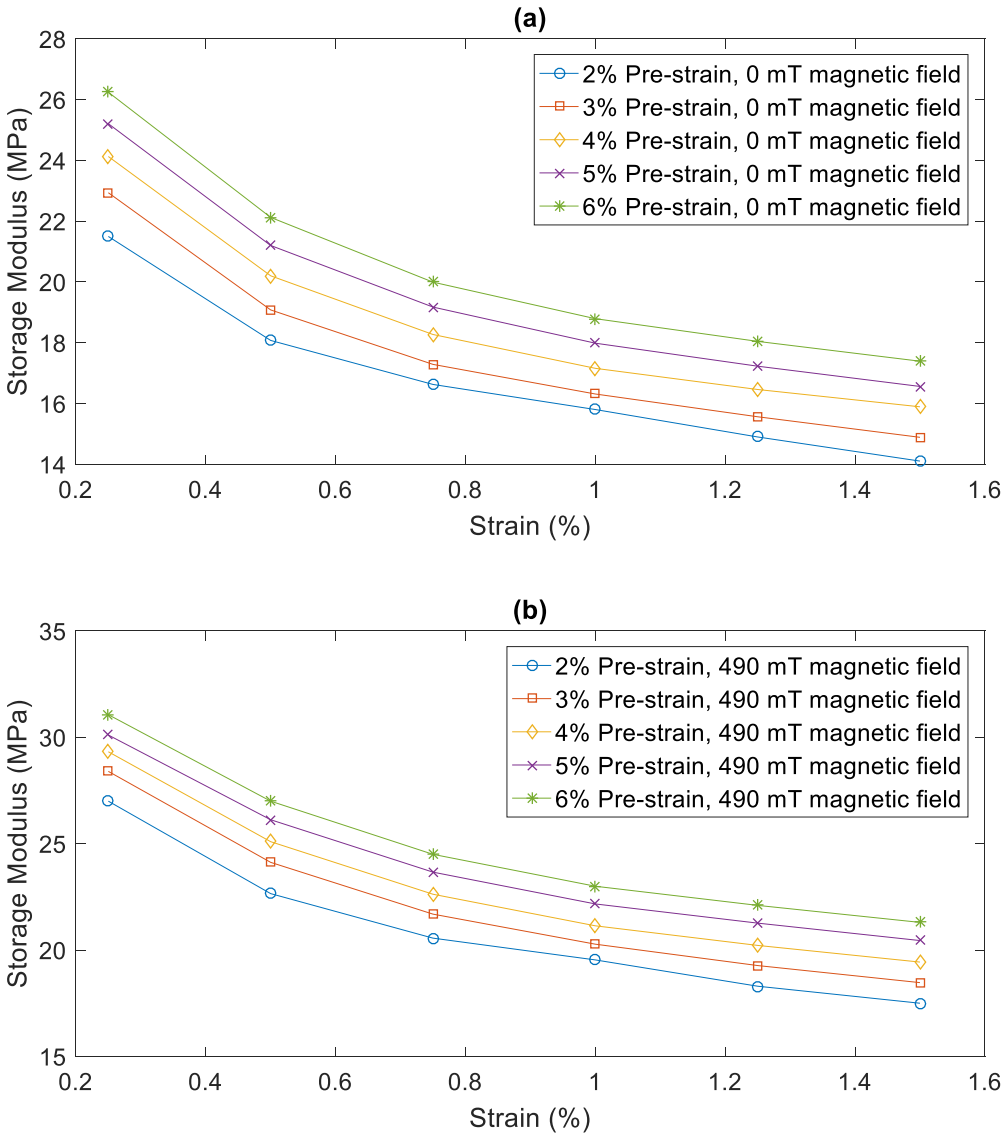

Figure 5.12 Compression storage modulus of MRE with 30% iron powder under different pre-strain amplitude with 10 Hz frequency (a) under 0 mT magnetic field (b) under 490 mT magnetic field

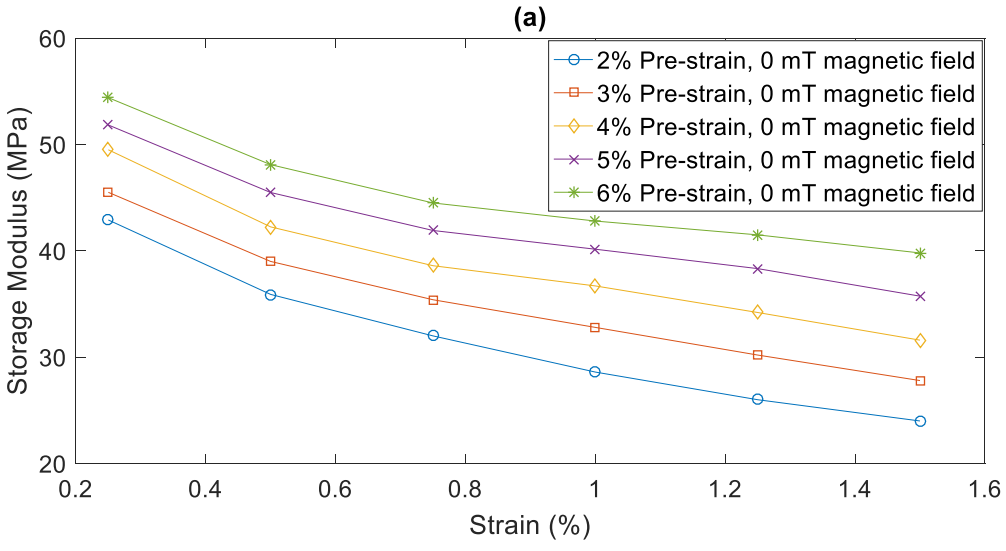

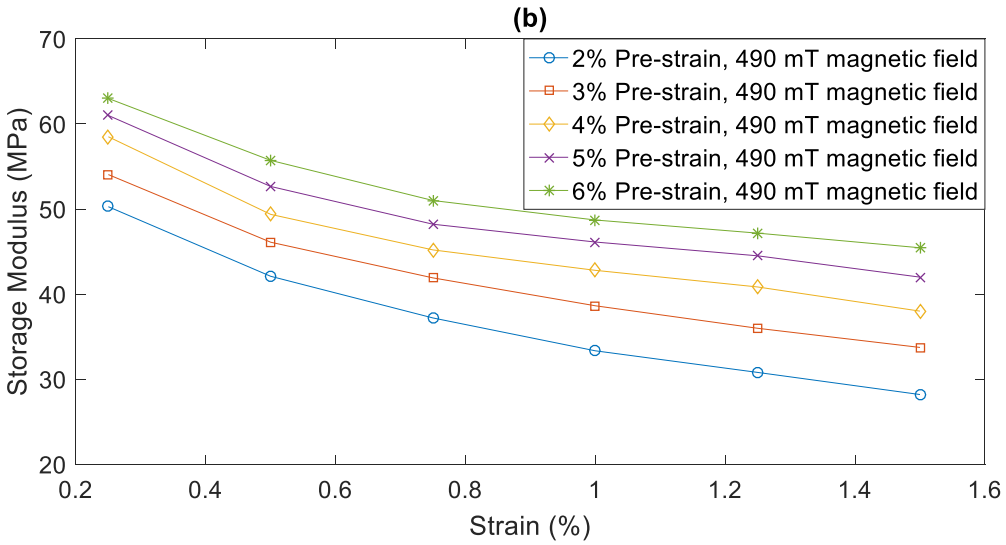

Figure 5.13 Compression storage modulus of MRE with 50% iron powder under different pre-strain amplitude with 10 Hz frequency (a) under 0 mT magnetic field (b) under 490 mT magnetic field

Figure 5.11-5.13 demonstrate compression pre-strain effect and strain amplitude coupling effect on the dynamic compression storage modulus of MRE with 10%, 30% and 50% iron particle concentrations. The excitation frequency is set to 10 Hz. Two magnetic field strengths 0 mT and 490 mT are selected for strain amplitude sweep tests. The compression storage modulus decreases with an increase strain amplitude from 0.25% to 1.5% for all MRE samples. MRE under compression loading is stiffer at smaller strain amplitude. This phenomenon is described as Payne effect which is also observed for MRE with shear tests (Figure 4.11-4.13). The compression storage modulus decreases rapidly as strain amplitude increases from 0.25% to 0.5%. Then, a steady decrease of compression storage modulus is observed for strain amplitude further increase. Compression pre-strain effects on the dynamic storage modulus of MRE for strain amplitude sweep show similar results comparing with those of the frequency sweep. Compression pre-stain leads to a steady increase of storage modulus for MRE with different iron particle concentrations with strain amplitude from 0.25% to 1.5%. The plots of compression storage modulus with different compression pre-strains for strain amplitude from 0.25% to 1.5% are parallel with each other. The trend of storage modulus at different compression pre-strain does not change with strain amplitude. Then, it is said that the dependence of compression pre-strain on storage modulus of MRE is independent of strain amplitude. Coupling effect between compression pre-strain and strain amplitude is weak and can be neglected.

Figure 5.11 (b) - 5.13 (b) show the effect of compression pre-strain on the dynamic storage modulus of MRE with different strain amplitudes at 490 mT magnetic field. An external magnetic field does not change the dependence of compression pre-strain and strain amplitude on storage modulus, but induces an increment of storage modulus.

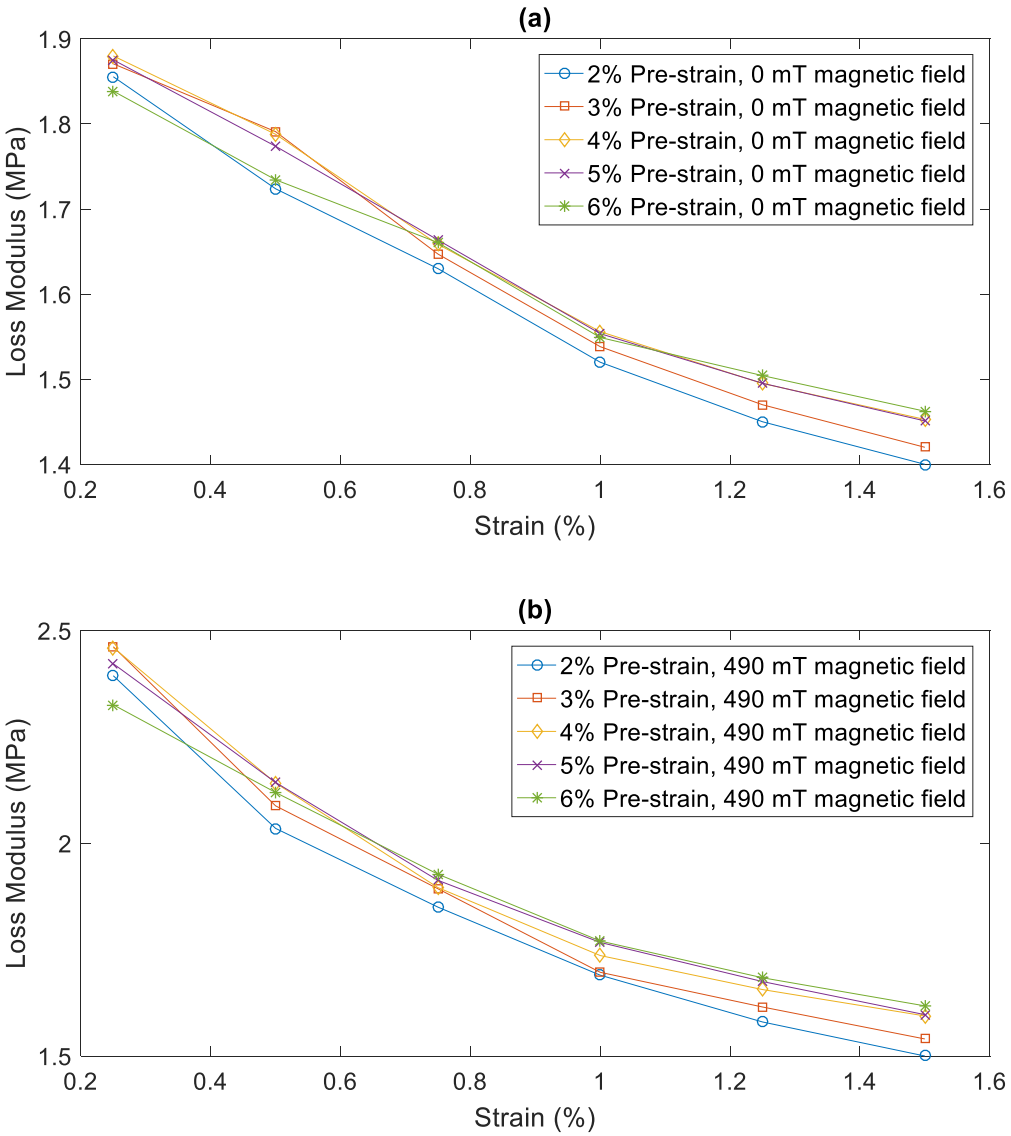

Figure 5.14 Compression loss modulus of MRE with 10% iron powder under different pre-strain amplitude with 10 Hz frequency (a) under 0 mT magnetic field (b) under 490 mT magnetic field

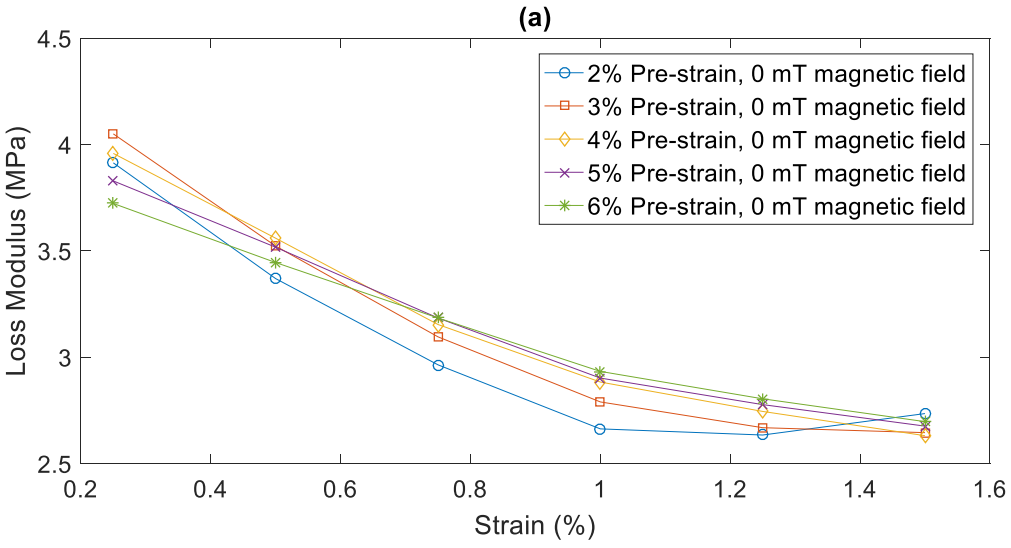

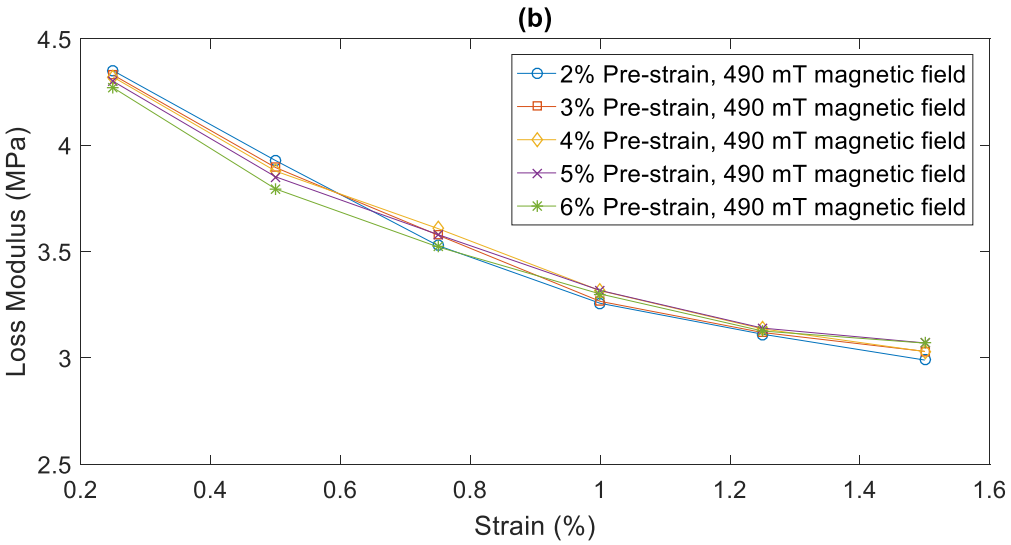

Figure 5.15 Compression loss modulus of MRE with 30% iron powder under different pre-strain amplitude with 10 Hz frequency (a) under 0 mT magnetic field (b) under 490 mT magnetic field

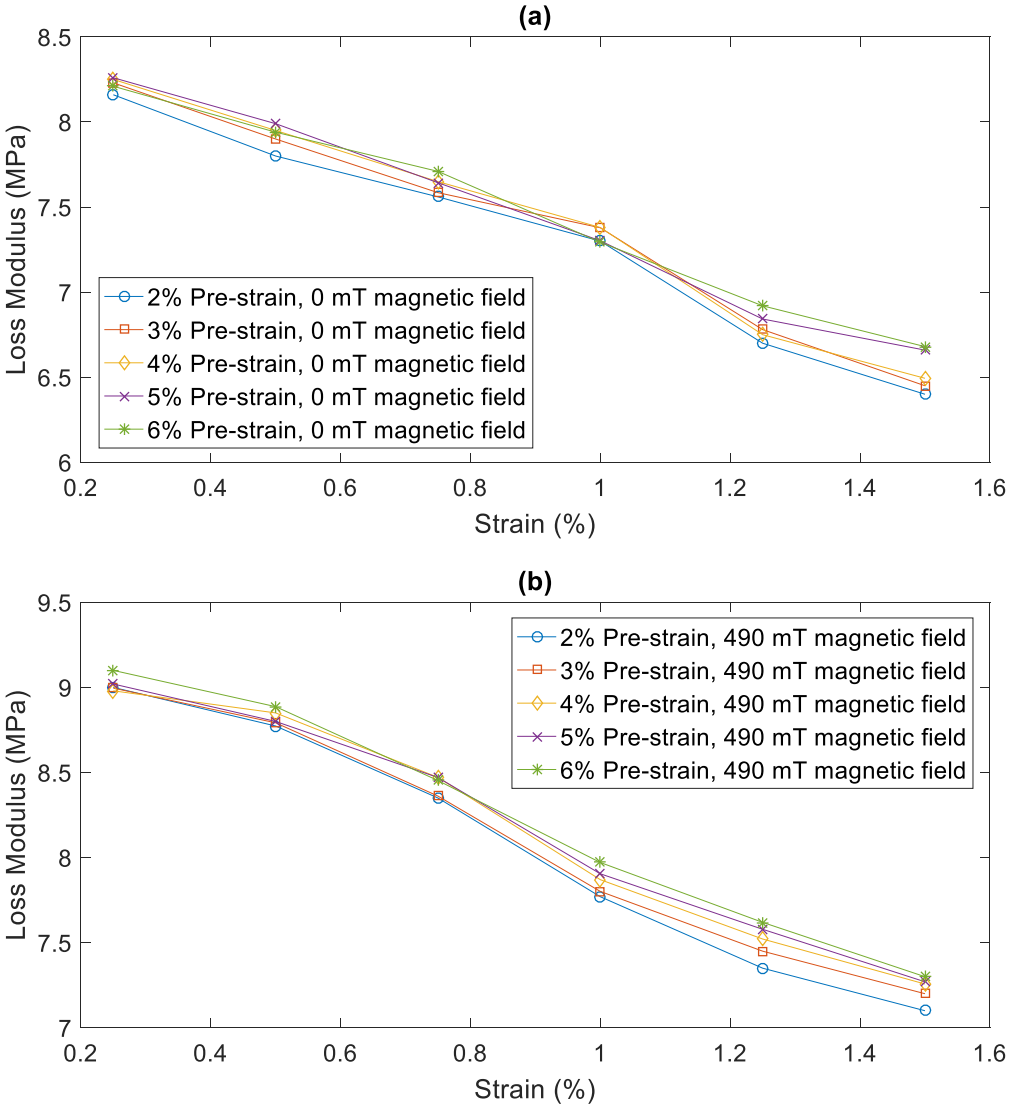

Figure 5.16 Compression loss modulus of MRE with 50% iron powder under different pre-strain amplitude with 10 Hz frequency (a) under 0 mT magnetic field (b) under 490 mT magnetic field

Figure 5.14-5.16 demonstrate compression pre-strain and strain amplitude coupling effect on the dynamic loss modulus of MRE with 10 Hz at two magnetic fields strength 0 mT and 490 mT. Loss modulus decreases with an increase strain amplitude for MRE with different iron particle concentrations. Loss modulus decreases steadily as strain amplitude increases from 0.25% to 1.5%. This phenomenon is described as Payne effect which is also observed for MRE samples with shear test. Loss modulus at 2% compression pre-stain with 0 mT magnetic field is slightly lower comparing with those of higher compression pre-strain. This phenomenon is more clearly observed for 10% and 30% iron particle MRE samples. As iron particle concentration increases to 50%, the effect of compression pre-stain on loss modulus decays. By increasing a compression pre-strain amplitude from 2% to 3%, a slight increase of loss modulus is observed. There are no noticeable variations of loss modulus as compression pre-strain further increase. Since the trend of loss modulus remains unchangeable as compression pre-strain increases from 2% to 6%. The dependence of strain amplitude on loss modulus is independent of compression pre-strain. An external magnetic field induces a higher loss modulus for all MRE samples. Meanwhile, the dependent of compression pre-strain amplitude on loss modulus remains the same.

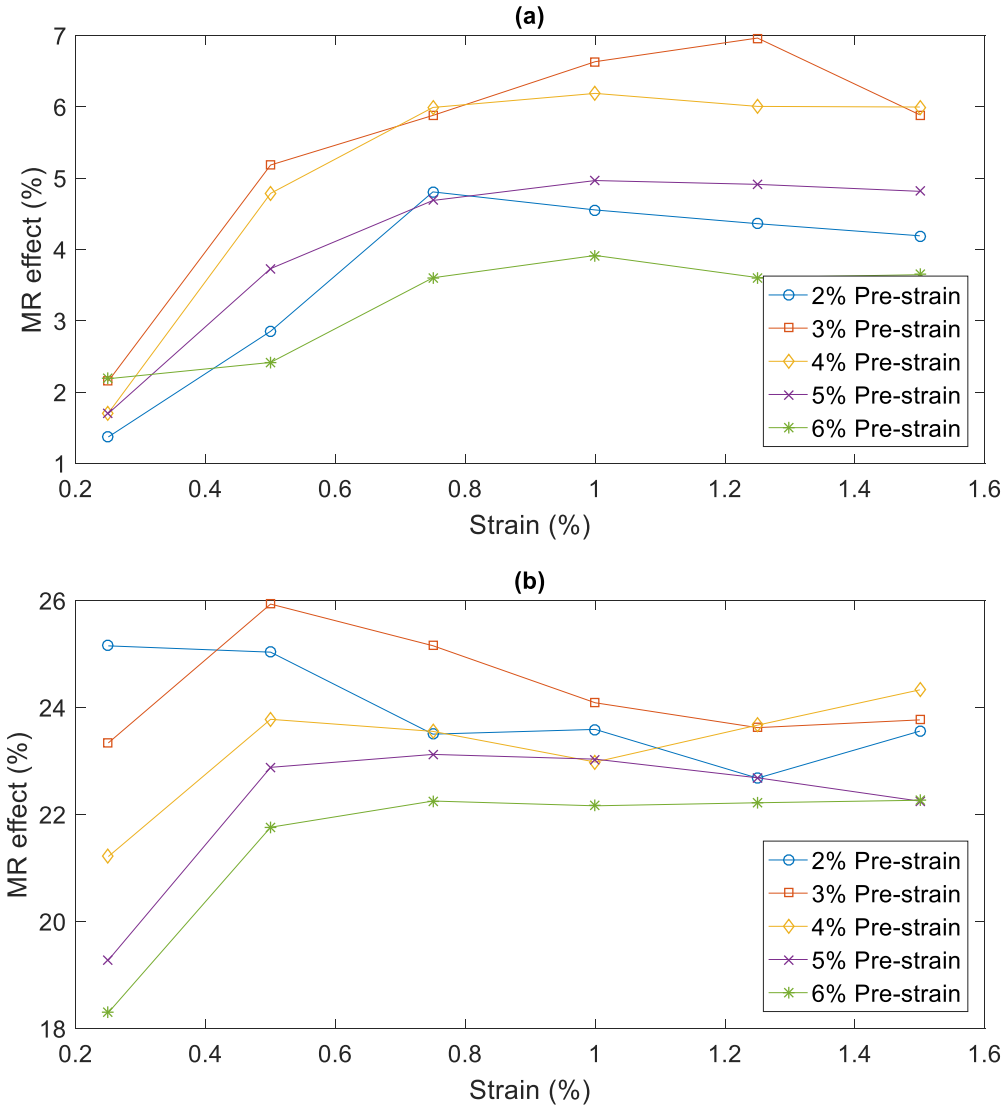

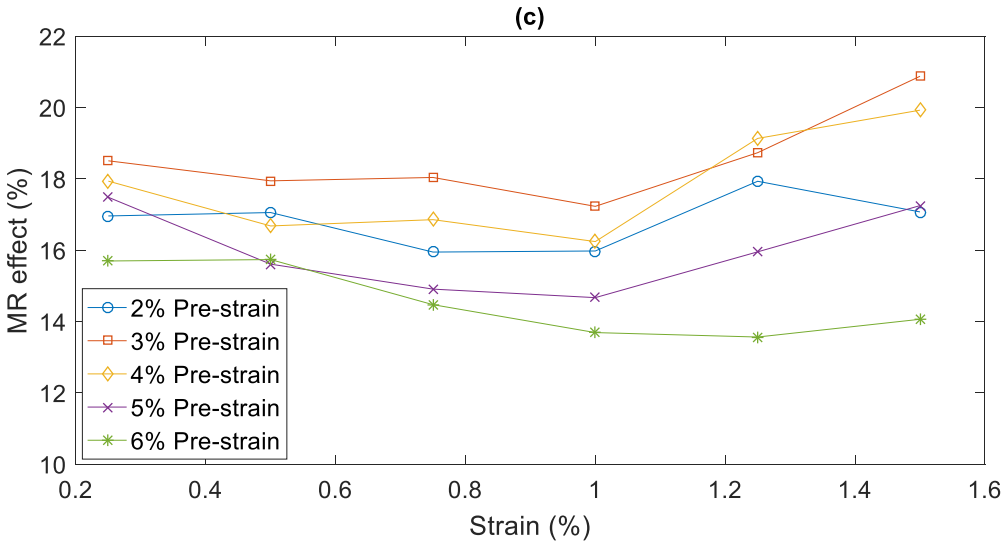

Figure 5.17 MR effect of MRE samples under different compression pre-strain amplitude with 10 Hz at 490 mT magnetic field (a) 10% iron particle sample (b) 30% iron particle sample (c) 50% iron particle sample

The MR effect of MRE samples with 10%, 30% and 50% iron particle concentrations under different compression pre-strains with stain amplitude varies from 0.25% to 1.5% is shown in Figure 5.17. It is seen that the trend of the MR effect with the an increase strain amplitude is different for MRE with different iron particle concentrations. For MRE with 10% iron particle concentration (Figure 5.17 (a)), the MR effect demonstrates a steady increase as strain amplitude increases from 0.25% to 1%. Then, the MR effect remains stable for strain amplitude further increases. For the 30% iron particle concentration MRE (Figure 5.17 (b)), an increment of the MR effect is obtained as strain amplitude increases to 0.5%. After that, the MR effect becomes stable for stain amplitude further increases. Figure 5.17 (c) shows that the MR effect remains stable for the 50% iron particle concentration as strain amplitude increases from 0.25% to 1% and increases slightly for strain amplitude further increase. Compared with the results of MRE with shear test, the controllability of MRE with compression tests do not deteriorate as strain amplitude increases. As the compression pre-stain increases from 2% to 3%, an increment of the MR effect is observed for all MRE samples. As compression pre-strain continues to increase, MRE becomes stiffer at zero magnetic field. Then, the MR effect starts to decrease.

5.5 Pre-strain effect on the dynamic compression properties of MRE under different magnetic fields

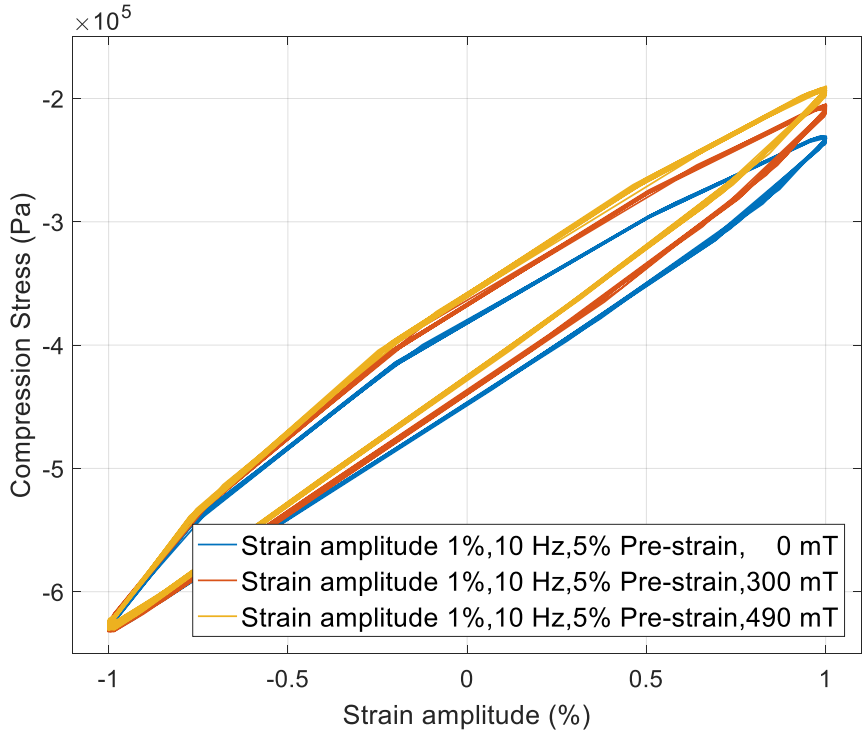

Figure 5.18 Stress-strain hysteresis curve plot of the 30% iron particle concentration MRE with 0 mT, 300 mT and 490 mT at 10 Hz frequency with 1% strain amplitude

The Stress-strain hysteresis curves of the 30% iron particle concentration MRE under 0, 300 mT and 490 mT magnetic fields at 10 Hz, 1% strain amplitude with 5% compression pre-strain condition are shown in Figure 5.18. It can be seen that the slope of the stress to strain increases with an increase magnetic field strength. An obvious increase of MRE compression modulus is achieved as a magnetic field increases from 0 mT to 300 mT. As magnetic field continues increasing to 490 mT, the magnetic saturation is happened and the increase rate of the compression modulus subsides. This phenomenon is also observed for MRE samples with shear test (Figure 4.18).

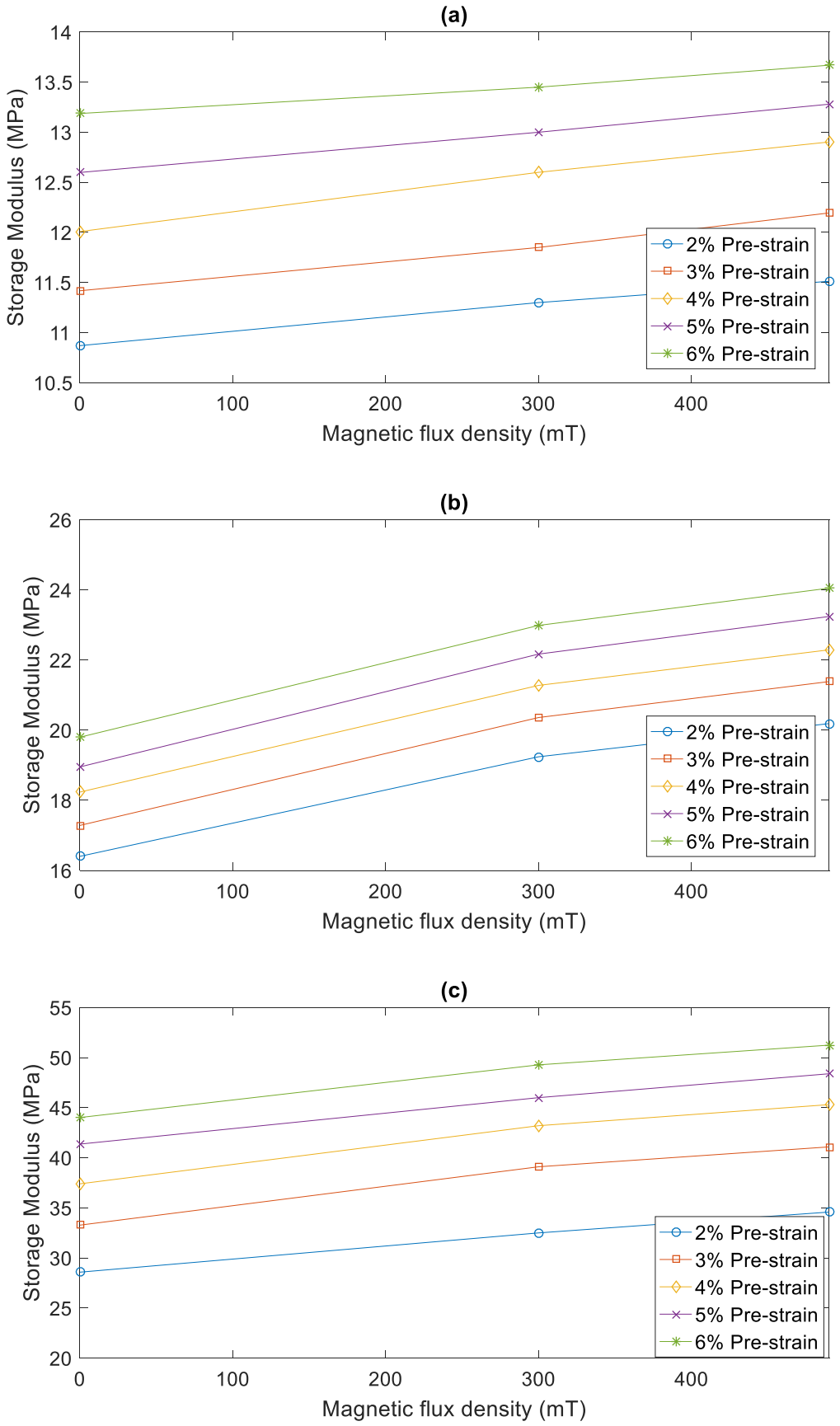

Figure 5.19 Compression storage modulus of MRE under different magnetic field with 1% strain amplitude at 10 Hz (a) 10% iron particle concentration (b) 30% iron particle concentration (c) 50% iron particle concentration

Figure 5.19 (a)-(c) illustrate the compression storage modulus of MRE with different iron particle concentrations under different magnetic fields. Storage modulus is increased by increasing a magnetic field strength. Magnetic field induces magnetic interactions among iron particle chains. This makes MRE material stiffer. By increasing a magnetic field, the interactions among iron particle chains becomes stronger. Thus, storage modulus is increased. Storage modulus also increases with iron particle concentration. More iron particles in MRE form stronger iron particle chains which also increase the interactions among iron particle chains due to a magnetic field. The same conclusion is drawn for MRE with shear test.

Compression pre-strain induces an increment of storage modulus. By applying a magnetic field, the plots of storage modulus are parallel with each other and the trend of storage modulus due to a magnetic field at different compression pre-strain remains the same. In Section 4.5, it is found that pre-strain affects the micro-structure of MRE. The distance between the iron particles is changed by a pre-strain. Hence, the coupling between magnetic field and pre-strain has an effect on storage modulus. However, this phenomenon is not observed for compression pre-strain tests. This may because the increase of storage modulus due to pre-strain is more significant compared with storage modulus increase due to a magnetic field. Thus, coupling between compression pre-stain and magnetic field effect on the storage modulus is not observed.

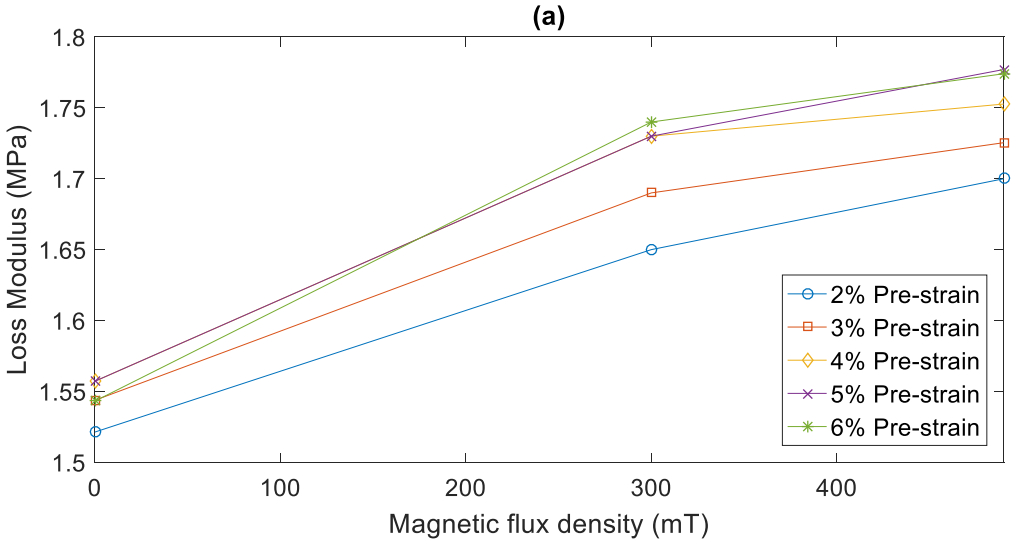

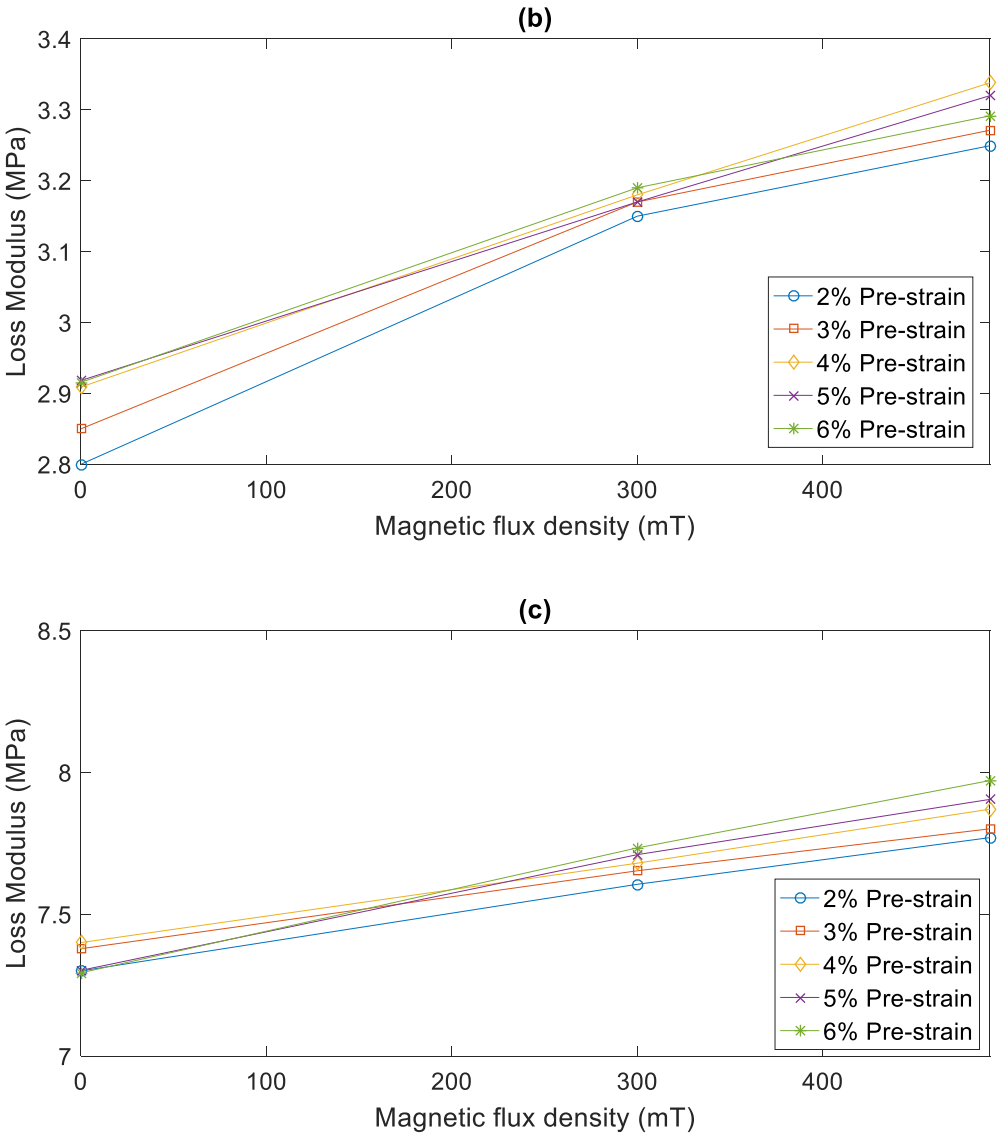

Figure 5.20 Compression loss modulus of MRE under different magnetic field with 1% strain amplitude at 10 Hz (a) 10% iron particle concentration (b) 30% iron particle concentration (c) 50% iron particle concentration

Figure 5.20 (a)-(c) illustrate loss modulus of MRE sample with 10%, 30, and 50% iron particle concentrations under different compression pre-strain amplitude with magnetic field strengths from 0 mT to 490 mT. Loss modulus also increases with a magnetic field strength. An external magnetic field induces iron particles becomes more aggregate. The frictions between iron particles are increased. These frictions between iron particles generate more dissipated energy which lead to an increase of loss modulus. In the same reason, loss modulus also increases by increasing iron particle concentration of MRE. This phenomenon is also observed for MRE with shear test. There is no clear relationship obtained between compression pre-strain and magnetic field effect on loss modulus of MRE. Compression pre-strain induces a slight increase of loss modulus as compression pre-strain amplitude increases from 2% to 4%. Loss modulus remains at a stable value as compression pre-strain further increases.

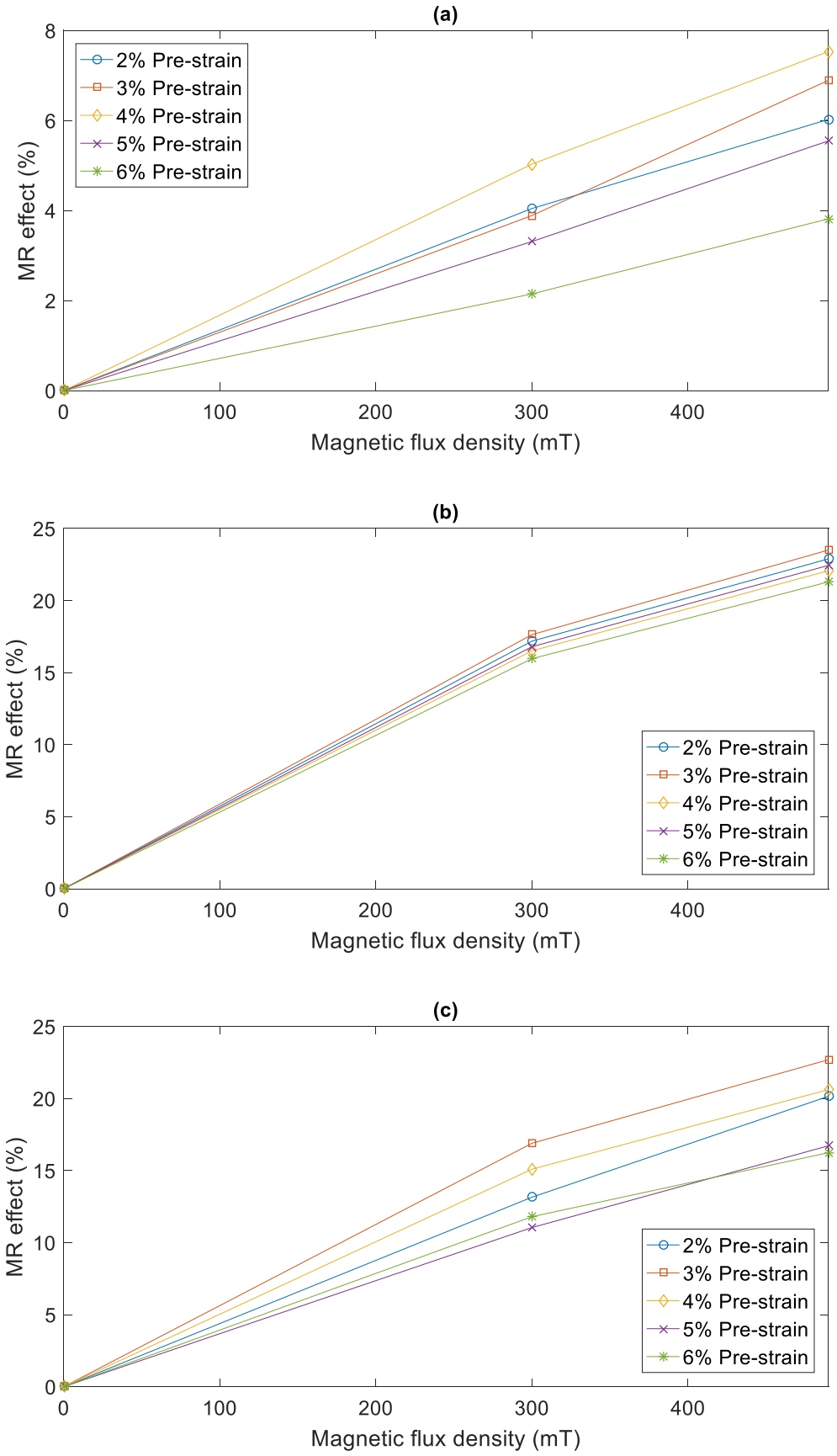

Figure 5.21 MR effect of MRE under different magnetic field with 1% strain amplitude at 10 Hz (a) 10% iron particle sample (b) 30% iron particle sample (c) 50% iron particle sample

Figure 5.21 shows the MR effect of MRE samples with 10%, 30% and 50% iron particle concentrations with different compression pre-stains at magnetic field from 0 mT to 490 mT. The MR effect increases with magnetic field for all MRE samples. The highest MR effect is achieved by 30% iron particle concentration MRE sample. Compression pre-strain induces a slight increase of the MR effect as compression pre-strain increases from 2% to 3%. Then, the MR effect demonstrates a steady decrease as compression pre-strain further increases. This phenomenon is magnified by increasing magnetic field.

5.6 Coupling effect between strain amplitude and frequency on the dynamic compression properties of MRE

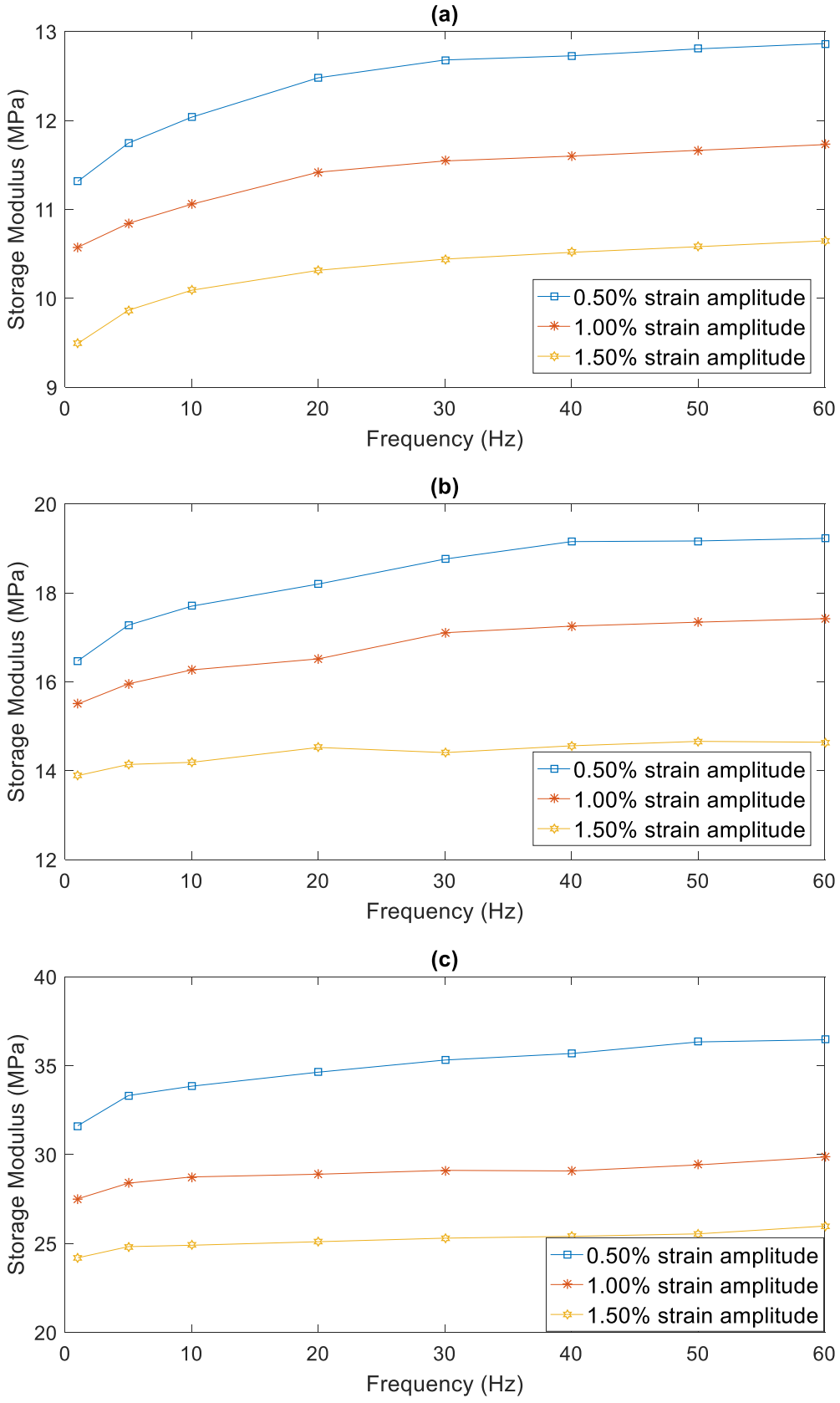

Figure 5.22 Strain amplitude and frequency coupling effect on the compression storage modulus of MRE at 0 mT magnetic field (a) 10% (b) 30% (c) 50% iron particle concentration MRE sample

The strain amplitude and frequency coupling effects on compression storage modulus with different iron particle concentrations of MRE are shown in Figure 5.22. There is an obvious storage modulus reduction as strain amplitude increases. This is explained by Payne effect. Meanwhile, the storage modulus increases smoothly as frequency increase. The increase trend of storage modulus with frequency is different with different strain amplitudes. The increment of storage modulus is higher for smaller strain amplitude from frequency 1 Hz to 60 Hz. Payne effect becomes more obviously at a higher frequency. The same phenomenon is also observed for MRE with shear test. It is concluded that the coupling between strain amplitude and frequency has an effect on the dynamic compression storage modulus.

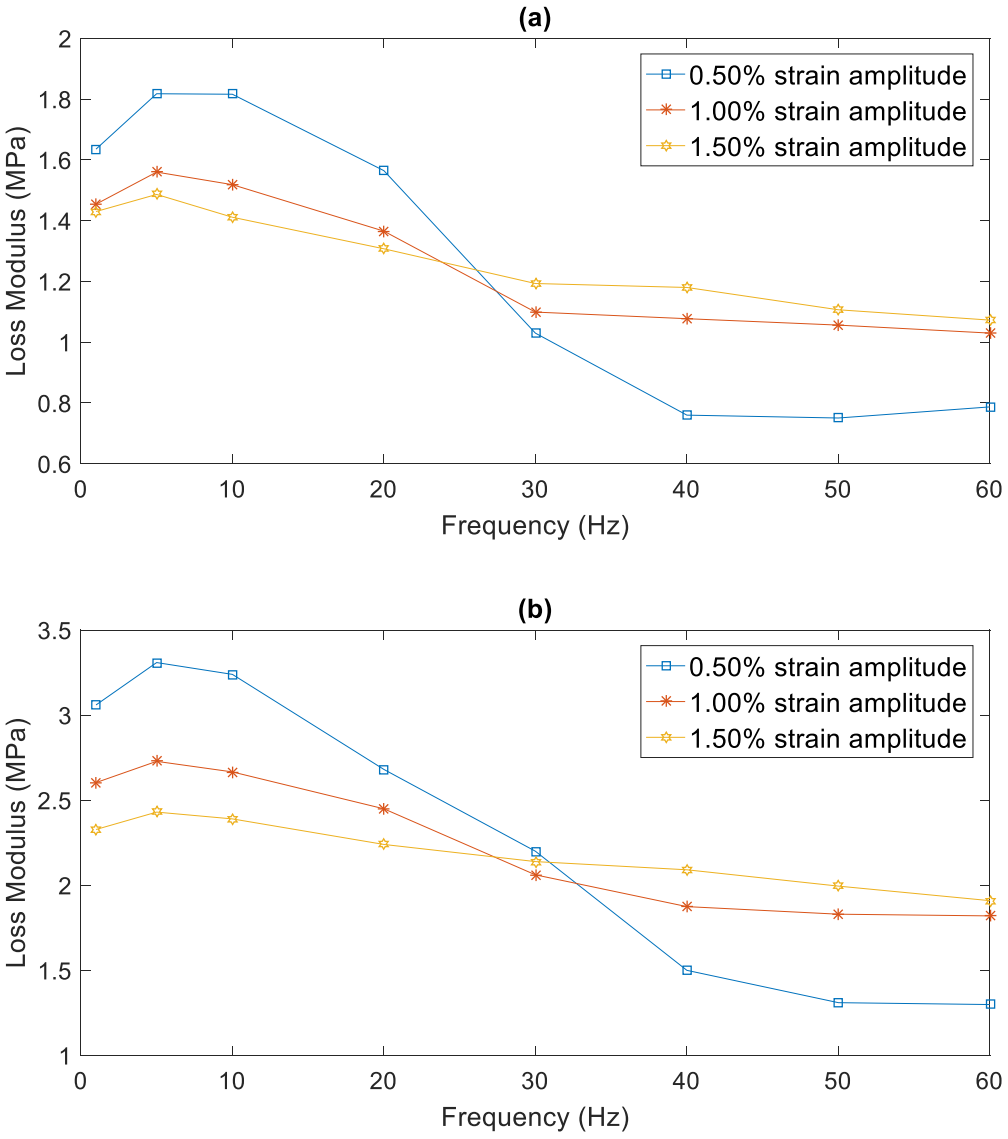

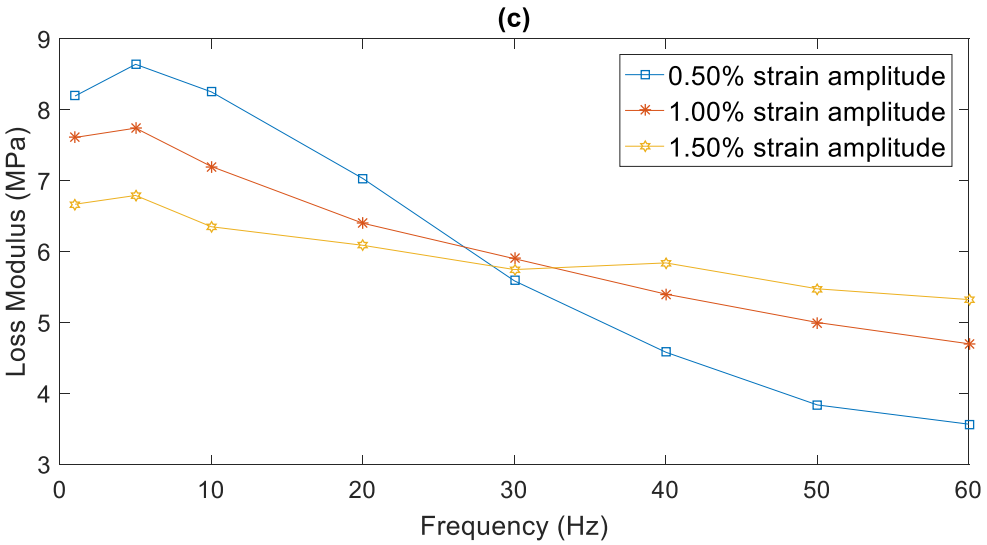

Figure 5.23 Strain amplitude and frequency coupling effect on the compression loss modulus of MRE at 0 mT magnetic field (a) 10% (b) 30% (c) 50% iron particle concentration MRE sample

Figure 5.23 (a)-(c) demonstrates the coupling of stain amplitude and frequency effect on compression loss modulus of MRE with 10%, 30% and 50% iron particle concentrations. It is clearly seen that there is an obvious coupling effect between strain amplitude and frequency on compression loss modulus of MRE. By increasing frequency, loss modulus increases to a peak value around 10 Hz and then decreases steadily as frequency further increases. Meanwhile, a decrease reduction rate of loss modulus with an increase stain amplitude is obtained. The value of loss modulus demonstrates a faster reduction for smaller strain amplitude. This phenomenon is also observed for the shear test MRE samples.

5.7 Coupling effect between strain amplitude and magnetic field on the dynamic compression properties of MRE

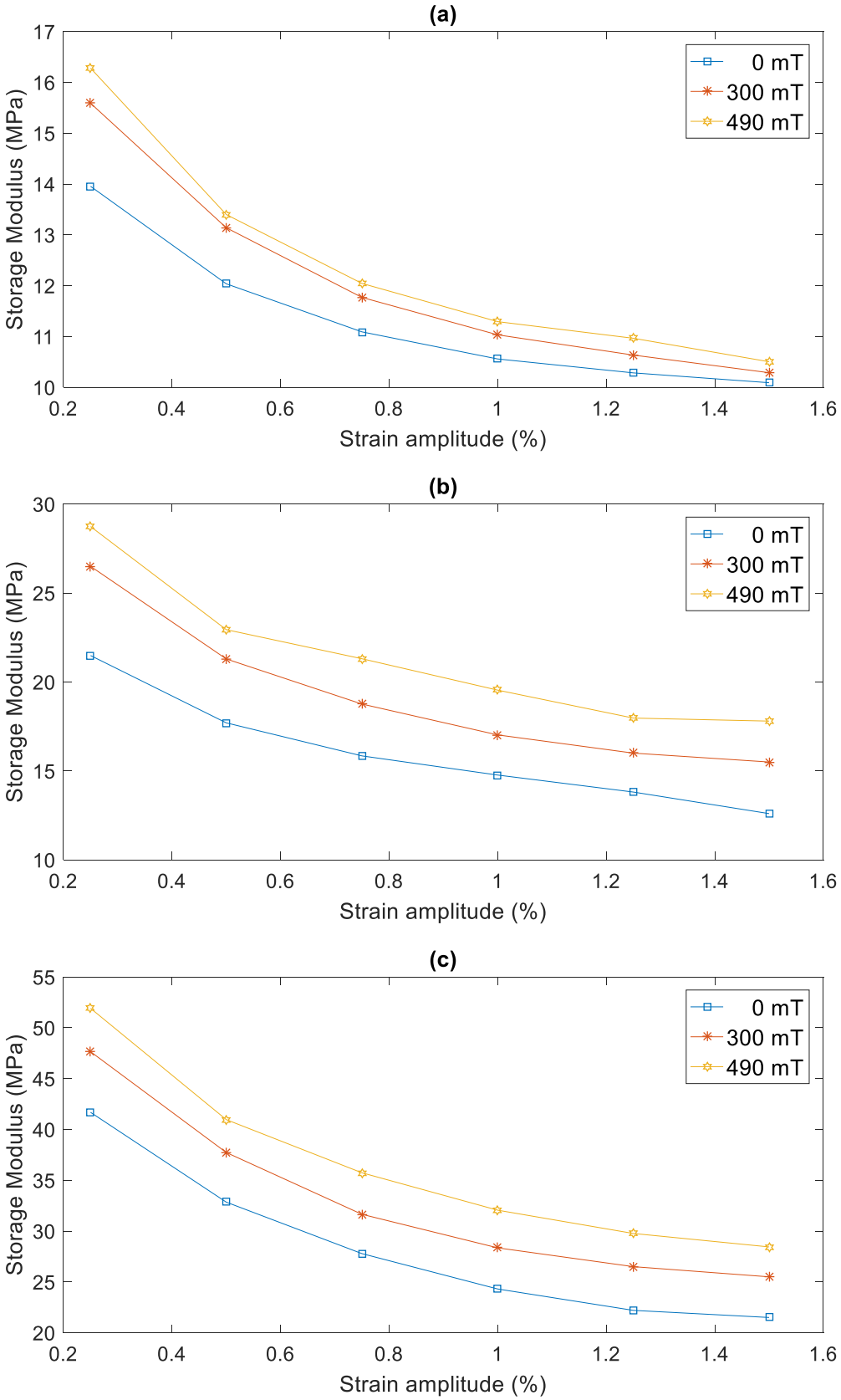

Figure 5.24 Strain amplitude and magnetic field coupling effect on the compression storage modulus of MRE at 10 Hz (a) 10% (b) 30% (c) 50% iron particle concentration MRE sample

The strain amplitude and magnetic field coupling effect on compression storage modulus of MRE is shown in Figure 5.24 (a)-(c). An external magnetic field induces an increment of storage modulus. A more obvious increment of storage modulus due to external magnetic field is obtained at smaller strain amplitude (less than 0.5%). By increasing stain amplitude, the effect of magnetic field on storage modulus is attenuated. It is concluded that the coupling between strain amplitude and magnetic field has an effect on storage modulus of MRE. The coupling effect is more obvious for the 10% iron particle concentration MRE.

Figure 5.25 (a)-(c) demonstrates strain amplitude and magnetic field coupling effect on compression loss modulus of MRE with 10%, 30% and 50% iron particle concentrations. The increment of loss modulus due to an external magnetic field is more notable at smaller strain amplitude. By increasing strain amplitude, the effect of magnetic field to the loss modulus of MRE diminishes.

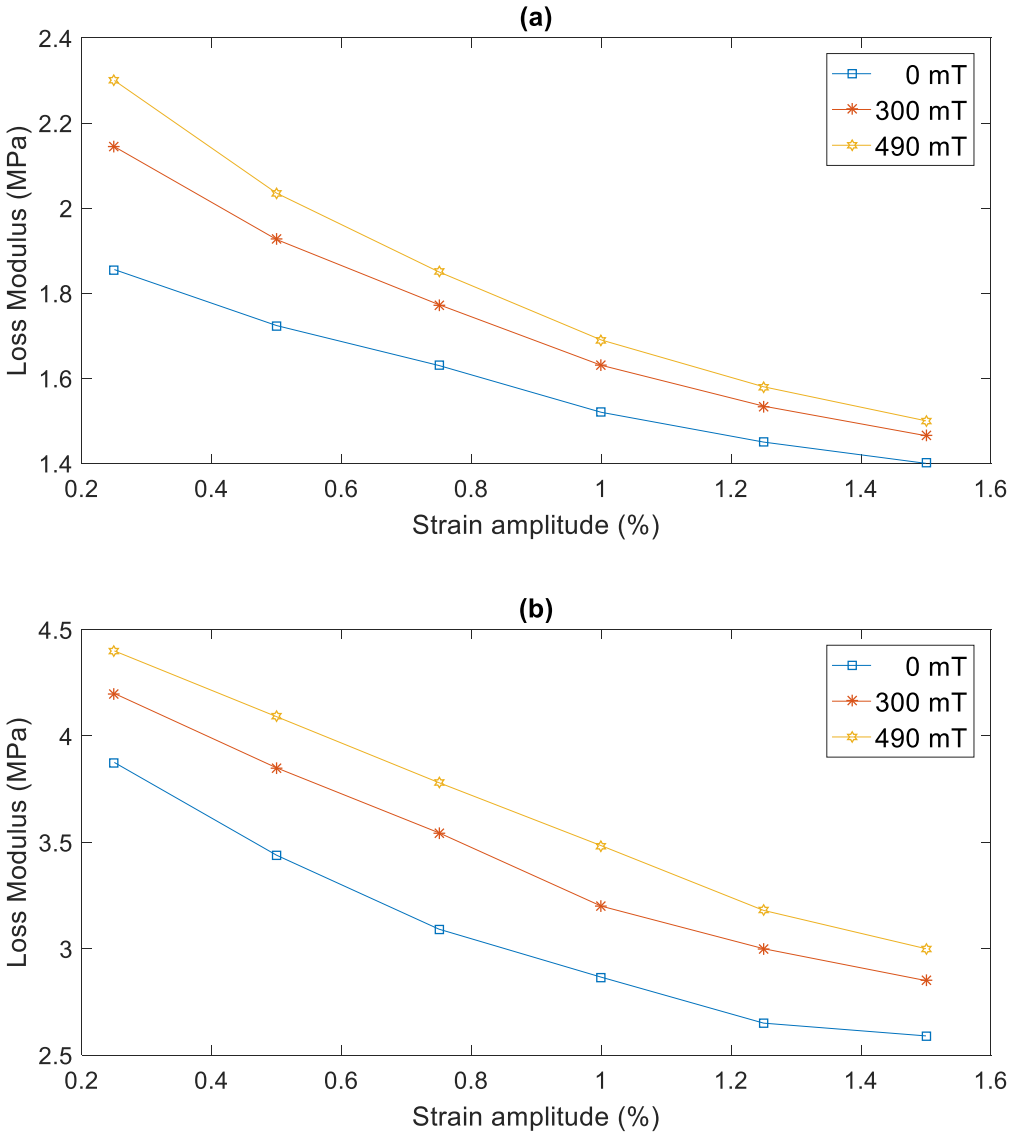

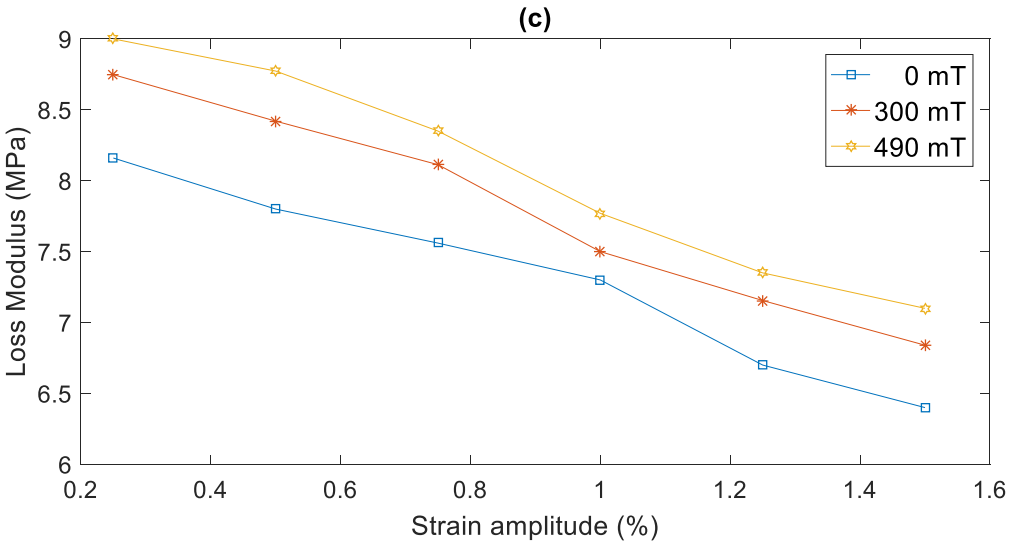

Figure 5.25 Strain amplitude and magnetic field coupling effect on the compression loss modulus of MRE at 10 Hz (a) 10% (b) 30% (c) 50% iron particle concentration MRE sample

5.8 Coupling effect between frequency and magnetic field on the dynamic compression properties of MRE

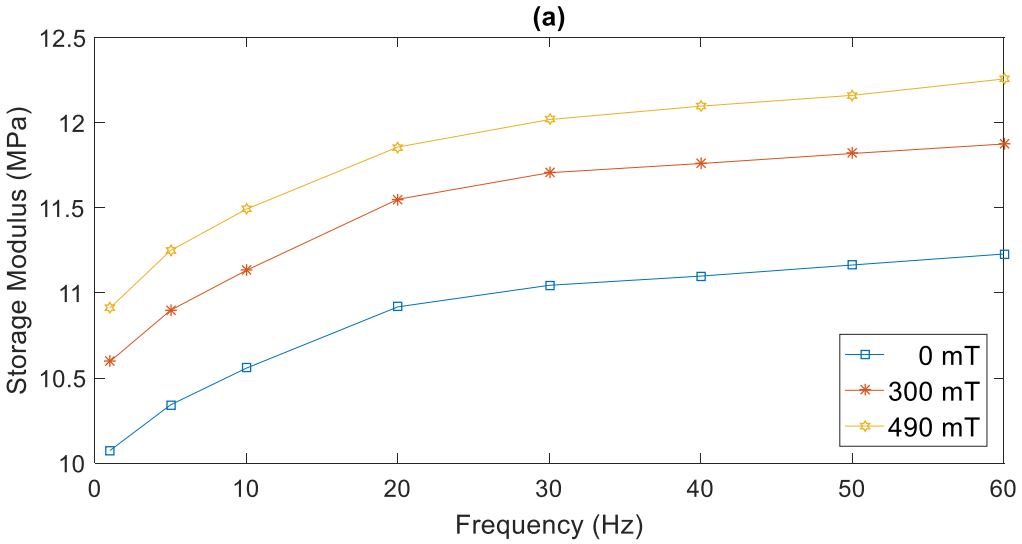

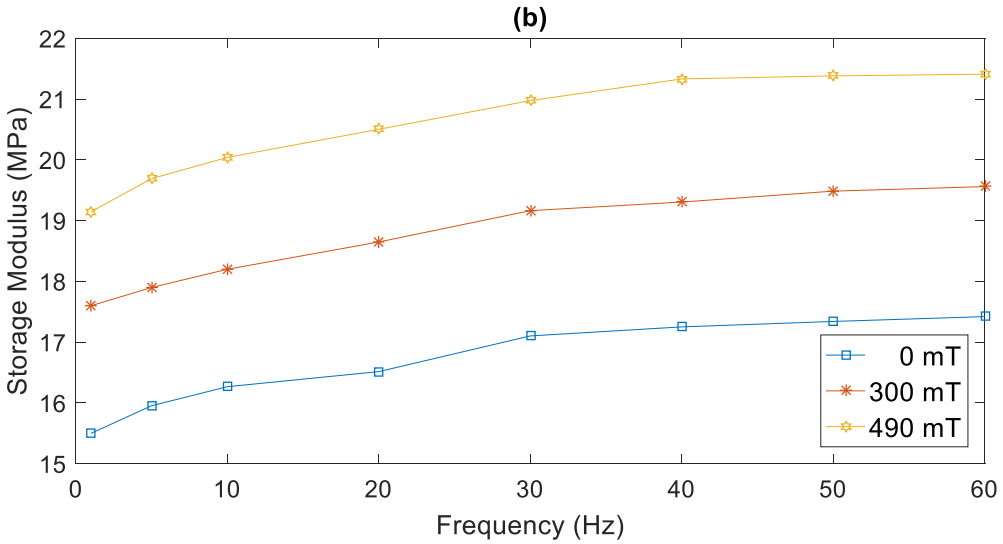

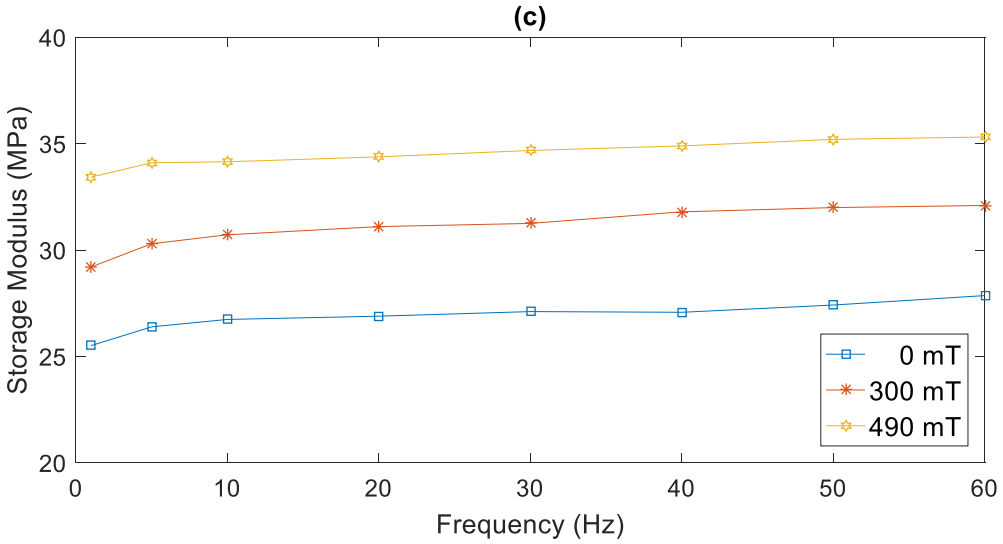

Figure 5.26 Frequency and magnetic field coupling effect on the compression storage modulus of MRE at 1% strain amplitude (a) 10% (b) 30% (c) 50% iron particle concentration MRE sample

Figure 5.26 and Figure 5.27 demonstrate frequency and magnetic field coupling effect on compression storage modulus and loss modulus of MRE. It is found that the trends of storage modulus and loss modulus with different frequency are not affected by a magnetic field. The plots of storage modulus and loss modulus are parallel with each other with different magnetic field. Then, it is concluded that there is no coupling effect between frequency and magnetic field on storage modulus and loss modulus. The same conclusion is also drawn from MRE samples with shear test.

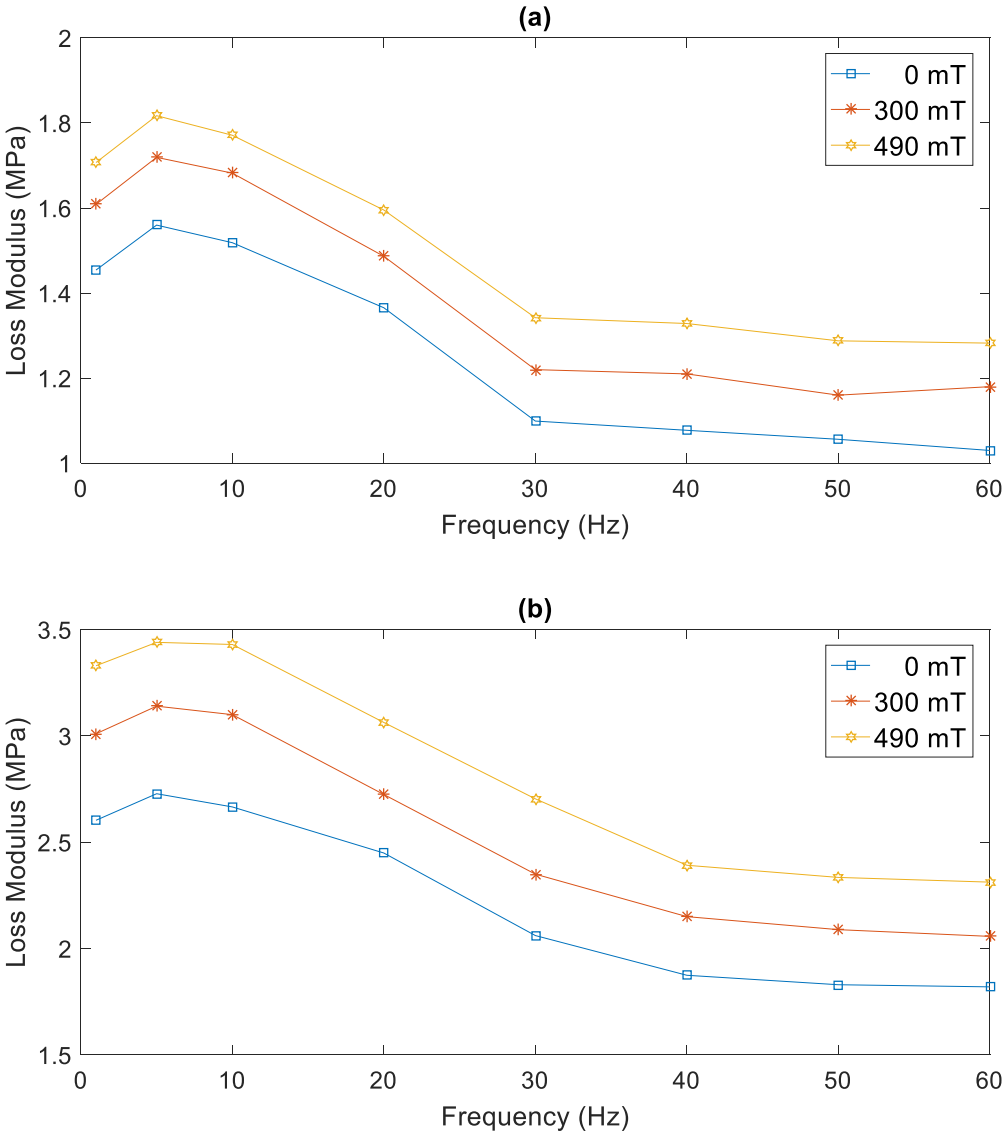

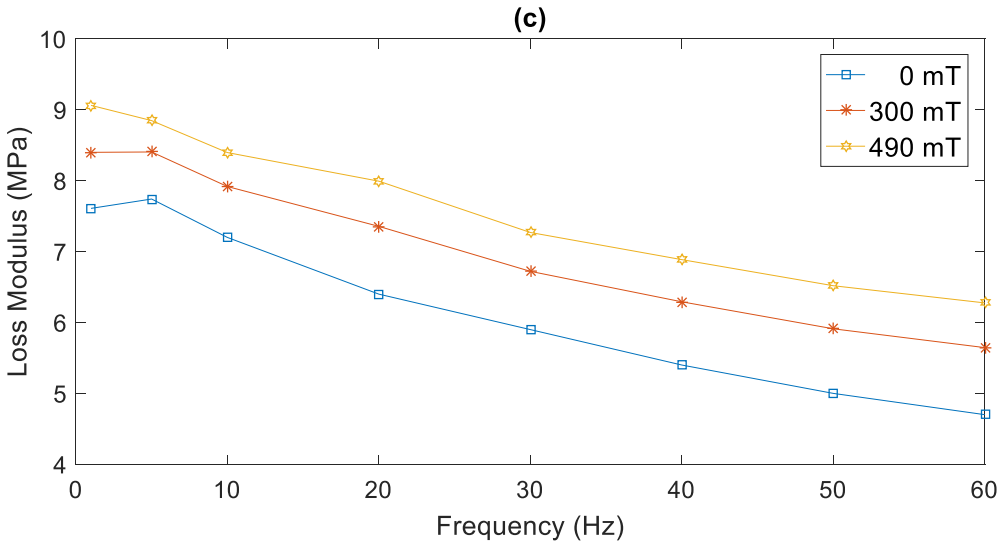

Figure 5.27 Frequency and magnetic field coupling effect on the compression loss modulus of MRE at 1% strain amplitude (a) 10% (b) 30% (c) 50% iron particle concentration MRE sample

5.9 Experimental error analysis of dynamic shear tests of MRE

For dynamic compression tests of MRE, three MRE samples are used for each test condition. Error bar is used to represent the experiment error of the dynamic compression test of MRE. The equation to calculate the error bar is given in equation 4.2.

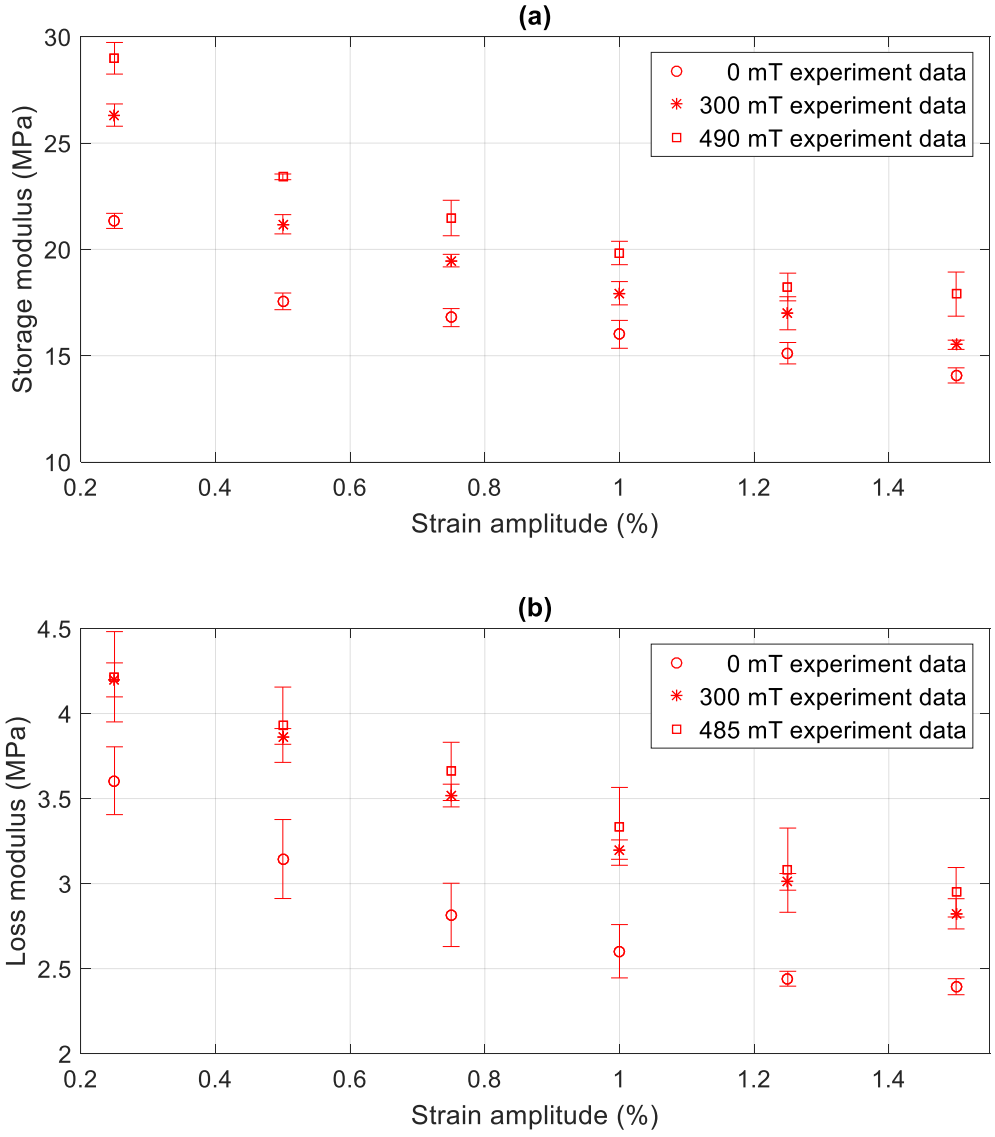

Figure 5.28 Error bar of (a) compression storage modulus and (b) compression loss modulus of 30% iron particle concentration MRE samples at 10 Hz with 0 mT, 300 mT and 485 mT.

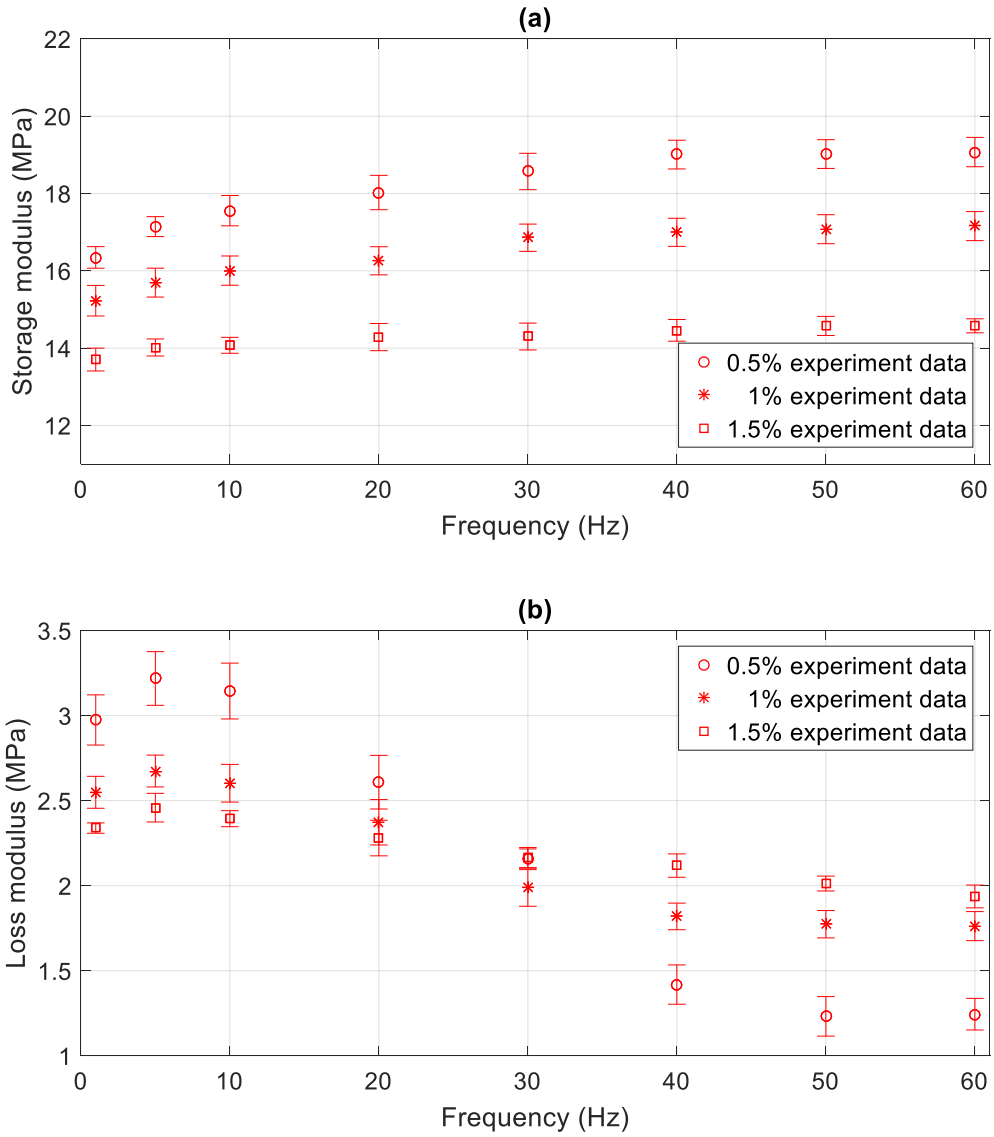

Figure 5.29 Error bar of (a) compression storage modulus and (b) compression loss modulus of 30% iron particle concentration MRE samples at 0.5%, 1% and 1.5% strain amplitude at 0 mT.

For experiment error of compression MRE tests, it is found that the error of compression loss modulus is also higher comparing with that of compression storage modulus. Loss modulus is the ability of MRE dissipating energy as heat. The dissipating energy of MRE is mainly due to the friction between iron particle chains and matrix material. The error of loss modulus of MRE may indicate that there is a microstructure difference between each MRE samples.

5.10 Summary

In this chapter, the dynamic compression mechanical properties of MRE are investigated. The dependences considered include pre-strain, frequency, strain amplitude and magnetic field. The coupling effects between different dependences are also analysed. MRE samples used for compression tests are comprised silicone rubber ELASTOSIL 4644 A/B and 9 μm carbonyl iron powder (ALDRICH-44890) and cured at a 260 mT magnetic field. Three groups of MRE samples with different iron particle concentrations (10%, 30% and 50%) are fabricated and tested. For stress relaxation test of compression MRE, it is found that a steady state compression stress response is achieved at 40 seconds. Then, a dynamic sinusoidal excitation is applied to MRE at a 40-second delay after a pre-strain is applied. The dependences and their coupling effects on the dynamic compression mechanical properties of MRE are summarized as followed.

- The compression pre-strain induces an obvious increase of compression storage modulus for all MRE samples. The increasing pre-strain leads to a further increase of storage modulus. The dependence of the pre-strain on compression storage modulus is independent of frequency and strain amplitude. The coupling effect between compression pre-strain and magnetic field is also not observed.
- The pre-stain effect on compression loss modulus is not obvious compared with that on storage modulus. By increasing compression pre-strain amplitude, loss modulus increases slightly and remains stable for compression pre-strain (4% to 6%) further increase. There is no clear coupling effect observed between compression pre-stain with frequency, strain amplitude and magnetic field.
- The same coupling effect between frequency and strain amplitude for compression test is observed compared with the shear tests. For smaller strain amplitude, a higher increment of storage modulus is achieved with increasing frequency. The decreasing rate of loss modulus for smaller strain amplitude is higher.
- For strain amplitude and magnetic field coupling effect on compression mechanical properties of MRE, it is found that by increasing strain amplitude, the effect of magnetic field to storage and loss modulus of MRE diminishes. The same conclusion is drawn for MRE with shear test.
- The coupling effect between frequency and magnetic field on compression mechanical properties of MRE is weak and can be neglected.
- The compression MR effect is different comparing with that of the shear test. For shear test, the MR effect decreases with increasing strain amplitude and frequency. While, for compression test, the value of the MR effect is fluctuated (less than 2%) with frequency from 1 Hz to 60 Hz. The MR effect does not deteriorate as strain amplitude increases for compression tests. The MR effect increases as compression pre-strain increases from 2% to 3%, and starts to decrease for compression pre-strain further increases. The compression MR

effect for the 30% iron particle concentration MRE sample is the highest among all MRE samples.

Chapter 6: Mathematical Modelling of Dynamic Properties of MRE

6.1 Introduction

To propose an accurate mathematical model to describe the dynamic mechanical properties of MRE is important not only for better and deeper understanding of this material but also to provide a better control of MRE as used in engineering application.

Currently, modelling of the mechanical properties of MRE can be classified into two groups. The first group is to model the magnetic induced modulus of MRE by using the dipole method (section 2.4.1). However, this method does not include the dependence of frequency, so this method is incapable of describing the dynamic properties of MRE. The second group is to use viscoelastic model to model the dynamic properties of MRE. The dynamic properties of MRE are dependent on pre-strain amplitude, frequency, strain amplitude and magnetic field strength. Coupling effects between the dependences also have effects on the dynamic properties of MRE. The current viscoelastic models can not consider all there four dependences. The investigations of the coupling effects between the dependences are also limited.

In this chapter, the dynamic properties of MRE are modelled based on a classical viscoelastic Kelvin-Voigt model. The dependences of strain amplitude, frequency, magnetic field and pre-stain are considered. Coupling effects between strain amplitude, frequency and magnetic field are also included. The proposed model use polynomial to express storage modulus and loss modulus with respect to strain amplitude, frequency, magnetic field and their coupling effects. Since, coupling effects between pre-strain, frequency and pre-strain, strain amplitude are weak and can be neglected. Then, the dependent of pre-strain is defined as a function of pre-strain amplitude and magnetic field strength. The dependence of pre-strain is used as a compensation value to the total storage modulus and loss modulus. In this chapter, the experiment results of the 30% iron particle concentration MRE samples are used to identify the relevant parameters of the mathematical model. This is because the MR effect of 30% iron particle concentration MRE samples is higher compared with 10% and 50% iron particle concentration MRE samples.

6.2 Modelling the nonlinear dynamic properties of MRE without pre-strain

Based on the experimental results shown in Chapter 4 and 5, it is concluded that the dynamic properties of MRE depend on the motion strain amplitude, frequency, magnetic field strength and the pre-strain condition. The coupling effects between strain amplitude, frequency and magnetic field strength also affect the mechanical properties of MRE. The dependence of pre-strain on the mechanical properties of MRE is independence of the frequency and strain amplitude. The pre-strain effect on the mechanical properties is modelled as a function of pre-strain amplitude and magnetic field strength and regarded as a compensation value to storage and loss modulus of MRE.

6.2.1 Modified Kelvin-Voigt model

The dynamic properties of MRE without pre-strain condition are modelled initially. A modified classical viscoelastic Kelvin-Voigt model is proposed to express the nonlinear dynamic properties of MRE. As can be seen from Figure 6.1, the Kelvin-Voigt model consists of a viscous damper and a Hookean elastic spring connected in parallel with each other.

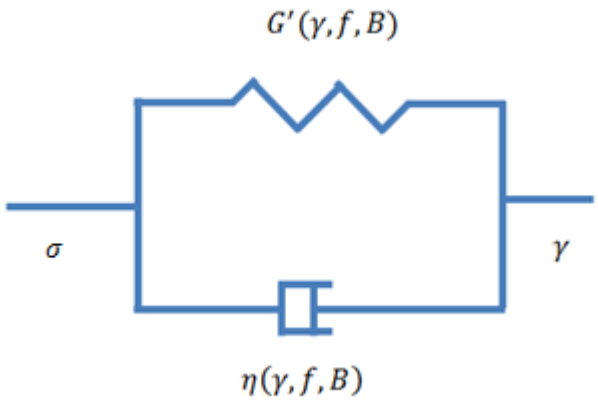

Figure 6.1 Viscoelastic Kelvin-Voigt model for MRE

For the viscoelastic Kelvin-Voigt model, σ is the stress, γ is the strain, $G'(\gamma, f, B)$ is storage modulus contribution to the elastic part, $\eta(\gamma, f, B)$ is viscosity damper contribution to the viscosity part.

The stress-strain relationship for the modified Kelvin-Voigt model is given in Eq. 6.1.

$$\sigma(t) = G'(\gamma, f, B) * \gamma(t) + \eta(\gamma, f, B) * \dot{\gamma}(t) \quad \text{Eq. 6.1}$$

$\sigma(t)$ is the stress output, $\gamma(t)$ is the strain input, $\dot{\gamma}(t)$ is strain rate which is the derivative of the strain with respect to time, $G'(\gamma, f, B)$ is real storage modulus and is a function of strain, frequency and magnetic flux density, $\eta(\gamma, f, B)$ is the viscosity, the definition of the of the viscosity is given in Eq. 6.2.

$$\eta(\gamma, f, B) = \frac{G''(\gamma, f, B)}{2\pi f} \quad \text{Eq. 6.2}$$

$G''(\gamma, f, B)$ is the loss modulus of the materials and is also defined as a function of strain, frequency and magnetic flux density.

For the experiment, a harmonic sinusoidal excitation strain is used, so the input strain function is defined in Eq. 6.3.

$$\gamma(t) = \gamma_0 \sin(2\pi f t) \quad \text{Eq. 6.3}$$

By substituting the Eq. 6.2 to 6.4 into Eq. 6.1, the stress-strain relationship for the Kelvin-Voigt model is defined as

$$\sigma(t) = G'(\gamma, f, B) * \gamma_0 \sin(2\pi f t) + \frac{G''(\gamma, f, B)}{2\pi f} * 2\pi f * \gamma_0 \cos(2\pi f t) \quad \text{Eq. 6.5}$$

By simplifying the Eq. 6.5,

$$\sigma(t) = \gamma_0 * (G'(\gamma, f, B) * \sin(2\pi f t) + G''(\gamma, f, B) * \cos(2\pi f t)) \quad \text{Eq. 6.6}$$

Then, the expression of the storage modulus and loss modulus are given in Eq. 6.7 and Eq. 6.8.

$$G'(\gamma, f, B) = G_0' + \boldsymbol{A_1'} \cdot \boldsymbol{\gamma} + \boldsymbol{A_2'} \cdot \boldsymbol{f} + \boldsymbol{A_3'} \cdot \boldsymbol{B} + \boldsymbol{A_4'} \cdot \boldsymbol{\gamma_f} + \boldsymbol{A_5'} \cdot \boldsymbol{\gamma_B} + \boldsymbol{A_6'} \cdot \boldsymbol{f_B} \quad \text{Eq. 6.7}$$

$$G''(\gamma, f, B) = G_0'' + \boldsymbol{A_1''} \cdot \boldsymbol{\gamma} + \boldsymbol{A_2''} \cdot \boldsymbol{f} + \boldsymbol{A_3''} \cdot \boldsymbol{B} + \boldsymbol{A_4''} \cdot \boldsymbol{\gamma_f} + \boldsymbol{A_5''} \cdot \boldsymbol{\gamma_B} + \boldsymbol{A_6''} \cdot \boldsymbol{f_B} \quad \text{Eq. 6.8}$$

where $\boldsymbol{A_1}$ to $\boldsymbol{A_6}$ are the parameters vectors for storage and loss modulus of MRE. The number 1 to 6 is the parameter vector corresponding to strain, frequency, magnetic field strength, strain frequency interaction, strain magnetic interaction and frequency magnetic interaction, respectively. The dimensions for all the vectors are given in Appendix I. A third order polynomial is used to represent the storage and loss modulus dependence on strain and frequency and a second order polynomial is used to describe the storage and loss modulus on magnetic field. The interaction between strain, frequency and magnetic field effect on storage modulus and loss modulus are discussed in Section 4.6-4.8 and 5.6-5.8. From experiment results, it is found that the interactions between strain-frequency and strain-magnetic field is stronger compared with the interaction between frequency-magnetic field. Then, a third order polynomial is used to demonstrate the interaction between strain-frequency and strain-magnetic field and a first order polynomial is used to express the interaction between frequency and magnetic field.

The parameter vectors from $\boldsymbol{A_1}$ to $\boldsymbol{A_6}$ are given in Eq. 6.9 to 6.14 below, these vectors can be used either for the storage modulus and loss modulus.

$$\boldsymbol{A_1} = [G_1 \quad G_2 \quad G_3] \qquad \text{Eq. 6.9}$$

$$\boldsymbol{A_2} = [G_4 \quad G_5 \quad G_6] \qquad \text{Eq. 6.10}$$

$$\boldsymbol{A_3} = [G_7 \quad G_8] \qquad \text{Eq. 6.11}$$

$$\boldsymbol{A_4} = [G_9 \quad G_{10} \quad G_{11}] \qquad \text{Eq. 6.12}$$

$$\boldsymbol{A_5} = [G_{12} \quad G_{13} \quad G_{14}] \qquad \text{Eq. 6.13}$$

$$\boldsymbol{A_6} = [G_{15}] \qquad \text{Eq. 6.14}$$

The vectors for strain, frequency, magnetic flux density and their interaction are given in Eq. 6.15 to 6.20.

$$\boldsymbol{\gamma} = [\gamma \quad \gamma^2 \quad \gamma^3] \qquad \text{Eq. 6.15}$$

$$\boldsymbol{f} = [f \quad f^2 \quad f^3] \qquad \text{Eq. 6.16}$$

$$\boldsymbol{B} = [B \quad B^2] \qquad \text{Eq. 6.17}$$

$$\boldsymbol{\gamma_f} = [\gamma f \quad \gamma^2 f \quad \gamma f^2] \qquad \text{Eq. 6.18}$$

$$\boldsymbol{\gamma_B} = [\gamma B \quad \gamma^2 B \quad \gamma B^2] \qquad \text{Eq. 6.19}$$

$$\boldsymbol{f_B} = [fB] \qquad \text{Eq. 6.20}$$

6.2.2 Parameters identification procedures

The parameters in Eq. 6.7 and 6.8 are identified based on the experiment results. The procedures to derive these parameters are given in Eq. 6.21 to Eq. 6.27. There are 32 parameters needed to identify, 16 parameters for shear modulus and the others for loss modulus. Storage modulus and loss modulus are dependent on three variables which are strain amplitude, frequency and magnetic flux density, respectively. The multivariate polynomial regression method is used to identify the parameters $G_0' \; to \; G_{15}'$ and $G_0'' \; to \; G_{15}''$ in Eq. 6.7 and 6.8. By transforming the Eq. of 6.7 and 6.8 into a matrix form

$$\boldsymbol{G} = \boldsymbol{X}\boldsymbol{R} \qquad \text{Eq. 6.21}$$

Where, $\boldsymbol{G}$ is the experiment results of storage modulus and loss modulus of shear and compression properties of MRE, $\boldsymbol{X}$ is the matrix of the variable of strain, frequency and magnetic field. $\boldsymbol{R}$ is a parameter vector which need to be calculated for the storage and loss modulus.

$$\boldsymbol{G} = (G_{1,1,1} \quad G_{2,1,1} \quad \cdots \quad G_{i,j,k} \quad \ldots \quad G_{n,m,p})^{T} \qquad \text{Eq. 6.22}$$

$$\boldsymbol{X} = \begin{bmatrix} 1 & \gamma_1 & \gamma_1^2 & \cdots & f_1 & \cdots & B_1 & \cdots & \gamma_1 B_1 \\ 1 & \gamma_2 & \gamma_2^2 & \cdots & f_1 & \cdots & B_1 & \cdots & \gamma_2 B_1 \\ \vdots & \vdots & \vdots & \cdots & \vdots & \cdots & \vdots & \cdots & \vdots \\ 1 & \gamma_i & \gamma_i^2 & \cdots & f_j & \cdots & B_k & \cdots & \gamma_i B_k \\ \vdots & \vdots & \vdots & \cdots & \vdots & \cdots & \vdots & \cdots & \vdots \\ 1 & \gamma_n & \gamma_n^2 & \cdots & f_m & \cdots & B_p & \cdots & \gamma_n B_p \end{bmatrix} \qquad \text{Eq. 6.23}$$

$$\boldsymbol{R} = [G_0 \quad G_1 \quad G_2 \quad \cdots \quad G_{14} \quad G_{15}]^T \qquad \text{Eq. 6.24}$$

where$i = 1,2, \ldots, n \; j = 1,2, \ldots m, k = 1,2, \ldots, p$. For the shear MRE model, $n = 8, m = 8, p = 5$ and for compression MRE model, $n = 6, m = 8, p = 3$. The dimensions of the matrix $\boldsymbol{X}$ and dimension of vectors $\boldsymbol{G}$ and $\boldsymbol{R}$ for shear and compression model of MRE are given in Appendix I. Eq. 6.21 is over determined equations with 16 variables. In order to obtain the solution of the over-determined-equation, the least square method is applied. The least square method is to select a group of most appropriate parameters to obtain the minimum mean square error. The mean square error is defined in Eq. 6.25.

$$\varepsilon\,(\boldsymbol{R}) = \|\boldsymbol{X}\boldsymbol{R} - \boldsymbol{G}\|^2 \qquad \text{Eq. 6.25}$$

$\varepsilon\,(\boldsymbol{R})$ is the mean square error and is defined as a function of $\boldsymbol{R}$, as $\boldsymbol{R} = \widehat{\boldsymbol{R}}$, the minimum $\varepsilon(\widehat{\boldsymbol{R}})$ is achieved, then the value of $\widehat{\boldsymbol{R}}$ is regarded as the solution of the over determined function. The calculation of $\widehat{\boldsymbol{R}}$ is given in Eq. 6.26 and 6.27.

$$\boldsymbol{X}^{\boldsymbol{T}}\boldsymbol{X}\widehat{\boldsymbol{R}} = \boldsymbol{X}^{\boldsymbol{T}}\boldsymbol{G} \qquad \text{Eq. 6.26}$$

$$\widehat{\boldsymbol{R}} = (\boldsymbol{X}^{\boldsymbol{T}}\boldsymbol{X})^{-1}\boldsymbol{X}^{\boldsymbol{T}}\boldsymbol{G} \qquad \text{Eq. 6.27}$$

The parameters for the storage modulus and loss modulus in Eq. 6.7and 6.8 from the presented method are given in Table 6.1 and 6.2 below. These parameters are derived with Eq. 6.21 to Eq. 6.27.

Table 6.1 Parameter identification for shear storage and loss modulus of 30% iron particle concentration MRE

Parameters for shear storage modulus

G_0', MPa	G_1', Mpa	G_2', Mpa	G_3', Mpa	$G_4', Mpa \cdot s$	$G_5', Mpa \cdot s^2$
2.5233	-1.4926	1.1104	-2.8156E-01	3.6301E-02	-7.1999E-04
$G_6', Mpa \cdot s^3$	$G_7', Mpa/mT$	$G_8', Mpa/mT^2$	$G_9', Mpa \cdot s$	$G_{10}', Mpa \cdot s$	$G_{11}', Mpa \cdot s^2$
5.5086E-06	3.2651E-03	-1.4042E-06	-1.1970E-02	2.5806E-03	5.5061E-05

$G_{12}', Mpa/mT$	$G_{13}', Mpa/mT$	$G_{14}', Mpa/mT^2$	$G_{15}', Mpa \cdot s/mT$
-2.0618E-03	5.1335E-04	4.1771E-07	1.6288E-06

Parameters for shear loss modulus

G_0'', MPa	G_1'', Mpa	G_2'', Mpa	G_3'', Mpa	$G_4'', Mpa \cdot s$	$G_5'', Mpa \cdot s^2$
3.9281E-01	-2.5206E-01	9.3013E-02	-1.0594E-02	-1.8638E-03	-2.0133E-04
$G_6'', Mpa \cdot s^3$	$G_7'', Mpa/mT$	$G_8'', Mpa/mT^2$	$G_9'', Mpa \cdot s$	$G_{10}'', Mpa \cdot s$	$G_{11}'', Mpa \cdot s^2$
2.1477E-06	5.1209E-04	-3.5775E-07	7.5232E-03	-1.9958E-03	-5.4784E-06

$G_{12}'', Mpa/mT$	$G_{13}'', Mpa/mT$	$G_{14}'', Mpa/mT^2$	$G_{15}'', Mpa \cdot s/mT$
-1.8422E-05	-2.8808E-05	7.7118E-08	-1.9974E-06

Table 6.2 Parameter identification for compression storage and loss modulus of 30% iron particle concentration MRE

Parameters for compression storage modulus

G_0', MPa	G_1', Mpa	G_2', Mpa	G_3', Mpa	$G_4', Mpa \cdot s$	$G_5', Mpa \cdot s^2$
2.4743E+01	-2.6325E+01	2.4664E+01	-8.0225E+00	1.8797E-01	-2.3834E-03
$G_6', Mpa \cdot s^3$	$G_7', Mpa/mT$	$G_8', Mpa/mT^2$	$G_9', Mpa \cdot s$	$G_{10}', Mpa \cdot s$	$G_{11}', Mpa \cdot s^2$
7.8632E-06	2.5505E-02	-9.7413E-06	-1.2159E-01	1.6033E-02	1.0279E-03

$G_{12}', Mpa/mT$	$G_{13}', Mpa/mT$	$G_{14}', Mpa/mT^2$	$G_{15}', Mpa \cdot s/mT$
-2.9185E-02	9.1529E-03	1.3919E-05	5.8856E-06

Parameters for compression loss modulus

G_0'', MPa	G_1'', Mpa	G_2'', Mpa	G_3'', Mpa	$G_4'', Mpa \cdot s$	$G_5'', Mpa \cdot s^2$
4.7245E+00	-3.7506E+00	1.7645E+00	-2.4115E-01	-4.0880E-02	-1.9691E-03
$G_6'', Mpa \cdot s^3$	$G_7'', Mpa/mT$	$G_8'', Mpa/mT^2$	$G_9'', Mpa \cdot s$	$G_{10}'', Mpa \cdot s$	$G_{11}'', Mpa \cdot s^2$
2.5220E-05	2.1204E-03	-2.6387E-06	9.2451E-02	-2.5688E-02	-1.4411E-04

$G_{12}'', Mpa/mT$	$G_{13}'', Mpa/mT$	$G_{14}'', Mpa/mT^2$	$G_{15}'', Mpa \cdot s/mT$
1.7641E-03	-1.0957E-03	8.0177E-07	-2.0208E-05

Based on Eq.6.7 and Eq. 6.8, shear and compression storage modulus and loss modulus with respect to the strain amplitude and frequency and magnetic strength by the proposed model are plotted in Figure 6.2 and 6.3. The x, y and z-axis of the three-dimensional-plot are strain amplitude, frequency and magnetic strength. The colour shown in the figure represents the value of storage modulus or loss modulus. The red colour means the value is high and the blue means the value is low. For the storage modulus, smaller strain amplitude, at higher excitation frequency and with higher magnetic strength will lead to a higher storage modulus of the MRE. For the loss modulus, larger loss modulus is achieved with smaller strain amplitude, lower excitation frequency and with higher magnetic strength. The changes of the storage modulus and loss modulus for the three-dimensional plots are in accordance with the experimental results.

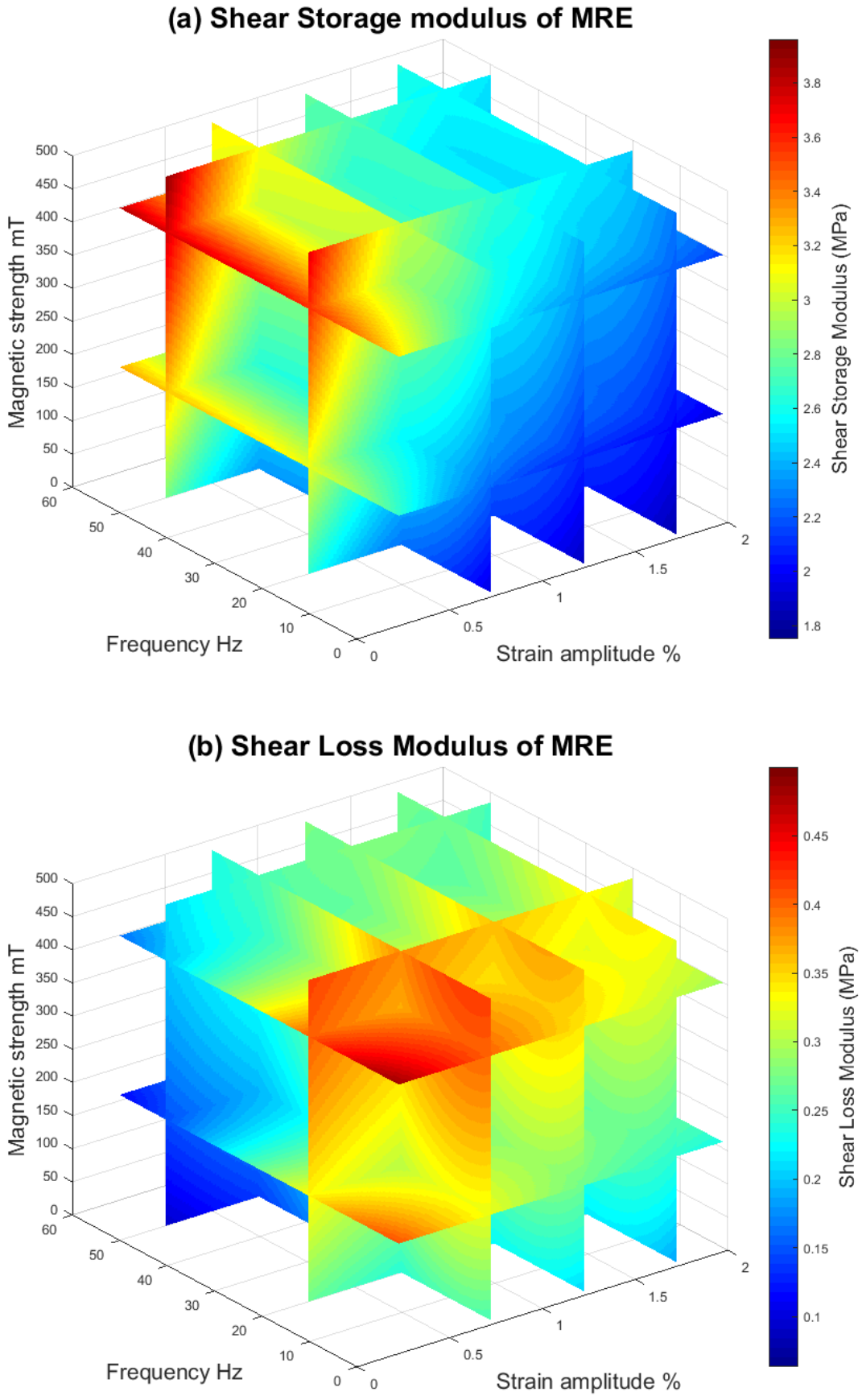

Figure 6.2 Three-dimensional slice plots of the (a) Shear Storage modulus and (b) Shear Loss modulus of 30% iron particle concentration MRE by the proposed model

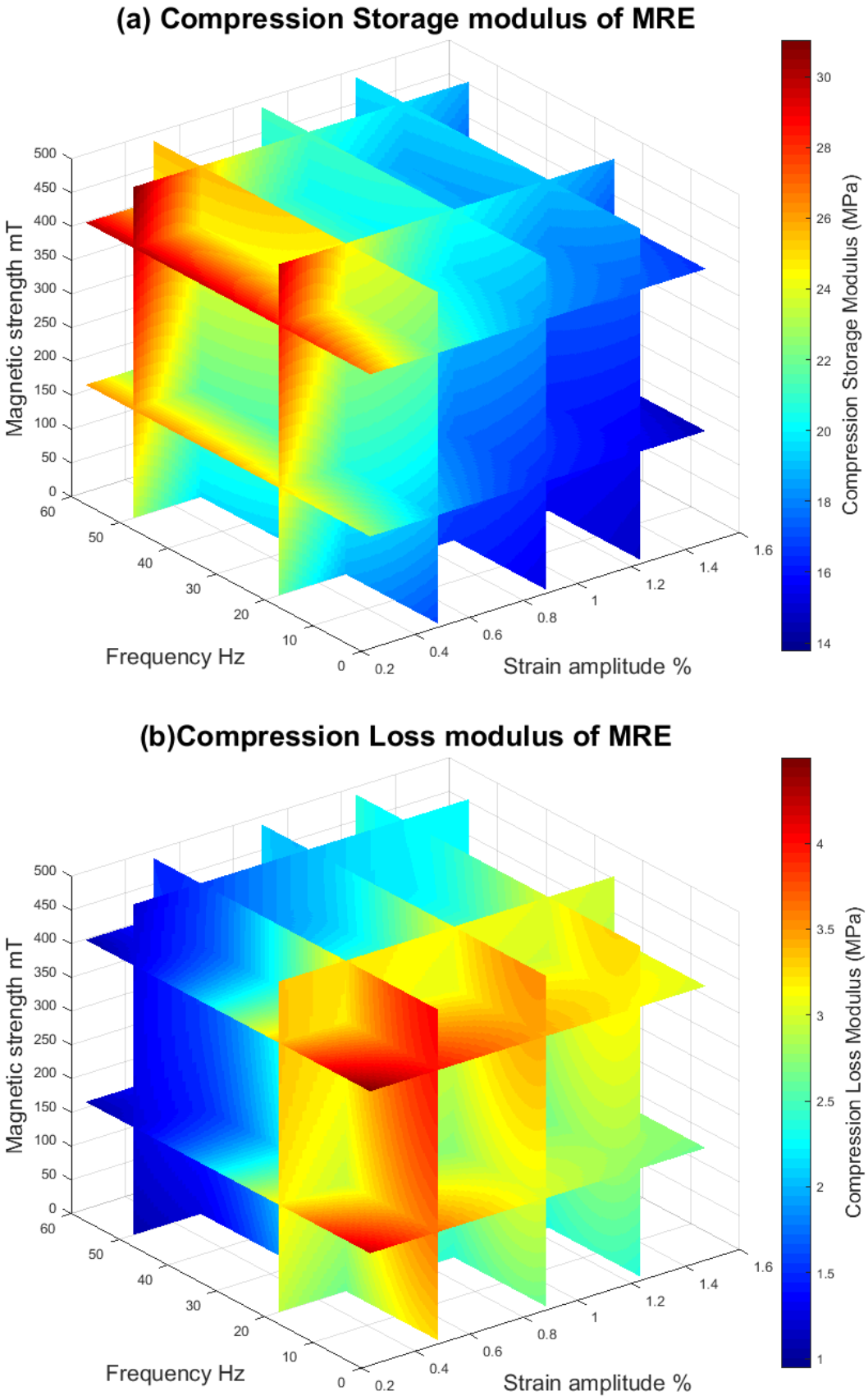

Figure 6.3 Three-dimensional slice plots of the (a) Compression Storage modulus and (b) Compression Loss modulus of 30% iron particle concentration MRE by the proposed model

6.2.3 Accuracy of the proposed model and comparison between the experiment results

The accuracy of the proposed model is examined at two parts. The first one is the accuracy of the simulation of strain-stress hysteresis curve of MRE. The other one is the accuracy of prediction of storage modulus and loss modulus of MRE with respect to strain, frequency and magnetic field. The simulations of strain-stress hysteresis curves for both shear and compression test of MRE are initially checked. The comparison of the hysteresis curves between the simulated results and experiment results for the MRE samples with shear and compression are shown in Figure 6.4 and 6.5, respectively. The experiment data is plotted with strain amplitude and shear/compression stress. The simulated data is plotted based on Eq. 6.6. For the results of MRE with shear test, the proposed model are validated with 1% and 2% strain amplitude at 10 Hz and 30 Hz with 0 mT and 300 mT and 485 mT magnetic field. For the validation of the compression test, the parameters selected are 1% and 1.5% strain amplitude, 10 Hz and 30 Hz with 0 mT, 300 mT and 490 mT magnetic field strength.

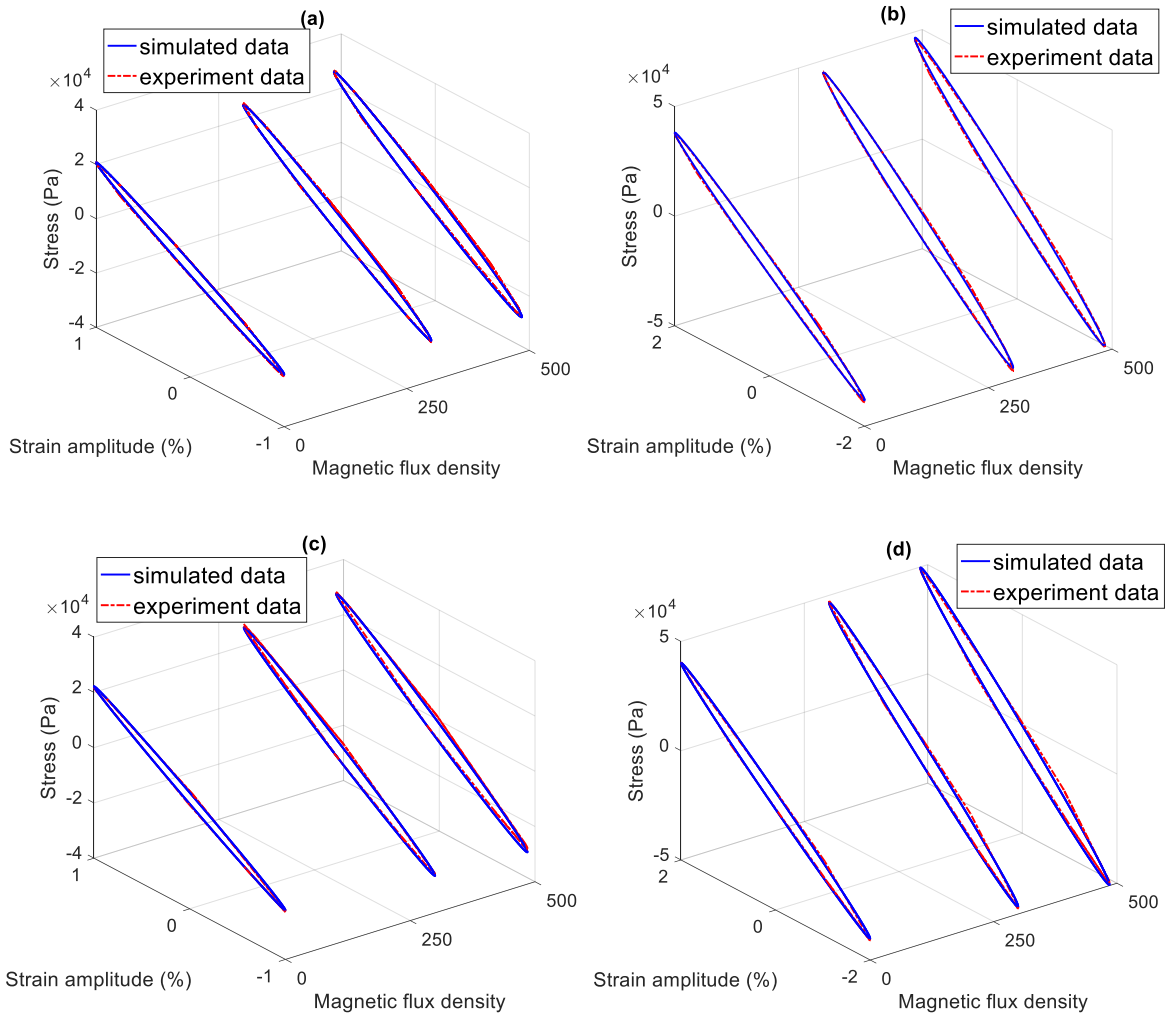

Figure 6.4 Comparison the experiment data and simulated data of shear stress-strain hysteresis curves (a) 1% strain amplitude at 10 Hz (b) 2% strain amplitude at 10 Hz (c) 1% strain amplitude at 30 Hz (d) 2% strain amplitude at 30 Hz with 0 mT, 300 mT, and 485 mT magnetic field strength.

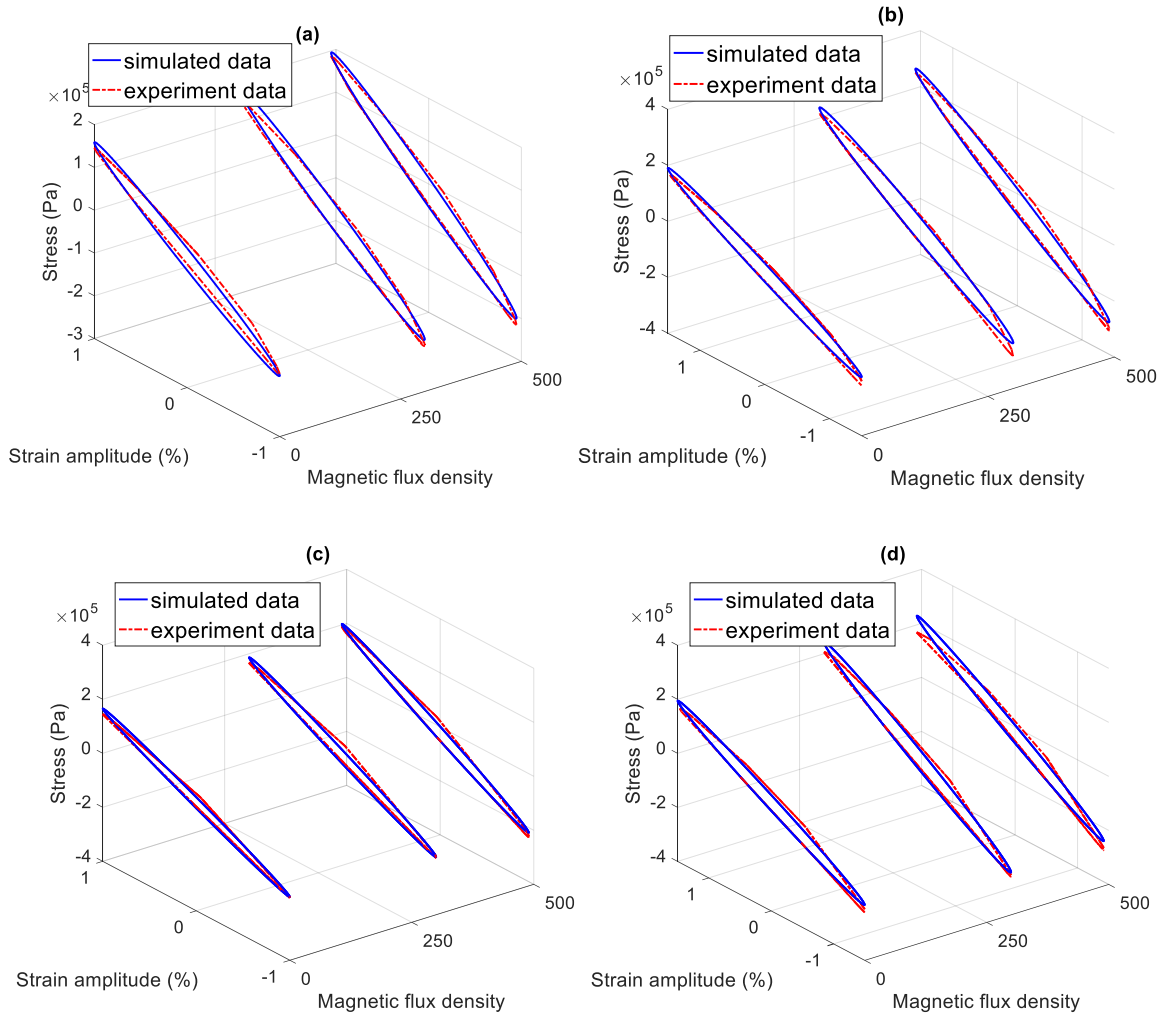

Figure 6.5 Comparison the experiment data and simulated data of compression stress-strain hysteresis curves (a) 1% strain amplitude at 10 Hz (b) 1.5% strain amplitude at 10 Hz (c) 1% strain amplitude at 30 Hz (d) 1.5% strain amplitude at 30 Hz with 0 mT, 300 mT, and 485 mT magnetic field strength.

It can be seen from the Figure 6.4 and 6.5 that the simulated stress-strain hysteresis curves substantially coincide with the experimental results. The simulated results demonstrate a better agreement with the experimental results for shear test. By increasing the magnetic flux density and excitation frequency, the shear and compression modulus of MRE increase. This phenomenon is well predicted by the current model. Comparing with the results of Figure 6.4-6.5, it is concluded that the proposed model could accurately describe the hysteresis stress-strain relationship of MRE.

Then, the simulated results of the storage modulus and loss modulus are plotted in Figure 6.6-6.9 based on the Eq. 6.7 and 6.8 and compared with the experimental data. The error bar of the experiment results are calculated based on Eq. 4.2.

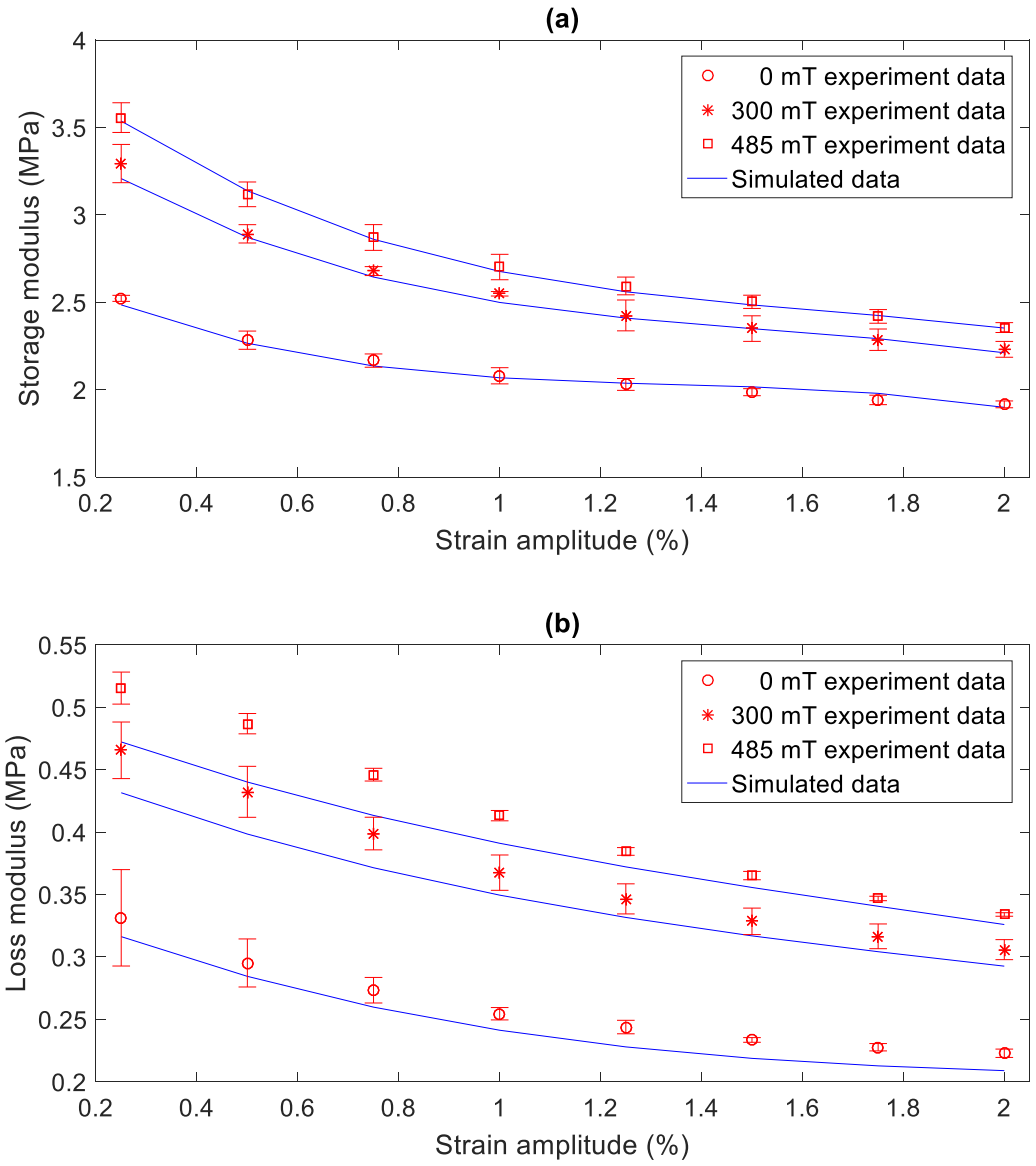

Figure 6.6 Comparison of the experimental data and simulated data of (a) shear storage modulus and (b) shear loss modulus of MRE at 10 Hz with 0 mT, 300 mT and 485 mT.

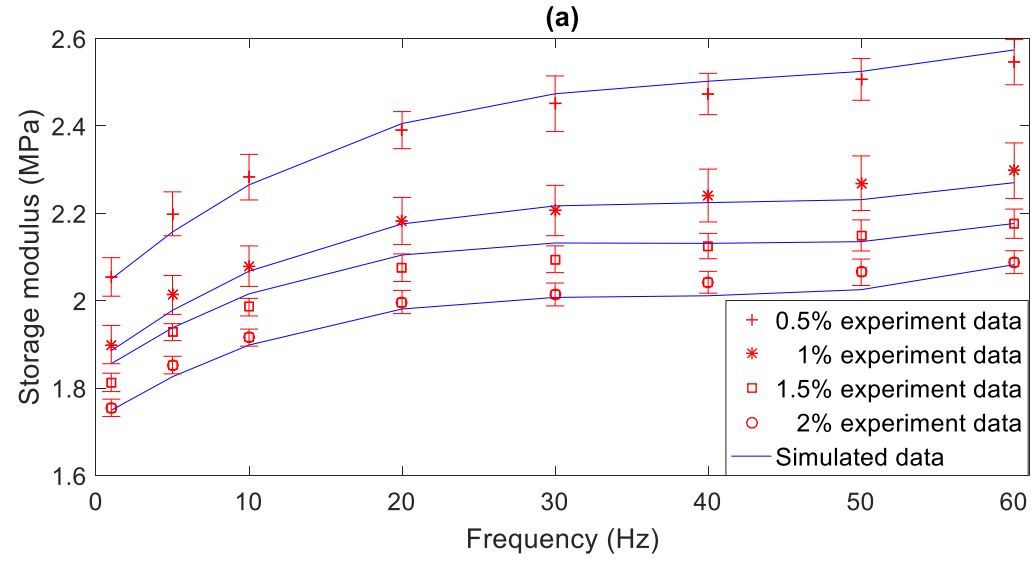

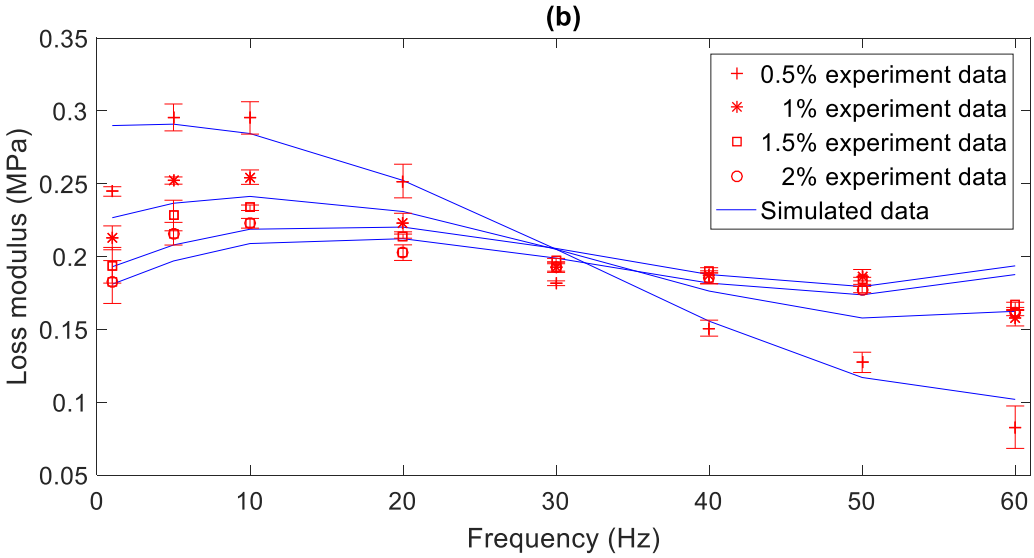

Figure 6.7 Comparison of the experimental data and simulated data of (a) shear storage modulus and (b) shear loss modulus of MRE at 0.5%, 1%, 1.5% and 2% strain amplitude at 0 mT.

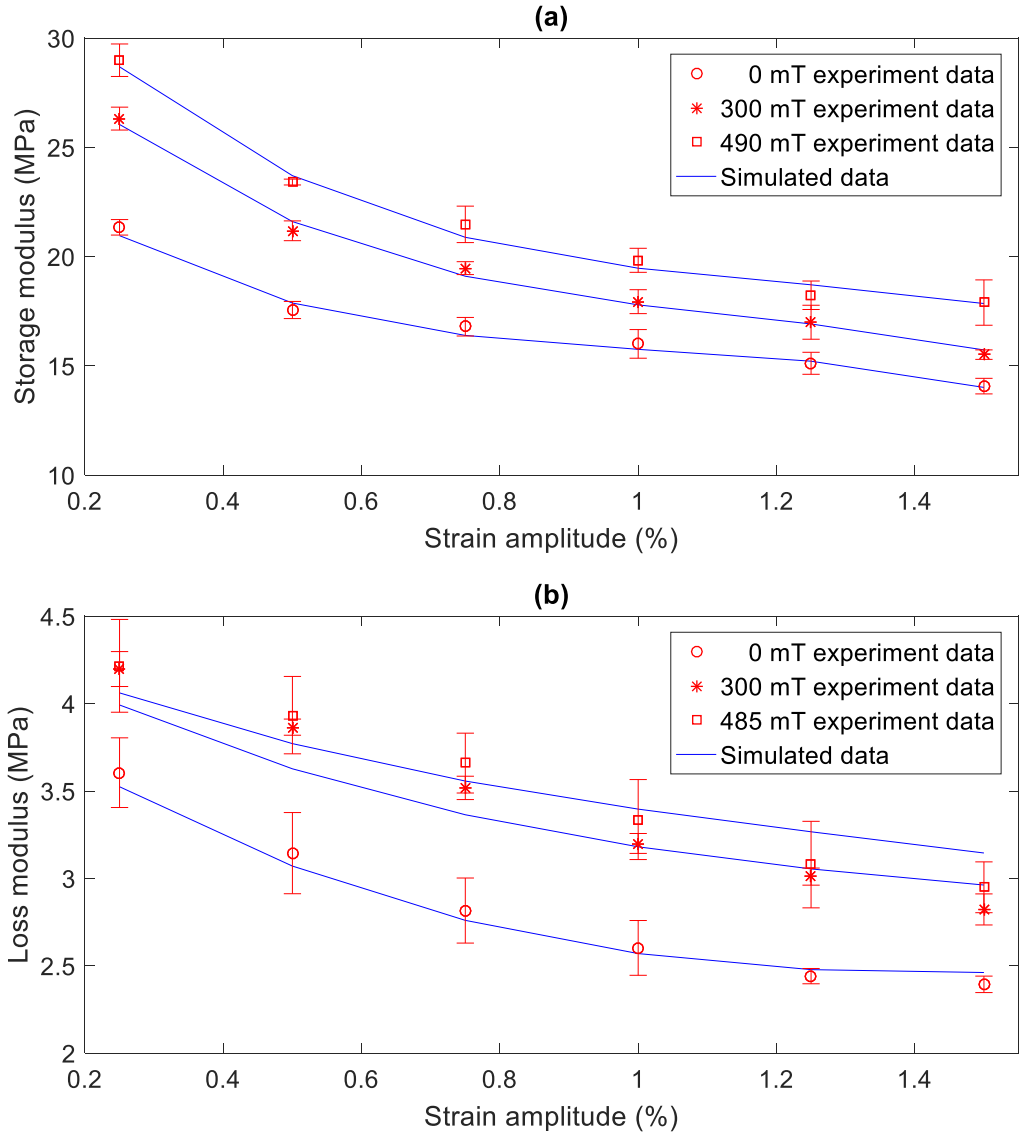

Figure 6.8 Comparison of the experimental data and simulated data of (a) compression storage modulus and (b) compression loss modulus of MRE at 10 Hz with 0 mT, 300 mT and 485 mT.

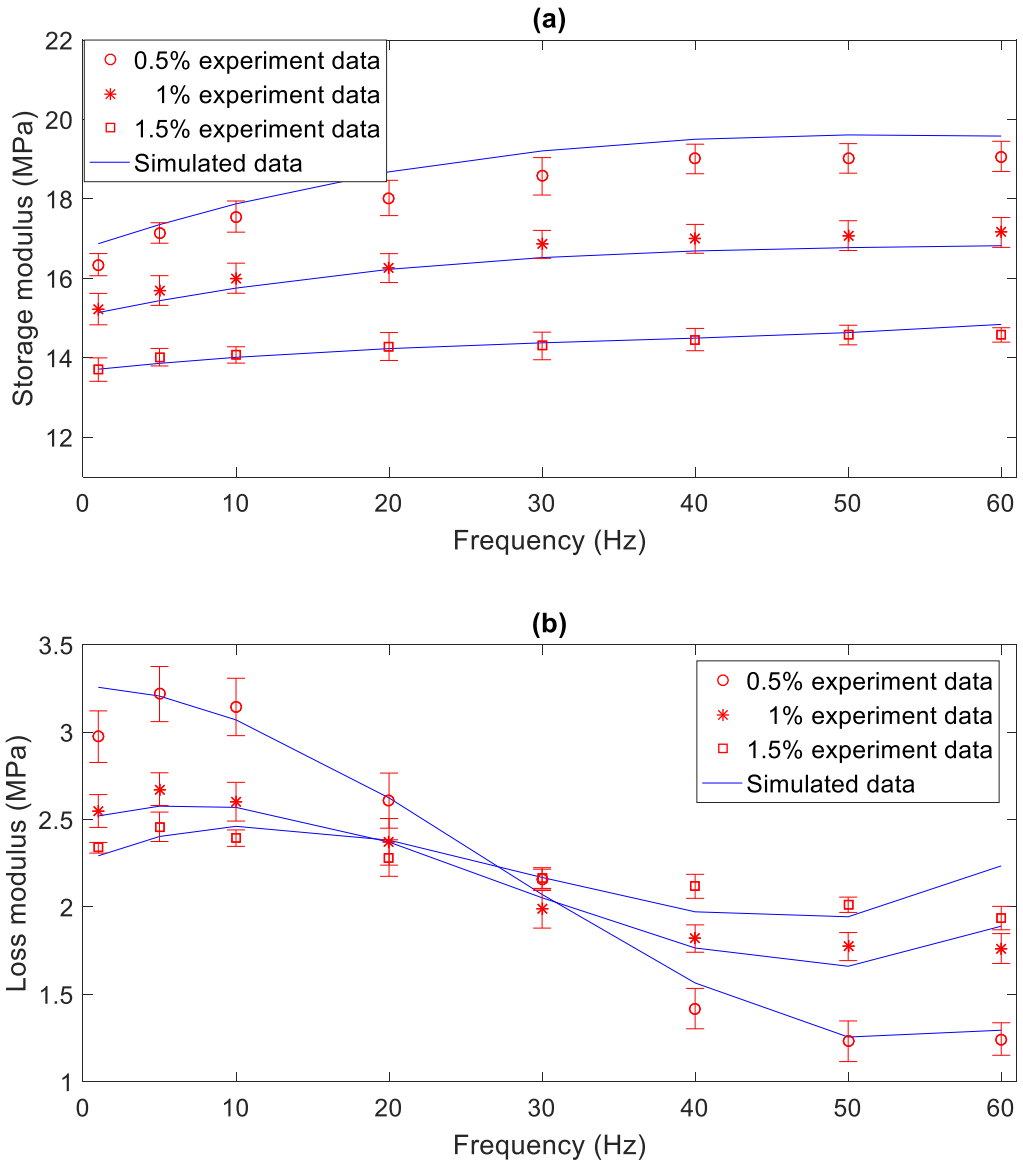

Figure 6.9 Comparison of the experimental data and simulated data of (a) compression storage modulus and (b) compression loss modulus of MRE at 0.5%, 1% and 1.5% strain amplitude at 0 mT.

The simulated results of storage modulus and loss modulus by the proposed model are compared with experimental results for two cases for both dynamic shear and compression mechanical properties of MRE. Figure 6.7 and Figure 6.9 compare the experimental data and simulated data of the storage modulus and loss modulus with different magnetic field strength at 10 Hz with increasing strain amplitude for dynamic shear and compression properties of MRE. Figure 6.8 and 6.10 illustrate the differences between experimental results and simulation results of strain-frequency coupling effect of storage modulus and loss modulus. As can be seen from Figure 6.7 to 6.10, the proposed model can accurately simulate both shear and compression storage and loss modulus of MRE. The proposed model is capable of capturing storage and loss modulus dependence on the strain, frequency and magnetic field. Most importantly, the coupling effects between strain-frequency and strain-magnetic-field are also well described. The simulation results for storage modulus illustrate a better

agreement with the experimental data comparing with loss modulus, since the non-linear properties of loss modulus are higher.

Then, the fitness value is used to evaluate the accuracy of the proposed model. The calculation of fitness value is given in Eq. 6.28.

$$fitness\ value\ (\%) = 100 * (1 - \left|\frac{\overline{G_e} - G_s}{\overline{G_e}}\right|) \quad \text{Eq. 6.28}$$

Where, $\overline{G_e}$ is the mean experiment data, G_s is the simulation data. $\overline{G_e}$ and G_s can be used to express storage modulus or loss modulus. The fitness value of storage modulus and loss modulus for the dynamic shear and compression properties of MRE are listed in Table 6.3 to 6.6 below.

Table 6.3 Fitness value of shear storage modulus of the presented model

Strain amplitude %	1Hz	5Hz	10Hz	20Hz	30Hz	40Hz	50Hz	60Hz
Magnetic flux density (0 mT)								
0.25	99.88	98.34	98.51	99.15	99.29	99.57	99.82	98.23
0.5	99.76	98.11	99.23	99.37	99.07	98.82	99.28	98.90
0.75	98.66	97.47	98.57	99.58	99.61	99.62	98.96	99.60
1	99.27	98.25	99.44	99.69	99.52	99.28	98.34	98.81
1.25	99.30	99.11	99.65	99.74	99.02	99.58	98.63	99.04
1.5	97.63	99.49	98.46	98.60	98.23	99.71	99.33	99.98
1.75	97.39	98.91	98.06	98.42	98.15	99.48	99.75	99.30
2	99.68	98.56	99.11	99.20	99.67	98.48	98.07	99.73
Magnetic flux density (485 mT)								
0.25	96.27	99.10	99.43	98.95	99.30	98.80	97.83	98.97
0.5	96.95	99.17	99.35	98.88	98.03	98.68	98.99	98.35
0.75	99.37	98.98	99.64	99.86	99.20	99.91	99.81	99.44
1	98.63	98.26	99.06	98.74	99.80	99.07	98.81	99.64
1.25	99.05	98.02	98.71	98.58	99.57	98.82	98.34	99.47
1.5	99.88	98.90	99.29	99.06	99.85	99.10	98.87	99.90

1.75	99.68	99.39	99.78	99.50	99.41	99.84	99.64	98.82
2	99.76	99.00	99.89	99.32	99.52	99.88	99.94	98.09

Table 6.4 Fitness value of shear loss modulus of the presented model

Strain amplitude %	1Hz	5Hz	10Hz	20Hz	30Hz	40Hz	50Hz	60Hz
Magnetic flux density (0 mT)								
0.25	72.57	97.75	95.45	95.25	96.94	85.54	64.71	80.31
0.5	81.51	98.43	96.37	99.84	87.15	96.83	91.85	76.97
0.75	86.57	96.61	95.04	95.08	84.52	99.43	78.55	97.93
1	93.52	93.82	94.80	96.61	93.63	94.35	84.84	97.22
1.25	98.14	90.54	93.48	94.16	94.80	97.07	91.06	90.60
1.5	99.47	91.13	93.68	97.09	95.92	99.02	97.22	83.95
1.75	98.19	89.95	93.44	95.21	95.12	99.83	99.23	81.59
2	99.17	91.32	93.75	95.27	96.67	98.25	97.96	83.58
Magnetic flux density (485 mT)								
0.25	91.46	94.68	91.63	94.97	87.16	92.82	99.28	94.74
0.5	95.01	91.46	90.40	96.57	80.12	76.51	98.80	65.53
0.75	94.01	93.30	92.68	99.82	84.18	93.95	85.41	98.88
1	94.59	94.45	94.64	95.45	92.70	99.54	86.43	96.89
1.25	93.63	95.29	96.78	92.60	94.64	97.00	89.19	97.76
1.5	92.74	96.77	97.39	91.49	95.89	97.62	92.10	96.49
1.75	92.65	97.40	98.20	91.09	96.25	97.66	92.46	96.49
2	92.56	98.16	97.59	94.17	98.72	93.99	89.90	98.24

The fitness value for storage modulus is higher comparing with that for loss modulus. It is because the loss modulus of MRE behaves a higher non-linear property comparing with the storage modulus. The mean fitness value for shear storage modulus and loss modulus is 99.06% and 92.94%. For the compression storage modulus and loss modulus, the mean fitness value is 98.46% and 95.22%. It is concluded that the proposed model is capable of accurately describing dynamic shear and compression mechanical properties of MRE. The results of storage and loss modulus of MRE material are accurately simulated by the dependence of strain amplitude, frequency and magnetic field.

Table 6.5 Fitness value of compression storage modulus of the presented model

Strain amplitude %	1Hz	5Hz	10Hz	20Hz	30Hz	40Hz	50Hz	60Hz
Magnetic flux density (0 mT)								
0.25	98.91	98.85	98.21	99.20	99.77	99.55	98.63	99.21
0.5	96.78	98.77	98.18	96.35	96.56	97.39	96.89	97.32
0.75	98.95	97.26	97.63	99.46	98.19	98.14	98.36	98.14
1	99.43	98.37	98.44	99.81	98.03	98.20	98.23	98.06
1.25	97.66	99.33	99.37	98.70	98.86	99.01	99.20	98.65
1.5	99.93	98.89	99.58	99.63	99.45	99.75	99.58	98.19
Magnetic flux density (490 mT)								
0.25	88.41	97.63	97.76	97.66	95.45	98.01	93.11	77.01
0.5	90.50	99.64	97.65	99.41	95.86	89.66	98.04	95.96
0.75	93.64	97.89	98.00	99.53	96.95	93.76	89.33	94.57
1	98.89	96.36	98.75	99.94	96.68	97.04	93.64	92.75
1.25	97.10	97.15	98.48	98.26	99.64	92.75	93.05	89.75
1.5	98.03	97.74	97.17	95.51	99.77	93.11	96.59	84.58

Table 6.6 Fitness value of compression loss modulus of the presented model

Strain amplitude %	1Hz	5Hz	10Hz	20Hz	30Hz	40Hz	50Hz	60Hz
Magnetic flux density (0 mT)								
0.25	99.35	99.37	98.95	99.99	98.47	98.99	99.78	99.67
0.5	97.51	99.55	98.75	98.01	98.17	98.92	98.18	98.47
0.75	99.03	97.21	97.24	98.27	98.57	97.66	98.08	97.97
1	99.01	98.15	98.18	98.75	98.21	98.00	98.11	98.35
1.25	97.33	98.07	97.38	96.54	96.01	96.30	97.07	96.47
1.5	99.76	98.52	99.76	99.17	99.00	98.93	98.49	99.51
Magnetic flux density (490 mT)								
0.25	95.16	98.69	96.33	96.27	98.12	99.59	99.89	90.30
0.5	96.57	96.25	95.86	97.36	97.03	76.61	70.58	99.43
0.75	99.28	95.80	97.19	99.92	98.82	94.28	92.11	90.84
1	95.44	98.34	98.21	96.76	97.79	95.85	90.16	96.52
1.25	99.58	98.25	93.91	90.70	97.27	92.20	89.06	98.39
1.5	96.19	99.26	93.35	93.01	99.91	92.39	92.67	95.02

6.3 Modelling the pre-strain effect on the dynamic properties of MRE

The experimental results in Section 4.3-4.5 and 5.3-5.5 demonstrate pre-strain effect to the dynamic shear and compression mechanical properties of MRE. The effect of the shear pre-strain and compression pre-strain on the dynamic mechanical properties is different. The pre-strain effect on the storage modulus and loss modulus is also different for MRE with different iron particle concentrations. In this chapter, the dynamic mechanical properties of MRE with 30% iron particle concentration are simulated, since the controllability of MRE with 30% iron particle concentration is relatively higher compared with the others.

For shear pre-strain effect on the dynamic shear mechanical properties of MRE, it is concluded that a shear pre-strain induces magnitude reduction of shear storage modulus. As shear pre-strain amplitude continues to increase, MRE becomes stiffer and storage modulus starts to increase. Shear loss modulus demonstrates a slight increase as shear pre-strain is applied. Loss modulus starts to decrease as shear pre-strain continues to increase (1% to 2%). The dependence of pre-strain effect on shear mechanical properties of MRE is independence of strain amplitude and motion frequency. In the meantime, a magnetic field magnifies the effect of pre-strain. Then, the effect of shear pre-strain on the dynamic mechanical properties is modelled as a function of shear pre-strain amplitude and magnetic field strength. The value change on the dynamic properties of MRE due to pre-strain is regarded as a compensation value to shear storage modulus and shear loss modulus without the pre-strain.

For compression pre-strain effect on the dynamic compression properties of MRE, it is also found that the dependence of compression pre-strain effect on the dynamic mechanical properties is independence of strain amplitude and frequency. The coupling effect between pre-strain amplitude and magnetic field strength for dynamic compression properties is not obvious comparing with that of MRE with shear test. This is because the effect of the compression pre-strain on the dynamic mechanical properties is more significant which diminishes the effect of magnetic field. The effect of compression pre-strain on the dynamic compression mechanical properties is modelled as a function of compression pre-strain amplitude and magnetic flux density which has the same form as the shear pre-strain.

The expressions of the compensation value of pre-strain for storage modulus and loss modulus are given in Eq. 6.29 and 6.30.

$$G_p' = C_{s1}\gamma_p + C_{s2}\gamma_p^2 + C_{s3}\gamma_p B \quad \text{Eq. 6.29}$$

$$G_p'' = C_{l1}\gamma_p + C_{l2}\gamma_p^2 + C_{l3}\gamma_p B \quad \text{Eq. 6.30}$$

G_p' and G_p'' are the compensation value of the storage modulus and loss modulus due to pre-strain, $C_{s1}\ to\ C_{s3}$ and $C_{l1}\ to\ C_{l3}$ are parameters need to determine from the experiment, γ_p is the pre-strain amplitude. For the compression pre-strain γ_c,

$$\gamma_p = \gamma_c - 2\% \quad \text{Eq. 6.31}$$

The parameters are derived by the multivariate polynomial regression method. The procedures to derive these parameters are given in Eq. 6.21 to Eq. 6.27. The compensation parameters of storage and loss modulus due to pre-strain effect for both dynamic shear and compression properties of MRE are given in Table 6.7 and Table 6.8.

Table 6.7 Compensation parameters for shear storage modulus and loss modulus

Compensation Parameters for shear storage modulus		
C_{s1}	C_{s2}	$C_{s3},/mT$
-2.26E-02	6.45E-04	-6.80E-05
Compensation Parameters for shear loss modulus		
C_{l1}	C_{l2}	$C_{l3},/mT$
8.47E-03	-5.83E-03	6.62E-06

Table 6.8 Compensation parameters for compression storage modulus and loss modulus

Compensation Parameters for compression storage modulus		
C_{s1}	C_{s2}	$C_{s3},/mT$
1.00E+00	-4.15E-02	2.93E-04
Compensation Parameters for compression loss modulus		
C_{l1}	C_{l2}	$C_{l3},/mT$
5.92E-02	-8.11E-03	-3.91E-05

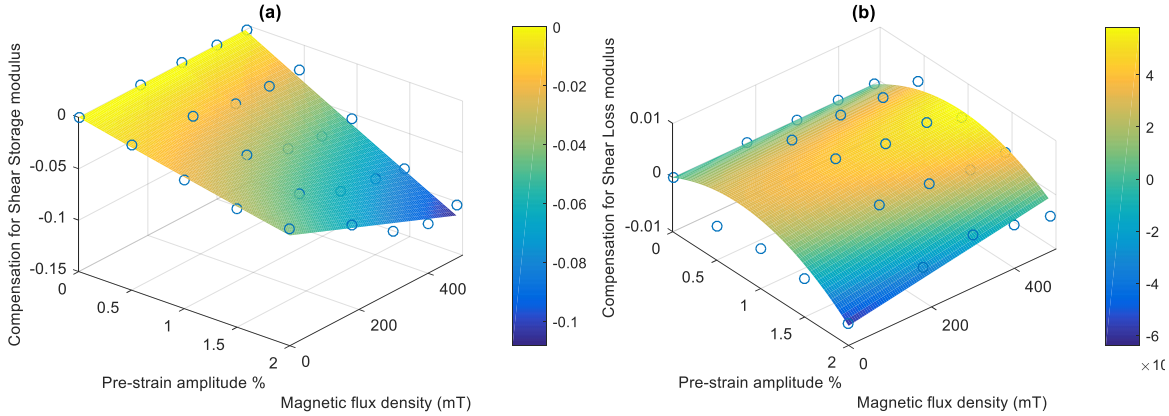

Figure 6.10 Compensation value due to pre-strain for (a) shear storage modulus (b) shear loss modulus

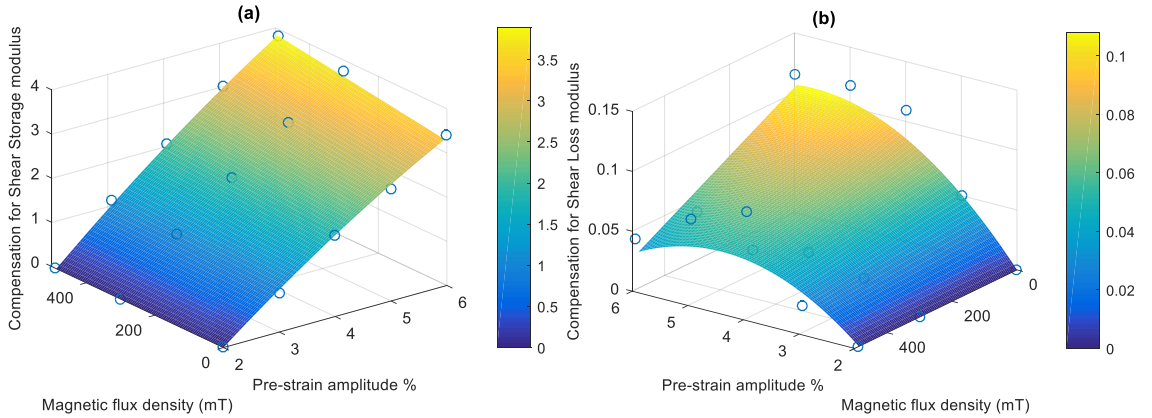

Figure 6.11 Compensation value due to pre-strain for (a) compression storage modulus (b) compression loss modulus

Figure 6.10 and Figure 6.11 compare the simulated and experimental compensation value due to pre-strain. The plot of the simulated compensation value is based on Eq. 6.29 and Eq. 6.30. From these two figures, it is found that the simulated results show a better agreement for the compensation value for storage modulus.

6.4 Summary

The dynamic shear and compression properties of MRE with 30% iron particle concentration are modelled in this chapter. The dynamic mechanical properties of MRE are dependent on the strain amplitude, frequency, magnetic field and pre-strain. The couplings between these dependences also have effects on the dynamic mechanical properties of MRE.

The modelling procedures include two steps. The first step is to model the dynamic properties of storage modulus and loss modulus of MRE with dependence of strain, frequency and magnetic field. The coupling effect between strain-frequency, strain-magnetic-field and frequency-magnetic-field are considered. A modified classical viscoelastic Kelvin-Voigt model is developed to model the dynamic properties of MRE without pre-strain condition. The storage modulus and loss modulus are expressed by a three order polynomial and multivariate polynomial regression method is applied to identify the parameters of this polynomial. The simulation results show that the proposed model can accurately and continuously describe storage modulus and loss modulus for both dynamic shear and compression mechanical properties of MRE. The simulated results of storage modulus are more accurate compared with those of loss modulus. This is because loss modulus demonstrates higher non-linear properties.

The second step is to simulate pre-strain effect on the dynamic properties of MRE. Since, the pre-strain effect is independent of strain amplitude and frequency while dependent on pre-strain amplitude and magnetic field. Then, pre-strain effect is modelled as a function of pre-strain amplitude and magnetic field and is regarded as a compensation value to the total storage modulus and loss modulus.

Storage modulus and loss modulus of the dynamic shear and compression properties of MRE can be expressed as a function of strain, frequency, magnetic field and pre-stain are given in Eq. 6.32 and 6.33 below.

$$G'_{total} = G' + G'_p \qquad \text{Eq. 6.32}$$

$$G''_{total} = G'' + G''_p \qquad \text{Eq. 6.33}$$

G'_{total} and G''_{total} are storage modulus and loss modulus considered the dependence of strain, frequency, magnetic field and pre-strain. G' and G'' are storage modulus and loss modulus without pre-strain defined in Eq. 6.7 and 6.8. G'_p and G''_p are the compensation value of the pre-strain effect to the storage modulus and loss modulus.

The proposed model in this chapter is capable of continuously describing the dynamic properties of MRE by including the dependences of strain, frequency, magnetic field and pre-strain. And this

model is used to evaluate the performance of MRE for the dynamic isolation problem in the following chapter.

Chapter 7: Design novel hybrid squeeze and shear MRE isolator

7.1 Introduction

The operation mode of MRE can be classified into two groups, which are squeeze mode and shear mode. Both of these modes have their own advantages and disadvantages. The MR effect for MRE operated in shear mode is relatively higher compared with that for squeeze mode, which indicates that the control bandwidth for MRE shear mode based vibration control device is wider. Meanwhile, a MRE squeeze mode based vibration control device has higher stiffness with higher load capacity.

Engine vibration is usually the main vibration source in many engineering applications, such as maritime vessels or automotive vehicles. For engine vibration isolation, a designed isolator should have certain properties. The first one is a designed isolator should have enough stiffness to support an engine. Revolutions per minute (RPM) of engine varies with different working conditions. Especially, during the engine starting procedure, vibration frequency increases from zero and rises to the desired working frequency. Then, it is required that the designed isolator should have a wider effective bandwidth.

A vibration isolator withstands the gravity force of the engine. This initial loading cause a pre-strain on a MRE based vibration isolator. The previous chapter analyse the pre-strain effect on both shear and compression dynamic mechanical properties of MRE and it is found that large pre-strain amplitude deteriorates the controllability of MRE.

In order to control the pre-strain within a reasonable region, the squeeze mode of MRE is used which provides a high stiffness to support the engine. In the meantime, the operation of MRE in shear mode is also used to enhance the overall controllability of the isolator.

In this chapter, a hybrid squeeze and shear based MRE isolator is developed. By combining the squeeze and shear mode of MRE, the new designed MRE isolator has a high load capacity, wide effective control bandwidth and with compact size. Comparing with a traditional rubber isolator, one important issues need to resolve for MRE isolator is to provide sufficient magnetic field to control the stiffness and damping properties of MRE. In this chapter, firstly, the structure of a hybrid squeeze and shear based MRE isolator is proposed. Then, the design of a closed magnetic circuit for MRE isolator and the calculation of the magnetic flux density generated by the proposed design are provided. Then, a prototype of the hybrid squeeze and shear based MRE isolator is developed.

7.2 Structure of hybrid MRE isolator

The structure design of the proposed hybrid squeeze and shear MREs isolator is given in Figure 7.1 and 7.2 below.

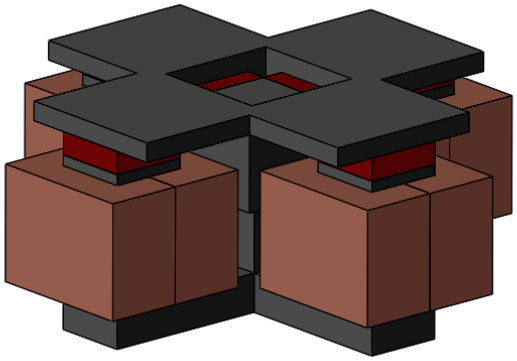

Figure 7.1 Hybrid squeeze and shear mode based MRE isolator

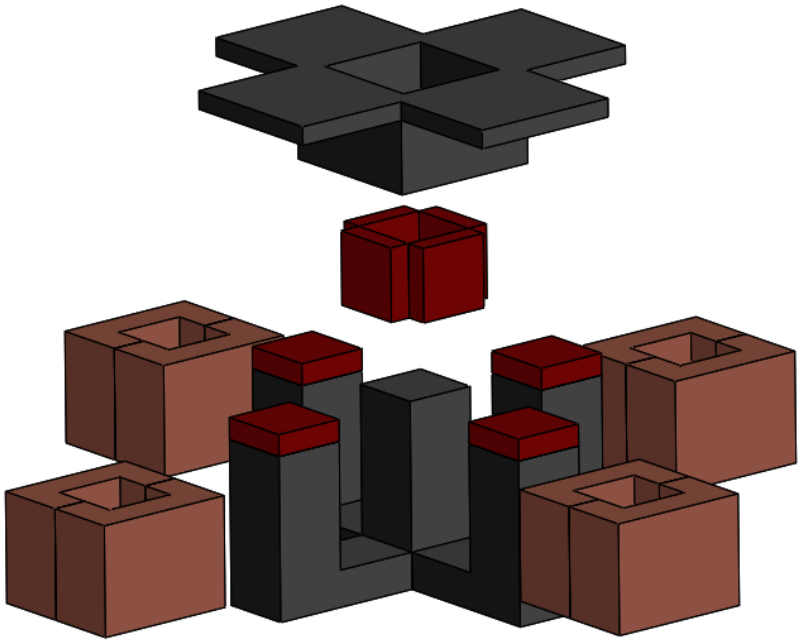

Figure 7.2 Exploded view of the hybrid squeeze and shear mode based MRE isolator

The cross-shaped hybrid MRE isolator contains four parts, which are bottom base, coils, MRE and top cover. From Figure 7.1 and 7.2, the red parts are MRE material, the dark black are the bottom base and top cover, the copper part are the metal copper coils. The four vertical MRE materials (shown in Figure 7.2) in the centre part of the isolator are glued by adhesive (Araldite ®, extra strong adhesive) to the middle column of the bottom base and the inner side of the top cover. As hybrid MRE in working condition, the surface of MRE glued to the middle column of bottom base remains

stationary. A shear force is applied to the other surface of MRE through the top cover. Then, it is said that the operation mode of these four part MRE materials is regarded as shear mode. The operation mode for the other four MRE materials glued to the top surface of the side column of the bottom base is regarded as squeeze mode.

The design procedure of a MRE based isolator is different comparing with a traditional rubber-based isolator. The design procedures for a traditional rubber-based isolator include: specify an equipment to be isolated (weight, size, etc.), identify dynamic disturbances (sinusoidal, random, etc.), select rubber material and calculate the dimension of the rubber for desired stiffness working condition, etc. (Gent, 2012). For the design procedure of a MRE based isolator, there is another important procedure which is to design the magnetic circuit to provide magnetic field to control MRE material.

For the hybrid shear and compression MRE based isolator, 30% iron particle concentration MRE sample is selected for the designed MRE based isolator. The controllability of 30% iron particle concentration MRE sample is relatively higher comparing with the other two MRE samples. The geometry of MRE sample is used as the same as MRE samples used for shear and compression test. One import issue which limits the application of MRE is how to generate magnetic field to control MRE material.

In this chapter, special consideration is given to the magnetic circuit design. The designed magnetic circuit aims to have light weight, low power consumption and compact size. The design of the magnetic circuit is given in Section 7.3.

7.3 Design and optimisation of magnetic circuit

The purpose of a magnetic circuits design is to assess how many turns of coil is needed at a desired current input to generate the required magnetic field. The design procedures for a magnetic circuit are listed as followed:

- Specify the magnetic field strength needed to generate
- Calculate the total magnetic reluctance of the magnetic circuit
- Evaluate number of windings and current to generate the desired magnetic field
- Measure the dimensions of the solenoid and check whether it suits for the isolator structure.

For application of MRE isolator in engineering field, there is always limit space for MRE isolator to install. The magnetic circuit is usually bulky and heavy. In order to enhance the application of MRE based isolator, an optimisation process is required to ensure the designed MRE isolator has compact size and lower weight. Power consumption is another factor that limits the application of MRE isolator. The power consumption of magnetic circuit could be high. The designed MRE isolator also needs to be optimised to have lower power consumption.

In order to have a wider control bandwidth of the proposed hybrid shear and squeeze mode MRE isolator, the designed magnetic circuit is required to generate a 0.5 Tesla magnetic field strength.

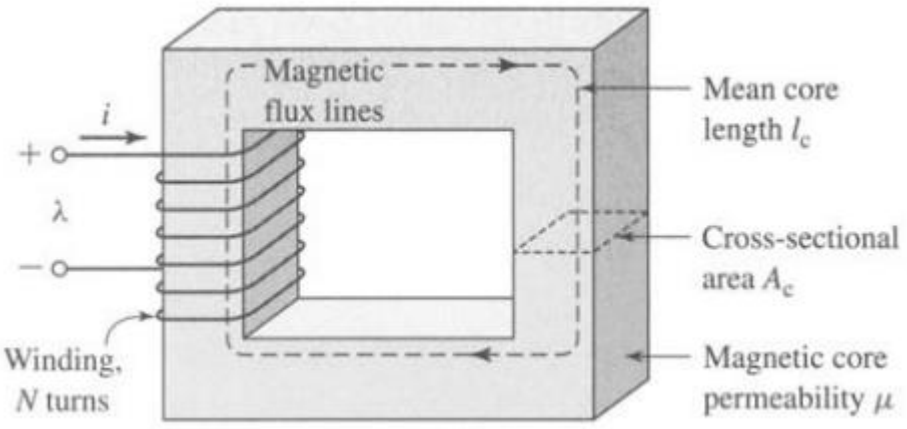

Figure 7.3 Magnetic circuit (Fitzgerald et al., 2003, p.3)

Figure 7.3 demonstrates a basic magnetic circuit. The magnetic circuit consists of a high magnetic permeability core and a solenoid. Magnetic flux traveling through the core is dependent on the current, winding numbers, cross-section area, mean core length and the magnetic core permeability.

In physics, magnetomotive force is used to describe the magnetic flux in a magnetic circuit.

$$mmf = \Phi * R \qquad \text{Eq. 7.1}$$

where mmf is the magnetomotive force, Φ is the magnetic flux through the magnetic circuit, R is the magnetic reluctance. The Eq. 7.1 is known as Hopkinson's law. The magnetomotive force in Eq. 7.1 is analogous to the voltage in Ohm's law. The magnetic reluctance is analogous to resistance in Ohm's law.

The magnetomotive force is also equal to the product of the number of turn N and current i.

$$mmf = N * i \quad \text{Eq. 7.2}$$

Then, combining the Eq. 7.1 and 7.2 yield,

$$\Phi * R = N * i \quad \text{Eq. 7.3}$$

Φ also equals to the product of the magnetic flux density B and cross section area A.

$$\Phi = B * A \quad \text{Eq. 7.4}$$

The definition of the magnetic reluctance (R) is given in Eq. 7.5,

$$R = \frac{l}{A * \mu_0 * \mu} \quad \text{Eq. 7.5}$$

where, μ_0 is the magnetic permeability in vacuum, μ is the relative magnetic permeability of the core material. Since the cross-section of the proposed magnetic circuits is not a constant, so the magnetic flux instead of the magnetic flux density is used to calculate the number of winding turn. Then, the number of turn is defined as

$$N = \frac{\Phi * R}{i} \quad \text{Eq. 7.6}$$

The magnetic reluctance in Eq. 7.6 is the total reluctance in the magnetic circuit. For each magnetic circuit of the integral MRE isolator, the total magnetic reluctance is equal the summation of the magnetic reluctance of the MRE samples both in shear and squeeze mode, magnetic reluctance of one quarter bottom base and top cover.

The magnetic reluctance is dependent on the magnetic permeability of the materials. The magnetic permeability is a term which describes the ability of the material to allow the magnetic flux pass through it. A larger magnetic permeability means the magnetic flux is easier to pass through. Usually, a high magnetic permeability material is selected as the core material. The Table 7.1 lists the relative permeability of the magnetic materials.

Table 7.1 Relative permeability of the magnetic material (Engineeringtoolbox.com, 2017)

Material	Relative Magnetic Permeability (μ)
Silicon Steel	40000
Iron (99.8% pure)	5000
Ferritic Stainless steel	1000-1800
Nickel (99% iron)	600

As can be seen from Table 7.1, the magnetic permeability varies significantly for different magnetic materials. The relative magnetic permeability of the silicone steel is the highest. However, the price of the silicone steel is also the highest. Due to limit budget, the iron (99.8% pure) is selected as the core material of the magnetic circuit.

The data of the relative magnetic permeability of the MRE is difficult to obtain. Kallio (2005) used stationary coil method to measure the magnetic permeability of the anisotropic MRE with 30% iron particle cued at 260 mT. The relative permeability of the anisotropic MRE is around 3.34. Based on author's experience, using the stationary coil method will underestimate the relative magnetic permeability of the material. So, the relative magnetic permeability of the anisotropic MRE is assumed to be 3.5.

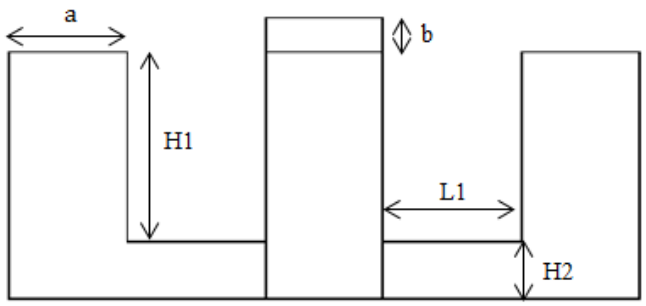

Figure 7.4 Front view of the bottom base of the designed isolator

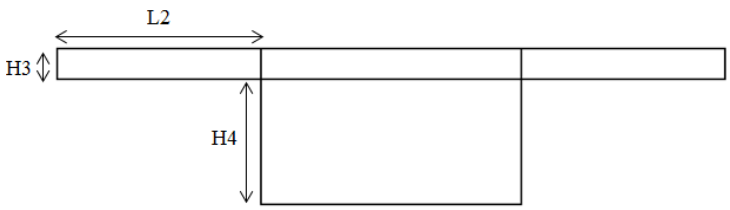

Figure 7.5 Front view of the top cover of the designed isolator

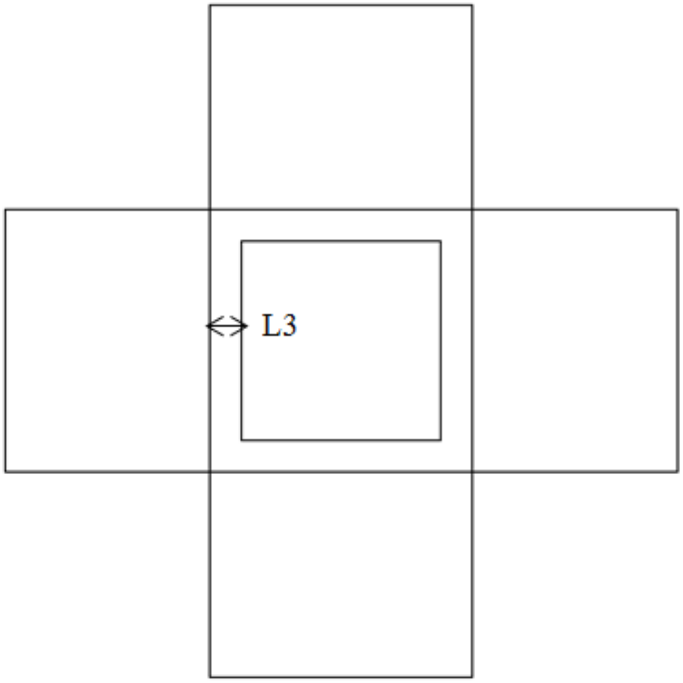

Figure 7.6 Top view of the top cover of the designed isolator

The magnetic reluctance of the one quarter of the designed isolator will be calculated first. The magnetic circuit will start from the side column of the bottom base and go through the MRE material working as the squeeze mode. After that, the magnetic flux will go through the top cover and cross the MRE material again, and then return back to the middle column of the bottom based. The Figure 7.4-7.6 show the dimension parameters of the bottom base and top cover of the designed isolator. For these parameters, a and b are respectively the length and height of the MRE sample used to design the isolator. The maximum magnetic field cross the MRE is 0.5 T and the magnetic saturation of the Iron is 2.1 T. In order to optimise the design isolator to have lower weight, the parameter of H3 and L3 are selected as a quarter of the length of MRE. H2 is defined as half of the length of MRE to ensure the centre gravity of the isolator low. The dimension parameters are given in Table 7.2 below.

Table 7.2 Dimension parameters of the design isolator

Parameter	Value (mm)
a	22
b	6.5
H2	11
H3	5.5
H4	22
L2	10+L1
L3	5.5
L1	L1
H1	H1

Then, the only dimension parameters need to be specified are L1 and H1. The magnetic reluctance of the one quarter of the isolator designed is calculated based on the Eq. 7.5. The magnetic reluctance of the one quarter of the integral structure is provided in Table 7.3.

Table 7.3 Magnetic reluctance of the MRE isolator

Part	Magnetic reluctance ($ampere - turns/weber$)
Top cover	$\frac{\mathrm{L1}}{968\pi} * 10^7 + 57410$
Bottom Base	$\frac{\mathrm{H1} + \mathrm{L1}}{1936\pi} * 10^7 + 33752$
Two MREs	6109987
Total	$6201149 + \frac{\mathrm{H1} + 3\mathrm{L1}}{1936\pi} * 10^7$

Then, the number of coil winding is calculated with Eq. 7.6. The magnetic flux Φ through the MRE isolator is calculated by the Eq. 7.4. The magnetic flux density is 0.5T and the cross-section area is

obtained as 0.000484 m^2. The magnetic flux is equal to 0.000242 Wb. The parameters needed to calculate the solenoid coil are listed in Table7.4.

Table 7.4 Parameters for the coil winding

Parameter	Symbol	Parameter	Symbol
Current (A)	i	Number of Layer	N_l
Wire Diameter (mm)	d	Total Length of Wire (m)	L_t
Winding Length (mm)	L_w	Resistance (ohm)	R_r
Number of Turns	N	Voltage at Rated Current (V)	V
Turns per Layer	N_t	Power at Rated Current (W)	P

The winding length is equalled to side column of the bottom base while a three millimetre margin is remained from both ends.

$$L_w = H1 - 6 \quad \text{Eq. 7.7}$$

The number of turn is calculated based on the Eq. 7.6 which is given in Eq. 7.8

$$N = \left\lceil \frac{\Phi * R_m}{i} \right\rceil \quad \text{Eq. 7.8}$$

The turn per layer and number of each layer is defined below

$$N_t = \left\lfloor \frac{L_w}{d} \right\rfloor \quad \text{Eq. 7.9}$$

$$N_l = \left\lceil \frac{N}{N_t} \right\rceil \quad \text{Eq. 7.10}$$

Total length of wire is defined as

$$L_t = \left(\pi d * N_t + 4 * \left(a + d(N_l - 2)\right)\right) * (N_l - 1) + \left(\pi d + 4a + 8d(N_l - 1)\right) * (\mathrm{N} - N_t * (N_l - 1)) \quad \text{Eq. 7.11}$$

The electric resistance R_r is

$$R_r = \frac{4 * \rho_r * L_t}{\pi * d^2} * 10^6 \quad \text{Eq. 7.12}$$

where $\rho_r = 1.72 * 10^{-8}\ ohm * meter$ is the resistivity of the copper wire. Then, the power consumption of the designed magnetic circuit is defined as

$$P = i^2 * R_r \quad \text{Eq. 7.13}$$

The deigned magnetic circuit is required to have low power consumption, compact size and light weight. The weight of the magnetic circuit includes two parts. The first part is the weight of the copper coil. The second part is the weight of the magnetic core which is the sum of the weight of the bottom base and top cover. The weight of the coil is calculated in Eq. 7.14.

$$W_{coil} = \rho_{copper} * L_t * \frac{\pi d^2}{4} \quad \text{Eq. 7.14}$$

ρ_{copper} is the density of the copper which equals to $8.96\ g/cm^3$. The weight of the magnetic core is defined as a function of H1 and L1.

$$W_{core} = 505.45 + 15.54 * L1 + 19.00 * H1 \quad \text{Eq. 7.15}$$

The total weight of the magnetic circuit is the sum of the weight of the coil and core.

$$W_{total} = W_{coil} + W_{core} \quad \text{Eq. 7.16}$$

Then, next step is to find an optimised value of power consumption and total weight of the magnetic circuit to manufacture the hybrid shear and squeeze MRE based isolator. Power consumption of the designed isolator is defined in Eq. 7.13 which contains variable of current i, wire diameter d and the height of the side column of bottom base $H1$. Total weight of the design isolator given in Eq. 7.16 contains variable of current i, wire diameter d and two dimensions of the bottom base $H1$ and $L1$.

Then, a multi-objective optimisation problem is formulated for the designed hybrid shear and squeeze MRE based isolator. Two conflicted objectives are lighter weight and lower power consumption. In order to have lower power consumption, both of the current i and electric resistance R_r are required to be small. According to Eq. 7.6 and 7.12, in order to generate the same magnetic field strength, a lower current induces more turns of the copper coil. To maintain the electric resistance R_r at a smaller value, a thick wire diameter d is required. More turns of copper coil and thicker wire diameter increase both of size and weight of the magnetic circuit. Conversely, in order to achieve a compact size and low weight of the magnetic circuit, a higher current with thinner wire diameter are needed. In the meanwhile, the power consumption of the magnetic circuit increases accordingly.

For optimisation of the designed isolator, minimum weight of the isolator is chosen as the main optimisation objective. If power consumption is selected as the main optimisation object, the size of

the optimised isolator becomes large and the corresponding weight of the isolator is heavy. Total weight of the isolator includes the weight of the core material and the weight of the copper coil. To optimise total weight of the isolator, the weight of both core material and the copper coil is optimised. Less weight of the core material makes the size of the isolator more compact and less weight of the cooper coil means less power consumption for the specified current and coil diameter.

The variable ranges and constrains are given in Eq. 7.17 and 7.18.

$$\begin{cases} 1\ ampere\ \leq i \leq 3\ ampere \\ 0.5\ mm \leq d \leq 1\ mm \\ 20\ mm \leq H1 \leq 100\ mm \\ 20\ mm \leq L1 \leq 100\ mm \end{cases} \quad \text{Eq. 7.17}$$

$$\begin{cases} (1)\ N_l * d \leq L1 * 0.5 \\ (2)\ N_l * d + 15 \leq L1 \\ (3)\ i * R_r \leq 15 \end{cases} \quad \text{Eq. 7.18}$$

For the optimisation process, the four variables are selected because i, d, $H1$ and $L1$ are the parameters influenced the weight and power consumption of the designed isolator. The variable range of current i is dependent on power supply and taken as an integer between 1 ampere and 3 ampere. The diameter of wire is selected from 0.5mm to 1mm with an interval of 0.1mm. For the wire diameter below 0.5 mm, the electric resistance R_r will increase significantly. And for the wire diameter above 1 mm, the weight and the space required for the coil winding will be relatively large. Then, both of these two ranges are excluded for the optimisation process. The range of the dimension $H1$ and $L1$ are selected based on author's experience. The manufacturing precision for the available workshop to fabricate the designed isolator is 0.5 mm, therefore the interval of $H1$ and $L1$ is taken as 1mm.

The constraints are placed to satisfy the geometric and physical rationality, where the optimisation results may not be able to manufacture without the constraints. The first constrain in Eq. 7.18 is to avoid the overlap between the winding coils. The second constrain is to prevent the overlap between the winding coil and the top cover and a 3 mm margin is left between the coil and top cover. The third constrain is the limited by the output of the power supply.

The optimisation processes are summarized as follow:

- Specify the value of current i and coil diameter d
- Calculate the total weight of the designed isolator with all the dimensional variables $H1$ and $L1$
- Comparing the total weight and find the minimum value of the total weight

- Identify the dimensional variable $H1$ and $L1$ to achieve the minimum value of the total weight
- Calculate the power consumption with the optimised $H1$ and $L1$.

The optimised results of the weight of the isolator and the power consumption are given in Figure 7.7. Each point is the optimised value of the total weight and power consumption of the isolator for a specified current and coil diameter. The relevant parameters for each case are given in Table 7.5 and 7.6.

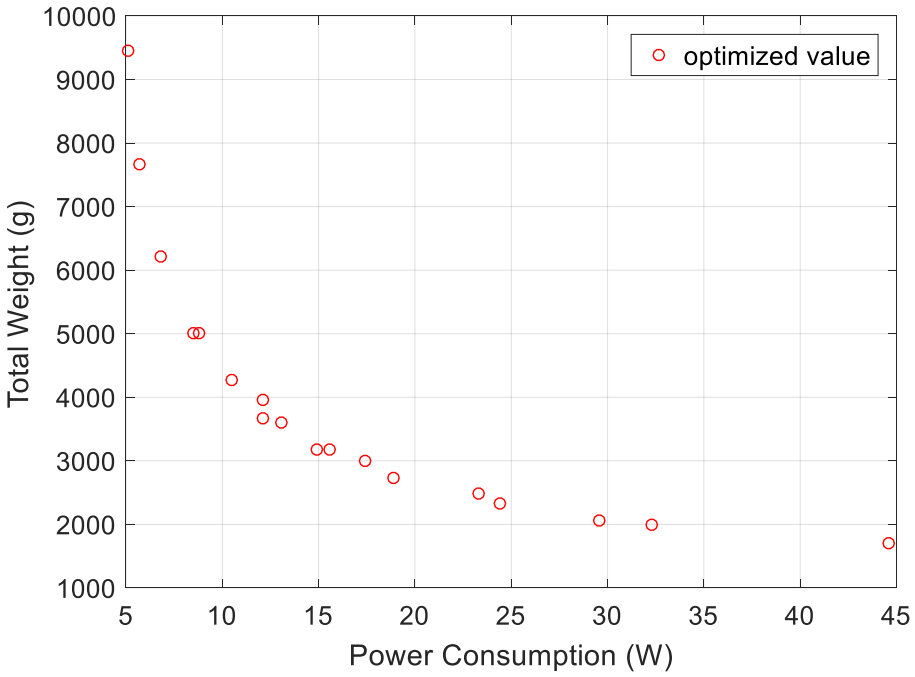

Figure 7.7 Optimised results of total weight and power consumption of the designed isolator

Table 7.5 The optimised parameter for designed isolator with specified current and coil diameter

d (mm)	1	0.9	0.8	1	0.7	0.9	0.6	1	0.8
i (A)	1	1	1	2	1	2	1	3	2
H1 (mm)	100	100	90	72	72	60	54	54	50
L1 (mm)	36	31	27	27	27	27	27	26	27
L_t (m)	230.6	209.2	198.2	96.4	196.8	96.5	198.0	61.4	95.7
N	1584	1578	1569	781	1562	779	1555	518	777
N_t	94	104	105	66	94	60	80	48	55

N_l	17	16	15	12	17	13	20	11	15
R_r (ohm)	5.1	5.7	6.8	2.1	8.8	2.6	12.1	1.3	3.3
V (V)	5.1	5.7	6.8	4.2	8.8	5.2	12.1	4.0	6.6
P (W)	5.1	5.7	6.8	8.5	8.8	10.5	12.1	12.1	13.1
W_{coil} (g)	6492.2	4770.0	3570.0	2713.7	2714.8	2201.1	2006.2	1729.1	1724.4
W_{core}(g)	2964.7	2887.0	2634.8	2292.9	2292.9	2064.9	1950.9	1935.4	1875.0
W_{total}(g)	9456.9	7657.0	6204.8	5006.6	5007.7	4266.0	3957.2	3664.5	3599.4

Table 7.6 The optimised parameter for designed isolator with specified current and coil diameter

d (mm)	0.5	0.9	0.7	0.8	0.6	0.7	0.5	0.6	0.5
i (A)	1	3	2	3	2	3	2	3	3
H1 (mm)	59	42	39	38	32	32	32	27	23
L1 (mm)	23	27	27	26	26	25	23	24	23
L_t (m)	169.2	63.9	97.3	61.3	95.5	60.5	84.4	58.9	56.4
N	1552	517	775	516	773	515	771	514	513
N_t	106	40	47	40	43	37	52	35	34
N_l	15	13	17	13	18	14	15	15	16
R_r (ohm)	14.9	1.7	4.4	2.1	5.8	2.7	7.4	3.6	5.0
V (V)	14.9	5.2	8.7	6.3	11.6	8.1	14.8	10.8	14.9
P (W)	14.9	15.6	17.4	18.9	23.3	24.4	29.6	32.3	44.6
W_{coil} (g)	1190.4	1458.0	1342.5	1105.0	967.4	834.6	593.8	596.5	397.0
W_{core}(g)	1983.8	1723.0	1666.0	1631.5	1517.5	1501.9	1470.8	1391.4	1299.9
W_{total}(g)	3174.1	3181.0	3008.5	2736.5	2484.8	2336.5	2064.7	1987.9	1696.9

The Figure 7.7 presents the optimised results of the total weight and power consumption of the designed isolator. As it expected, lower power consumption will induce a heavier isolator. In order

to make the designed isolator compact and light weight, the power consumption will increase. For current project, the selection of the coil diameter and the current for the hybrid squeeze and shear MRE isolator are dependent on the manufacture difficultly and power consumption. In order to have a moderate power consumption of the designed isolator, the power consumption for single solenoid coil is limited by 20W. The number of turns is selected to around 500 to reduce the manufacture difficultly. Then, the current and coil diameter are selected as 3 ampere and 0.8 mm. The other relevant parameters related to the design isolator are given in Table 7.6 and marked in red colour. The total weight of the designed hybrid MRE isolator is 2736.5 gram and power consumption for single solenoid coil is 18.9 W.

7.4 Simulation the magnetic circuit in COMSOL MULTIPHYSICS

The magnetic circuit of the hybrid MRE isolator is simulated in the commercial software COMSOL MULTIPHYSICS by using the parameters calculated in Section 7.3. The aim of this process is to exam whether the designed magnetic circuit can produce sufficient magnetic field strength to control the mechanical properties of the MRE and the overall magnetic flux distribution among the integrated hybrid MRE isolator. The detailed settings of simulation of the magnetic circuit by COMSOL MULTIPHYSICS are given in Appendix II.

Figure 7.8 (a) and (b) below demonstrate the simulation domain of the magnetic circuit and the mesh of the domain. The magnetic flux generated by the solenoid not only just passes through the designed magnetic circuit, some magnetic flux will also leak in the air. In order to make this physical problem more realistic, an air domain is considered to the MRE isolator. The dimension of the isolator is $118mm \times 118mm \times 61mm$ and the dimension of the air domain is $500mm \times 500mm \times 400mm$. The centre of the isolator and the air-box are coincident. Since the magnetic flux through the isolator is the main problem of concern, a finer mesh is selected to mesh the isolator and a relatively coarse mesh is used to mesh the air domain.

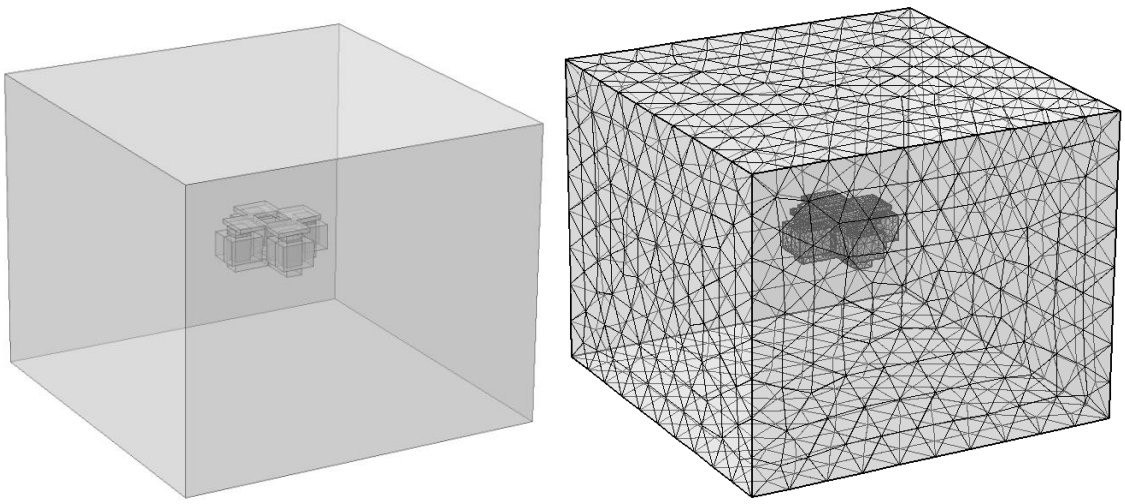

(a) (b)

Figure 7.8 (a) Simulation domain (b) mesh of the integral domain

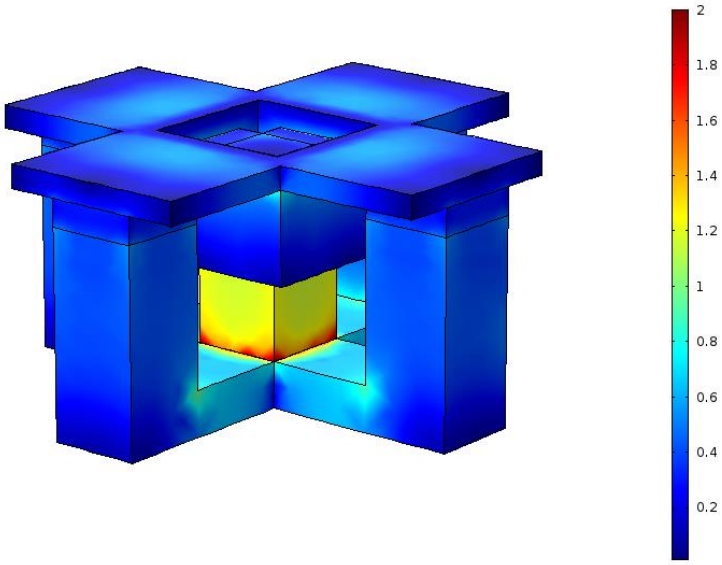

Figure 7.9 Surface plot of the magnetic flux density of the entire MRE isolator

Figure 7.9 illustrates the magnetic flux density on the surface of the entire MRE isolator. As can be seen from this figure, the magnetic flux density on the surface of the MRE isolator is relatively low. The value of the magnetic flux density on the surface of the middle column of the bottom base is higher, since the magnetic flux generated from the side columns will joint into the middle column.

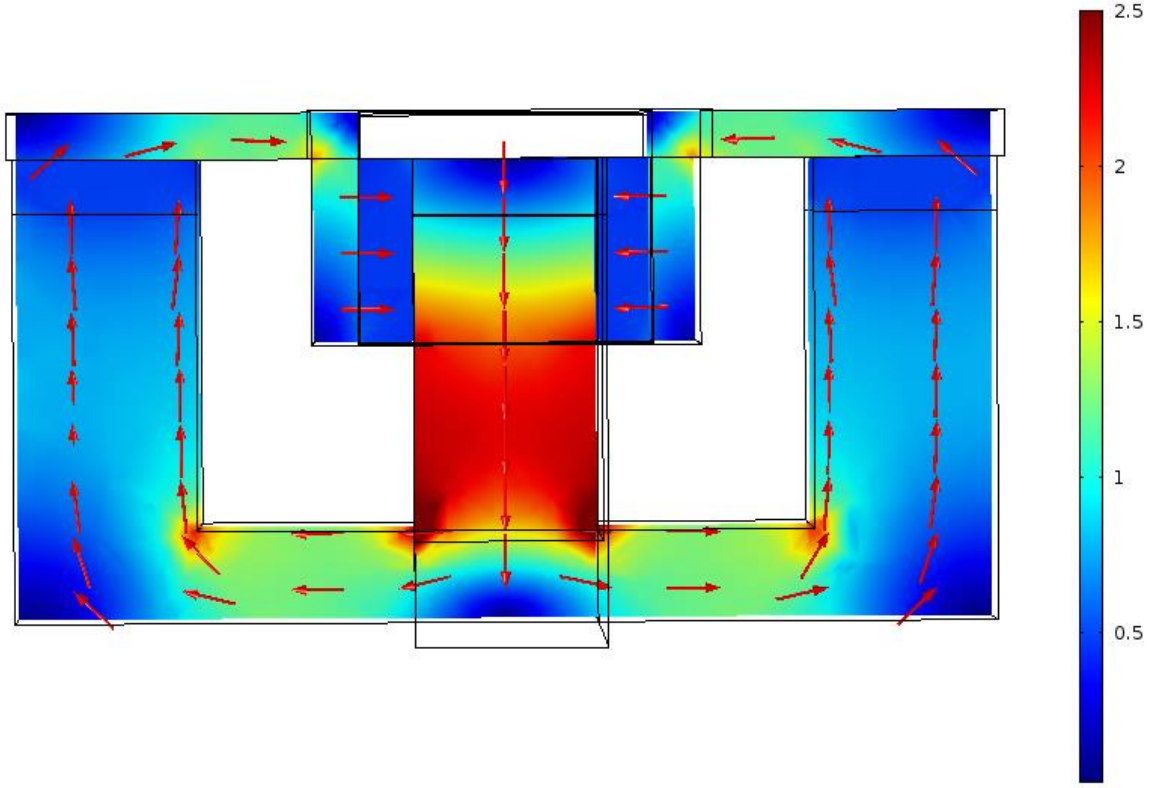

Figure 7.10 Magnetic flux density (T) and magnetic flux vector plot of the mid-section of the MRE isolator

Figure 7.10 indicates the magnetic flux density distribution and the magnetic flux vector inside the MRE isolator. The red arrow represents the magnetic flux vector. The current for the solenoid is set

as an anti-clock direction and an upward magnetic flux is generated. The path of the magnetic flux is described as follow. The magnetic flux initially goes upward through the side column of the isolator bottom base. Then, the magnetic flux goes through the squeeze MRE sample, top cover, shear MRE sample and returns back to the bottom based. A closed loop magnetic circuit is formed as expected.

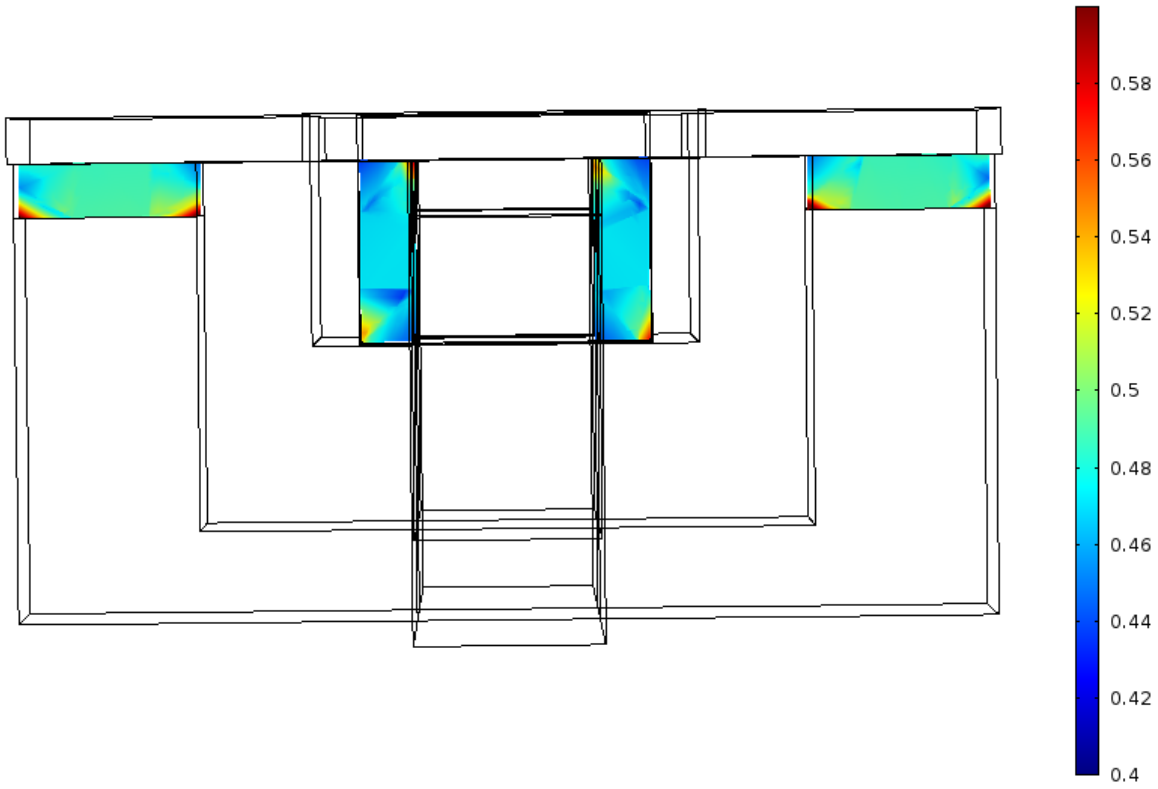

Figure 7.11 Magnetic flux density (T) plot of the MRE material

From Figure 7.10, the magnetic flux density inside the MRE isolator and the magnetic flux vector is obtained. However, it is difficult to obtain the value of magnetic flux density of the shear and squeeze MRE from the legend since the magnetic flux density of the MRE is relatively low compared with the value of other parts of the structure. So the magnetic flux density of the shear part and squeeze part MRE are plotted separately from the entire structure. As can be seen from the Figure 7.11, the magnetic flux density at the squeeze part MRE is slightly higher compared with the shear part MRE. The magnitude of the magnetic flux density for the compression MRE is around 0.49T to 0.51T and for the shear part MRE the magnitude of magnetic flux density is between 0.46T to 0.48T.

It is concluded that the design structure can provide sufficient magnetic flux density for both of the shear and squeeze mode MRE.

7.5 Manufacture and assembly of the hybrid MRE isolator

The hybrid squeeze and shear MRE isolator is manufactured based on the optimised results obtained in Section 7.3. The values of L1 and H1 are 26 mm and 38 mm, respectively. The other relevant dimensions of the bottom based and top cover of the designed isolator are listed in Table 7.2. The coil diameter is selected as 0.8 mm. The isolator top cover and bottom base (shown in Figure 7.12) are manufactured by the EDMC workshop in the University of Southampton.

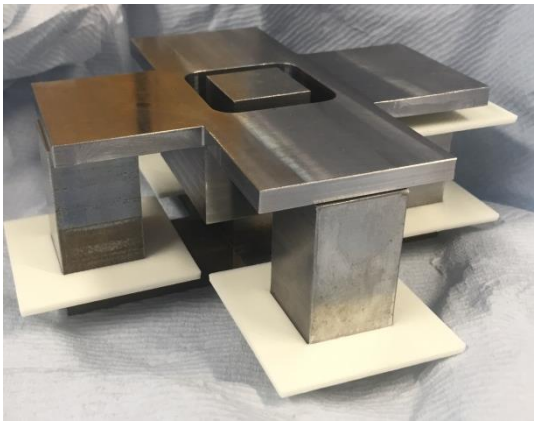

Figure 7.12 Top cover and bottom base of designed isolator with optimised dimension parameter

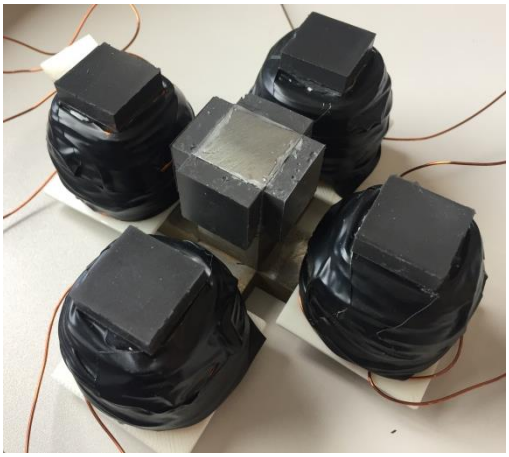

Figure 7.13 Bottom base of the hybrid squeeze and shear MRE isolator

The white plastic slices inserted on the side column of bottom base are used for supporting the winding coils. The first step to assemble the hybrid MRE isolator is to wind copper coils at the four side columns of bottom base. After winding coils, four set copper coils are welded together. Then, eight pieces of MRE samples are glued to the bottom base by adhesive (Araldite ®, extra strong adhesive). Four pieces are glued on the top surface of side column of the bottom base and the other four pieces are glued on the centre column of the bottom base (shown in Figure 7.13). The final step is to glue the top cover to the isolator. Figure 7.14 presents the assembled hybrid squeeze and shear MRE isolator.

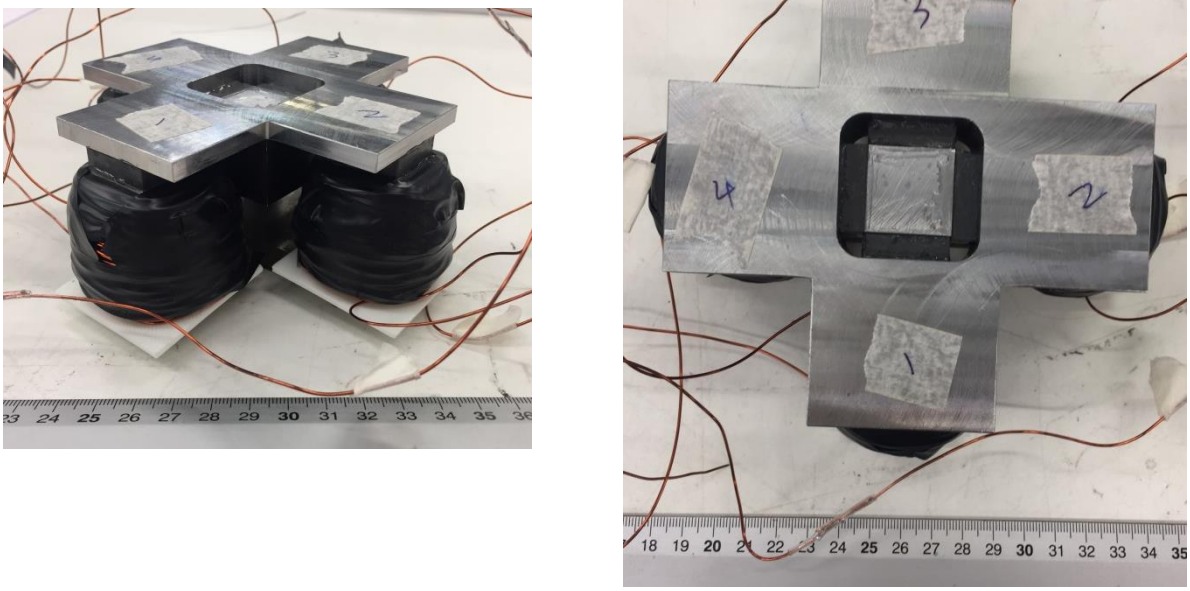

Figure 7.14 The assembled hybrid squeeze and shear MRE isolator.

During the manufacture and assemble processes, there is one issue arising that affect the performance of the designed hybrid MRE isolator. The designed isolator requires 516 turns of copper coil. The space designed for 516 turns coil is assumed that each coil is tightly and neatly winded. The winding of copper coil is done manually and it is difficult to maintain each turn of copper coil tightly winded. Especially, the layer number of winding increases to 5. Even through, a three millimetre space margin is remained for winding. It is still difficult to achieve the required 516 turns copper coil. A 320 turns copper coil is achieved. The magnetic field strength generated by the manufactured isolator is measured by a Gauss meter. Magnetic field strength generated by the isolator is around 270 mT at the current of 3A.

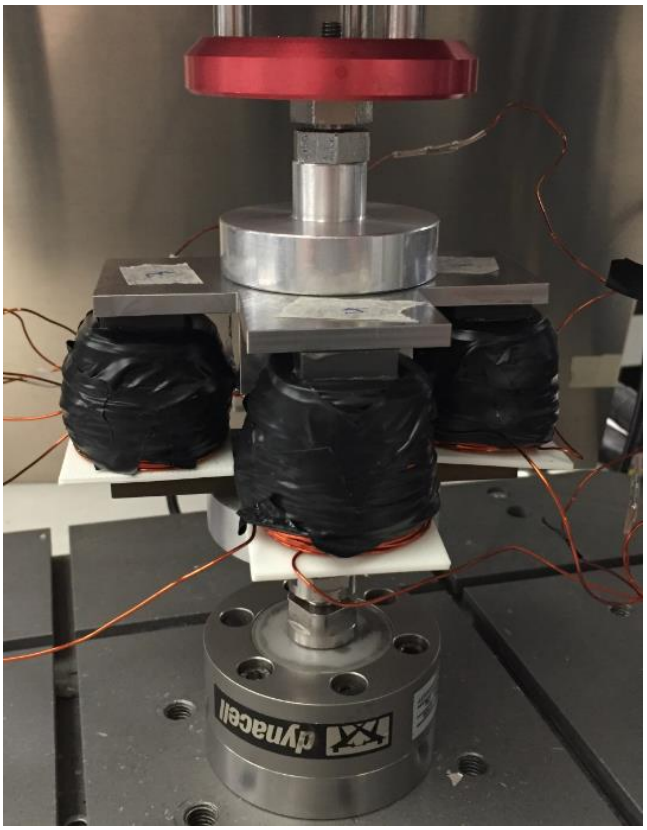

Figure 7.15 Dynamic testing of the designed hybrid MRE isolator

The ElectroPlus E1000 is used to test the dynamic and isolation properties of the hybrid squeeze and shear MRE isolator (as shown in Figure 7.15). The experiment results of the dynamic properties and analysis of the isolation efficiency of the hybrid isolator are given in Chapter 8.

7.6 Summary

In this chapter, a hybrid shear and squeeze mode MRE based isolator is designed and developed. The advantages of the hybrid MRE isolator are highlighted below:

1. Combine the squeeze mode and shear mode of the MRE into an integral structure which increases the loading capacity and effective control bandwidth of the isolator.
2. Compact structure is designed with the space used effectively.
3. Easy to maintain and replace. The designed isolator is assembled with several independent parts. If some part of the isolator is broken and out of work, instead of replace the integral isolator, the broken part can be replaced individually.

Magnetic reluctance of the structure and solenoid parameters are evaluated based on the magnetic circuit theory. Magnetic circuit is optimised to have light weight, low power consumption and compact size. Then, magnetic circuit of the MRE isolator is simulated by commercial software COMSOL MULTIPHYSICS. Based on the simulation results, it is concluded that the structure with calculated solenoid coil parameters can generate sufficient magnetic flux density for both shear and squeeze mode MRE.

Based on the calculated dimension parameters of the magnetic circuit, the hybrid MRE isolator is manufactured and assembled. Magnetic field strength required by the hybrid shear and squeeze MRE isolator is 0.5 T. However, due to manufacture difficulty, 320 turns of copper coil is achieved for the designed isolator which is less than the design value. The magnetic field strength is measured by Gauss meter. The magnetic field strength generated by the isolator is around 270 mT at 3 Ampere current.

The dynamic test of MRE isolator is performed with the Electroplus E1000. The dynamic properties and isolation efficiency of hybrid isolator are given in the next chapter.

Chapter 8: Analysis of the efficiency of the Designed MRE Isolator

8.1 Introduction

In this chapter, the isolation efficiency of hybrid shear and squeeze isolator is analysed. The methodology to evaluate efficiency of MRE isolator is introduced, initially. Then, the experimental results of the dynamic properties of the hybrid MRE isolator are presented. The experimental results are compared with the simulated results. The isolation efficiency of the hybrid MRE isolator is evaluated by the force transmissibility.

8.2 Equation of Motion

The forced vibration of single degree of freedom with damping is used to describe the vibration system. The vibration system contains a mass and a Kelvin-Voigt chain which comprises of a spring and a damper. The mass represents the isolated object. The Kelvin-Voigt chain represents the hybrid MRE isolator. The stiffness and damping properties of the hybrid MRE based isolator are dependent on the frequency, amplitude, external magnetic field and the pre-strain conditions. The couplings between these dependences also have effects on the dynamic properties of MRE isolator.

The single degree of freedom vibration system is illustrated in figure 8.1 below.

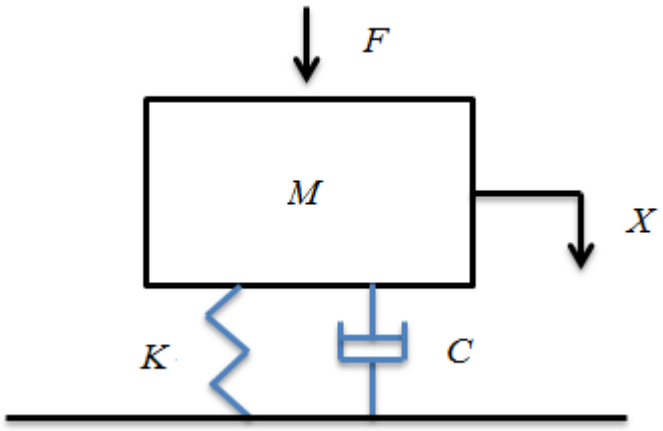

Figure 8.1 Single degree of freedom MRE isolation system

The standard form of the equation of motion is given in Eq. 8.1 below.

$$M\ddot{X} + C\dot{X} + K(X + x) = F + Mg \quad \text{Eq. 8.1}$$

Where M is the mass of the isolated object, X is the dynamic displacement of the system, the over dot means the derivate to time. Then, $\dot{X}$ is the velocity of the isolated object and $\ddot{X}$ is the acceleration of the isolated object. K is the stiffness of the system, C is the damping, F is the excitation force and x is the static deflection due to the gravity of the mass.

The force F is assumed to a harmonic sinusoidal force which is described as

$$F = F_0 sin(2\pi ft) \quad \text{Eq. 8.2}$$

where F_0 is the magnitude of the excitation force and f is the excitation frequency.

For the forced vibration with damping system, the mass will vibrates rapidly to its steady-state response. Then, the steady-state response of the system is considered only and the transitional stage is neglected. The general form of the response for the forced vibration with damping is given in Eq. 8.3.

$$X = X_1 sin(2\pi ft) + X_2 cos(2\pi ft) \quad \text{Eq. 8.3}$$

The first order and second order time derivate of the response X is given in Eq. 8.4 and 8.5

$$\dot{X} = 2\pi f * (X_1 cos(2\pi ft) - X_2 sin(2\pi ft)) \quad \text{Eq. 8.4}$$

$$\ddot{X} = (2\pi f)^2 * (X_1 sin(2\pi ft) - X_2 cos(2\pi ft)) \quad \text{Eq. 8.5}$$

The restoring force due to the static deflection Kx is equal to the gravity force of the mass Mg and can be cancelled from both side of Eq. 8.1. Then, replace the $X, \dot{X}, \ddot{X}$ and F in Eq. 8.1 according to the Eq. 8.2 to 8.5. The Eq. 8.1 can be rewritten as

$$\begin{aligned}(2\pi f)^2 * M(-X_1 sin(2\pi ft) - X_2 cos(2\pi ft)) + 2\pi f * C(X_1 cos(2\pi ft) \\ - X_2 sin(2\pi ft)) + K(X_1 sin(2\pi ft) + X_2 cos(2\pi ft)) = F_0 sin(2\pi ft)\end{aligned} \quad \text{Eq. 8.6}$$

Then, equating the sine terms and cosine terms in Eq. 8.6

$$\begin{cases}(-(2\pi f)^2 * MX_1 - 2\pi f * CX_2 + KX_1) * sin(2\pi ft) = F_0 sin(2\pi ft) \\ (-(2\pi f)^2 * MX_2 + 2\pi f * CX_1 + KX_2) * cos(2\pi ft) = 0\end{cases} \quad \text{Eq. 8.7}$$

Cancel the sine terms and cosine terms the Eq. 8.7 can be written as

$$\begin{cases}(K-(2\pi f)^2 * M)X_1 - 2\pi f * CX_2 = F_0 \\ 2\pi f * CX_1 + (K-(2\pi f)^2 * M)X_2 = 0\end{cases} \quad \text{Eq. 8.8}$$

Then, arrange the Eq. 8.8 into a matrix form

$$\begin{bmatrix}K-(2\pi f)^2 * M & -2\pi f * C \\ 2\pi f * C & K-(2\pi f)^2 * M\end{bmatrix}\begin{bmatrix}X_1 \\ X_2\end{bmatrix} = \begin{bmatrix}F_0 \\ 0\end{bmatrix} \quad \text{Eq. 8.9}$$

In the Eq. 8.9, the stiffness K and the damping C are field dependent parameters representing the dynamic properties of the MRE, the stiffness K contributed to the elastic part of the MRE and the damping C can be used to express the viscous part of the MRE. The stiffness and damping of the MRE can be derived from the storage modulus and loss modulus of the MRE. The equations are given below.

$$K = \frac{G'_{total} * A}{H} \quad \text{Eq. 8.10}$$

$$C = \frac{G''_{total} * A}{H * 2\pi f} \quad \text{Eq. 8.11}$$

where, G'_{total} and G''_{total} are the dynamic shear modulus and loss modulus of the MRE, A is the contact area of the MRE with respect to squeeze or shear deformation and H is the thickness of the MRE sample. The storage and loss modulus of the MRE are dependent on the strain amplitude, frequency, external magnetic field and pre-strain and are defined in Eq. 8.12 and 8.13.

$$G'_{total} = G' + G'_p \quad \text{Eq. 8.12}$$

$$G''_{total} = G'' + G''_p \quad \text{Eq. 8.13}$$

where G'_p and G''_p are the compensation value of the storage modulus and loss modulus due to pre-strain which is defined as an equation of pre-strain amplitude and magnetic flux density.

$$G'_p = C_{s1}\gamma_p + C_{s2}\gamma_p^2 + C_{s3}\gamma_p B \quad \text{Eq. 8.14}$$

$$G''_p = C_{l1}\gamma_p + C_{l2}\gamma_p^2 + C_{l3}\gamma_p B \quad \text{Eq. 8.15}$$

C_{s1} to C_{s3} and C_{l1} to C_{l3} are the parameters contribute to the compensation value of the storage modulus and loss modulus due to the pre-strain condition. The values of these parameters are obtained from the experiment. γ_p is the pre-strain amplitude and is defined as

$$\gamma_p = \frac{x}{H} \quad \text{Eq. 8.16}$$

The storage modulus and loss modulus of the MRE without pre-strain condition are defined in Eq. 8.17 and 8.18

$$G'(\gamma, f, B) = G_0' + \boldsymbol{A_1'} \cdot \boldsymbol{\gamma} + \boldsymbol{A_2'} \cdot \boldsymbol{f} + \boldsymbol{A_3'} \cdot \boldsymbol{B} + \boldsymbol{A_4'} \cdot \boldsymbol{\gamma_f} + \boldsymbol{A_5'} \cdot \boldsymbol{\gamma_B} + \boldsymbol{A_6'} \cdot \boldsymbol{f_B} \quad \text{Eq. 8.17}$$

$$G''(\gamma, f, B) = G_0'' + \boldsymbol{A_1''} \cdot \boldsymbol{\gamma} + \boldsymbol{A_2''} \cdot \boldsymbol{f} + \boldsymbol{A_3''} \cdot \boldsymbol{B} + \boldsymbol{A_4''} \cdot \boldsymbol{\gamma_f} + \boldsymbol{A_5''} \cdot \boldsymbol{\gamma_B} + \boldsymbol{A_6''} \cdot \boldsymbol{f_B} \quad \text{Eq. 8.18}$$

where $\boldsymbol{A_1}$ to $\boldsymbol{A_6}$ are the parameter matrices for storage and loss modulus of the MRE, respectively. The number 1 to 6 is the parameter matrices corresponding to the dependence on strain, frequency, magnetic flux density, strain frequency interaction, strain magnetic interaction and frequency magnetic interaction, respectively. The parameter matrices of $\boldsymbol{A_1}$ to $\boldsymbol{A_6}$ are given below.

$$\boldsymbol{A_1} = [G_1 \quad G_2 \quad G_3] \quad \text{Eq. 8.19}$$

$$\boldsymbol{A_2} = [G_4 \quad G_5 \quad G_6] \quad \text{Eq. 8.20}$$

$$\boldsymbol{A_3} = [G_7 \quad G_8] \quad \text{Eq. 8.21}$$

$$\boldsymbol{A_4} = [G_9 \quad G_{10} \quad G_{11}] \quad \text{Eq. 8.22}$$

$$\boldsymbol{A_5} = [G_{12} \quad G_{13} \quad G_{14}] \quad \text{Eq. 8.23}$$

$$\boldsymbol{A_6} = [G_{15}] \quad \text{Eq. 8.24}$$

Table 8.1 Parameter identification for storage and loss modulus of the hybrid MRE isolator with 30% iron particle concentration

Parameters for storage modulus

G_0', MPa	G_1', Mpa	G_2', Mpa	G_3', Mpa	$G_4', Mpa \cdot s$	$G_5', Mpa \cdot s^2$
1.3633E+01	-1.3909E+01	1.2887E+01	-4.1521E+00	1.1214E-01	-1.5517E-03
$G_6', Mpa \cdot s^3$	$G_7', Mpa/mT$	$G_8', Mpa/mT^2$	$G_9', Mpa \cdot s$	$G_{10}', Mpa \cdot s$	$G_{11}', Mpa \cdot s^2$
6.6860E-06	1.4385E-02	-5.5730E-06	-6.6780E-02	9.3070E-03	5.4150E-04

$G_{12}', Mpa/mT$	$G_{13}', Mpa/mT$	$G_{14}', Mpa/mT^2$	$G_{15}', Mpa \cdot s/mT$
-1.5624E-02	4.8332E-03	7.1685E-06	3.7572E-06

Parameters for loss modulus

G_0'', MPa	G_1'', Mpa	G_2'', Mpa	G_3'', Mpa	$G_4'', Mpa \cdot s$	$G_5'', Mpa \cdot s^2$
2.5587E+00	-2.0014E+00	9.2875E-01	-1.2587E-01	-2.1372E-02	-1.0852E-03

$G_6'', Mpa \cdot s^3$	$G_7'', Mpa/mT$	$G_8'', Mpa/mT^2$	$G_9'', Mpa \cdot s$	$G_{10}'', Mpa \cdot s$	$G_{11}'', Mpa \cdot s^2$
1.3684E-05	1.3163E-03	-1.4983E-06	4.9987E-02	-1.3842E-02	-7.4795E-05

$G_{12}'', Mpa/mT$	$G_{13}'', Mpa/mT$	$G_{14}'', Mpa/mT^2$	$G_{15}'', Mpa \cdot s/mT$
8.7285E-04	-5.6225E-04	4.3945E-07	-1.1103E-05

The matrices for strain, frequency, magnetic flux density and their interaction are given in Eq. 8.25 to 8.30.

$$\boldsymbol{\gamma} = [\gamma \quad \gamma^2 \quad \gamma^3] \qquad \text{Eq. 8.25}$$

$$\boldsymbol{f} = [f \quad f^2 \quad f^3] \qquad \text{Eq. 8.26}$$

$$\boldsymbol{B} = [B \quad B^2] \qquad \text{Eq. 8.27}$$

$$\boldsymbol{\gamma_f} = [\gamma f \quad \gamma^2 f \quad \gamma f^2] \qquad \text{Eq. 8.28}$$

$$\boldsymbol{\gamma_B} = [\gamma B \quad \gamma^2 B \quad \gamma B^2] \qquad \text{Eq. 8.29}$$

$$\boldsymbol{f_B} = [fB] \qquad \text{Eq. 8.30}$$

where γ is the strain amplitude defined in Eq. 8.31.

$$\gamma = \frac{\sqrt{X_1^2 + X_2^2}}{H} \qquad \text{Eq. 8.31}$$

Then, substituting the Eq. 8.8-8.29 into Eq. 8.7, the steady state response of X_1 and X_2 can be calculated.

The force transmissibility of the SDOF system can be evaluated as the ratio of the amplitude of the transmitted force to the base respect to the amplitude of the applied force.

$$T_f = \frac{\sqrt[2]{(C|\dot{X}|)^2 + (K|X|)^2}}{F_0} \qquad \text{Eq. 8.32}$$

8.3 Dynamic properties of the designed hybrid MRE isolator

The dynamic properties of the designed hybrid shear and squeezed MRE isolator are experimentally tested at 2% pre-strain amplitude with two different magnetic fields (0 mT and 270 mT). The

experiment setup is shown in figure 7.15. For the dynamic test of the designed MRE isolator, 2% static pre-strain amplitude is initially applied. Then, the static pre-strain is maintained for 40 second. After that, the dynamic tests of the MRE isolator are performed along with different excitation frequency (1-60 Hz), stain amplitude (0.25% -1.5%).

The dynamic shear and compression mechanical properties of the MRE are discussed in Chapter 4 and 5. It is concluded that the dynamic mechanical properties of MRE are dependent on the strain amplitude, frequency, pre-strain amplitude and magnetic field strength. These dependences also have effects on the dynamic properties of the hybrid MRE isolator. The experiment results of the stiffness and damping properties of the designed MRE isolator are recorded and plotted. Figure 8.2 demonstrates the stiffness and damping properties of the MRE isolator without the magnetic field at 2% pre-stain amplitude. Figure 8.3 shows the stiffness and damping properties of the hybrid MRE isolator at 270 mT magnetic field strength. The black and green circles in figure 8.2 and 8.3 are the stiffness and damping value from experiment. The surface plot in figure 8.2 and 8.3 are based on Eq. 8.10 and Eq. 8.11. As can be seen from both Figure 8.2 (a) and 8.3 (a) that, stiffness of MRE isolator shows an obvious decrease as dynamic strain amplitude increases. In the meantime, stiffness of the isolator increases with the increasing frequency. From Figure 8.2 (b) and 8.3 (b), it is observed that damping of MRE isolator decreases significantly as frequency increases. By comparing with Figure 8.2 and 8.3, it is found that the stiffness and damping properties of the MRE isolator increase with the presence of the magnetic field.

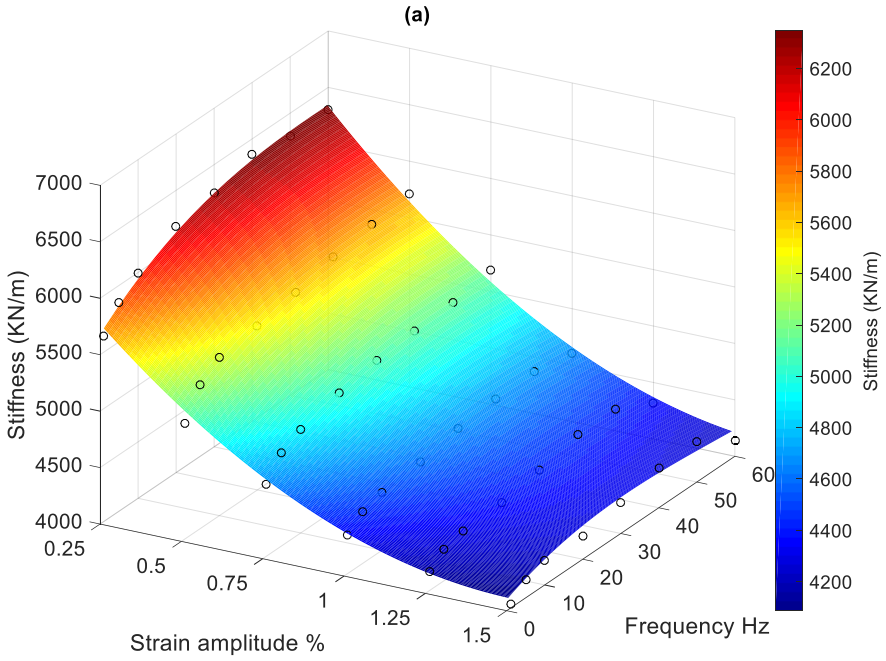

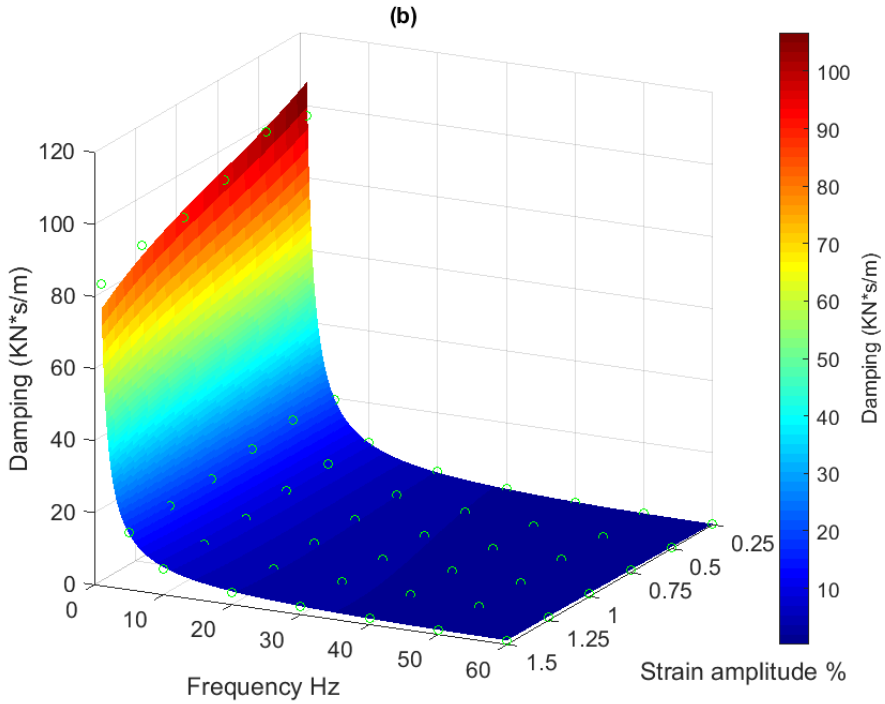

Figure 8.2 The stiffness (a) and damping (b) properties of the designed hybird MRE isolator at 0 mT magnetic field strength with 2% pre-strain amplitude

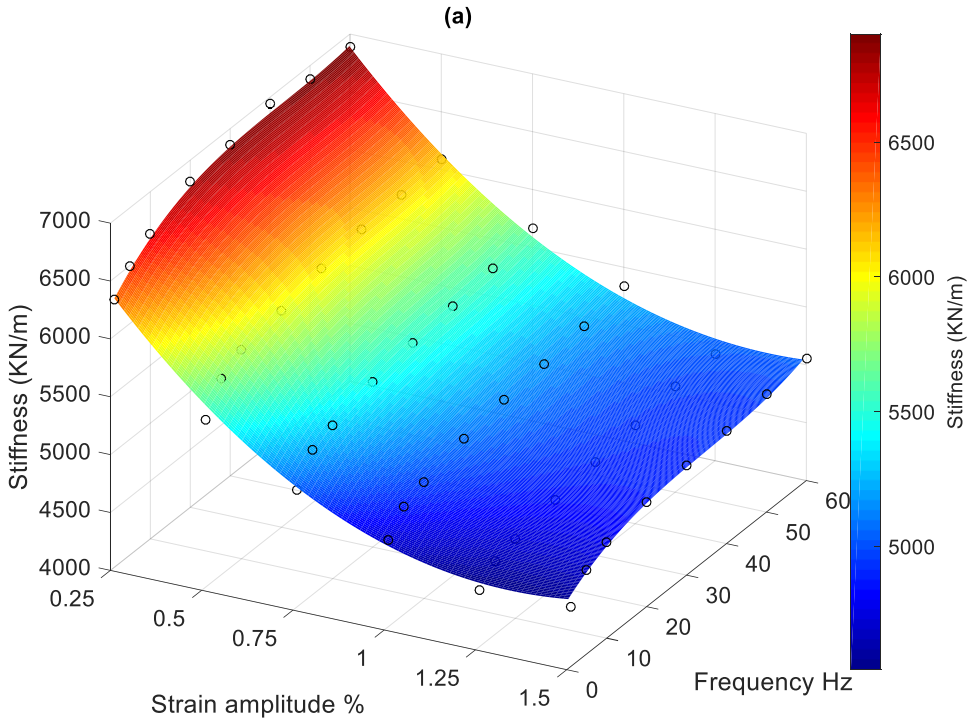

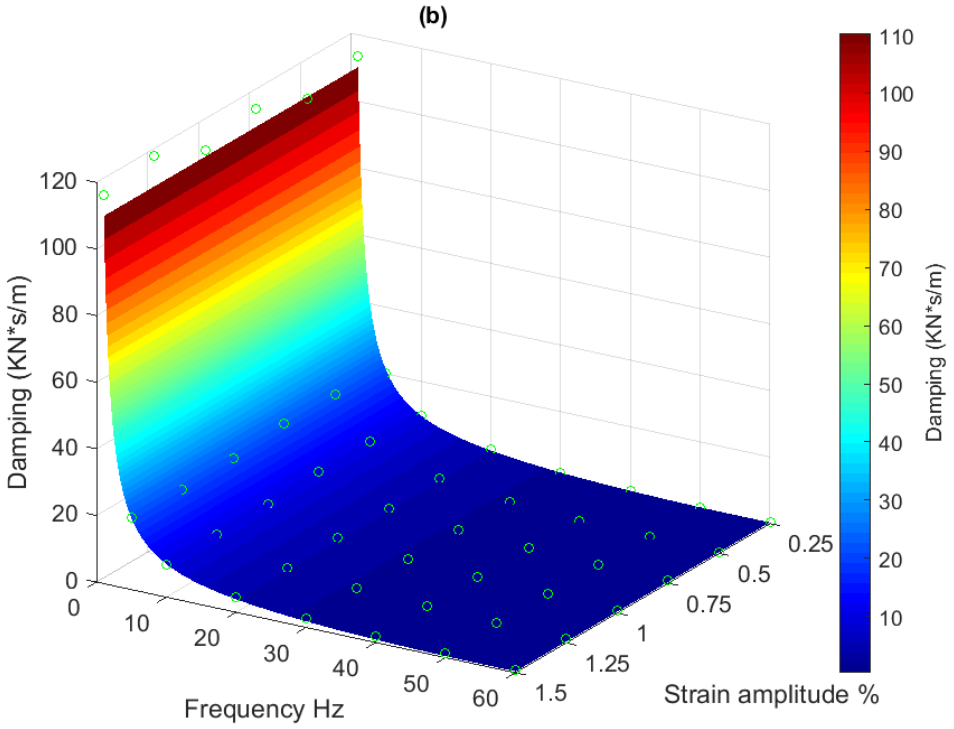

Figure 8.3 The stiffness (a) and damping (b) properties of the designed hybird MRE isolator at 270 mT magnetic field strength with 2% pre-strain amplitude.

8.4 Analysis of non-linear MRE based isolation system

The isolation properties test of the hybrid MRE isolator is performed at a 2% pre-strain amplitude condition. The hybrid shear and compression MRE isolator can provide a 490 N vertical suspension force at 2 % pre-strain amplitude condition. The mass of the isolation object is selected as 50 kg for MRE isolator to perform the isolation test. By applying a magnetic field to the isolator, the stiffness of the isolator increase and a higher vertical suspension force is provided at 2% pre-strain amplitude. Then, pre-strain induce by 50 kg isolated object is less than 2%. The quasi-static stiffness of MRE isolator at 0 mT and 260 mT are shown in Appendix III. It is seen that the pre-strain amplitude induced by a 50 kg isolated object decreases from 1.98% to 1.91% at 260 mT magnetic field strength. The change of pre-strain amplitude for the isolator is of very small magnitude (less than 0.1%). Then, it is assumed that the pre-strain amplitude induced by 50 kg isolated object remains the same value as a magnetic field is applied at a quasi-static state. For the isolation performance test of the MRE isolator, the excitation force (F) is defined in Eq. 8.33. The frequency sweep for the isolation test is chosen from 1 Hz to 60 Hz.

$$F = 150 * sin(2\pi ft) \quad \text{Eq. 8.33}$$

The dynamic properties of the designed isolator are shown in Figure 8.2 and 8.3. It is concluded that the stiffness and damping of the designed isolator has non-linear properties with different strain amplitudes, frequencies and magnetic fields. In order to better understand and analyse the dynamic behaviour of MRE based isolation system, the non-linear properties of MRE system should be considered.

The non-linear dynamic isolation system is defined in Eq. 8.1 to Eq. 8.31. The processes to achieve the solution of displacement response at a specified frequency of the non-linear system are:

1. Input the initial value (excitation frequency f, displacement X, magnetic field strength B and pre-strain γ_p) of the isolation system
2. Calculate the stiffness and damping properties of MRE based isolation system
3. Solve the motion of equation of the system (Eq. 8.1) with the stiffness and damping achieved in step 2 and get displacement response X_{new} at the excitation frequency.
4. Compare the value of X and X_{new}. If the error between these two is less than 10^{-9}, then the problem is solved. Otherwise, replace X with X_{new} and go back to step 2.

The comparisons of the experimental results and simulation results of displacement response of the isolated object are plot in Figure 8.6. It is seen from Figure 8.6 that, the experimental results are missing around the resonance excitation frequency. This is because at resonance frequency, the vibration of the system becomes significantly violent. The displacement response increase sharply and exceed the safety margin of the testing machine. Consequently, the data of displacement response near resonance frequency is not obtained from the experiment.

The modelling of the non-linear stiffness and damping properties of MRE are dependent on the experimental results (in Chapter 6). This proposed mathematical model can provide an accurate prediction of the dynamic mechanical properties (stiffness and damping) of MRE within certain regions. The effect regions of the proposed model are frequency (1-60 Hz), strain amplitude (0-2%), magnetic field strength (0-500mT) and pre-strain amplitude (0-2%). As dependences out of these effect regions, the dynamic mechanical properties of MRE simulated by the proposed model may lose its accuracy.

Due to Payne effect, the stiffness of MRE decreases with increasing strain amplitude. For current model, the stiffness of MRE decrease to a negative value as strain amplitude keeps increasing (more

than 3% strain amplitude). For hybrid MRE isolation system, strain amplitude around the resonance frequency increases significantly. At this time, the non-linear stiffness and damping properties of MRE isolator cannot be accurately described by the proposed model. In order to predict the dynamic behaviour of the MRE isolator near the resonance frequency, an alternative method is used to evaluate the dynamic response of the system around the resonance frequency.

The methodology to evaluate the displacement response around resonance frequency of the isolation system is summarized as follow:

1. Find the specified frequency (f) where there is no solution for the non-linear dynamic system
2. Calculate the natural frequency (f_{na}) of the system at the frequency f
3. Calculate the stiffness K_{na} of the isolation system with the natural frequency (f_{na})
4. Find the corresponding damping C_{na} of the isolation system with natural frequency (f_{na})
5. Solve the dynamic motion equation using the stiffness and damping value find in step 3 and 4.
6. Find the response displacement X_{na} at the specified frequency

The overall methodology flow chart of the entire processes to solve the non-linear MRE based isolation system is given in Figure 8.4.

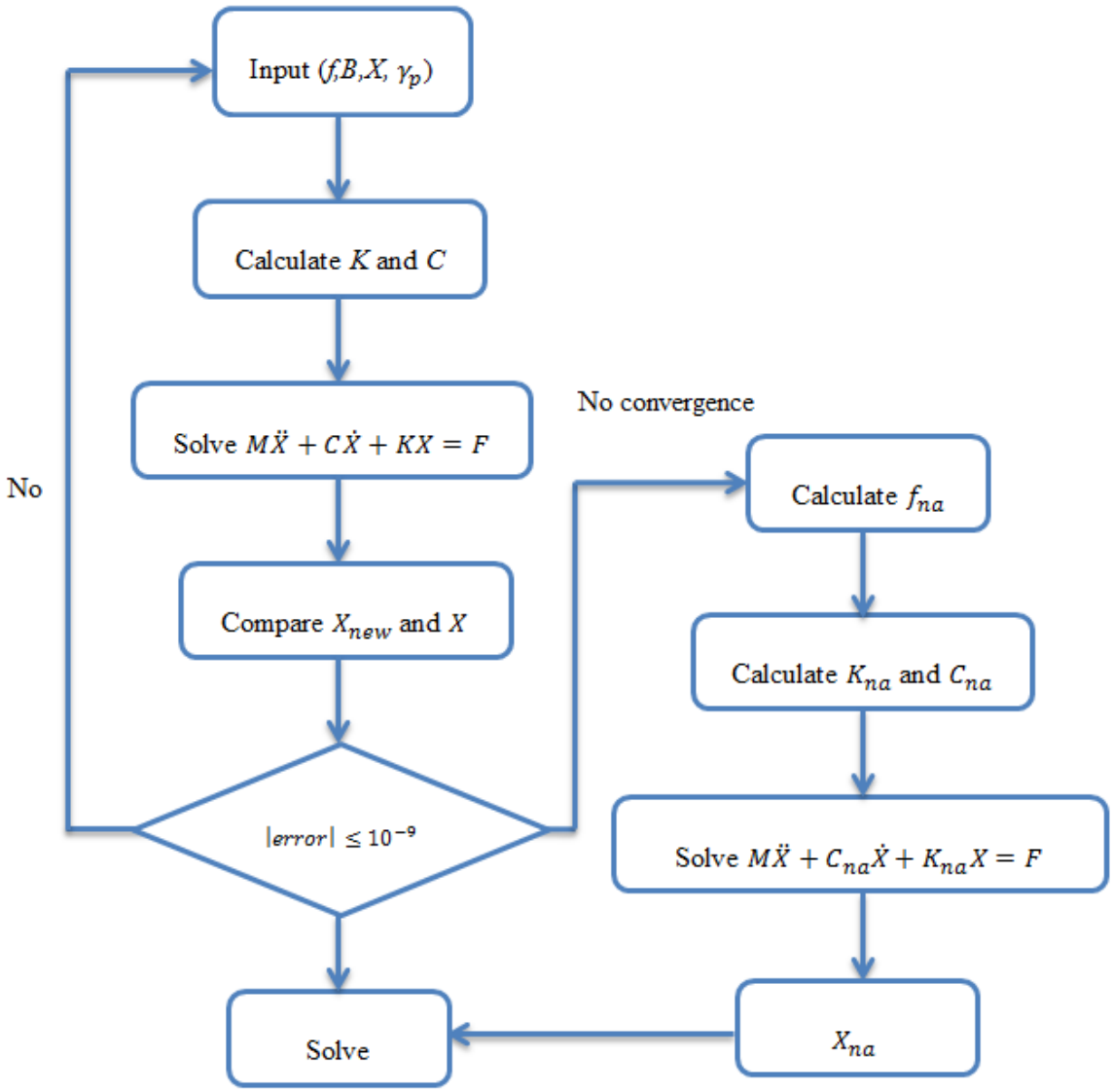

Figure 8.4 Processes to solve the non-linear MRE based isolation system

Natural frequency of the isolation system with an increasing frequency with different magnetic fields is plot in Figure 8.5. It is observed from Figure 8.5 that natural frequency of the system increases steadily as excitation frequency increases from 1 Hz to 20 Hz. As excitation frequency continues to increase, natural frequency of the isolation system starts to decrease. A sharp decrease of natural frequency is observed for excitation frequency near 30 Hz for isolation system without magnetic field. By applying a magnetic field, the sharp drop of natural frequency is shifted toward to higher frequency. The resonance phenomenon of MRE isolator happens between the sharp drop regions of natural frequency. It is clearly seen from Figure 8.5 that resonance frequency is shifted by applying a magnetic field. There is a surge increase of natural frequency observed as excitation frequency continually increases. Then, natural frequency of MRE based isolation system increases at a decreasing rate.

$$f_{na} = \sqrt{\frac{k}{m}} \qquad \text{Eq. 8.34}$$

The variation of natural frequency with excitation frequency is divided into three parts. The value of MRE stiffness is small at a low excitation frequency. As excitation frequency increases, the stiffness of MRE increases. The definition of natural frequency of an isolation system is given in Eq. 8.34. An increasing stiffness leads to an increasing of natural frequency of the system. The displacement response at low frequency is small (Figure 8.6). Then, it is concluded the variation of natural frequency in region one is dominated by frequency. For region two, a violent variation of natural frequency is observed. As excitation frequency increases and approaches to resonance frequency, the displacement starts to increase. Chapter 4 and 5 state that, an increasing of strain amplitude leads to a decrease of MRE stiffness. The effect of strain amplitude on natural frequency is greater than excitation frequency in region two. Hence, the natural frequency in region two is dominated by displacement response (i.e. strain amplitude). For region three, the excitation frequency starts to move away from resonance frequency. The value of displacement decreases as excitation frequency moves away from natural frequency. The decreasing displacement and the increasing frequency both lead to an increment of stiffness of the isolation system. Then, stiffness of the system is affected by both of increasing frequency and decreasing displacement. It is concluded that natural frequency in region three is dominated by both excitation frequency and displacement response.

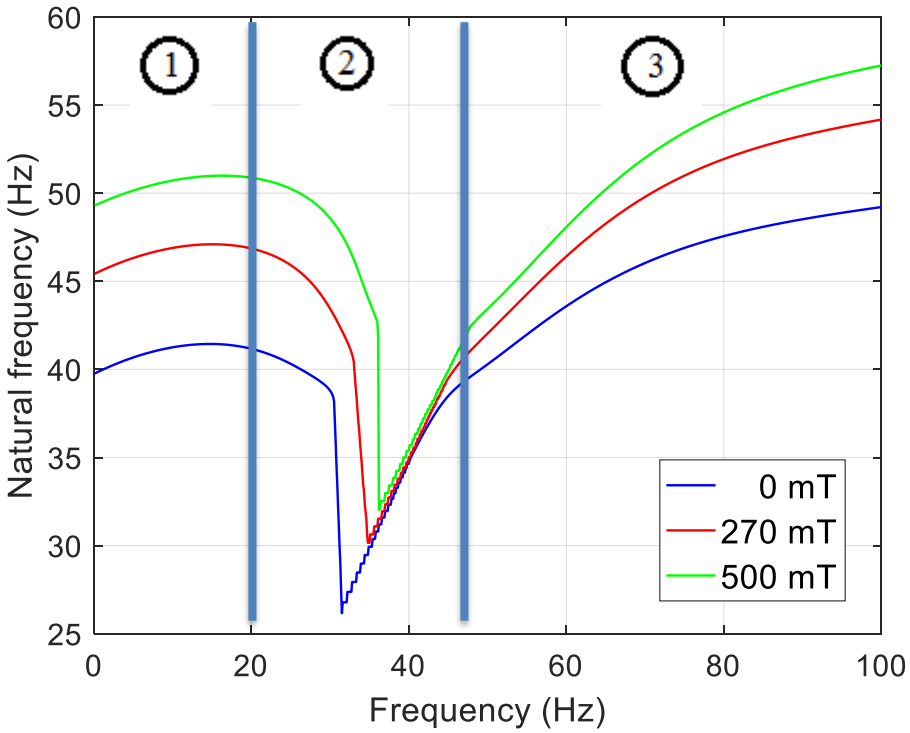

Figure 8.5 Natural frequency variation of the hybrid MRE isolation system with increasing frequency with different magnetic fields

Figure 8.6 (a) and (b) present the comparison of the experimental results and simulation results without magnetic field and at 270 mT magnetic field strength. The experiment setup is shown in

Figure 7.15. The displacement response is calculated by Eq. 8.1 – 8.31. In order to verify applicability of the proposed mathematical model, the simulation results are run from 1 Hz to 100 Hz. As can be seen from Figure 8.6, displacement response increases with the increasing frequency from 1 Hz with different magnetic field strengths. As excitation frequency increases to resonance frequency, a sharp increase of displacement is observed. Due to violent vibration, displacement response is not obtained from experiment around resonance frequency. However, a sharp increase of displacement is recorded by experiment. The simulation results demonstrate that there is a drop of displacement response after the excitation frequency pass resonance frequency. Then, as excitation frequency continually increases, displacement response decreases at a decreasing rate. The trend of displacement response of the isolation system is the same with different magnetic field strengths.

The sharp increase of displacement as excitation frequency increases to resonance frequency can be explained as below. As excitation frequency approach to resonance frequency, the response of isolator increases. The increasing of displacement response leads to a reduction of stiffness of the isolator. Then, the natural frequency of MRE isolator is reduced (shown in Figure 8.5). The shift direction of natural frequency comes towards to excitation frequency. A sharp increase of displacement response is observed as excitation frequency comes closed to resonance frequency. As excitation frequency passes the resonance frequency and continues to increase, displacement response starts to decrease. The reduction of response leads to an increase of the stiffness of MRE isolator. Meanwhile, natural frequency of the isolation system also increases (Figure 8.5). Natural frequency of the system moves towards to excitation frequency. Then, displacement response decreases at a reduction rate is observed as excitation frequency continually increases.

The simulation results demonstrate a good agreement of the experimental results. The simulation results of displacement response are slightly lower between 20 Hz and 30 Hz compared with the experiment results at 270 mT magnetic field. However, both of sharp increase and slow decrease of displacement response are well predicted by the proposed model. For applicability of the proposed model, it is found that the effective regions of the proposed model in frequency region could go up to 100 Hz. However, in strain amplitude region, as strain amplitude increase over 2%, the proposed model loses its effectiveness. The peak value of displacement at resonance frequency predicted by the proposed model may not be completely correct. But, the identification of resonance frequency is relative accurate.

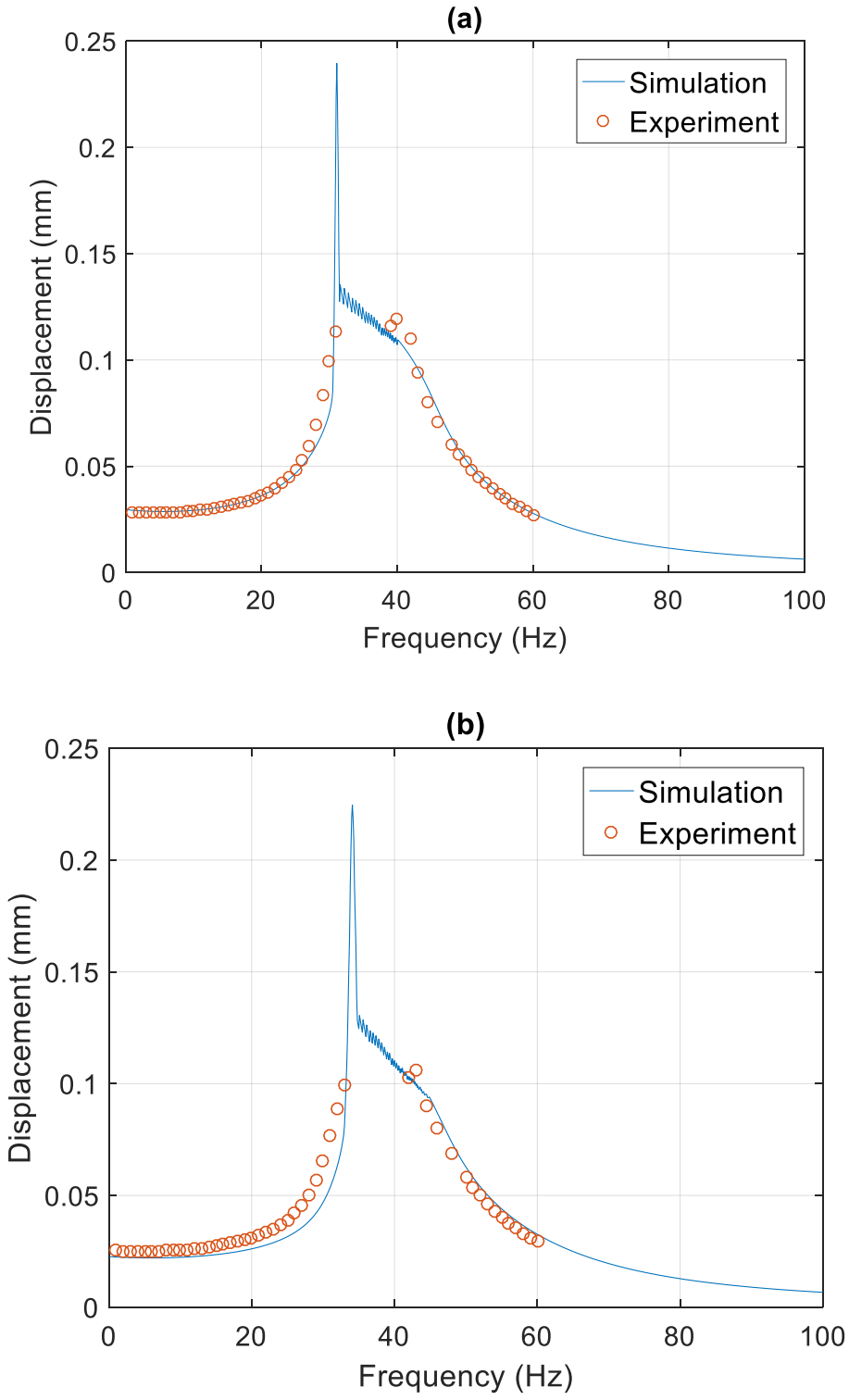

Figure 8.6 Comparison of displacement response of hybrid MRE isolator at 150N excited force (a) 0 mT magnetic field strength (b) 270 mT magnetic field strength

Figure 8.7 compares the response of hybrid MRE isolator with 0 mT, 270 mT and 500 mT magnetic field strengths. Since, the maximum magnetic field strength generated by MRE isolator is 270 mT. The simulated result of the 500 mT magnetic field strength is not experimentally verified. The simulation results are compared with the experimental results in Figure 8.7 and show good agreement. Then, it is concluded that the proposed model could well describe the dynamic vibration properties of MRE based isolation system.

The presenting of simulation results at 500 mT magnetic field strength is to analyse the dynamic response of isolator at a high magnetic field strength. It is clearly seen from Figure 8.7 that the resonance frequency of MRE isolation system is shifted by presence of a magnetic field. The resonance frequency of the system is shifted from 30.1 Hz to 36.8 Hz with a magnetic field strength of 500 mT. For displacement response of the system at excitation frequency below resonance frequency, an increasing magnetic field strength leads to a reduction of displacement response. As excitation frequency increases pass the resonance frequency, the isolation system without magnetic field demonstrates a lower value of displacement response comparing with the results with magnetic field. In order to control the response of MRE isolator to avoid violent vibration, it is recommended that a higher magnetic field should be applied as excitation frequency below the resonance frequency. For high frequency (over 36 Hz) excitation, in order to achieve a lower response value of MRE isolation system, the magnetic field should be removed.

Figure 8.8 illustrates an optimised response of hybrid MRE isolation system. Magnetic field strength is controlled by a simple on-off control. For excitation frequency below 36 Hz, electric power is applied to MRE isolator and a magnetic field is generated. For excitation above 36 Hz, electric power is removed and the magnetic field is vanished. It is clearly seen from Figure 8.8 that by a simple on-off control of the magnetic field, the resonance peak of displacement response is significantly reduced.

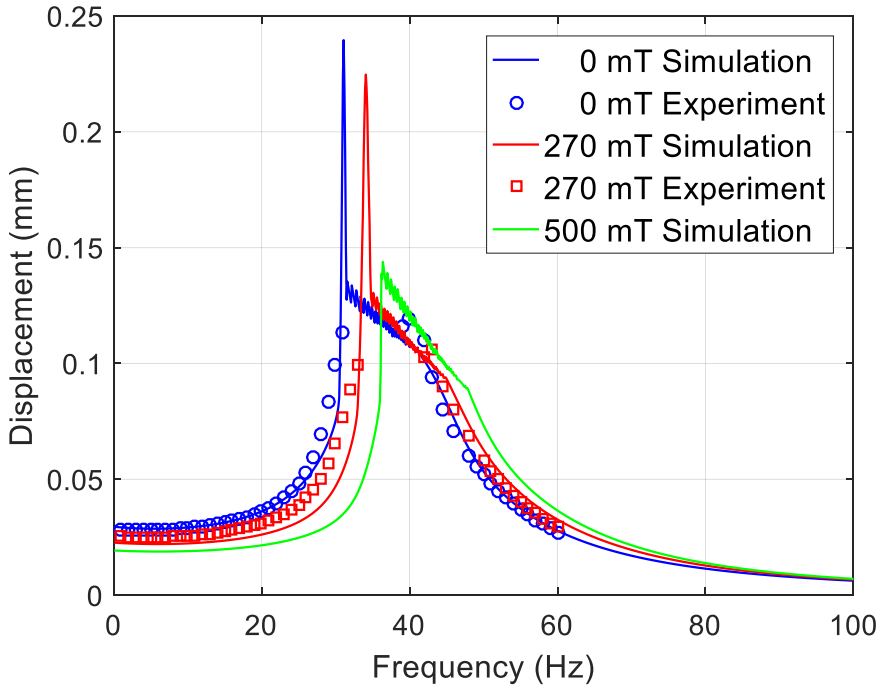

Figure 8.7 Comparison of the displacement of hybrid MRE isolation system with different magnetic fields

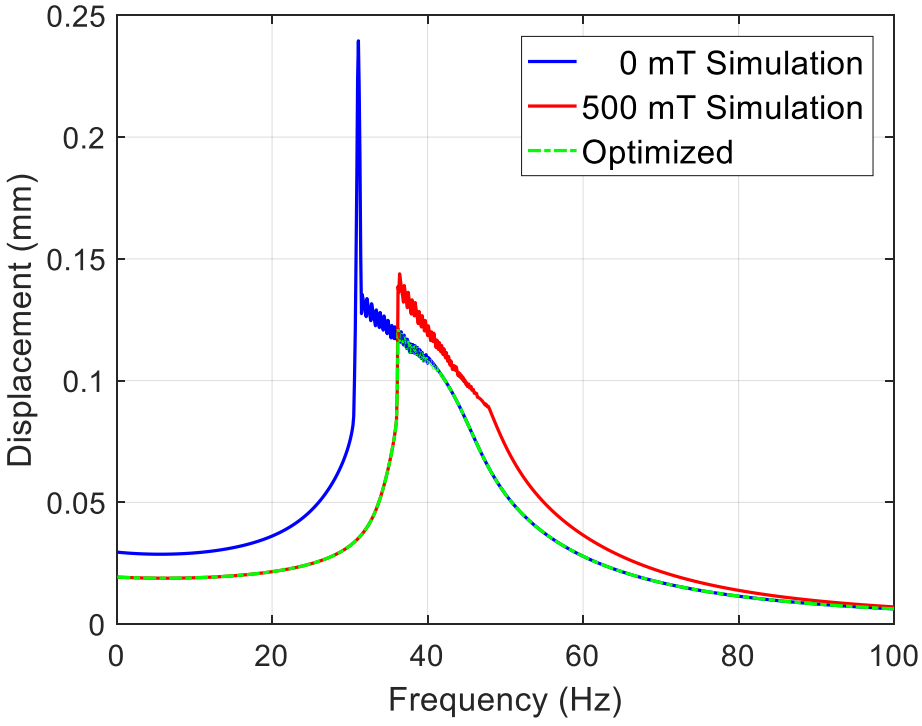

Figure 8.8 Optimisation of displacement response of MRE isolation system

Figure 8.9 compares experimental results and simulation results of force transmissibility of MRE isolator with 0 mT and 270 mT magnetic field strength. Force transmissibility is calculated by Eq. 8.32. Force transmissibility remains at a low value (near 1) for excitation frequency below 10 Hz. There is an obviously increase of force transmissibility as excitation frequency continues to increase. A sharp increase of force transmissibility is obtained as excitation frequency approaches resonance frequency. The value of force transmissibility is not obtained from experiment around resonance frequency due to a violent vibration. The force transmissibility of MRE isolation system around resonance region is evaluated by Xna. The methodology to calculate Xna is shown in Figure 8.4. As excitation frequency passes the resonance frequency, there is a sudden drop of force transmissibility observed. Then, a steady increase of force transmissibility is predicted by proposed model as excitation frequency continues to increase. The steady increase of force transmissibility is because the natural frequency of isolation system increases towards to the increasing frequency. Force transmissibility remains at a relatively high value as excitation frequency is closed to the natural frequency. After the force transmissibility reaching the second peak value, the force transmissibility of MRE isolator stars to decrease. The trends of force transmissibility are the same for results with different magnetic field strengths.

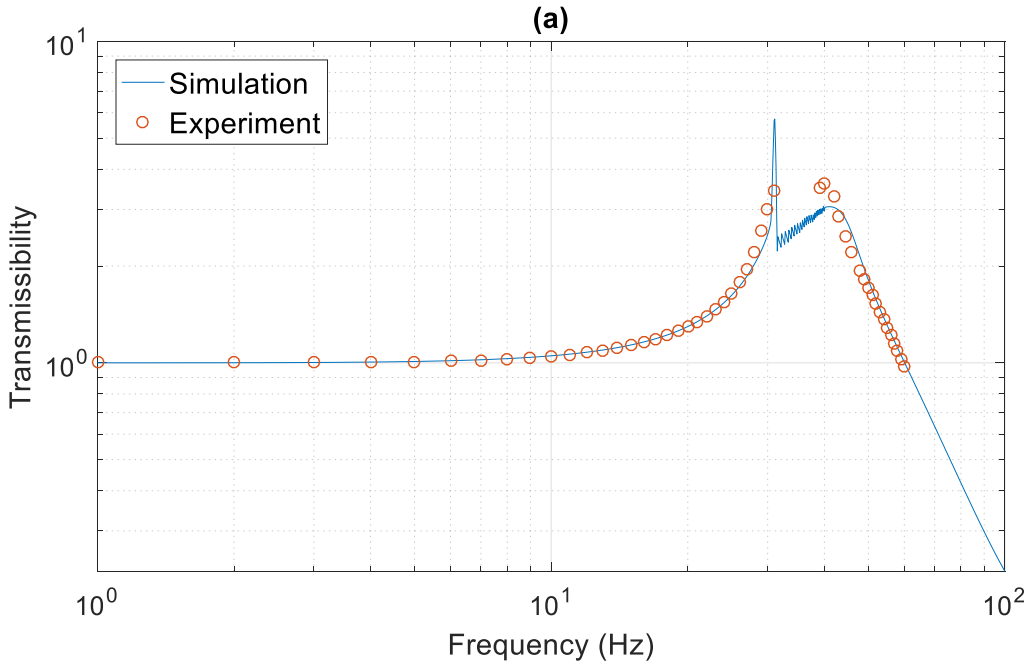

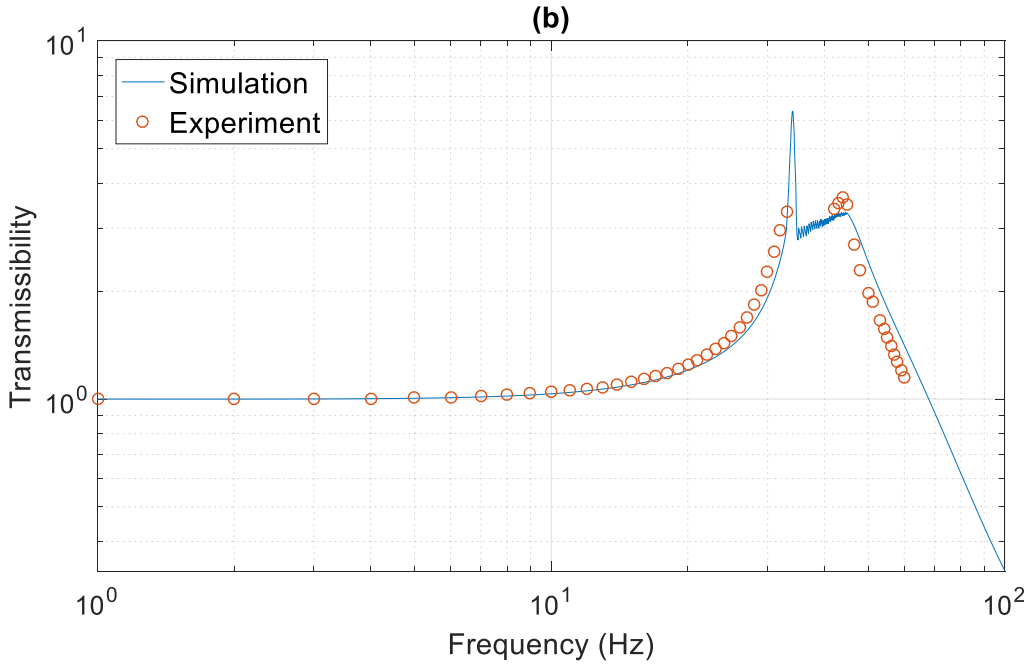

Figure 8.9 Comparison of force transmissibility of hybrid MRE isolator at 150N excited force (a) 0 mT magnetic field strength (b) 270 mT magnetic field strength

Figure 8.10 compares the force transmissibility of hybrid MRE isolator with different magnetic field strengths. It is clearly seen that the peak of force transmissibility is shifted by an applying magnetic field. A higher magnetic field induces a larger shift of resonance frequency. Figure 8.11 shows the optimised force transmissibility of the designed isolator by a simple on-off control. It is seen that the performance of hybrid MRE based isolation system is improved at resonance frequency region. For hybrid MRE based isolation system, by using a magnetic field to control the stiffness and damping properties of MRE isolator, the force transmissibility at the resonance frequency is controlled. The maximum force transmissibility of MRE isolation system is reduced from 6.6 to 3.2 (51.5%). By largely reducing the force transmissibility around resonance frequency and shifting the resonance frequency by a magnetic field, a wider frequency bandwidth and lower force transmissibility isolation system is achieved.

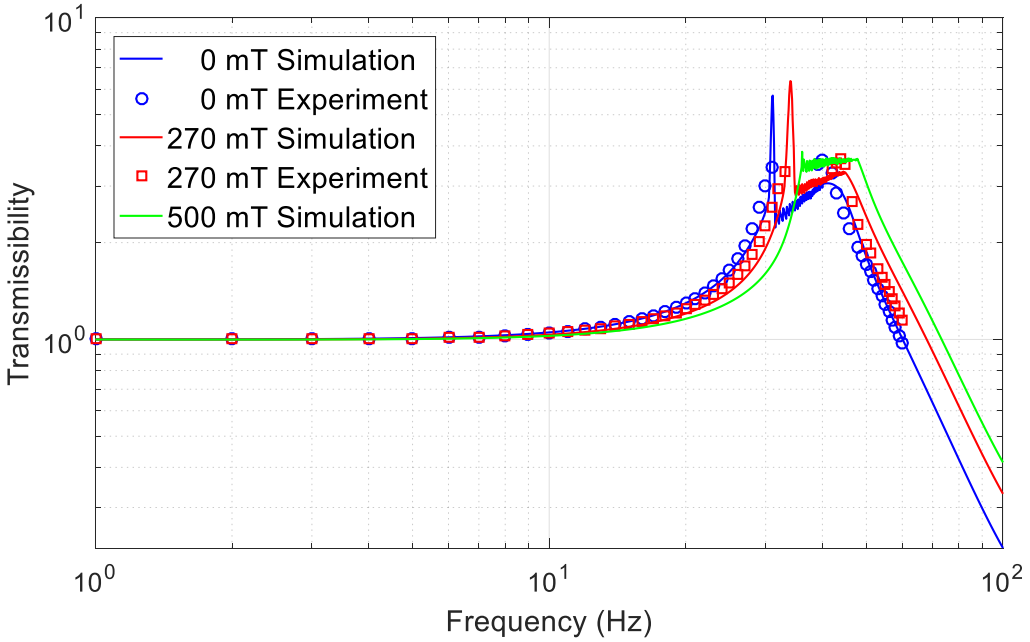

Figure 8.10 Comparisons of force transmissibility of hybrid MRE isolation system with different magnetic fields

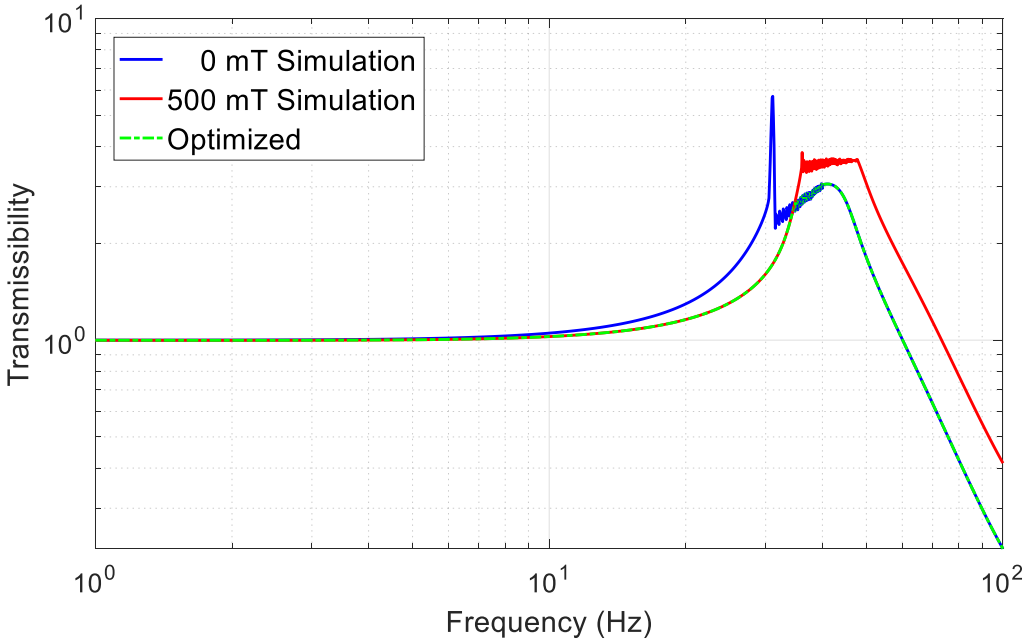

Figure 8.11 Optimisation of force transmissibility of hybrid MRE isolation system

8.5 Summary

In this chapter, the isolation efficiency of designed hybrid shear and squeeze MRE based isolator is analysed. Equation of motion of the dynamic isolation system is formulated with harmonic forced single degree of freedom with non-linear stiffness and damping.

The isolation efficiency test of hybrid isolator is performed at a 2% pre-strain amplitude condition. A sinusoidal force with amplitude of 150 N is selected as excitation force. Due to a violent vibration at resonance frequency, experimental results of displacement response around resonance frequency are not obtained experimentally. While, the sharp increase of displacement response before resonance frequency and the steady decrease of response after resonance frequency is experimentally recorded. For the proposed model, as strain amplitude increase over 2%, the model loses its effectiveness. An alternative methodology is applied to solve the dynamic equation of motion as strain amplitude over 2%. The limitation of the proposed model is that the prediction of displacement response at resonance frequency may not be completely correct, while the identification of resonance frequency of MRE isolation system is relatively accurate. The experiment results show good agreement with the simulation results. It is concluded that the proposed model can accurately describe the dynamic motion of MRE isolator.

By comparing with the experimental results and the simulation results, it is found that resonance frequency of the isolation system is shifted from 30.1 Hz to 36.8 Hz by a magnetic field strength of 500 mT. The maximum force transmissibility of hybrid MRE based isolation system is reduced at 51.5% (from 6.6 to 3.2). By using a simple on-off control on the magnetic field, the performance of MRE based isolation system is improved. The designed hybrid compression and shear MRE based has a wider effective frequency bandwidth and lower force transmissibility.

Chapter 9: Conclusions and Future Work

9.1 Conclusions

The work in this thesis can be categorised into three parts: dynamic mechanical properties of MRE, mathematical modelling of MRE and MRE isolator development and assessment. The conclusions of each part are given below:

1. Dynamic properties of MRE

In this thesis, the dynamic shear and compression properties of MRE are investigated. Three different samples with 10%, 30% and 50% iron particle concentration are tested. The dependences considered are pre-strain, frequency, strain amplitude and magnetic field.

For dynamic shear properties of MRE

- The pre-strain effect on shear storage modulus is different with different iron particle concentration samples. For MRE samples with low iron particle concentration (10%), pre-strain induces a decrease of storage modulus. For higher iron particle concentration samples (30% and 50%), as pre-strain amplitude further increase (more than 1%), MRE material becomes stiffer and storage modulus starts to increase. The dependence of pre-strain on shear storage modulus is independent of frequency and strain amplitude. The magnetic induced modulus is reduced by presence of pre-strain. This phenomenon is more obvious for MRE with higher pre-strain amplitude and iron particle concentration.
- The pre-strain effect induces an increase of shear loss modulus of MRE with 10% iron particle concentration. For higher iron particle concentration samples (30% and 50%), loss modulus starts to decrease for large pre-strain amplitude (1.5-2%). The magnetic field induce a decrease of loss modulus and becomes more obvious for larger pre-strain amplitude and higher iron particle concentration. The dependence of pre-strain on shear loss modulus is independent of frequency and strain amplitude.
- The coupling effect between frequency and strain amplitude, strain amplitude and magnetic field is noticeable. These two effects should be considered in mathematical model. The coupling effect between frequency and magnetic field is weak and can be ignored.
- The MR effect decreases with increasing strain amplitude, frequency and pre-strain amplitude, while increase with increasing magnetic field. The MR effect of the 10% iron particle concentration MRE is the lowest. The MR effect for the 30% and 50% iron particle concentration MRE samples are almost the same. The stiffness and damping of the 50% iron particle concentration samples are the highest among all three samples.

For dynamic compression properties of MRE

- Compression pre-strain induces an obvious increment of compression storage modulus. The dependence of pre-strain on compression storage modulus is independent of frequency and strain amplitude. There is also no obvious coupling effect between compression pre-strain and magnetic field.
- The pre-strain effect on compression loss modulus is not obvious compared with the effect on compression storage modulus. Compression loss modulus increases slightly by presence of pre-stain. There is no clearly coupling effect observed between compression pre-strain with frequency, strain amplitude and magnetic field.
- The coupling effects between frequency and strain amplitude, strain amplitude and magnetic field are obvious. These two effects should be considered in mathematical model. The coupling effect between frequency and magnetic field is weak can be neglected. The same conclusions are drawn from MRE with shear test.
- The value of the MR effect for compression MRE sample is fluctuated (less than 2%) with frequency increases from 1 Hz to 60 Hz. The MR effect does not deteriorate as strain amplitude increase. The MR effect increases slightly as compression pre-strain increases from 2% to 3%. For compression pre-strain continuing increase, the MR effect starts to decrease. For compression test, the MR effect of the 30% iron particle concentration MRE achieves the highest value.

2. Mathematical modelling of MRE

A modified classical viscoelastic Kelvin-Voigt model is developed to model the dynamic properties of MRE. The dependences of pre-strain amplitude, frequency, strain amplitude and magnetic field are considered. The coupling effects between these dependences are also included. The proposed mathematical model can accurately and continuously describe the dynamic shear and compression properties of MRE material. By comparing with the experimental results, it is found that the simulated results of storage modulus are more accurate than loss modulus. This is because loss modulus demonstrates higher non-linear properties.

3. MRE isolator development and assessment

- A hybrid shear and squeeze mode MRE based isolator is designed. The designed isolator has a high load-bearing capacity, compact size and low power consumption.

- By comparing with the simulation results and experimental results, resonance frequency of MRE based isolation system is shifted from 30.1 Hz to 36.8 Hz at a magnetic field strength of 500 mT.
- With a simple on-off control, the maximum force transmissibility of hybrid MRE based isolation system is reduced at 51.5% (from 6.6 to 3.2). The isolation performance of MRE isolation system is improved.
- The proposed mathematical model is able to predict and describe the non-linear dynamic properties of MRE isolation system.

9.2 Recommendations for future work

1. Mathematical model of MRE

In this thesis, the modelling of non-linear stiffness and damping properties of MRE are dependent on the experiment results. The effectiveness of proposed model is within certain regions of the dependences. In order to develop the current model to deal with more vibration problem, more experiments need to be done to improve the database of this mathematical model.

2. Dynamic testing of hybrid MRE isolator

The isolation performance of MRE based isolator is evaluated with a harmonic excitation. The harmonic excitation is classified as a steady state input. Depend on the types of vibration inputs, there are also transient input (shock) and random input. In order to broaden the applications of MRE in engineering field, the investigations of isolation performance of MRE based isolator with the transient and random input are essential. The dynamic behaviour and isolation performance of MRE based isolator will remain for further study.

3. New manufacture technology to fabricate MRE material

It is known that microstructure of iron particle in MRE significantly affect MRE mechanical properties. Depend on the distribution of iron particles, MRE is classified as isotropic and anisotropic MRE material. The conventional manufacture procedures of MRE include: mixing, forming pre-configuration and solidification. An anisotropic MRE is fabricated by applying a magnetic field to MRE martial during the curing procedure. In order to manufacture MRE with specified microstructure and simplify manufacture procedure, a new manufacture technology should be used to fabricate MRE. 3D printing technology can fabricate geometrically complicated structure quickly with low cost. Thus, 3D printing technology will be used to manufacture the MRE. A preliminary study on 3D printing to manufacture MRE material has been done. The 3D printing results are in AppendixIV.

List of References

Aguiar, R.A., Savi, M.A. and Pacheco, P.M. (2012) 'Experimental investigation of vibration reduction using shape memory alloys', *Journal of Intelligent Material Systems and Structures*, vol. 24, Issue: 2, pp. 247-261.

Aguib, S., Nor, A., Djedid, T., Bossis, G. and Chikh, N (2016) 'Forced transverse vibration of composite sandwich beam with magnetorheological elastomer core', vol. 30, no. 1, pp. 15-24.

Andre, P. (2011) *Vibration Control of Active Structures 3rd Edition*, Berlin, Germany: Springer.

Ausanio, G., Iannotti, V., Ricciardi, E., Lanotte, L. and Lanotte, L. (2014) 'Magneto-piezoresistance in magnetorheological elastomers for magnetic induction gradient or position sensors', *Sensors and Actuators A: Physical*, vol. 205, pp.235-239.

Baranwal, D. and Deshmukh, T.S. (2012) 'MR-Fluid technology and its application-A review', *International journal of emerging technology and advanced engineering*. vol. 2, no. 12, pp.563-569.

Boczkowska, A., Awietjan, S.F., Wroblewski, R. (2007) 'Microstructure-property relationships of urethane magnetorheological elastomers', *Smart Materials and Structures.* vol. 16, pp. 1924-1930.

Boczkowska, A. and Awietjan, S. (2012) 'Chapter 6: Microstructure and properties of magnetorheological elastomers', *Advanced Elastomers – Technology, properties and applications*, In: Boczkowska, A. (eds.) ISBN 978-953-51-0739-2. InTech.

Bogue, R. (2014) 'Smart materials: a review of capabilities and applications', *Assembly Automation*, vol. 34, no. 1, pp.16-22.

Bose, H., (2007) 'Viscoelastic properties of silicone-based magnetorheological elastomers', *International Journal of Modern Physics B*, vol. 21, no. 28n29 , pp.4790-4797.

Bose, H. and Roder, R. (2009) 'Magnetorheological elastomers with high variability of their mechanical properties', *Journal of Physics: Conference Series.* vol. 149, 012090.

Bose, H., Rabindranath, R. and Ehrlich, J. (2012) 'Soft magnetorheological elastomers as new actuators for valves', *Journal of Intelligent Material Systems and Structures*, vol. 23, no. 9, pp.989-994.

BSI (2011) BS ISO 4664-1:2011: *Rubber, vulcanized or thermoplastic – Determination of dynamic properties, Part 1: General guidance*, London, British Standards Institution.

Carlson, J.D. and Jolly, M.R. (2000) 'MR fluid, foam and elastomer devices', *Mechatronics.* vol. 10, pp.555-569.

Chen, L., Gong, X.L., Li, W.H. (2007) 'Microstructures and viscoelastic properties of anisotropic magnetorheological elastomers' *Smart Material and Structure,* vol. 16, pp. 2645-2650.

Chen, L., Gong, X.L., Jiang, W.Q., Yao, J.J., Deng, H.X. and Li, W.H. (2007) 'Investigation on magnetorheological elastomers based on natural rubber', *Journal of Materials Science,* vol. 42, pp. 5483-5489.

Coquelle, E. and Bossis, G. (2006) 'Mullins effect in elastomers fileld with particles aligned by a magnetic field', *International journal of solids and structures*. vol. 43, pp. 7659-7672.

Davis, L.C. (1999) 'Model of Magnetorheological elastomers', *Journal of applied physics,* vol. 85, no. 6, pp. 3348-3351.

Deng, H. X., Gong, X. L. and Wang, L. H. (2006) 'Development of an adaptive tuned vibration absorber with magnetorheological elastomer', *Smart Material and Structure,* vol. 15, no. 5, pp. 111-116.

Deng, H. X. and Gong, X. L. (2007) 'Adaptive tuned vibration absorber based on magnetorheological elastomer', *Journal of Intelligent Material System and Structures,* vol. 18, pp.1205–1210.

Du, H., Li, W. and Zhang, N. (2011) 'Semi-active variable stiffness vibration control of vehicle seat suspension using an MR elastomer isolator', *Smart materials and structure.* vol. 20, 105003.

Eem, S.H, Jung, H.J. and Koo, J.H. (2012) 'Modelling of magneto-rheological elastomers for harmonic shear deformation', *IEEE Transaction on magnetic,* vol. 48, no. 11, pp. 3080-3083.

Engineeringtoolbox.com (2017). Permeability. [online] Available at: http://www.engineeringtoolbox.com/permeability-d_1923.html [Accessed 29 Sep. 2017].

Fan, Y.C., Gong, X.L., Jiang, W.Q., Zhang, W., Wei, B. and Li, W.H. (2010) 'Effect of maleic anhydride on the damping property of magnetorheological elastomers', *Smart Material and Structures,* vol. 19, 055015.

Fan, Y.C., Gong, X.L., Xuan, S.X., Qin, L.J. and Li, X.F. (2013) 'Effect of Cross-Link density of the matrix on the damping properties of magnetorheological elastomers', *Industrial & Engineering Chemistry Research,* vol. 52, pp. 771-778.

Farshad, M. and Benine, A. (2004) 'Magnetoactive elastomer composites', *Polymer Testing*. vol. 23, pp. 347-353.

Fitzgerald, A.E., Kingsley, C. and Umans, S.D. (2009) Electric Machinery, 6th edn, New York, McGraw-Hill, p. 3, figure.

Genc, S. and Phule, P.P. (2002) 'Rheological properties of magnetorheological fluids', *Smart Material and Structures*, vol. 11, pp. 140-146.

Gent, A.N. (2012) *Engineering with rubber: How to Design Rubber Components*, 3rd edn, Munich, Hanser Publications.

Ginder, J. M., Clark, S. M., Schlotter, W. F. and Nichols, M. E. (2002) 'Magnetostrictive phenomena in magnetorheological elastomers', *International Journal of Modern Physiscs B*, vol. 16, pp. 2412–2418.

Ginder, J.M., Scholotter, W.F. and Nichols, M.E. (2001) 'Magnetorheological elastomers in tunable vibration absorbers', *Proc. SPIE.* vol. 4331, pp.103–110.

Gong, X.L., Chen, L. and Li, J.F. (2007) 'Study of the utilizable magnetorheological elastomers', *International Journal of Modern Physics B.* vol. 21, nos. 28&29, pp. 4875-4882.

Gong, X.L., Zhang, X.Z. and Zhang, P.Q. (2005) 'Fabrication and characterization of isotropic magnetorheological elastomers', *Polymer Testing*, vol. 24, pp. 669-676.

Gong, X., Xu, Y., Xuan, S., Guo, C. and Zong, L. (2012) 'The investigation on the nonlinearity of plasticine-like magnetorheological materials under oscillatory shear rheometry', *Journal of the society of rheology*, vol. 56, no.6, pp. 1375-1391.

Gong, X.L., Fan, Y.C., Xuan, S.H., Xu, Y.G., and Peng, C. (2012) 'Control of the Damping Properties of Magnetorheological elastomers by using polycaprolactone as a temperature-controlling component', *Industrial and Engineering chemistry Researh*. vol. 51, pp. 6395-6403.

Guo, F., Du, C.B. and Li, R.P. (2014) 'Viscoelastic parameter model of magnetorheological elastomers based on Abel dashpot', *Advances in Mechanical Engineering*, vol. 6, 629386.

Hua, Y., Wang, Y.L., Gong, X.L., Gong, X.Q., Zhang, X.Z., Jiang, W.Q., Zhang, P.Q. and Chen, Z.Y. (2005) 'New magnetorheological elastomers based on polyurethane/si-rubber hybrid', *Polymer Testing.* vol. 24, pp. 324-329.

Huang, J., Zhang, J.Q., Zhu, Y. and Wei, Y.Q. (2002) 'Analysis and design of a cylindrical magneto-rheological fluid brake', *Journal of Materials Processing Technology*, vol. 129, pp. 559-562.

Instron. (2008) 'WaveMatrix Software application program – V1.3 Onwards Software Reference Manual. M22-16102-EN Revision A'. pp. 233- 248.

Jani, H. M., Leary, M., Subic, A. and Gibson, M.A. (2014) 'A review of shape memory alloy research, applications and opportunities', *Materials and Design.* vol. 56, pp. 1078-1113.

Jeong, U.C., Yoon, J.H., Yang, I.H., Jeong, J.E., Kim, J.S., Chung, K.H. and Oh, J.E. (2013) 'Magnetorheological elastomer with stiffness-variable characteristics based on induced current applied to differential mount of vehicles', *Smart Materials and Structures,* vol. 22, 115007.

Jiang, W.Q., Yao, J.J., Gong, X.L. and Chen, L. (2008) 'Enhancement in Magnetorheological effect of Magnetorheological elastomers by surface modification of iron particles', *Chinese Journal of Chemical Physics,* vol. 21, no. 1, pp. 87-92.

Jolly, M.R., Carlson, J.D and Munoz, B.C. (1996) 'A model of the behaviour of magnetorheological materials', *Smart Materials and structure,* vol. 5, pp. 607-614.

Kallio, M. (2005). *The elastic and damping properties of magnetorheological elastomers*. Ph.D Thesis. Tampere University of Technology.

Kallio, M., Lindroos, T., Aalto, S., Jarvinen, E., Karna, T. and Meinander, T. (2007) 'Dynamic compression testing of a tunable spring element consisting of a magnetorheological elastomer', *Smart Mater.Struct*. vol. 16, pp. 506-514.

Kashima, S., Miyasaka, F. and Hirata, K. (2012) 'Novel soft actuator using magnetorheological elastomer' *IEEE Transactions on Magnetics*, vol. 48, no. 4, pp.1649-1652.

Kavlicoglu, B., Wallis, B., Sahin, H. and Liu, Y. (2011) 'Magnetorheological elastomer mount for shock and vibration isolation', *proceeding of SPIE,* vol. 7977, 79770Y.

Kciuk, M. and Turczyn, R. (2006) 'Properties and application of magnetorheological fluids', *Journal of Achievements in Materials and Manufacturing Engineering,* vol.18, no. 1-2, pp.127-130.

Lejon, J and Kari, L. (2009) 'Preload, frequency, vibrational amplitude and magnetic field strength dependence of magnetosensitive rubber', *Plastics, Rubber and Composites,* vol. 38, no. 8, pp. 321-326.

Lokander, M. and Stenberg, B. (2003) 'Performance of isotropic magnetorheological rubber materials', *Polymer Testing,* vol. 22, pp. 245-251.

Li, R. and Sun, L.Z. (2013) 'Viscoelastic responses of silicone-rubber-based magnetorheological elastomers under compressive and shear loadings', *Journal of Engineering materials and Technology,* vol. 135, 021008.

Li, W.H., Kostidis, K., Zhang, X.Z. and Zhou, Y. (2009) 'Development of a force sensor working with MR Elastomers', *2009 IEEE/ASME International Conference on Advanced Intelligent Mechatronics.* Singapore, July 14-19, 2009. pp. 233-238, IEEE.

Li, W.H., Zhang, X.Z. and Du, H. (2013) 'Magnetorheological elastomers and their applications', in Visakh, P.M., Thomas S., Chandra A.K. & Mathew A.P. (eds.), *Advances in Elastomers I: Blends and Interpenetrating Networks,* Berlin, Germany, Springer, pp. 357-374.

Li, W.H., Zhou, Y. and Tian T.F. (2010) 'Viscoelastic properties of MR elastomers under harmonic loading', *Rheologica Acta,* vol.49, pp. 733-740.

Li, Y., Li, J., Tian, T. and Li, W. (2013) 'A highly adjustable magnetorheological elastomer base isolator for application of real-time adaptive control', *Smart materials and structures,* vol. 22, 095020.

Lokander, M. and Stenberg, B. (2003) 'Improving the Magnetorheological effect in isotropic Magnetorheological rubber materials', *Polymer Testing.* vol. 22, no. 6, pp. 677-680.

Maxwell-Garnett J.C. (1904) 'Colour in metal glasses and metallic films', *Phil. Trans. R. Soc.* vol. 203, pp. 385-420.

Mitsumata, T., Sakai, K. and Takimoto, J.I. (2006) 'Giant reduction in dynamic modulus of κ-carrageenan magnetic gels', *The Journal of Physical Chemistry B,* vol. 110, no. 41, pp.20217-20223.

Mitsumata, T., Horikoshi, Y. and Negami, K. (2008) 'High-power actuators made of two-phase magnetic gels', *Japanese Journal of Applied Physics*, vol. 47, no. 9, pp.7257-7261.

Mitsumata, T. and Ohori, S. (2011) 'Magnetic polyurethane elastomers with wide range modulation of elasticity', *Polymer Chemistry,* vol. 2, pp.1063-1067.

Mullins, L. (1969) 'Softening of rubber by deformation', *Rubber Chemistry and Technology,* vol. 42, no. 1, pp. 339-362.

Munoz, B.C. and Jolly, M.R. (2001) 'Composites with field responsive rheology', in Brostow, W. (ed) *performance of plastics,* Munich, Carl Hanser Verlag, pp. 553-574.

Nayak, B., Dwivedy, S.K. and Murthy, K.S.R.K. (2011) 'Dynamic analysis of magnetorheological elastomer-based sandwich beam with conductive skins under various boundary conditions', *Journal of sound and vibration,* vol. 330, pp. 1837-1859.

Neelakanta, S.P. (1995) *Handbook of Electromagnetic materials Monolithic and composite Versions and their applications,* CRC Press LLC press, USA.

Norouzi, M., Alehashem, S.M.S., Vatandoost, H., Ni, Y.Q. and Shahmardan, M.M. (2015) 'A new approach for modeling of magnetorheological elastomers', *Journal of Intelligent Material Systems and Structures,* vol. 27, no. 8, pp. 1121-1135.

Ogden, R.W. and Roxburgh, D.G. (1999) 'A pseudo-elastic model for the Mullins effect in filled rubber', *Proceedings of the Royal Society of London. Series A: Mathematical, Physical and Engineering Sciences,* vol. 455, pp. 2861-2877.

Olabide, I.A., Lion, A. and Elejabarrieta, M.J. (2017) 'A new three-dimensional magneto-viscoelastic model for isotropic magnetorheological elastomers', *Smart Material and Structure,* vol. 26, 035021.

Opie, S. and Yim, W. (2011), 'Design and control of a real-time variable modulus vibration isolator', *Journal of intelligent material system and structures,* vol. 22, pp. 113-125.

Padalka, O., Song, H.J., Wereley, N.M., Filer II, J.A. and Bell, R.C. (2010) 'Stiffness and damping in Fe, Co, and Ni nanowire-based magnetorheological elastomeric composites', *IEEE Transactions on Magnetics*, vol. 46, no. 6, pp.2275-2277.

Payne, A.R. (1962) 'The dynamic properties of carbon black loaded natural rubber vulcanizates. Part I', *Journal of Applied Polymer Science*, vol. 6, no. 19, pp. 57-63.

Popp. K.M., Kroger, M., Li W.H., Zhang, X.Z. and Kosasih, P.B. (2009) 'MRE properties under shear and squeeze modes and applications', *Journal of intelligent material system and structures,* vol. 21, pp. 1471-1477.

Rabinow, J. (1948) 'The Magnetic Fluid Clutch', *American Institute of Electrical Engineers transactions.* vol. 67, pp. 1308-1315.

Ruddy, C., Ahearne, E. and Byrne, G. (2012) 'A review of magnetorheological elastomers: properties and applications', *Advanced Manufacturing Science (AMS) Research,* [Online]. http://www. ucd. ie/mecheng/ams/news_items/Cillian% 20Ruddy. pdf Accessed, 20.

Shen, Y, Golnaraghi, M.F. and Heppler, G.R. (2004) 'Experimental Research and Modelling of Magnetorheological Elastomers', *Journal of Intelligent Materials Systems and Structures,* vol. 15, pp. 27-35.

Sorokin, V.V., Ecker, E., Stepanov, G.V., Shamonin, M., Monkman, G.J., Kramarenko, E.Y. and Khokhlov, A.R. (2014) 'Experimental study of the magnetic field enhanced Payne effect in magnetorheological elastomers', *Soft matter,* vol. 10, pp. 8765-8776.

Stepanov, G., Borin, D. and Odenbach, S. (2009) 'Magnetorheological effect of magneto-active elastomers containing large particles', *Journal of Physics: Conference Series*, vol. 149, 012098.

Sun, S.S., Deng, H.X., Yang, J., Li, W.H., Du, H.P., Alici, G. and Nakano, M. (2015) 'An adaptive tuned vibration absorber based on multi-layered MR elastomers'. *Smart Material and Structure,* vol. 24, 045045.

Sun, S.S., Yildirm, T., Wu, J.C., Yang, J., Du, H., Zhang, S.W. and Li, W.H. (2017) 'Design and verification of a hybrid nonlinear MRE vibration absorber for controllable broadband performance', *Smart Material and Structure,* vol. 26, 095039.

Thorsteinsson, F., Gudmundsson, I. and Lecomte, C., össur hf, (2017) *Prosthetic and orthotic devices having magnetorheological elastomer spring with controllable stiffness,* U.S. Patent 9724210.

Tian, T.F., Li, W.H., Alici, G., Du, H. and Deng, Y.M. (2011) 'Microstructure and magnetorheology of graphite-based MR elastomers', *Rheol Acta,* vol. 50, pp. 825-836.

Turczyn, R. and Kciuk, M. (2008) 'Preparation and study of model magnetorheological fluids', *Journal of Achievements in Materials and Manufacturing Engineering,* vol.27, no. 2, pp. 131-134.

Ubaidillah, Imaduddin, F., Li, Y.C., Mazlan, S.A., Sutrisno, J., Koga, T., Yahya, I. and Choi, S.B. (2016) 'A new class of magnetorheological elastomers based on waste tire rubber and the characterization of their properties', *Smart Materials and Structures,* vol. 25, 115002.

Ubaidillah, Sutrisno, J., Purwanto, A. and Mazlan, S.A. (2015) 'Recent progress on magnetorheological solids: materials, fabrication, testing and application', *Advanced engineering materials,* vol. 17, no. 5, pp. 563-597.

Varga, Z., Filipcsei, G. and Zrinyi, M. (2005) 'Smart composites with controlled anisotropy', *Polymer.* vol. 46, pp. 7779-7787.

Wahab, N.A., Mazlan, S.A., Ubaidilah, Kamaruddin, S., Ismail, N.I.N., Choi, S.B. and Sharif, A.H.R. (2016) 'Fabrication and investigation on field-dependent properties of natural rubber based magneto-rheological elastomer isolator', *Smart materials and structures,* vol. 25, 107002.

Wang, Y.L., Hu, Y., Deng, H.X., Gong, X.L., Zhang, P.Q., Jiang, W.Q. and Chen, Z.Y. (2006) 'Magnetorheological elastomers based on Isobutylene-Isoprene rubber', *Polymer Engineering and Science.* vol. 46, no. 3, pp. 264-268.

Wang, Y.L., Hu, Y., Chen, L., Gong, X.L., Jiang, W.Q., Zhang, P.Q. and Chen, Z.Y. (2006) 'Effects of rubber/magnetic particle interactions on the performance of Magnetorheological elastomers', *Polymer Testing.* vol. 25, no.2, pp.262-267.

Ward, I.M. and Sweeney, J. (2004) *An Introduction to The Mechanical Properties of Solid Polymers*, 2nd ed, John Wiley & Sons.

Wen, Q., Wang, Y. and Gong, X. (2017) 'The magnetic field dependent dynamic properties of magnetorheological elastomers based on hard magnetic particles', *Smart material and structure,* vol. 26, 075012.

Wu, D.F., Huang, L., Pan, B., Wang, Y.W. and Wu, S. (2014) 'Experimental study and numerical simulation of active vibration control of a highly flexible beam using piezoelectric intelligent material', Aerospace Science and Technology. vol. 37, pp.10-19.

Xu, Y., Gong, X., Xuan, S., Zhang, W. and Fan, Y. (2011) 'A high-performance magnetorheological material: preparation, characterization and magnetic-mechanic coupling properties', *Soft Matter*, vol. 7, pp.5246-5254.

Yang, J., Du, H.P., Li,W.H., Li, Y.C., Li, J.C., Sun,S.S. and Deng, H.X. (2013) 'Experimental study and modelling of a novel magnetorheological elastomer isolator', *Smart Material and structure,* vol. 22, 117001.

You, J.L., Park, B.J. and Choi, H.J. (2008) 'Magnetorheological characteristics of Carbonyl Iron embedded suspension polymerized poly (Methyl Methacrylate) Micro-bead', *IEEE Transactions on magnetics,* vol.44, no. 11, pp. 3867-3870.

Zajac, P., Kaleta, J., Lewandowski, D. and Gasperowicz, A. (2010) 'Isotropic magnetorheological elastomers with thermoplastic matrices: structure, damping properties and testing', *Smart Materials and Structure.* vol. 19, no.4, 045014.

Zhang, W., Gong, X.L., Xuan, S.H. and Xu, Y.G. (2010) 'High-performance hybrid magnetorheological materials: Preparation and Mechanical Properties', *Industrial and Engineering chemistry Researh,* vol. 49, pp. 12471-12476.

Zhou, G.Y. and Wang, Q. (2006) 'Study on the adjustable rigidity of magnetorheological-elastomer-absed sandwich beams', *Smart material and structure,* vol. 15, 59-74.

Zhu, G., Xiong, Y.P., Daley, S. and Shenoi, R.A. (2015) 'Magnetorheological elastomer materials and structures with vibration energy control for marine application', *Analysis and Design of Marine Structure V.* pp, 197-204.

Zhu, J.T., Xu, Z.D. and Guo, Y.Q. (2012) 'Magnetoviscoelasticity parametric model of an MR elastomer vibration mitigation device', *Smart Materials and Structures*, vol. 21, 075034.

Zhu, J.T., Xu, Z.D. and Guo, Y.Q. (2013) 'Experimental and modelling study on magnetorheological elastomers with different matrices', *Journal of materials in civil engineering,* vol. 25, no. 11, pp. 1762-1771.

Zhu, W. and Rui, X.T. (2014) 'Semiactive vibration control using a magnetorheological damper and a magnetorheological elastomer based on the Bouc-Wen model', *Shock and Vibration,* vol. 2014, 405421.

Zhu, Y.S., Gong, X.L., Dang, H., Zhang, X.Z. and Zhang, P.Q. (2006) 'Numerical Analysis on Magnetic-induced Shear Modulus of Magnetorheological Elastomers Based on Multi-chain Model', *Chinese Journal of Chemical Physics,* vol. 19, no.2, pp. 126-130.

List of Publications

Wang, W. and Xiong, Y.P. (2017) ‘Pre-strain effect on the dynamic shear properties of the magnetorheological elastomer’, *Smart Material and Structure, (Submit)*

Wang, W., Xiong, Y.P. and Yang, S.F. (2017) ‘Smart Magnetorheological elastomer for vibration control’, Poster, FSI away day, Southampton.

Wang, W. and Xiong, Y.P. (2016) ‘Dynamic shear properties of MRE considering of pre-strain, strain amplitude, magnetic fields strength and frequencies and their coupling effects’, *15th International Conference on Electrorheological Fluid and Magnetorheological Suspensions.* 4-8 July, Incheon, Korea.

Wang, W. and Xiong, Y.P. (2014) ‘Novel approach to high-performance smart MRE material for vibration control of marine structure’, Poster, FSI away day, Southampton.

Appendix I

Table A.I 1 Vectors and matrices dimension for mathematical model of shear and compression MRE

	Shear	Compression
$\boldsymbol{A_1'}$	1×3	1×3
$\boldsymbol{A_2'}$	1×3	1×3
$\boldsymbol{A_3'}$	1×2	1×2
$\boldsymbol{A_4'}$	1×3	1×3
$\boldsymbol{A_5'}$	1×3	1×3
$\boldsymbol{A_6'}$	1×1	1×1
$\boldsymbol{A_1''}$	1×3	1×3
$\boldsymbol{A_2''}$	1×3	1×3
$\boldsymbol{A_3''}$	1×2	1×2
$\boldsymbol{A_4''}$	1×3	1×3
$\boldsymbol{A_5''}$	1×3	1×3
$\boldsymbol{A_6''}$	1×1	1×1
$\boldsymbol{\gamma}$	1×3	1×3
$\boldsymbol{f}$	1×3	1×3
$\boldsymbol{B}$	1×2	1×2
$\boldsymbol{\gamma_f}$	1×3	1×3
$\boldsymbol{\gamma_B}$	1×3	1×3
$\boldsymbol{f_B}$	1×1	1×1
$\mathbf{G}$	960×1	432×1
$\mathbf{X}$	960×16	432×16
$\mathbf{R}$	16×1	16×1

Appendix II

Simulation of magnetic circuit in COMSOL MULTIPHYSICS

1. In the new window, click Model Wizard. For Select Space Dimension, select 3D. Then, in the Select Physics, select AC/DC>Magnetic fields (mf).

2. Import the MRE isolator to COMSOL and create an air domain to this simulation (shown in figure 7.8 (a)). The dimension of the isolator is $118mm \times 118mm \times 61mm$ and the dimension of the air domain is $500mm \times 500mm \times 400mm$.

3. The aim of this simulation is to simulate the magnetic flux density through MRE material by a direct current. The magnetic field induced by an electric current in space obeys ampere law. For the simulation in COMSOL MULTIPHYSICS, choose Ampere' Law for the domain of air domain, MRE isolator top and bottom and MRE samples. The magnetic field in these domains obey ampere law.

4. The settings of relative magnetic permeability for each part of this model are given in Table A.II 1.

Table A.II 1 Relative magnetic permeability for each domain

Domain	Material	Relative magnetic permeability
Air domain	Air	1
Isolator top	Iron (99.8% pure)	5000
Isolator Bottom	Iron (99.8% pure)	5000
MRE	MRE	3.5

5. The magnetic field in this simulation is generated by copper coils. In COMSOL, Multi-Turn Coil is chosen for the domain of four copper coils. The settings of the domain of Multi-Turn Coil are given in Table A.II 2.

Table A.II 2 Multi-Turn Coil Setting

Domain Type	Multi-Turn Coil
Coil Current	3 Ampere
Number of Turns	516
Current Direction	Anti-clockwise

6. For meshing of the simulation domain, a finer mesh is selected to mesh the isolator and a relatively coarse mesh is used to mesh the air domain. This is because magnetic flux through the isolator is the main problem of concern. Mesh of the integral domain is shown in Figure 7.8 (b).

7. For the setting of solver, the first step of the simulation is to run the Coil Geometry Analysis. Then, the magnetic field generated by copper coil is achieved. Then, use the default setting of the stationary analysis of COMSOL to solve the magnetic circuit of the integral domain.

Appendix III

Figure A.III 1 Stress strain curve of MRE isolator

Table A.III 1 Experiment results of static stiffness of MRE isolator with different magnetic field

Magnetic field strength	Test 1	Test 2	Test 3	Average
0 mT	3805 KN/m	3778 KN/m	3813 KN/m	3798 KN/m
260 mT	3935 KN/m	3969 KN/m	3924 KN/m	3942 KN/m

Appendix IV

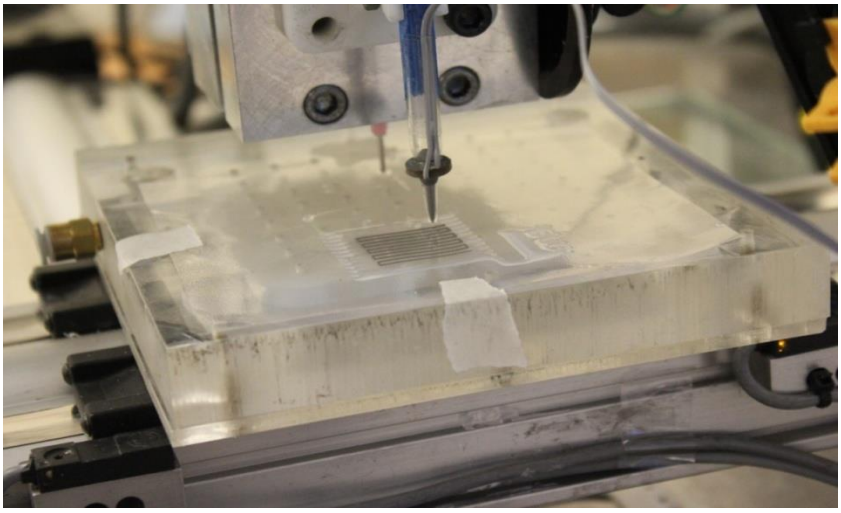

Figure A.IV 1 3D printing for MRE material

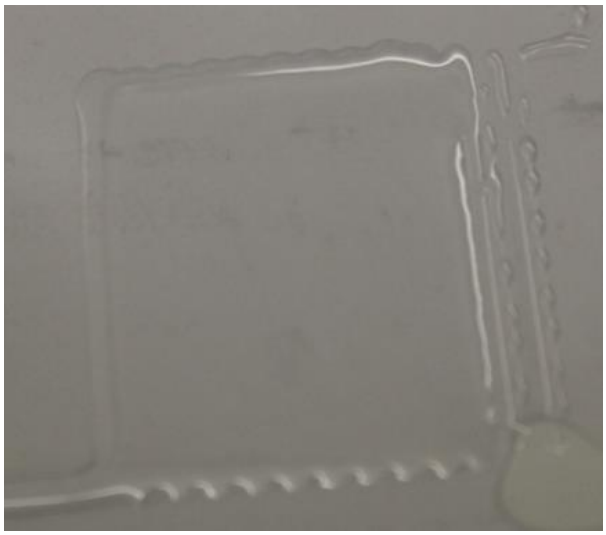

Figure A.IV 2 Single layer of silicone rubber printing

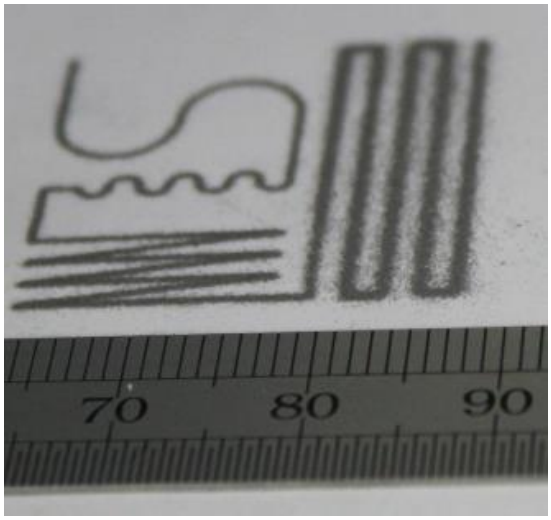

Figure A.IV 3 (a) Iron powder printing

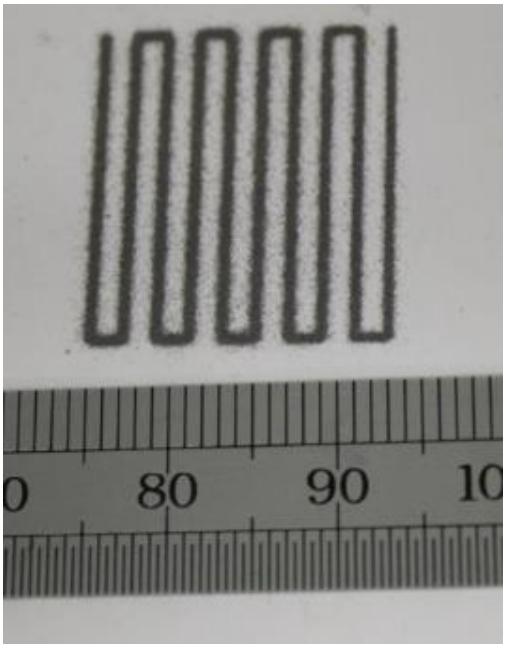

Figure A.IV 3 (b) Iron powder printing

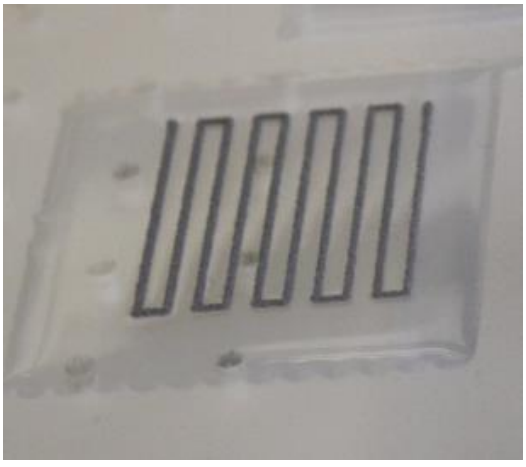

Figure A.IV 4 Printing of two layers of silicone rubber and one layer of iron powder

(a) (b)

Figure A.IV 5 Multi-layer printing (a) three layers of silicone rubber, (b) four layer of silicone rubber